NTNU
Norwegian University of
Science and Technology

Optimisation of Manganese Alloy Multi-plant Production Planning

Martin Naterstad Digernes
Lars Rudi

Industrial Economics and Technology Management
Submission date: June 2017
Supervisor: Magnus Stålhane, IØT
Co-supervisor: Brage Rugstad Knudsen, ITK
Henrik Andersson, IØT

Norwegian University of Science and Technology
Department of Industrial Economics and Technology Management

Problem Description

The purpose of this Master's Thesis is to develop an optimisation model to manage manganese alloy production. Efficient allocation of resources across multiple plants is essential to ensure optimal production. The primary objectives of this thesis are to formulate a model that handles complex chemical and pooling restrictions and to apply a solution method to verify the global optimum.

Main contents:

1. Description of the problem.
2. Presentation of the mathematical formulation developed for the problem.
3. Presentation of the solution method applied to solve the problem.
4. Implementation and testing of the mathematical formulation using the appropriate software.
5. Presentation and discussion of the results and an evaluation of the applicability of the model.

Preface

This Master's Thesis is the concluding part of our Master of Science in Industrial Economics and Technology Management with a degree specialisation in Managerial Economics and Operations Research at the Norwegian University of Science and Technology (NTNU), spring 2017. The Master's Thesis is a continuation of the work done by *Digernes and Rudi (2016)* in the specialisation project in Managerial Economics and Operations Research, Fall 2016.

We would like to thank our supervisors Associate Professor Magnus Stålhane (Department of Industrial Economics and Technology Management, NTNU), Professor Henrik Andersson (Department of Industrial Economics and Technology Management, NTNU), and Postdoctoral Brage Rugstad Knudsen (Department of Engineering Cybernetics, NTNU) for their valuable guidance throughout the work. We would also like to thank our industrial partner Eramet Norway for providing us with industrial data.

Trondheim, June 7, 2017

Martin Naterstad Digernes

Lars Rudi

Abstract

The average concentration of manganese in the earth's crust is nearly 0.1%, making it the fourth most abundant of the metals in commercial use. Manganese alloys are mainly consumed as alloying elements in the steel industry. Manganese ores are extracted at mining sites and smelted to manganese alloys at smelting sites. In the production of manganese alloys, the problem is to find the optimal combination of ores, fluxes, coke, and slag to feed the furnaces that yields alloys that meet customer specifications and to optimally decide the volume, composition, and allocation of the produced slag between furnaces. The alloys are either sold or further refined and then sold. The authors name the problem as the manganese alloy multi-plant production problem.

Current decisions in the industry are based on experience and process knowledge and are denoted as single furnace optimisation. Single furnace optimisation is the practice of optimising the profit for each single furnace without considering the overall production. A multi-plant optimisation model can provide decision support to the industry and improve the current practice.

A pooling problem formulation is presented to solve the problem. To the authors' knowledge, little work has been done on formulating the pooling problem for production of manganese alloys, and no formulations for multi-plant production exist in this industry. The formulation presented is flow and quality based and is a hybrid between the standard and the general pooling problem. The model is, however, subject to simplifying assumptions that may limit how realistic it is in its current state.

The bilinear terms in the mathematical formulation are linearised using the Multiparametric Disaggregation Technique (MDT) and the formulation is implemented in the linear solver FICO® Xpress. To the authors' knowledge, this is the first model that applies the MDT to solve large-scale, real instances. The model is applied to test instances based on the industrial partner Eramet Norway's plant layout and solved to a global optimality within 3% using the MDT-algorithm. The computational study shows that the optimisation model presented can solve problem sizes of up to ten furnaces to a global optimality gap within 8% for the allotted run time, that the MDT scales well with the problem sizes tested, and that our model outperforms single furnace optimisation. It should be noted that the single furnace optimisation practice is based on mimicking the actual practice by using our model and not actual practice results. Comparing the model to real production data remains an objective, but the results indicate that multi-plant production planning can be of considerable value to manganese alloy production.

A paper based on the contents of this thesis has been written in cooperation with the supervisors. This paper, with the title *"Optimisation of Manganese Alloy Production"*, is appended to the end of the thesis. As the paper is based on this thesis, there is overlapping content.

Sammendrag

Gjennomsnittlig mangankonsentrasjon i jordskorpen er rundt 0.1%. Mangan er dermed det fjerde mest forekommende metallet blant metaller i kommersiell bruk. Manganlegeringer blir hovedsakelig konsumert som legeringselementer i stålindustri. Manganmalm blir utvunnet gjennom gruvedrift og legeringer produseres i smelteverk ved å smelte malm sammen med andre råstoffer i ovner. Legeringene har gitte kvalitetsspesifikasjoner og kan selges som de er, eller videre raffineres og selges.

Problemet i manganlegeringsproduksjon er å finne en optimal kombinasjon av malmer, flussmiddel, koks og slagg å benytte i ovnene til å produsere de sluttproduktene som tilfredsstiller kundenes krav, samt å bestemme volum, komposisjon og transport av slaggstoff som kommer fra ovnene. Dette problemet blir betegnet som multifabrikks-manganlegeringproduksjons-problemet. I dag baseres produksjonsbeslutninger på erfaring og prosesskunnskap, dette blir betegnet som enkeltovnsoptimering. Enkeltovnsoptimering er praksisen med å optimere profitt for hver enkelt ovn og tar ikke hensyn til den helhetlige produksjonen. En multifabrikkmodell kan bidra som beslutningsstøtte til industrien og forbedre den nåværende praksisen.

En optimeringsmodell basert på poolingproblemet presenteres for å løse problemet. Etter det forfatterne kjenner til, er lite arbeid gjort for å formulere et poolingproblem for manganlegeringsproduksjon og ingen multifabrikkmodell eksisterer for denne industrien. Modellen er flyt- og kvalitetsbasert og er en kombinasjon av en standard og en generell poolingproblemformulering. Modellen inneholder forenklinger og antagelser som begrenser hvor realistisk den er i sin nåværende tilstand.

De bilineære leddene i den matematiske formuleringen er lineærisert ved bruk av multiparametrisk disaggregeringsteknikk (MDT). Formuleringen er deretter implementert i det lineære optimeringsprogrammet FICO® Xpress. Til forfatternes kunnskap er modellen som presenteres den første hvor MDT benyttes til å løse store, reelle probleminstanser. Modellen benyttes til å teste probleminstanser basert på Eramet Norge sitt fabrikkoppsett og disse løses til et globalt optimalitetsgap innenfor 3% ved bruk av MDT-algoritmen. En beregningsstudie viser at optimeringsmodellen kan løse probleminstanser på størrelser opp til ti ovner til et globalt optimalitetsgap innenfor 8% på tillatt kjøretid, at MDT skalerer godt med størrelsen på probleminstansene som testes og at vår modell presterer bedre enn enkeltovnsoptimering. Det gjøres oppmerksom på at praksisen med enkeltovnsoptimering er basert på en etterligning av den virkelige produksjonen ved å bruke vår optimeringsmodell og ikke resultater fra en faktisk produksjon. Sammenligning av modellen mot reelle data gjenstår fremdeles som et mål, men resultatene indikerer at bruk av vår optimeringsmodell kan være av betraktelig verdi for manganlegeringsproduksjon.

En artikkel basert på innholdet i denne masteroppgaven har blitt skrevet i samarbeid med veilederene. Denne artikkelen, med tittelen *"Optimisation of Manganese Alloy Production"*, er lagt ved i slutten av oppgaven. Siden artikkelen er basert på masteroppgaven, er det overlappende innhold.

Table of Contents

List of Tables

List of Figures

Dictionary

Abbreviations

LS – Left side
NA – Not applicable
RS – Right side

Industry Terminology

Calcine – To convert to calx by heating or burning
Calx – The oxide substance that remains after metals have been thoroughly roasted
HC – High Carbon
LC – Low Carbon
MC – Medium Carbon
MOR – Manganese Oxygen Refining
Reactant – Any substance that undergoes a chemical change in a given reaction
Redox – Reduction-oxidisation
Resultant – The result from the combination of two or more reactants
Tonne – Metric tonne, 1000kg

Optimisation Terminology

BLP – Bilinear Program
GOP – Global Optimisation Algorithm
LP – Linear Program
MAMP – Manganese Alloy Multi-plant Production problem
MDT – Multiparametric Disaggregation Technique
MILP – Mixed Integer Linear Program
MINLP – Mixed Integer Nonlinear Program
NLP – Nonlinear Program
RLT – Reformulation-Linearisation Technique
SLP – Successive Linear Programming

Elements and Oxides

Al – Aluminium
Al_2O_3 – Aluminium oxide
C – Carbon
$CaCO_3$ – Limestone
$CaMg(CO_3)_2$ – Dolomite
CaO – Calcium oxide
CO – Carbon monoxide
CO_2 – Carbon dioxide
Cu – Copper
Fe – Iron
FeMn – Ferromanganese
FeO – Iron(II) oxide
Fe_2O_3 – Iron(III) oxide
Fe_3O_4 – Iron(II, III) oxide
FeSi – Ferrosilicon
Mg – Magnesium
MgO – Magnesium oxide
Mn – Manganese
MnO – Manganese(II) oxide
MnO_2 – Manganese dioxide
Mn_2O_3 – Manganese(III) oxide
Mn_3O_4 – Manganese(II, III) oxide
P – Phosphorus
Si – Silicon
SiMn – Silicomanganese
SiO_2 – Silicon dioxide

Chapter 1

Introduction

Manganese is a hard, brittle, silvery metal that exists in nature in the form of minerals, mainly as oxides *(Olsen et al., 2007)*. It is an important element in steel and aluminium alloys. In steel, manganese improves strength, wear resistance, and workability. Steel alloys are used to create railway tracks, safes, and prison bars among other applications *(Royal Society of Chemistry, 2016)*. Manganese in aluminium alloys increases the resistance against corrosion. Such alloys are used in beverage cans, kitchenware, roofing, and car radiators *(Metalpedia, 2016)*.

There is an increasing focus on environmental impacts caused by production industries *(United Nations Environment Programme, 2016; Olsen et al., 2007)*. Consequences of unsustainable production of manganese alloys are environmental degradation, resource depletion, and emissions of carbon dioxide and other pollutants into the atmosphere. Efficient production and resource consumption are, consequently, necessary to address. Producers of manganese alloys are, therefore, looking for ways to better utilise available resources and to make the production more sustainable.

The manganese alloy industry is world spanning and can be divided into two parts: ore mining and alloy production. In the alloy production, manganese ores are melted in furnaces to create manganese alloys. Some by-products are also produced in the furnaces, where the most significant by-product is slag. The slag can either be discarded or reused to save raw materials. A more thorough presentation of the industry and its production methods is given in Chapter 2.

The total production of manganese alloys has been approximately twenty million tonnes annually in the recent years *(d'Harambure, 2015)*. An average price for manganese alloys around 2 USD/kg *(InvestmentMine, 2017)* makes the manganese alloy production a multi-billion dollar industry. One actor in the industry is the Eramet Group who is a world leader in production of alloying metals, employing about 14 000 people in 21 countries *(Eramet Group, 2016b)*. A division of this company, Eramet Norway, is our industrial partner. They produce manganese alloys mostly for the European and North American markets and have three plants located in Norway, producing ferromanganese and silicomanganese alloys *(Eramet Norway, 2016a)*.

The industry partner's current operational practice is, according to the problem owner, to make decisions based on the metallurgist's experience, process knowledge, and to optimise the production for each furnace separate instead of considering the overall production. Slag is sent to the furnaces where the transportation costs are the lowest. The industry partner is uncertain whether this is a good operational practice or if it could be improved. Finding the best way to utilise the

slag while accounting for the overall production can result in more efficient resource consumption. The industrial partner is interested in a decision support tool that can help them make complex decisions for the production across multiple plants instead of optimising the production in each furnace separately. An optimisation model that considers the integrated production of ferromanganese and silicomanganese alloys across multiple plants can improve the current practice. In the remainder of the thesis, the considered problem is denoted as the Manganese Alloy Multi-plant Production problem (MAMP).

Optimisation literature is studied to investigate if the problem is addressed in previous work. The production problem is identified as a pooling problem. The pooling problem is solved for various problems in multiple industries, but little work has been done on formulating it for manganese alloy production. To the authors' knowledge, only one paper is written on the topic, where the model presented is only capable of calculating the production for single ferromanganese and silicomanganese furnaces. As the manganese alloy production industry is a large and complex industry, an optimisation model can provide the industry with production planning support that can result in better utilisation of resources, less waste, and less energy consumption in the furnaces per tonne alloy produced. Thus, resulting in savings for both the manganese alloy producer and the environment. The objective of this thesis is therefore to formulate a general model that can be used as a decision support tool for multi-plant production planning of manganese alloys.

The contributions of this thesis are:

- A clear description and definition of a multi-plant manganese production problem previously not analysed.
- A general nonlinear formulation of the problem in consideration, applicable to any alloy production with similar processes as manganese alloy production.
- Linearisation of the nonlinear formulation using the Multiparametric Disaggregation Technique so that the MAMP can be solved using a linear solver.
- Showing that the Multiparametric Disaggregation Technique can be applied to a large-scale, industrial pooling problem.
- Results indicating that multi-plant production planning is superior to the current practice of single furnace optimisation.

The thesis has the following structure: Chapter 2 is a background chapter where an overview of the manganese alloy production industry, the operational processes including power consumption and furnace chemistry, and information about our industrial partner are presented. The problem description outlining the MAMP is provided in Chapter 3. A review of the relevant literature to the MAMP is conducted in Chapter 4. In Chapter 5, simplifications and underlying assumptions are presented before the mathematical formulation of the MAMP is given. Chapter 6 presents the solution method applied to solve the MAMP. The implementation of the MAMP and a computational study are presented in Chapter 7. Concluding remarks are presented in Chapter 8, before thoughts on future research are described in Chapter 9.

A paper based on the contents of this thesis has been written in cooperation with the supervisors. This paper, with the title *"Optimisation of Manganese Alloy Production"*, is appended to the end of the thesis in its unreviewed and unpublished form, in Appendix F. As the paper is based on this thesis, there is overlapping content.

Chapter 2

Industry Insight

This chapter outlines the manganese alloy manufacturing industry. The motivation is to give the reader a thorough understanding of the manganese alloy industry, both of its markets and production processes. This industry overview is a necessity for understanding the complexities of the production and the structure of the Manganese Alloy Multi-plant Production problem (MAMP).

An overview of the industry is provided in Section 2.1. The supply chain is outlined in Section 2.2 and a detailed description of the alloy production process is given in Section 2.3. Production methods are presented in Section 2.4. An approximation of the furnace power consumption for manganese alloy production is presented in Section 2.5. In Section 2.6, the chemical reactions occurring in the furnaces are presented. Lastly, an overview of our industrial partner Eramet Norway and the locations of the company's plants in Norway are given in Section 2.7.

2.1 Market Overview

The average concentration of manganese (Mn) in the earth's crust is nearly 0.1%, making it the fourth most abundant of the metals in commercial use *(Gasik, 2013)*. Only iron (Fe), aluminium (Al), and copper (Cu) are ranked higher than manganese in abundance *(Kalagadi Manganese, 2013)*. Although there is an abundance of manganese ore, it is only mined in a few countries. South Africa, Australia, China, and Gabon stand for 70% of the total manganese ore mined in 2011. Together with Brazil and Ukraine, these countries hold 90% of the world's confirmed manganese reserves *(Cannon, 2014)*. South Africa, Australia, Gabon, and Brazil are the main suppliers of high-grade ore, while Australia, South Africa, and India are the main suppliers of medium-grade ore. China dominates the market for low-grade ore by producing more than 90% of the world's low-grade manganese ore *(Risk & Policy Analysts Limited, 2015)*.

Manganese is widely used in everyday life. As an alloy, manganese decreases the brittleness of steel and imparts strength *(Cannon, 2014)*, toughness, and hardness *(Gasik, 2013)*. Figure 2.1 illustrates high-carbon ferromanganese (HC FeMn), a manganese alloy. There has not yet been identified satisfactory substitutes for manganese as an alloying element that combines the low production costs and the key properties manganese possesses. These traits make it an attractive metal to use in steel alloys *(Kalagadi Manganese, 2013)*. Manganese is mainly consumed in the steel industry,

which consumes about 90% of the total manganese supply *(International Manganese Institute and Hatch, 2015)*. Thus, the world consumption of manganese alloys heavily depends on the consumption of steel. On average, 10 kg manganese alloy is used per tonne (1000 kg) produced steel *(Gasik, 2013)*.

Figure 2.1: High-carbon ferromanganese. Photo reproduced from *Marmara Metal (2016)*.

2.1.1 Market Supply and Demand

The production of manganese alloys has been steadily increasing the recent years, in correlation with the increasing crude steel production. This increase can be seen from Figures 2.2 and 2.3. The supply and demand in 2014 for the most important manganese alloys can be seen in Table 2.1. Asia is by far both the largest supplier and consumer of manganese alloys with a market share of around 70 - 80% within both sectors for all the manganese alloy types listed in Table 2.1 *(d'Harambure, 2015)*. For manganese alloy production, there has been a shift in demand away from HC FeMn towards medium carbon silicomanganese (MC SiMn) and refined alloys of both *(Olsen et al., 2007)*, primarily for economic reasons *(Olsen and Tangstad, 2004)*.

Table 2.1: Supply and demand in 2014 for the most important manganese alloys: silicomanganese (SiMn), high-carbon ferromanganese (HC FeMn), and refined ferromanganese (medium carbon ferromanganese (MC FeMn) and low carbon ferromanganese (LC FeMn)). Based on data from *d'Harambure (2015)*.

Manganese alloys	Supply (in million tonnes)	Supply increase Year-over-Year (%)	Demand (in million tonnes)	Demand increase Year-over-Year (%)
SiMn	12.80	-4.3%	13.20	-2.5%
HC FeMn	4.90	9.0%	4.97	5.0%
Refined FeMn	1.84	7.3%	1.86	7.7%

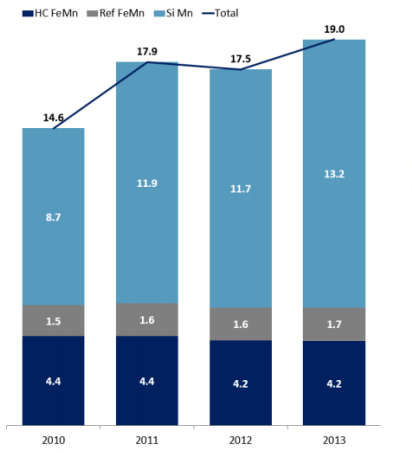

Figure 2.2: Global manganese alloy production 2010 - 2013 in million tonnes. Figure reproduced from *Risk & Policy Analysts Limited (2015)*.

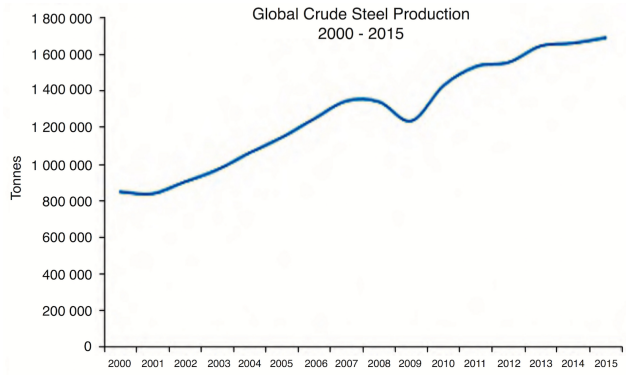

Figure 2.3: Global crude steel production 2000 - 2015 in million tonnes. Figure reproduced from *d'Harambure (2015)*.

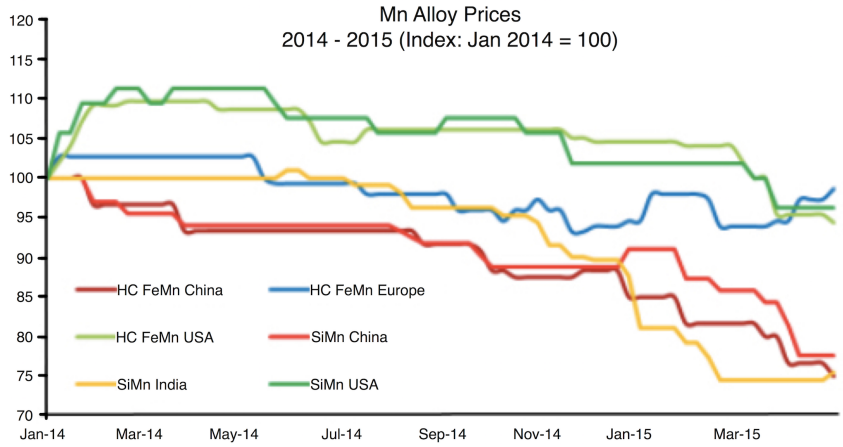

Figure 2.4: Manganese alloy prices 2014 - 2015 for China, India, USA, and Europe. Figure reproduced from *d'Harambure (2015)*.

The global crude steel production driving the consumption of manganese alloys has shown a steady increase in production since the early 2000s, as seen from Figure 2.3, and the crude steel demand is expected to increase by a 2% compound annual growth rate. Despite the fact that the demand for manganese alloys and steel are highly correlated, prices for most manganese alloys have been decreasing in the period 2014 - 2015, illustrated in Figure 2.4. This decrease is primarily due to the slowing steel demand in China combined with cheap manganese alloys becoming abundant *(d'Harambure, 2015)*.

2.2 The Supply Chain

The manganese industry can be divided into two categories: ore mining and alloy production. The supply chain is illustrated in Figure 2.5. The ore mining process consists of extracting ore from the ground, hauling the ore to a processing plant where the ore is crushed, separated and beneficiated, transportation of ores to sinter plants, and sintering *(Olsen et al., 2007)*. Sintering is the solidification of powder, forming a compact material after temperature treatment below the material's melting point *(Foundry Lexicon, 2016)*, making it possible to use fine ores which otherwise are unusable in the furnace *(Olsen et al., 2007)*. The alloy production process consists of smelting ores, fluxes, quartz, and coke in a furnace, tapping and casting, further refining, crushing, and reuse of by-products *(International Manganese Institute and Hatch, 2015)*. The focus of this thesis is on the alloy production process of the supply chain, illustrated inside the blue rectangle in Figure 2.5.

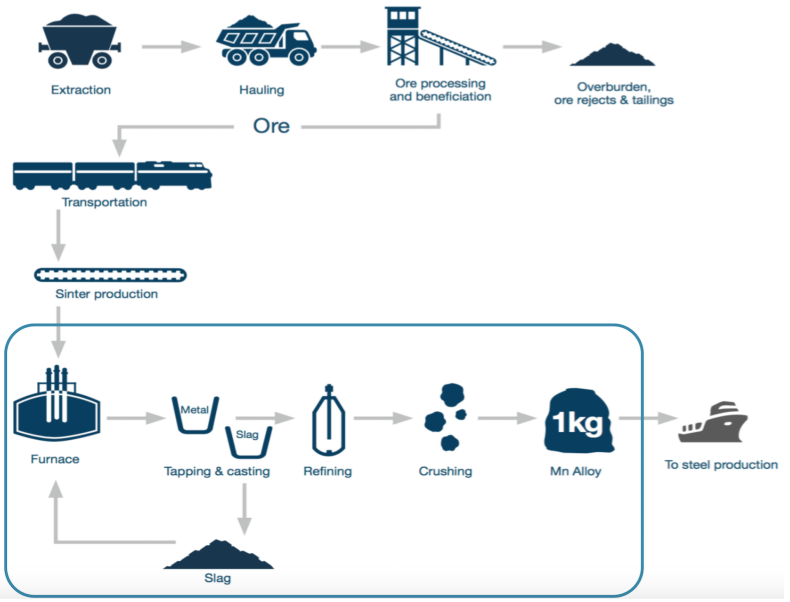

Figure 2.5: Overview of the manganese alloy industry supply chain. Figure reproduced from *International Manganese Institute and Hatch (2015)*. The alloy production process is inside the blue rectangle.

2.3 The Production Process

This section offers a detailed description of the different stages in the alloy production process. Figure 2.6 provides an overview of the material flow between the processes under consideration. The FeMn and SiMn production paths are separated with slag being the only coupling between the two. The production path flows for both the FeMn and SiMn production are described in detail in the following two sections. More information about the furnaces, refining, and crushing process is given in sections 2.3.4 - 2.3.7.

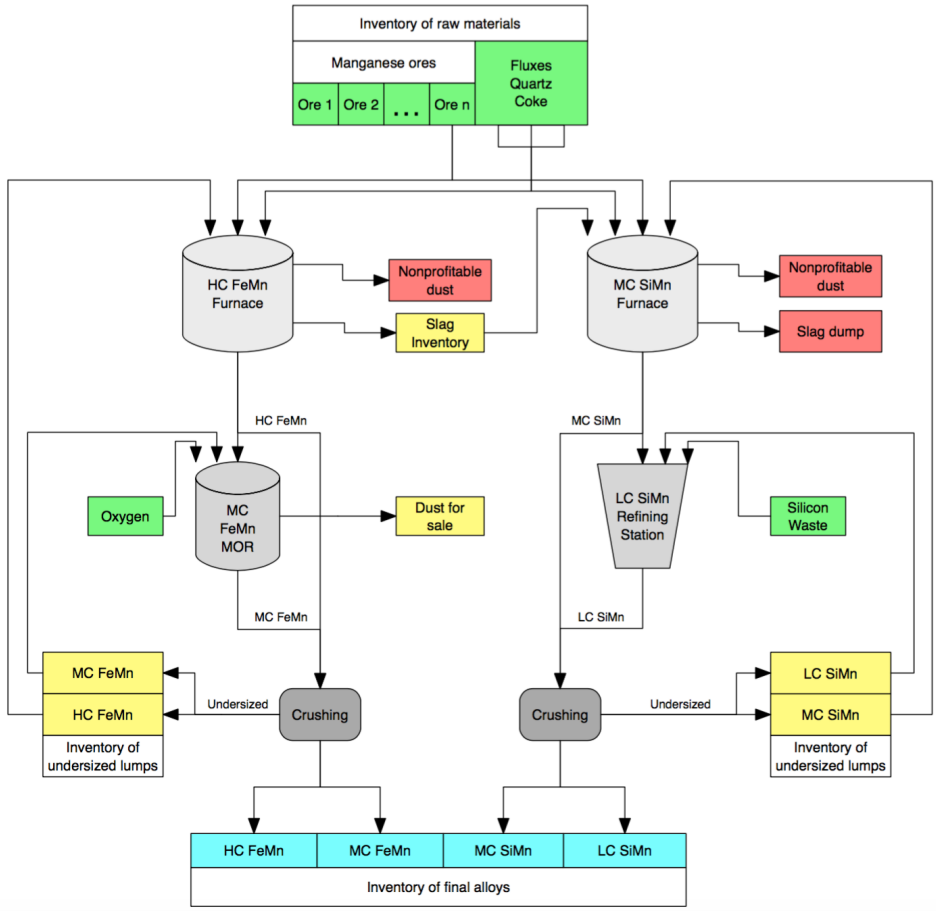

Figure 2.6: Overview of manganese alloy production material flow using the duplex method (presented in section 2.4.2). The figure is based on *Olsen et al. (2007)*. Green colour: raw materials. Red: wastes. Yellow: reusable/saleable materials. Blue: final alloys. Scales of grey: the furnace, refining, and crushing processes.

2.3.1 The FeMn Production

As seen from Figure 2.6, the inventory of raw materials supplies the necessary resources to the HC FeMn furnace. A furnace can be considered as a pool where the material constituents are blended into output products. The output products from the HC FeMn furnace are HC FeMn alloy, slag, nonprofitable dust, and off-gases. The HC FeMn alloy can follow two paths through the production chain: either directly to crushing or through the process of manganese oxygen refining (MOR), before crushing. In the MOR, oxygen is added to reduce HC FeMn to medium carbon ferromanganese (MC FeMn). MC FeMn is the primary output of the MOR, with saleable dust as a by-product. After crushing, the respectable alloy type is sent to a final inventory for that alloy. The leftover from the crushing, called undersized lumps, are sent to inventories for undersized lumps. Inventories are separated into HC FeMn and MC FeMn undersized lump inventories as lumps are used different processes. HC FeMn undersized lumps are reused in the HC FeMn furnace while MC FeMn undersized lumps are reused in the MOR.

2.3.2 The SiMn Production

As for the HC FeMn furnace, the same inventory of raw materials feeds the MC SiMn furnace. The only difference between the two feeding processes is that slag is fed to the MC SiMn furnace and that it originates from the HC FeMn furnace, not the inventory of raw materials. Mixing occurs in the furnace, and the outputs are MC SiMn, nonprofitable dust, slag dump, and off-gases. The MC SiMn alloy can follow two paths through the production: either directly to crushing or through the low carbon silicomanganese (LC SiMn) refining station before crushing. In the LC SiMn refining station, silicon waste is added to the process which alters the composition of the MC SiMn, yielding LC SiMn. Crushing and the rest of the SiMn production is identical to the FeMn production.

2.3.3 Ores, Fluxes, Quartz, and Coke

Blending manganese ores from different sources is common, for instance, to obtain a specific end-product specification. Manganese ores vary widely in their content, such as in Mn, Fe, silicon dioxide (SiO_2), Al, magnesium (Mg), limestone ($CaCO_3$), and phosphorus (P). Producers of alloys have considerable flexibility in the blending of ores, making it possible to produce the demanded alloy at a low production cost. Fluxes are added to secure proper furnace operation, high manganese yield, and to give the slag suitable chemical properties, viscosity, and smelting temperature. Commonly used fluxes are limestone and dolomite ($CaMg(CO_3)_2$). Quartz is a SiO_2 bearing raw material. Coke is the regular source of carbon (C) for manganese ore reduction *(Olsen et al., 2007)*.

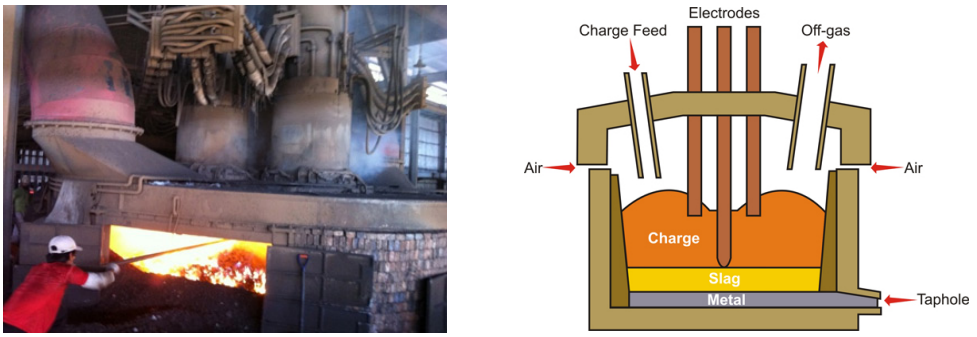

(a) **(b)**

Figure 2.7: **(a)** Submerged arc furnace. **(b)** Cross-sectional illustration of a submerged arc furnace. The photos are reproduced from *Gulf Manganese Corp. Ltd. (2017)*.

2.3.4 The Furnace

Today's furnaces are mainly of the submerged arc furnace variant, illustrated in Figure 2.7a and Figure 2.7b. This furnace type makes for a flexible production as it can be utilised for production of both HC FeMn and MC SiMn alloys *(Olsen et al., 2007)*. The furnaces are operated at high temperature ranges, varying with the type of alloy to be produced *(Gasik, 2013)*. The operation of the MC SiMn process is more difficult than the HC FeMn process since a higher process temperature is required to obtain the necessary silicon-specification of the alloy *(Olsen et al., 2007)*.

In the furnace, manganese ores are mixed with fluxes, quartz, and coke. Also, reusable slag and undersized alloy lumps can be added to the mix to replace some of the manganese ore. The producer's main objectives are to make sure that the furnace operates with a high and stable load, minimises coke and energy consumption, secures a high yield of manganese, and most importantly: produces alloy and slag of correct compositions. The main cost drivers for the furnace are the prices of electricity and coke *(Olsen et al., 2007)*.

2.3.5 The MOR

MORs have been used in Norway and the United States since 1976 and are in principle similar to the oxygen steelmaking processes *(Gasik, 2013)*. In this process, HC FeMn is reduced to MC FeMn by blowing oxygen into liquid HC FeMn. The output is MC FeMn, which is sent to crushing *(Olsen et al., 2007)*, and dust from off-gases. MC FeMn is used in special grades of steel where controlling the carbon content is essential. The MOR process happens at high temperatures (>1750°C), and there is excessive evaporation and oxidation of excess oxygen, mainly producing manganese(II, III) oxide (Mn_3O_4), which is collected in the gas cleaning system *(Gasik, 2013)*. The collected oxide dust can be sold. There is a considerable cost of electricity consumption in the MOR process *(Olsen et al., 2007)*.

2.3.6 The LC SiMn Refining Station

LC SiMn is produced using ladle refining *(Olsen et al., 2007)*, which raises the temperature and allows adjustment of the chemical composition of the molten alloy *(Inductotherm Corp., 2016)*. Adjustment of the chemical composition is done by adding silicon waste from the ferrosilicon industry to the MC SiMn. Silicon waste can even be favourable for MC SiMn production since it reduces the specific energy consumption and consequently allows for a larger production volume *(Olsen et al., 2007)*.

2.3.7 The Crushing Process

The finished alloys have to satisfy a certain lump size to meet the customer' specifications. Depending on the size of the uncrushed material, two types of crushers are commonly used: jaw crusher and sole roller crusher. A jaw crusher is suitable for materials that must be crushed in all directions, while a sole roller crusher can be applied to materials that have the correct size in one direction. As with all crushing activities, some of the output is undersized and not suitable for sale. The undersized lumps of unsatisfactory size can be re-melted in the proper process. The size limit of lumps is typically set to 10 mm, although some consumers accept sizes down to 4 mm *(Olsen et al., 2007)*. The output of sufficient size is stored in an inventory for finished alloys, ready to be shipped to customers.

2.3.8 By-products

The alloy production processes produce several by-products, some of which are of value. The by-products from the furnace, MOR, and crushing process are reusable slag, non-profitable slag, and profitable and non-profitable dust. Approximately 500 - 1000 kg slag is produced per tonne alloy in the HC FeMn furnace. This relationship is known as the slag-to-metal ratio and highly depends on the ore types combined in the furnace and the furnace temperature *(Olsen et al., 2007)*. The amount of reusable slag a furnace produces can, therefore, be manipulated. Non-profitable slag and dust produced in a furnace are wastes and must be discarded at a cost *(Eramet Norway, 2013)*. Profitable dust is sold for use in other industries.

The reusable slag couples the furnaces with different production settings, as seen in Figure 2.6. There may be a potential cost saving in using the slag from an HC FeMn furnace in an MC SiMn furnace by replacing ore with slag. Manganese(II) oxide (MnO) dust is another by-product from the furnace that can be sold as a valuable pigment, but due to the small quantities of MnO produced, it gives low economic value compared to the alloy production *(Westfall et al., 2016)*.

2.4 The Production Methods

There are two main operational practices in the industry, commonly referred to as the discard slag practice and the duplex method practice, also called high-MnO practice. The latter is the most common practice *(Olsen et al., 2007)*.

2.4.1 The Discard Slag Practice

The aim of this practice is to reduce the ore in one process step, yielding HC FeMn and a "throw-away" slag *(Olsen et al., 2007)*. This one step reduction is accomplished by the assistance of basic fluxes such as calcium oxide (CaO) or magnesium oxide (MgO), or by decreasing the silicon (Si) activity in the slag and increasing the MnO activity. The manganese recovery in the HC FeMn furnace is around 80%, where 15 - 20% MnO remains in the slag and is consequently discarded, as recovery of manganese at such concentrations is not economical *(Gasik, 2013)*. The operation involves high consumption of carbon and electricity *(Olsen et al., 2007)*.

2.4.2 The Duplex Method

Slag from the HC FeMn furnace can be an important manganese-bearing material for MC SiMn production *(Westfall et al., 2016)*. A blend of several ores is used to achieve the correct alloy and slag composition in the HC FeMn furnace, where the slag contains as much as 30 - 50% MnO. The slag can then be reprocessed and used in the production of MC SiMn. The result is that the MnO content in the slag output from the MC SiMn furnaces can be reduced to 5%, with an overall increase in manganese recovery of 85 - 90% with less use of coke and few or no fluxes needed *(Gasik, 2013)*. The duplex production method is shown in Figure 2.6.

2.5 Furnace Power Consumption

An essential cost driver in manganese alloy production is the electric power consumption in the furnaces. The energy consumption in a furnace is determined by the net effect of exothermic and endothermic reactions and the enthalpy of the materials entering and leaving the furnace *(Olsen et al., 2007)*. Since most metallurgical processes follow paths of substantially constant pressure, called isobaric processes, the change in heat content of a process is only dependent on the initial and final state of the process and not on the path of the process *(Ghosh and Ray, 1991)*. The change in enthalpy ΔH for an isobaric process can, therefore, be used to calculate the furnace power consumption. The change in enthalpy is given by equation (2.1) *(Ghosh and Ray, 1991)*, where H_{in} is the total enthalpy of the elements and oxides entering the system, H_{out} is the total enthalpy of the elements and oxides exiting the system, Q is the heat added to the system, and W is the work done on the system.

$$\Delta H \;=\; H_{\text{out}} - H_{\text{in}} \;=\; Q + W \tag{2.1}$$

Reformulating the equation with respect to W, equation (2.1) becomes (2.2).

$$W \;=\; H_{\text{out}} - H_{\text{in}} - Q \tag{2.2}$$

The total enthalpy consists of a formation enthalpy and a sensible enthalpy. The formation enthalpy is the energy required to form a compound from its elements at a certain temperature, usually defined at $25°\text{C}$. The formation enthalpy for elements is zero. The formation enthalpies make it possible to calculate the energy change in a chemical reaction based on the difference in formation enthalpies between the reactants and the resultants. This is known as Hess' Law *(Ghosh and Ray, 1991)*. Sensible enthalpy is the heat required to change the temperature of an element or oxide from an initial temperature to a given temperature and is defined to be zero at $25°\text{C}$. Following the given definitions; the enthalpy H_{out} becomes $H^{\text{F}}_{\text{out}} + H^{\text{S}}_{\text{out}}$, where $H^{\text{F}}_{\text{out}}$ represents the formation enthalpy and $H^{\text{S}}_{\text{out}}$ the sensible enthalpy of the resultants at the exit temperature. H_{in} becomes $H^{\text{F}}_{\text{in}} + H^{\text{S}}_{\text{in}}$, where H^{F}_{in} represents the formation enthalpy and H^{S}_{in} the sensible enthalpy of the reactants at the entry temperature. Equation (2.2) then becomes (2.3).

$$W \;=\; (H^{\text{F}}_{\text{out}} + H^{\text{S}}_{\text{out}}) - (H^{\text{F}}_{\text{in}} + H^{\text{S}}_{\text{in}}) - Q \tag{2.3}$$

The raw materials enter the furnaces at $25°\text{C}$. Thus, the term $H^{\text{S}}_{\text{in}} = 0$ by definition and equation (2.3) becomes (2.4). This equation gives the total electrical work required to produce alloys by the chemical reactions occurring in a furnace, in addition to the heat lost to the surroundings.

$$W \;=\; (H^{\text{F}}_{\text{out}} + H^{\text{S}}_{\text{out}}) - H^{\text{F}}_{\text{in}} - Q \tag{2.4}$$

As a result of the thermodynamic properties of the elements and oxides, different slag practices consume different amounts of energy. The discard slag practice consumes about 2900 - 3400 kWh/tonne alloy produced, while the duplex method consumes about 2650 - 3100 kWh/tonne alloy produced in the HC FeMn furnaces. The higher energy consumption from using the discard slag practice is due to the extra power used to calcine the fluxes and continue smelting to obtain a higher recovery of metal *(Downing, 2013)*.

The power required to produce standard MC SiMn alloy from mixing ores, HC FeMn slag, and Si-rich metallic remelts, is usually in the range of 3500 - 4500 kWh/tonne alloy. More energy is consumed for higher Si-content in the final alloy, as well as the amount of slag produced per tonne MC SiMn. About 50 kWh of extra energy is consumed per additional 100 kg slag produced, and 100 kWh/tonne alloy and some coke are saved if ascending carbon monoxide (CO) gas from the melt-reduction zone is utilised to reduce the ore fraction in the charge to MnO *(Olsen and Tangstad, 2004)*.

2.6 Chemical Reactions

The mass of the end-products is related to the mass of ores, fluxes, quartz, and coke used in the furnaces through a set of chemical reactions. The main chemical reactions occurring in a furnace are given in reactions (2.5) - (2.17), where parentheses denote the slag phase and underlines the metal phase. Note that these reduction-oxidisation (redox) reactions give a simplified description of a highly complex chemical process occurring over a wide range of temperatures. An illustration of a furnace and the most important chemical reactions is provided in Figure 2.8.

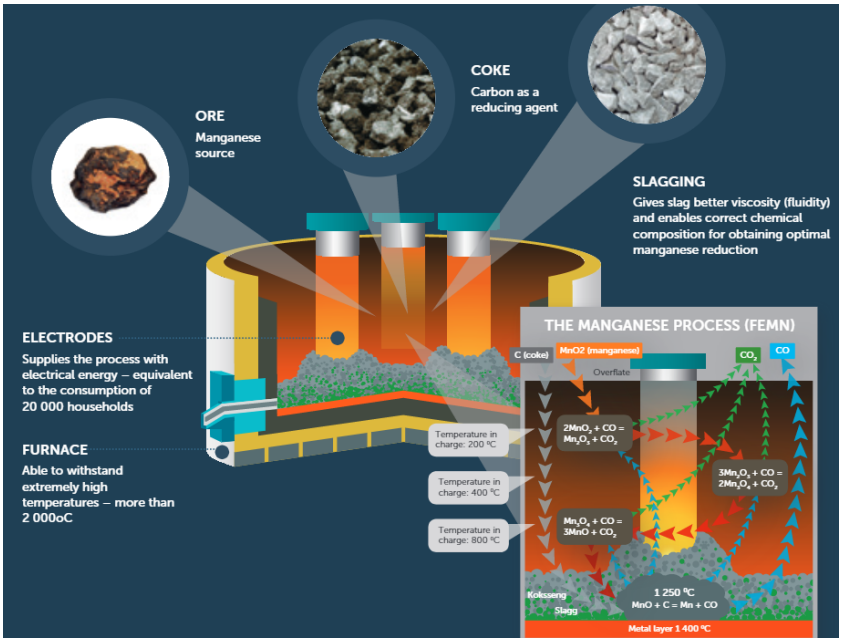

Figure 2.8: The furnace and the most important chemical reactions. The photo is reproduced from *Eramet Norway (2013)*.

Manganese oxides are present in the ores mainly as manganese dioxide (MnO_2), manganese(III) oxide (Mn_2O_3), Mn_3O_4, and MnO *(Olsen et al., 2007)*. In contact with CO in the furnace, MnO_2, Mn_2O_3, and Mn_3O_4 are reduced according to reactions (2.5) - (2.7). The resulting MnO, and supplied MnO from the ores, then react with solid carbon in the coke bed of the furnace, resulting in liquid manganese metal and CO-gas. This chemical reaction is given by reaction (2.8).

$$2\,\mathrm{MnO_2(l)} + \mathrm{CO\,(g)} \longrightarrow \mathrm{Mn_2O_3(l)} + \mathrm{CO_2(g)} \tag{2.5}$$

$$3\,\mathrm{Mn_2O_3(l)} + \mathrm{CO\,(g)} \longrightarrow 2\,\mathrm{Mn_3O_4(l)} + \mathrm{CO_2(g)} \tag{2.6}$$

$$\mathrm{Mn_3O_4(l)} + \mathrm{CO\,(g)} \longrightarrow 3\,(\mathrm{MnO}) + \mathrm{CO_2(g)} \tag{2.7}$$

$$(\mathrm{MnO}) + \mathrm{C\,(s)} \longrightarrow \underline{\mathrm{Mn}} + \mathrm{CO\,(g)} \tag{2.8}$$

The final alloy contains a certain amount of carbon. The carbon from the raw material feed dissolutes into the metal up to a saturation point *(Olsen et al., 2007)*. This dissolution is given by reaction (2.9).

$$\mathrm{C\,(s)} \longrightarrow \underline{\mathrm{C}} \tag{2.9}$$

Similar to the reduction of manganese oxides, iron oxides and silicon oxides are also reduced in the furnace. Iron(III) oxide (Fe_2O_3) and iron(II, III) oxide (Fe_3O_4) are reduced through chemical reactions with CO. The final reductions of iron(II) oxide (FeO) to Fe, and SiO_2 to Si, take place in the coke bed. The chemical reactions are provided in reactions (2.10) - (2.13).

$$3\,\mathrm{Fe_2O_3(l)} + \mathrm{CO\,(g)} \longrightarrow 2\,\mathrm{Fe_3O_4(l)} + \mathrm{CO_2(g)} \tag{2.10}$$

$$\mathrm{Fe_3O_4(l)} + \mathrm{CO\,(g)} \longrightarrow 3\,(\mathrm{FeO}) + \mathrm{CO_2(g)} \tag{2.11}$$

$$(\mathrm{FeO}) + \mathrm{C\,(s)} \longrightarrow \underline{\mathrm{Fe}} + \mathrm{CO\,(g)} \tag{2.12}$$

$$(\mathrm{SiO_2}) + 2\,\mathrm{C\,(s)} \longrightarrow \underline{\mathrm{Si}} + 2\,\mathrm{CO\,(g)} \tag{2.13}$$

In the furnace, carbon reacts with carbon dioxide (CO_2) resulting from the chemical reactions (2.5) - (2.7) and (2.10) - (2.11) and forms CO. This reaction is known as the Boudouard reaction and is given in reaction (2.14). The amount of CO_2 that enters the Boudouard reaction from reactions (2.7) and (2.10) - (2.11) is defined as the degree of pre-reduction. 100% pre-reduction is defined as when no CO_2 from the given reactions react with carbon and activate the Boudouard reaction, 0% pre-reduction is defined as when all CO_2 from the given reactions react with carbon according to the Boudouard reaction. CO_2 resulting from reactions (2.5) - (2.6) is not expected to react according to the Boudouard reaction under normal furnace operation. The specified degree of pre-reduction has a significant impact on consumed electrical power *(Olsen et al., 2007)*. The Boudouard reaction, together with the feed of CO resulting from the chemical reactions (2.8) and (2.12) - (2.13), is critical for the feeding of CO to the chemical reactions (2.5) - (2.7) and (2.10) - (2.11).

$$\mathrm{C\,(s)} + \mathrm{CO_2(g)} \longrightarrow 2\,\mathrm{CO\,(g)} \tag{2.14}$$

The feed to the furnace also contains oxides that do not enter the final alloy. These oxides are important constituents of the slag, giving it different thermodynamic and physical properties. The oxides are aluminium oxide (Al_2O_3), MgO, and CaO. The oxides enter the furnace as solids, and dissolute into the slag phase. The reactions are given by (2.15) - (2.17).

$$Al_2O_3(l) \longrightarrow (Al_2O_3) \tag{2.15}$$

$$MgO(l) \longrightarrow (MgO) \tag{2.16}$$

$$CaO(l) \longrightarrow (CaO) \tag{2.17}$$

2.7 Eramet Norway

Eramet Norway is our industry partner. The layout of the company's plants in Norway forms the basis for the instances used to test the formulation presented later in this thesis. Eramet Norway is a part of the Eramet Group, which is a French mining and metallurgical group and a world leader within its business sectors. The Eramet Group's businesses are manganese ore extraction and alloy production, nickel and ferronickel production, and alloy parts manufacturing by high-power closed die-forging *(Eramet Group, 2016b)*. The Eramet Group operates in 21 countries across five continents. Their main markets are Europe, Asia, and North America *(Eramet Group, 2016a)*.

Eramet Norway operates within the manganese alloy production sector and exports all of its production of manganese alloys primarily to Europe and North America. Around 98% of the export is transported by ship and the remaining percentages by road or rail *(Eramet Norway, 2013)*. There are three plants located in Norway: in Sauda, Porsgrunn, and Kvinesdal. Their locations can be seen in Figure 2.9. The Sauda plant has two 40 MW furnaces, with an annual power consumption of 750 GWh at full capacity. The Porsgrunn plant also has two furnaces, with an annual power consumption of 570 GWh, where 200 GWh of thermal energy in the form of CO gas is recovered to Yara. The Kvinesdal plant has three modern 30 MW furnaces, with an annual power consumption of 750 GWh.

The Porsgrunn plant manufactures 65 000 tonnes of SiMn and 115 000 tonnes refined FeMn alloys annually. Further, sales of gas to Yara and sales of manganese dust earned the factory an income of 41 MNOK and 57 MNOK in 2013, respectively *(Eramet Norway, 2013)*. Annual output is 180 000 tonnes of SiMn alloy at the Kvinesdal plant *(Eramet Norway, 2016b)*. Sauda is the largest plant in Norway measured in tonnes produced. It has the highest output of refined FeMn alloys, processing about 70% of the manganese ore imported by Eramet Norway *(Eramet Norway, 2014)*.

Figure 2.9: The industry partner's plant locations in Norway: Sauda, Porsgrunn, and Kvinesdal.

Chapter 3

Problem Description

This chapter contains the problem description of the Manganese Alloy Multi-plant Production problem (MAMP), presented in Section 3.1. The purpose of the MAMP is to optimise the integrated production of FeMn and SiMn alloys across multiple plants to maximise profit. The profit is determined by deciding the optimal volumes of end-products to produce by mixing raw materials while satisfying given quality specifications. Production costs are considerable, and the MAMP should, therefore, ensure optimal use of raw materials to the furnaces and refining processes. The solution to the MAMP should also describe the optimal slag volume and slag composition to be produced in the HC FeMn furnaces and the allocation of slag to the MC SiMn furnaces.

3.1 The Manganese Alloy Multi-plant Production Problem

A manganese alloy manufacturer has a set of furnaces located at plants to produce manganese alloys. The alloys produced are given by customer specifications. The production is, therefore, based on contracts that must be satisfied. Customer specifications include order volume and alloy composition, resulting in a wide range of possible order sizes and end-products. To meet the end-product specifications set by the customers, a set of raw materials, including ores, fluxes and coke sources, containing different concentrations of various elements and oxides is available to the production. The raw materials are blended in the furnaces and further processed to produce the desired end-products. Any excess end-product produced can be sold on optional contracts in the spot market or held as an inventory for later contracts. Producing manganese alloys also yields various by-products, where some are valuable, and others are not. The by-products can, therefore, either be sold or discarded.

The furnaces are used to smelt the raw materials. These can produce both HC FeMn and MC SiMn alloys, but only one alloy type at a time. Each furnace has a mass and electrical power capacity that limits the raw material feed to the furnace. The furnaces also have a limitation on the volume of undersized lumps from the crushing process it is possible to feed, as feeding too much undersized lumps is problematic for the furnace operation. An MOR and an LC SiMn refining station are required to produce MC FeMn and LC SiMn, respectively. These refining units have a mass and power capacity limiting the feed to each process. The crushing process is where all the alloy types are crushed into lumps of adequate size.

Each plant has inventories for storing resources and end-products. The inventories at each plant are divided into raw material inventories, refining resource inventories, and end-product inventories. The raw material inventories store all resources used in the furnaces and the refining inventories store all resources used in the refining processes. The end-product inventories store all of the end-products produced. All inventories have capacity limits.

The first step of the production is to blend raw materials together in a furnace to produce either HC FeMn or MC SiMn. Besides the alloys, by-products in the form of slag, nonprofitable dust, and off-gases are also outputs from the furnaces. The slag produced by the HC FeMn furnaces is in proportion to the metal produced, and this slag-to-metal ratio can fluctuate between a lower and upper bound dependent on furnace alloy and slag characteristics. It is possible to produce slag of varying element and oxide content in each HC FeMn furnace. Further, the HC FeMn furnace slag can be reused in the MC SiMn furnaces. The reuse of slag in MC SiMn furnaces is the only coupling between the FeMn and SiMn productions, which otherwise would have been completely separated productions. Slag from the MC SiMn furnaces and the non-profitable dust produced by both furnace types must be discarded.

The next step is to send the produced HC FeMn alloy and MC SiMn alloy either to further refining in the MOR and LC SiMn processes, respectively, or to the crushing process. In the MOR process, oxygen is added to liquid HC FeMn to get MC FeMn. The MOR process also produces a by-product in the form of a metallic-oxide dust which can be sold. In the LC SiMn refining process, silicon waste is added to the liquid MC SiMn to get LC SiMn *(Olsen et al., 2007)*. In the crushing process, the alloy from the furnaces and the refining processes is crushed and then sent to the end-product inventories. A given percentage of the crushed end-product is undersized and cannot be sold to the customer and is, therefore, sent back to the associated process inventories for resmelting.

Revenues and costs are linked to various parts of the production. The resources used in the production, except the undersized lumps, are associated with a procurement cost. Smelting the raw materials in the furnaces requires energy in the form of electricity. Thus, the furnace process incurs electricity costs. Reusing slag produced by HC FeMn furnaces in MC SiMn furnaces at other plants incurs a transportation cost per tonne slag transported. Slag from the HC FeMn furnaces can also be discarded instead of reused, which incurs a discard cost. The other by-products that must be discarded incur a discard cost. The metallic-oxide dust from the MOR process can be sold, and is, therefore, associated with a revenue. Each end-product is associated with a revenue per tonne sold on fixed and optional contracts.

The chemical reactions occurring in a furnace should be accounted for, and are given by reactions (2.5) - (2.17) in Chapter 2. These reactions are essential to correctly model the flow of mass in a furnace and the quality attributes of the slag and end-products. Mass-to-mole conversion and reactions for Mn, Fe, Si, C, Al, Mg, Ca, and oxides of these elements should be used to establish the relationship between the content of each element in a raw material fed to a furnace and the content of each output product.

An approximation of the furnace power consumption should be included to better model a realistic production, as the power consumption greatly affects the choice of raw materials to consume. The power consumption can be approximated by the thermodynamic relation given by equation (2.4) in Chapter 2. Enthalpies are commonly provided in kJ/mole and should be converted to kWh/tonne for the furnace to yield the conventional unit of electrical work per tonne produced alloy.

Chapter 4

Literature Review

In this chapter, a review of the literature relevant to the Manganese Alloy Multi-plant Production problem (MAMP) is presented. To the authors' knowledge, there is a limited number of operations research publications on manganese production optimisation. This literature review is, therefore, expanded to relevant optimisation literature covering industries with problems similar to the MAMP, like the petrochemical and wastewater management industries. Various solution techniques for the pooling problem are reviewed to identify a suitable method to linearise the bilinear constraints present in the MAMP.

In the problem description in Chapter 3, it is observed that the problem consists of raw material mixing of different qualities in the furnaces and refining processes. Based on this, the MAMP can be seen as either a blending or pooling problem. The raw materials correspond to sources. The furnaces, the MORs, and the LC SiMn refining stations are intermediate pools where blending occurs. End- and by-products are modelled as terminals. The problem is complicated by the coupling of intermediate pools. Slag flowing from the HC FeMn furnaces are of varying volume and quality and is sent to MC SiMn furnaces for further blending. It is therefore of interest to look into the literature on both the blending and the pooling problem to be able to define and formulate the MAMP.

In Section 4.1, the blending problem is described before the complicating factors that generalise it into the pooling problem are explained. Section 4.2 outlines the pooling problem. In Section 4.3, five classes of the pooling problem identified by *Misener and Floudas (2009)* are presented. The classifications are compared to the MAMP to determine the class the MAMP belongs to. In Section 4.4, different formulations for the pooling problem are presented. Existing problems solved in other industries using the pooling problem formulation are presented in Section 4.5 to place the MAMP into an industrial context. Solution methods developed for the pooling problem are reviewed in Section 4.6. A review of the multi-period pooling problem is conducted in Section 4.7. In Section 4.8, our contribution to the existing literature on the pooling problem within the manganese alloy industry is presented.

4.1 The Blending Problem Versus the Pooling Problem

A common problem in many industries is blending several raw materials into various end products. The blending problem appears in refinery processes where feeds with different attribute qualities, such as sulphur or octane number, are mixed directly into end-products at terminal nodes *(Audet et al., 2004)*, as shown in Figure 4.1a.

The pooling problem, a generalisation of the blending problem, is used to model systems that have intermediate mixing pools in the blending process *(Audet et al., 2004)*. This is confirmed by *Alfaki (2012)* who states that a special case of the pooling problem occurs when the intermediate nodes are not needed. The flows are directly blended at the terminal nodes, reducing the pooling problem to the blending problem. The difference between the blending and pooling problem, therefore, lies in the presence of intermediate pools, as illustrated in Figure 4.1a and Figure 4.1b.

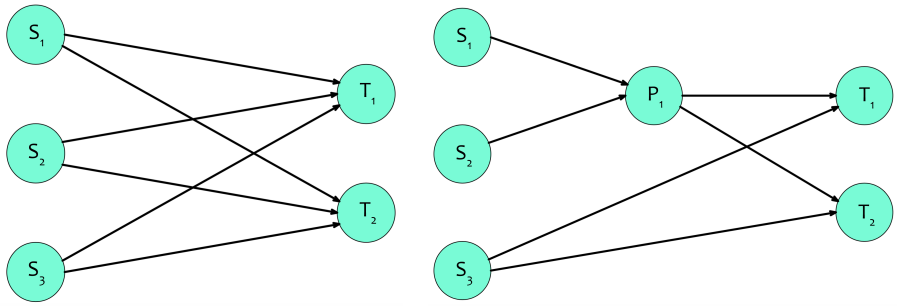

(a) Blending problem. **(b)** Pooling problem.

Figure 4.1: Illustration of the difference between the blending problem **(a)** and the pooling problem **(b)** defined by *Haverly (1978)*. $\mathcal{S}$ denotes sources, $\mathcal{P}$ pools, and $\mathcal{T}$ terminals. The figures are based on figures found in *Alfaki (2012)*.

The classical blending problem can be modelled as a linear program (LP), while the pooling problem has nonlinear terms yielding a bilinear program (BLP) *(Audet et al., 2004; Alfaki, 2012)*. Due to the blending constraints, the pooling problem can have multiple local optima *(Alfaki, 2012)*. Several intermediate pools are present in the MAMP, making it a pooling problem. The focus is, therefore, on literature related to the pooling problem in the rest of the literature review.

4.2 The Pooling Problem

The pooling problem usually occurs in chemical processing such as petroleum refining and wastewater treatment. It originates from the petrochemical industry where various process streams with different qualities are blended to form final products *(Gounaris et al., 2009)*.

The objective of the pooling problem is according to *Gounaris et al. (2009)* to find the most efficient combination of flows through the network that produces final products with the correct quality properties. The pooling problem involves a network of source nodes, intermediate nodes, terminal nodes, and arcs connecting the nodes. The source nodes represent the inventory of feeds, the intermediate nodes represent the intermediate pools and other production processes, and the terminal

nodes represent the final products. The arcs are the possible flows between processes. Intermediate pools are process stages where mixing of feeds into products of specified quality occurs. Usually, the products mixed at an intermediate pool are sent to another intermediate pool for further mixing, but the flow can also go straight to the terminal node.

Feeds can be of varying quality and composition, making blending of several feeds necessary to obtain the desired end-products. It is the restrictions on the properties of the end-products at the terminal nodes that set the framework for the feeds that can be mixed in the pools *(Misener and Floudas, 2009; Gounaris et al., 2009; Kolodziej et al., 2013b)*. The need for blending occurs when the requirements of a product are not met by any single feed, or there are fewer intermediate pools available than feeds or products. Linear blending of all qualities is assumed to occur in each intermediate and output node *(Gounaris et al., 2009)*. *Adhya et al. (1999)* point out that the pooling problem becomes harder to solve with multiple quality requirements. *Audet et al. (2004)* find that the complexity of a model increases when multiple pools are linked together in series or in parallel, where exiting blends are allowed to enter other intermediate pools.

When intermediate pools are present in the problem, monitoring pool composition requires either nonconvex trilinear or bilinear terms depending on whether there are pools in series or not. In both cases, the problem is a nonlinear program (NLP) *(Misener and Floudas, 2009)*. One of the early models attempting to solve the pooling problem is based on recursive linear programming techniques. It was observed that this procedure did not always converge due to the occurrence of local optima *(Haverly, 1978)*. The nonconvexities of the pooling problem prevents linear, convex, and stochastic solvers from verifying global optimality *(Misener and Floudas, 2009)*. Finding a global solution, particularly for large-scale, real instances, has proven difficult since the problem exhibit a multiplicity of local solutions due to these nonconvexities *(Gounaris et al., 2009)*.

4.3 Classifications of the Pooling Problem

Misener and Floudas (2009) present five sub-classes of pooling problems: standard pooling, generalised pooling, extended pooling, nonlinear blending, and crude oil operations. These sub-classes constitute the classifications used for the pooling problem in this literature review.

In the standard pooling problem, the source nodes, intermediate nodes, and terminal nodes are predetermined, and the flow rates are optimised to maximise profit subject to constraints on the quality of the final product constituents. The standard pooling problem only considers linear blending of qualities with one layer of intermediate pools, disregarding the possibility of further blending in other intermediate pools. This makes the bilinear terms that arise from the quality balances in the pools the only sources of nonconvexities *(Misener and Floudas, 2009)*.

Audet et al. (2004) and *Meyer and Floudas (2006)* generalise the pooling problem to allow a more general network topology, such as connections between intermediate pools. The generalised pooling problem is the extension of the standard pooling problem to the case where exiting blends of some intermediate pools feed other intermediate pools *(Audet et al., 2004)*. The generalised pooling problem is shown in Figure 4.2. In the generalised pooling problem, arcs between pools are allowed, and intermediate nodes are treated as discrete alternatives. This results in a nonconvex, disjunctive program that can be modelled as a mixed integer nonlinear program (MINLP). By not fixating the arcs, the problem becomes combinatorial complex with respect to the binary decision variables and bilinear terms *(Misener and Floudas, 2009)*.

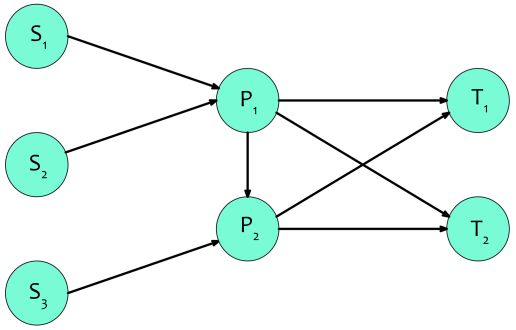

Figure 4.2: Illustration of the generalised pooling problem with an intermediate pool connection. $\mathcal{S}$ denotes sources, $\mathcal{P}$ intermediate pools, and $\mathcal{T}$ terminals. The figure is based on *Alfaki (2012)*.

The extended pooling problem adds a set of environmental constraints to the pooling problem formulation. For instance, the model sets upper limits on toxic emissions of reformulated gasoline, NO_X-gases, and volatile organic compounds, in addition to appending three sets of emission model equations to the standard pooling problem *(Misener and Floudas, 2009)*.

Nonlinear blending is a subclass of pooling problems and classifies problems where the simplifying assumption of linear blending is not valid. Examples of important fuel qualities that blends nonlinearly are Reid vapour pressure, motor octane number, and research octane number *(Misener and Floudas, 2009)*.

According to *Misener and Floudas (2009)*, crude oil operations span the subclass of pooling problems at the front-end of a refinery. The source nodes are arriving supply ships, the intermediate nodes are storage and charge tanks, and the terminal nodes are crude oil distillation units. The scheduling aspect is added to the pooling problem in the crude oil operations due to oil tankers arriving at discrete times.

In the MAMP, the flow through the production is optimised to maximise profit for a predefined set of plants and furnaces subject to quality restrictions on the end-products. Some of the properties of the standard pooling problem are, consequently, properties of the MAMP. Linear blending occurs in the MAMP, but there are multiple layers of pools, differentiating this problem from the standard pooling problem. In accordance with the generalised pooling problem, the exiting blends of intermediate pools feed other intermediate pools. Specifically for the MAMP, this is HC FeMn furnaces feeding slag to MC SiMn furnaces. Arcs between furnaces are allowed, but unlike the generalised pooling problem, nodes are fixed and not discrete alternatives. Arcs, on the other hand, are not fixed but treated as optional since an arc flow might be zero, making the MAMP combinatorial complex. The MAMP is not an extended pooling problem since emissions to the atmosphere are not included in the problem. The MAMP is excluded as a nonlinear blending problem since linear blending applies. The problem does not belong to the crude oil operations class either, since source nodes, intermediate nodes, and terminal nodes in the MAMP represent different processes than in the crude oil operations, and there is no scheduling aspect in the MAMP. The conclusion is that the MAMP is a hybrid of the standard and generalised pooling problem. In the subsequent sections, the literature review is therefore limited to papers related to the standard and generalised pooling problems.

4.4 Pooling Problem Formulations

Multiple optimisation formulations for the pooling problem are found in the literature. Formulating the standard pooling problem in different ways have varying ramifications for the problem size and relaxation tightness, although the formulations are mathematically equivalent *(Misener and Floudas, 2009)*. The most common formulations for the standard and generalised pooling problem are the P-formulation, the Q-formulation, and the PQ-formulation. Also, the TP-formulation, TSP-formulation, and the S-formulation are presented. An overview of the most significant pooling problem literature relevant to the MAMP formulation is provided in Table 4.1.

Table 4.1: Overview of pooling problem literature relevant to the formulation of the MAMP.

Paper	Formulation	Qualities	Findings
Haverly (1978)	P-formulation	Single	One of the first models to describe and represent the pooling problem.
Ben-Tal et al. (1994)	Q-formulation	Multiple	Introduces the Q-formulation.
Quesada and Grossmann (1995)	PQ-formulation	Single	Introduces the PQ-formulation.
Adhya et al. (1999)	P-formulation	Multiple	Compares single and multiple quality cases.
Audet et al. (2004)	P-, Q-, and PQ-formulation	Multiple	Introduces the generalised pooling problem.
Alfaki and Haugland (2013)	TP- and TSP-formulation	Multiple	Proposes two new formulations based on the PQ-formulation.
Hellemo and Tomasgard (2016)	Formulation S	Multiple	Presents a general formulation that allows interconnected pools and processing facilities.

The P-formulation originally used in *Haverly (1978)*, commonly used in chemical process industries *(Adhya et al., 1999)*, is based on total flows and component composition. The model seeks to find the optimal pooling of supply streams while satisfying the demand for a set of products with specified qualities. The objective is to minimise cost or maximise profit. Various stream qualities are estimated and fixed, and the resulting LP is solved. From the linear programming solution, the estimated properties are recalculated and the procedure repeated *(Haverly, 1978)*. The P-formulation of the pooling problem is illustrated in Figure 4.3a. The flow rate from a source i to a pool l is denoted by the variable f_{il}. Flow from a pool l to a terminal node j is denoted by the flow rate variable x_{lj}. Flow directly from a source i to a terminal j is denoted z_{ij}. Each pool has a level of quality for each attribute denoted by the variable p_{lk} for the level of quality k in pool l. *Audet et al. (2004)* identify the P-formulation to be advantageous when there are few quality attributes present because the number of complicating variables is small in this case. The P-formulation is perhaps the most intuitive formulation, as individual qualities in the streams are represented with mass fractions of the total flow *(Kolodziej et al., 2013b)*.

The Q-formulation used in *Ben-Tal et al. (1994)* does not explicitly use pool specifications as variables, but uses variables based on flow proportions that each exit stream supply to the total input stream of each pool *(Lotero et al., 2016)*. According to *Kolodziej et al. (2013b)*, this leads to a more compact formulation. In the Q-formulation presented by *Ben-Tal et al. (1994)*, the feedstock flow rate variables f_{il} are replaced with proportional flow rates q_{il} through the relation $f_{il} = q_{il} \sum_{j \in \mathcal{J}} y_{lj}$ where y_{lj} is the fraction of the total flow from intermediate pool l that flows

to terminal j. y_{lj} is equal to x_{lj} in the P-formulation. The flow z_{ij} is the bypass flow from source i directly to output j. An illustration of the Q-formulation is given in Figure 4.3b. Using the numbers from the figure, the equation $f_{il} = q_{il} \sum_{j \in \mathcal{J}} y_{lj}$ becomes $50 = 0.5(25+75)$, thus relating the variables of the P- and the Q-formulation. The corresponding transformation makes the p_{lk} variables redundant in the Q-formulation, thus, resulting in a formulation with fewer variables than the P-formulation *(Misener and Floudas, 2009)*. *Audet et al. (2004)* identify the Q-formulation to be advantageous in the case where the number of attributes increases because the number of bilinear variables and terms remain the same. According to *Misener and Floudas (2009)*, although the Q-formulation is smaller than the P-formulation for many configurations, P-formulations are often tighter after a convex relaxation due to the possibility of tightening the bounds of f_{il} and p_{lk}, while q_{il} are only known to vary between zero and one.

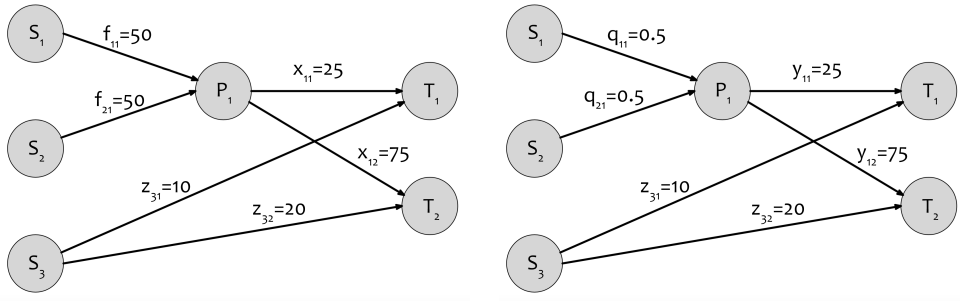

(a) P-formulation. **(b)** Q-formulation.

Figure 4.3: Illustration of the P- and Q-formulation. The difference is that q_{il} is a fraction of the total terminal flow in the Q-formulation, while f_{il} is the actual source-pool flow in the P-formulation.

The PQ-formulation is created from the Q-formulation by appending an additional set of constraints formulated using the Reformulation-Linearisation Technique (RLT) *(Sherali and Alameddine, 1992; Misener and Floudas, 2009)*. The formulation is first introduced in *Quesada and Grossmann (1995)* and later in *Sherali et al. (1998)* and *Tawarmalani and Sahinidis (2002)*. The PQ-formulation introduces no additional bilinear terms in the Q-formulation, but the result is a tighter relaxation than the Q- and P-formulation when term-wise convex envelopes are implemented to relax the formulation *(Misener and Floudas, 2009)*.

Two of the latest pooling problem formulations are proposed in *Alfaki and Haugland (2013)*. The formulations are based on the PQ-formulation and are the result of the extension of the idea of *Ben-Tal et al. (1994)* and *Sahinidis and Tawarmalani (2005)*. The first formulation, called the TP-formulation, uses terminal proportions instead of source proportions used in the PQ-formulation. The strengths of the TP-formulation and the PQ-formulation are not equal in general, but none of them dominates the other. The formulations are therefore comparable in strength. The second formulation, called the TSP-formulation, apply both source and terminal proportions, and is proven to be stronger than both the TP-formulation and the PQ-formulation *(Alfaki and Haugland, 2013)*.

Hellemo and Tomasgard (2016) present what they call formulation-S. The model explicitly models component flow, which allows easy inclusion of processing facilities that can alter the flow composition. Processing facilities are places in the network where some proportion of the components may be removed partially or entirely before the remainder continues downstream. *Hellemo and Tomasgard (2016)* finds that formulation-S is comparable but inferior to the formulations given

by *Alfaki and Haugland (2013)*, and that convergence is slower for formulation-S. Formulation-S, however, solves more general problems including processing facilities. *Hellemo and Tomasgard (2016)* conclude that for hard pooling problems without processing facilities, previous formulations may be preferable.

A common factor for the pooling problem formulations presented is that they are all formulated using bilinearities. *Audet et al. (2004)* state that the BLP problem is commonly formulated by introducing two subsets of variables: linear and nonlinear variables. By further dividing the nonlinear variables into two disjoint subsets of simple and complicating variables, it is possible to get an LP by fixating the variables from either subset. *Audet et al. (2004)* analyse two different formulations for the pooling problem, turning it into BLP problems. These formulations are based on partitioning the variables into either flow and attribute variables, or flow and proportion variables.

For the generalised pooling problem, *Audet et al. (2004)* state that the Q-formulation is not a BLP since the variables are not partitioned into two sets, but belongs to the class of quadratically constrained quadratic programs. They suggest that the hybrid formulation may be used instead to formulate a generalised pooling problem. In this case, the flow model is applied to all intermediate pools that have an input flow from at least one other intermediate pool, while the Q-formulation is used otherwise.

4.5 The Pooling Problem in Different Industries

The literature on manganese production optimisation is limited. To the authors' knowledge, only one paper on manganese production optimisation exists. *Jipnang et al. (2013)* present a FeMn/SiMn furnace process optimisation model based on mass and energy balances. It optimises a target function such as total operating costs, energy consumption, Mn-recovery, or the amount of slag produced. The model relies on software, hiding the modelling choices made in a "black box". It is only capable of calculating the production for single HC FeMn and MC SiMn-furnaces, and they state that connecting the two processes and adding possibilities for different production strategies are considered future research *(Jipnang et al., 2013)*.

The literature search is extended to similar industries as solutions to pooling problems in one may apply to similar problems present in other industries. The pooling problem has applications in petroleum refining, mining industry, supply chain operations, wastewater treatment, and communications *(Misener and Floudas, 2009)*. These problems, classified as bilinear process networks, are generally difficult to solve to global optimality since bilinear constraints are required to model the mixing of different streams *(Kolodziej et al., 2013b)*. The authors have been unsuccessful in finding literature on similar problems relevant to the formulation of the MAMP in other alloy production industries, such as the steel industry.

Ben-Tal et al. (1994) study the pooling problem in an oil refinery. In this case, it is a two-stage process consisting of intermediate pools and final blending of end-products. Given component procurement prices and product sales prices, the aim is to maximise total profit. *Amos et al. (1997)* also study the pooling problem within oil refining, but specifically with the aim to solve a problem for the New Zealand Refining Company. The problem is to decide the quantities of each crude oil to be processed in each crude distiller and to select the best cut points that yield the specified fractions. Cut points are the temperatures at which output streams are separated from the rest of the distillation. This cut point selection is done while trying to minimise the total cost of distil-

lation. Simplifications are made to the model. Examples are sulphur being distributed uniformly throughout all crude fractions and crude oils, and the end-products only having two quality properties. The end-products are assumed to blend directly from downstream fractions of the crude distillation units.

Boland et al. (2015) study a generalised pooling problem in the mining industry. They model the raw material blending in a mining supply chain where the inventory is of a given quantity and quality. Each time raw materials enter or exit the inventory, the quantity and quality change according to a weighted linear relationship between the inventory's old quality and the quality of the incoming raw materials. Instead of associating costs with network flows, costs are coupled to the deviation from the target qualities. Transfer time and costs are not considered between the supply points and the demand points. Aggregated demand can always be met. The problem is to decide how much inventory from each supply point that should be used to meet the demand to minimise the penalty of not meeting quality specifications. *Boland et al. (2015)* name the problem as the mining pooling problem, and it is formulated using the P-formulation.

The water network problem is a collection of processes that consume freshwater and cleanse wastewater. Source nodes of the process network are freshwater and wastewater disposal sites. Given a set of processes that use water and a set of treatment units that removes contaminants, the problem is to find a network configuration that minimises freshwater usage. Mixers and splitters are necessary to distribute the elements of the water network *(Jezowski, 2010)*. Mixers are process components where several streams are mixed into a single stream, while splitters are process components where single streams are split into multiple streams, as described in *Quesada and Grossmann (1995)*.

Meyer and Floudas (2006) study a wastewater problem. In this problem, the source nodes represent exit streams from a set of industrial plants where every stream contains a set of contaminants. The intermediate nodes represent wastewater treatment plants that may be used to reduce the contaminant levels in the streams. Each plant uses a different treatment technology, resulting in unique processing costs and contaminant reduction levels for each plant. The terminal nodes represent the rivers that the treated wastewater is released into. Regulations on contaminant concentration exist for each river. The complexity of the problem arises from the coupling of the nonconvex balance constraints and the combinatorial network configuration *(Meyer and Floudas, 2006)*.

The majority of the work done in the field of water network problems is related to continuous steady state operation mode *(Jezowski, 2010)*. According to *Kolodziej et al. (2013b)*, many blending constraints present in the water network problem are also present in the pooling problem, making advances in this field applicable to the pooling problem. An analysis of the water network problem formulation and an overview of different solution techniques are given in *Jezowski (2010)*. *Meyer and Floudas (2006)* concentrate on an industrial case involving seven streams, three stream components, ten plants and one terminal. Many feasible network configurations could be found by using the nonlinear optimisation software GAMS/DICOPT. The lower bound problem is formulated in three different ways: convex envelopes of bilinear terms, RLT, and a piecewise linear mixed integer linear program reformulated to a mixed integer linear program (MILP) through the introduction of additional binary variables *(Meyer and Floudas, 2006)*. *Jezowski (2010)* concludes there is still a need for flexible and robust approaches that have wider applications in practice.

4.6 Solution Methods for the Pooling Problem

Various solution methods for the pooling problem are discussed in the majority of the literature reviewed by the authors. The proposed solution methods can be classified into local and global optimisation methods *(Alfaki and Haugland, 2013)*. Guaranteeing global optimality is of major importance, as the objective function typically is related to an economic metric *(Teles et al., 2012)*. A summary of some of the different solution methods is found in *Misener and Floudas (2009)*, including Successive Linear Programming (SLP), Global Optimisation Algorithm (GOP), Lagrangian approaches, convex envelopes, RLT, piecewise-affine underestimators, and different branch-and-bound schemes. A more recent solution method is the Multiparametric Disaggregation Technique (MDT) found in *Teles et al. (2013)*, *Teles et al. (2012)*, *Kolodziej et al. (2013a)*, and *Kolodziej et al. (2013b)*. An overview of the literature on different pooling problem solution methods is presented in Table 4.2.

Haverly (1978) uses a recursive method where every quality variable is fixed to expected values. This fixation reduces the pooling problem into a solvable LP. The resulting optimal flow of the LP is then fixed, and new values are found for the quality variables. The method iterates between fixating the quality variables and fixating the flow until there are no changes in the values. The final solution of the method proves to be dependent on the initial fixation of the quality variables. Global optimum cannot be verified. However, the method is still acceptable for quickly computing good feasible solutions, as done by *Audet et al. (2004)*. They also simplify pooling problem instances by analysing the basic problem structure. Eliminating some flow variables reduces the size of the problem while the remaining flow variables are tightened *(Audet et al., 2004)*.

McCormick (1976) develops an efficient relaxation technique based on convex and concave envelopes for NLPs. *Foulds et al. (1992)* propose a pooling problem algorithm inspired by the work of *McCormick (1976)*. A standard branching step of branch-and-bound is used in this algorithm. Another branch-and-bound based algorithm, called branch-and-reduce, is developed by *Sahinidis and Tawarmalani (2005)* and applied to the PQ-formulation.

SLP linearly approximate the pooling problem by using a first-order Taylor expansion. The LP is then solved to obtain a new feasible point, then the problem is linearised at the new point, and the process iterates. SLP usually finds the global optimum when given an acceptable starting point, but fails for a nonphysical initialisation. As the method cannot guarantee global optimum, it is therefore mostly used for locally improving processes that already have a reasonable operating point *(Misener and Floudas, 2009)*.

Floudas and Visweswaran (1990) and *Visweswaran and Floudas (1990)* present the GOP. This is the first algorithm that guarantees convergence to a global optimal solution. The GOP approach and other Lagrangian based methods are built on Lagrangian relaxation and duality theory. The algorithms alternate between solving a projection of the upper bounding primal problem and lower bounding relaxed dual problems. Global optimality is attained when the upper bounding problem converges to the lower bounding problems *(Misener and Floudas, 2009)*. *Adhya et al. (1999)* introduce a new Lagrangian approach for developing lower bounds for the pooling problem. This approach provides stronger bounds for multi-quality pooling problems. Lagrangian relaxation is also used by *Ben-Tal et al. (1994)*, *Audet et al. (2000)*, and *Almutairi and Elhedhli (2009)*.

Table 4.2: Overview of solution method literature relevant to the pooling problem.

Paper	Solution Method	Findings
McCormick (1976)	McCormick envelopes	Demonstrates how convex underestimating problems can be generated for NLPs containing factorable terms.
Haverly (1978)	Recursive	Introduces the P-formulation. Cannot verify global optimum.
Al-Khayyal and Falk (1983)	Branch-and-bound	Proves that the applied algorithm converge to a global solution of the nonconvex program.
Floudas and Visweswaran (1990)	GOP	Propose a new theoretical approach for the determination of global optimum for several classes of nonconvex NLP problems.
Visweswaran and Floudas (1990)	GOP	Applies GOP algorithm to quadratic programming problems with linear and/or quadratic constraints.
Foulds et al. (1992)	Branch-and-bound	Replaces bilinear terms by their convex and concave envelopes.
Sherali and Alameddine (1992)	Branch-and-bound	Introduces the RLT to generate tight linear programming relaxations for jointly constrained BLPs.
Ben-Tal et al. (1994)	Branch-and-bound	Presents Lagrangean relaxation approaches to develop lower bounds for the pooling problem.
Quesada and Grossmann (1995)	RLT, spatial branch-and-bound search	Solves the PQ-formulation with a branch-and-bound procedure, obtains the global optimal solution.
Li and Chang (1998)	RLT	The proposed technique can theoretically solve a polynomial program to find a solution which is close to a global optimum.
Adhya et al. (1999)	Lagrangian relaxation	Proves Lagrangian approach gives tighter lower bounds than standard linear programming.
Audet et al. (2000)	Branch-and-cut	The method yields a global optimal solution of the nonconvex quadratically constrained quadratic programming problem.
Audet et al. (2004)	Branch-and-cut quadratic programming	Variable neighbourhood search heuristic. Solution of test problems from literature substantially accelerated.
Liberti and Pantelides (2006)	RLT	Spatial Branch-and-Bound algorithms applied to the reformulated problem usually obtains the global solution faster than that of the original NLP.
Meyer and Floudas (2006)	Convex envelopes, RLT, piecewise linear RLT	Propose an efficient way of implementing and solving MINLPs containing bilinear terms.
Almutairi and Elhedhli (2009)	Lagrangian relaxation	The approach is general and can be applied to problems with similar structure as the pooling problem.
Gounaris et al. (2009)	Piecewise linearisation	Some piecewise linearisation schemes are superior to their counterparts and should be preferred in pooling process optimisation.
Teles et al. (2012)	MDT	Provides close to zero estimated optimality gaps for problems where the global solver BARON struggles.
Alfaki and Haugland (2013)	Branch-and-bound	Suggests a new branching strategy that performs well in combination with the TSP-formulation.
Kolodziej et al. (2013a)	MDT	MDT scales more favourably than piecewise McCormick envelopes.
Kolodziej et al. (2013b)	MDT	MDT can outperform global solvers such as BARON for large problems.
Sherali and Adams (2013)	RLT	Comprehensive description of RLT.
Teles et al. (2013)	MDT	Introduces MDT, first published in 2011, republished in 2013. Approximates NLPs through successive parametrisation and disaggregation of bilinear variables.
Lotero et al. (2016)	Generalised disjunctive programming	Gives alternative formulation of the multi-period problem. Algorithm that decomposes the MINLP.

RLT is extensively described in *Sherali and Adams (2013)*, where the main objective is to develop and apply RLT as an automatic reformulation procedure and to formulate strong valid inequalities. RLT is divided into two phases; a reformulation phase and a linearisation/convexification phase *(Sherali and Adams, 2013)*. The first phase adds redundant constraints to the NLP model, such that when the problem is relaxed, the resulting underestimation is tighter than without the additional constraints *(Misener and Floudas, 2009)*. In the second phase, the extended problem is linearised, except in special cases where certain convex constraints are retained. The linearisation is done through defining suitable new variables that replace each bilinear term *(Sherali and Adams, 2013)*.

Advances in the pooling problem have the last decade mostly come from combining global optimisation algorithms. *Misener and Floudas (2009)* argue that when bilinear terms are present in equality constraints, the optimisation problem is not convexifiable and must, therefore, be solved using global optimisation techniques for optimality to be verifiable. The advances are in the form of branch-and-bound and relaxation techniques. Examples are the reduced RLT proposed by *Liberti and Pantelides (2006)* and the piecewise linear relaxation proposed by *Gounaris et al. (2009)*, called piecewise-affine underestimators.

Piecewise-affine underestimators are based on the observation that a bilinear envelope is tightest for small domains. The underestimators are constructed by partitioning the domain a priori and formulate sub-envelopes throughout the domain. This construction results in a tighter relaxation than that of the original envelope. Only one envelope is active at a given domain point. Thus, the problem can be represented as an MILP rather than an LP *(Misener and Floudas, 2009)*. Piecewise-affine underestimators are based on McCormick envelopes and are applied to improve the tightness of the formulation, as done by *Gounaris et al. (2009)*. Their computational study shows that piecewise relaxation schemes can significantly improve the lower bounding solution. It is worth noting that the improvement comes at the expense of computational effort and that one should be prudent with the extent in which the relaxation schemes are applied.

The presented solution methods each have their strengths and weaknesses. The recursive method of *Haverly (1978)* and the SLP method cannot verify global optimality *(Misener and Floudas, 2009)*. *Al-Khayyal and Falk (1983)* and *Foulds et al. (1992)* utilise LP relaxation techniques to obtain bounds for BLPs. LP relaxations are often weak *(Wicaksono and Karimi, 2008)*. McCormick relaxations can be weak or loose and may be slow in lifting the lower bound in a global optimisation algorithm *(Teles et al., 2012)*. The RLT, although promising in converging to global optimality, is difficult to implement due to several types of substituting constraints that must be formulated in a linearised form. Further, the algorithm always has to generate a huge amount of bounded constraints in which many are redundant, and there are many ways to design an RLT-process dependent on the problem structure *(Li and Chang, 1998)*. The most common global optimisation algorithms use a spatial branch-and-bound framework, which is similar to the standard branch-and-bound framework, but branches on continuous variables instead of discrete variables. The difficulties in using the spatial branch-and-bound framework lie in obtaining tight lower and upper bounds, to identify efficient procedures to obtain the bounds, and to come up with clever branching strategies to use *(Wicaksono and Karimi, 2008)*.

Due to the reasons mentioned above, other solution methods may be preferable. A promising linearisation technique developed in more recent times is the MDT. The method is introduced in *Teles et al. (2013)* and relies on a concept based on the characteristics of decimal representation of real numbers. The NLP is transformed into a suitably reformulated problem containing new sets of continuous and discrete variables. By disaggregating and parameterising the variables in the nonlinear terms, it is shown how to approximate the original NLP formulation as an MILP.

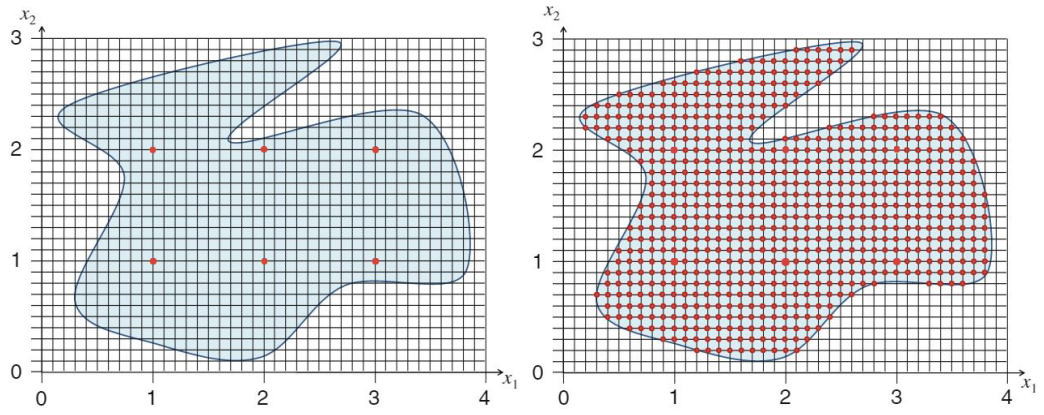

Figure 4.4: Illustration of the feasible region for different accuracy settings of the parameterised variables x_1 and x_2. Accuracy of one digit and two digits on the left and right, respectively, represented by coloured dots. Figure reproduced from *Teles et al. (2013)*.

For minimisation or maximisation problems, an upper and a lower bounding MILP can be derived. The MILPs can then be solved to global optimality through standard methods, where the original problem is approximated to a certain precision level, which can be as tight as desired *(Teles et al., 2013)*. The quality of the solution is dependent on the number of significant digits used to represent the number. One drawback with MDT is that only an infinite number of digits in the parametrisation can guarantee global optimum *(Teles et al., 2012)*. As a part of the research done by *Kolodziej et al. (2013a)*, two global optimisation algorithms are introduced with the MDT relaxation to locate the global optimum within a certain global optimality gap.

Kolodziej et al. (2013a) apply the MDT results in a relaxation which is shown to scale more favourably than the relaxation obtained by applying piecewise McCormick envelopes. The MDT yields smaller mixed-integer problems and faster solution times for similar optimality gaps. *Kolodziej et al. (2013a)* show that the MDT relaxation applied to large problems compares well with general global optimisation solvers. They also show that the solution from the upper and lower bound formulations converge towards the original nonlinear formulation in the limit of an infinite number of discretisation intervals.

Nonconvex nonlinear programming problems yielding multiple local optima, such as the pooling problem, make the application of local NLP solvers ineffective, due to a sub-optimal solution or failure to even locate a feasible one *(Teles et al., 2012; Wicaksono and Karimi, 2008)*. Compared to spatial branch-and-bound involving a continuous relaxation, the MDT involves a discrete partition of the feasible region *(Teles et al., 2012)*. An illustration of the discretisation is shown in Figure 4.4. This discretisation means one can simply use standard MILP solvers to generate a near to optimal solution, given that one exists for the selected accuracy settings. Further, the MDT does not require the specification of an initial point *(Teles et al., 2012)*. For these reasons, the MDT is selected to be the method for linearising the bilinear constraints present in the MAMP.

4.7 The Multi-period Pooling Problem

The pooling problem can be extended to allow for multiple time periods in which there can be variations in inventory, supply, and demand *(Lotero et al., 2016)*. Little literature exists on the pooling problem for a multi-period perspective. Papers that touch upon the subject are *Kolodziej et al. (2013b)* and *Lotero et al. (2016)*. *Kolodziej et al. (2013b)* introduce a generalised multi-period scheduling version of the pooling problem to represent blending systems varying in time. *Lotero et al. (2016)* address the problem from *Kolodziej et al. (2013b)* and propose an alternative formulation and a decomposition method. Binary variables are needed to impose operational constraints *(Kolodziej et al., 2013b)*, such as material movement to and from the tanks in addition to having control on fixed costs. General purpose global optimisation solvers fail to find a solution for even small instances *(Lotero et al., 2016)*.

4.8 Our Contribution

Based on the reviewed literature, little research has been done on the pooling problem in relation to the manganese alloy production industry. Due to the complexity of large-scale manganese alloy production and that no model currently exists, the authors conclude that there is a great potential for optimisation models in the manganese alloy industry.

Our contribution is a flow and quality based model specifically developed for manganese alloy production, named the MAMP. The MAMP is a hybrid between the standard and the generalised pooling problem. In formulating the problem, the P-formulation is used as this is the most common formulation used in chemical processing industries and it provides an intuitive understanding of the process flows and their qualities for this new problem. *Jipnang et al. (2013)* mention that a future extension of their model is to introduce the coupling between the HC FeMn and MC SiMn furnaces. The MAMP includes this coupling. It combines both multiple layers of intermediate pools, as it models the flow and mixing through the furnaces and refining processes, and multi-plant flow. One limitation of the MAMP compared to the model used in *Jipnang et al. (2013)* is that the MAMP does not delve into detailed thermodynamic balances for a furnace. The MAMP does, however, include enthalpy balances to approximate the power consumption in the furnaces.

Overall, the focus of the MAMP is on the economic aspects of the production. It attempts to solve production planning involving a predetermined set of furnaces located at multiple plants. The problem involves multiple quality components that are mixed into several final products. The model accounts for wastes in the production and how to model the reuse of already processed components in the production. A multi-period version of the MAMP is formulated to account for the time aspect of the production.

The formulations presented by *Ben-Tal et al. (1994)*, *Amos et al. (1997)*, and *Meyer and Floudas (2006)* for the oil refinery and water treatment industry, are in some aspects formulated similarly to the MAMP. *Amos et al. (1997)* and *Meyer and Floudas (2006)* formulate the problem using the P-formulation. The MAMP also uses this formulation. All the formulations include multiple quality components and multistage processes, but the MAMP and the wastewater treatment problem also include connections between intermediate pools. In the water network problem, flow between

intermediate pools are the flows between processing plants, while in the MAMP, this is the flow between furnaces. All the problems except the MAMP are formulated with the aim to minimise costs for a process, while the MAMP aims to maximise profit to capture the demand and market price effects on the production.

The MAMP has bilinear terms to correctly model mixing of the slag quality components and is, therefore, a nonconvex NLP with multiple local optima. The solution method MDT is applied to linearise the MAMP such that the problem is in the form of an MILP instead of an NLP. This solution method results in that the problem can be solved by linear solvers, and that global optimality is verified within a certain optimality gap when the problem is solved. To our knowledge, we are the first to apply the MDT to solve large, real problem instances and can, therefore, evaluate the scaleability of the MDT.

Chapter 5

Model Formulation

In this chapter, the deterministic, mathematical optimisation model of the Manganese Alloy Multi-plant Production problem (MAMP) is presented. Multi-plant production, blending, advanced chemistry, thermodynamics, and the coupling of the FeMn and SiMn productions that make up the MAMP, add a high degree of complexity to the formulation of the problem. This chapter starts with listing modelling choices, model assumptions, and the reasoning for each assumption in Section 5.1 to simplify and reduce the scope of the problem. In Section 5.2, the sets, indices, parameters, and variables used in the formulation are defined. The flow each variable represent is illustrated in Section 5.3. The mathematical formulation for a single time period is given in Section 5.4 with explanations of the objective function and constraints. Lastly, the mathematical formulation is extended to account for multiple time periods in Section 5.5.

5.1 Modelling Choices and Model Assumptions

This section outlines the modelling choices and the underlying assumptions used to model the MAMP. The section first describes the problem structure before production related assumptions, modelling choices, and chemical considerations are presented. At the end of the section, process and production options entirely disregarded are mentioned.

5.1.1 Problem Structure

The MAMP is formulated in such a way that the model is solved once and the production plan given by the solution can be used for the planning period in consideration. The time frame of the production can span days to years. The model can be re-run every time there is a change in the production conditions, meaning every time there is a significant change in sets or parameters. Examples are changes in the number of plants or furnaces that are available to the production, the availability of ores, or the end-products' composition requirements.

The end-product demands are assumed to originate from fixed and optional contracts. Fixed contracts are known ahead of production for the entire planning horizon, making a deterministic model appropriate. Optional contracts of any size are assumed to be found in the spot market, so the model provides the user with the quantity that should be sold in this market for each end-product. The chemical composition of the products is assumed to be specified for the fixed contracts, while it is possible to sell end-products of any composition in the spot market. Fixed contracts must be fulfilled while optional contracts can be chosen as desired. This modelling choice means that for every time period, the capacity of the production is always assumed to be greater than the cumulative fixed contract demand, and that is possible to choose between selling excess end-products on optional contracts or hold the end-products in an inventory for future contracts at a holding cost. The raw material procurement prices, electricity prices, and sale prices for end- and by-products are considered constant.

The electricity consumption in each furnace is approximated by the thermodynamic relations described in Chapter 2. The assumptions made about the chemical reaction temperatures to calculate the enthalpies for all elements and oxides are found in Appendix E. All furnaces are assumed to have no downtime, resulting in a continuous production. Switching furnace settings, or switching furnaces on and off, are not included in the model. These are reasonable assumptions as furnace downtime incurs costs and decreases production, and is therefore avoided as much as possible.

The mix of raw materials and slag to blend in a furnace must be decided to produce the demanded alloys. The flow from the furnaces through the refining processes also have to be decided. The formulation, therefore, includes intermediate variables to illustrate the material flow between the furnaces, refining, and crushing processes better. The model generates a production plan for each plant, illustrating the consumption and mixing of raw materials, slag flow between furnaces, material flow through the refining and crushing processes, and the total production of end- and by-products at each plant. Some of the important decisions are how much slag to feed to the MC SiMn furnaces, from which HC FeMn furnaces the slag should be allocated, and the composition of the slag. These decisions are both cost and quality motivated. From a cost perspective, the SiMn production costs may be significantly changed by feeding slag to the MC SiMn furnaces, as the slag replaces raw materials. From a quality perspective, slag of different qualities can be mixed to get the desired quality in an MC SiMn furnace. However, increasing the amount of slag fed also increases the power consumption as the oxides in the slag requires a greater amount of energy to be heated.

5.1.2 Raw Material Supply and Costs

Procurement of raw materials is outside the scope of the model. The raw material procurement cost is connected to the consumption of raw materials. The formulation assumes that inventories of undersized lumps exist and that undersized lumps are pulled from stock when needed. The lower cost of using the undersized lumps should ensure that it is favourable to feed this resource to the furnace. The undersized lumps that later exit the crushing process are sent to different inventories of undersized lumps and are disregarded for the rest of the problem. Another important aspect of the production problem is that a sustainable balance for the re-use of undersized lumps should be found; the process should not consume more undersized lumps than it produces for the result to be a sustainable production plan over time. The feed of undersized lumps is therefore bounded by the produced volume of undersized lumps. Inventories of undersized lumps, oxygen, and silicon waste added to the refining processes are separated from the raw material inventory since these raw materials are coupled to other processes than the furnace process.

5.1.3 Chemical Considerations

A large set of chemical reactions is involved in the production of manganese alloys. The model aims to keep the number of chemical reactions to a minimum, but still at a sufficient level to include the main reactions occurring in the furnaces to ensure the correct weight fractions of elements in the final alloy and oxides in the slag. Including chemical reactions to account for minor end-product constituents would limit the flexibility in end-product specifications in the model. The minor constituents are indirectly included in the model by making the total raw material fractions sum up to less than one. The mass entering the chemical reactions is thus less than the mass fed to the furnace, simulating the feeding of minor constituents, but not including them in the chemical reactions.

All chemical reactions are assumed to be complete. Thus, all chemical balances from reactions (2.5) - (2.17) in Chapter 2 translate into linear equality constraints. To enforce the correct chemical balances, there have to be three constraints for each chemical reaction; one that retains the correct total balance of the reaction and two that ensure correct ratio of the left and right side components. All reactions in the furnaces happen through mole balances as this often is the best way to model chemical relationships.

5.1.4 Slag Properties

In practice, many complicated chemical reactions and incomplete reactions constitute a significant amount of the slag, in addition to the most important oxides. It requires extensive chemical knowledge to model the slag production realistically. Therefore, slag is set to only consist of the most important oxides in the model. These oxides are MnO, FeO, SiO_2, Al_2O_3, MgO, and CaO. Elements and oxides considered of minor importance in the model are left out. The amount and composition of slag produced from each HC FeMn furnace can vary. It is assumed that the slag produced in the HC FeMn furnaces is sent for reuse in MC SiMn furnaces or discarded. In practice, the slag may also be sold, but this is disregarded.

As mentioned in Section 5.1.3, all chemical reactions are assumed to be complete. If this had been true in reality, all oxides would completely reduce to metal, and no slag would be produced. This is not the case, and the model needs to account for slag production. The slag is accounted for by removing a variable amount of the important oxides from the final chemical reactions before they react and form pure metals. The variable amount of important oxides then makes up the slag constituents. This modelling choice allows for the slag-to-metal ratio and slag composition to change depending on the demand, cost, and revenue for each end-product.

5.1.5 By-products

By-products resulting from the production processes pose a modelling challenge regarding the number of elements and oxides the by-products are made up of, as these involve complicated chemical reactions. In the furnaces, MOR, and LC SiMn refining station both the mass and the constituents of the by-products are dependent on the chemical reactions in the processes. Including chemical reactions to accurately model the by-products' mass and constituents is comprehensive. The authors, therefore, assume that a predetermined mix of elements and oxides ends up as by-

products. The mass of each by-product is set as a percentage of each element or oxide in the total feed to the process. The remaining feed available to the rest of the processes is then the total feed subtracted by the mass of the by-products produced by the respective process.

In the crushing process, the amount of crushed product that ends up as undersized lumps vary, but is for modelling purposes set as a fixed percentage of the total mass crushed of each end-product. The manganese alloy producers probably have good information on the crushing process to set an accurate estimate for this parameter, making it an acceptable modelling choice. All of the produced discardable by-products are assumed to be discarded immediately, thus removing the need to include inventory costs.

5.1.6 End-product Content Specifications

The specific carbon content of an end-product is only considered within medium and high range for FeMn and low and medium range for SiMn. Detailed classifications of product types by percentage carbon content within these ranges are disregarded, resulting in a reduced set of end-products. Each end-product must have a specified content of pure elements, which in the formulation is split into a subset of important and unimportant elements. The important elements are fixed requirements, while there are upper and lower bounds on the unimportant elements to ensure end-product specification flexibility.

5.1.7 Furnace Setup

The submerged arc furnaces used in the production of HC FeMn and MC SiMn are reversible. In the model, however, the furnace setup is predefined and not changeable during the run of the model. Should the setup of a furnace be changed, it must be done in the parameter settings.

5.1.8 Process Temperature

This model does not aim to have the answer for micromanaging pure process specific considerations. These considerations are best left to the experienced metallurgists who deal with the production on a daily basis. All processes are therefore assumed to happen at temperatures sufficient to yield the correct alloys and slag. The temperatures used to approximate electrical power consumption in the furnaces are given in Appendix E. Further temperature considerations are left out of the model.

5.1.9 Recovery of Thermal Energy

Some plants may have hot water systems in place for use by district heating or reuse in other plants relying on thermal energy. The heat generating processes in the production may contribute significant amounts of energy to these heating systems. Although interesting, it is not within the scope of the MAMP and is therefore disregarded.

5.2 Definition of Sets, Indices, Parameters, and Variables

Table 5.1: Sets.

Set			
$\mathcal{B}$	–	Set of by-products,	$\mathcal{B}$: {1,...,$\lvert\mathcal{B}\rvert$}
$\mathcal{C}$	–	Set of chemical reactions,	$\mathcal{C}$: {1,...,$\lvert\mathcal{C}\rvert$}
$\mathcal{E}$	–	Set of end-products,	$\mathcal{E}$: {1,...,$\lvert\mathcal{E}\rvert$}
$\mathcal{F}_p$	–	Set of furnaces at plant p,	$\mathcal{F}_p$: {1,...,$\lvert\mathcal{F}_p\rvert$}
$\mathcal{K}$	–	Set of elements and oxides,	$\mathcal{K}$: {1,...,$\lvert\mathcal{K}\rvert$}
$\mathcal{P}$	–	Set of plants,	$\mathcal{P}$: {1,...,$\lvert\mathcal{P}\rvert$}
$\mathcal{R}$	–	Set of raw materials,	$\mathcal{R}$: {1,...,$\lvert\mathcal{R}\rvert$}
$\mathcal{V}$	–	Set of variables present in the chemical reactions,	$\mathcal{V}$: {1,...,$\lvert\mathcal{V}\rvert$}
$\mathcal{F}_p^{\text{FeMn}}$	–	Subset of all HC FeMn furnaces at plant p,	$\mathcal{F}_p^{\text{FeMn}} \subseteq \mathcal{F}_p$
$\mathcal{F}_p^{\text{SiMn}}$	–	Subset of all MC SiMn furnaces at plant p,	$\mathcal{F}_p^{\text{SiMn}} \subseteq \mathcal{F}_p$
$\mathcal{C}^{\text{O}}$	–	Subset of original chemical reactions,	$\mathcal{C}^{\text{O}} \subset \mathcal{C}$
$\mathcal{C}^{\text{C}}$	–	Subset of critical chemical reactions,	$\mathcal{C}^{\text{C}} \subset \mathcal{C}$
$\mathcal{C}^{\text{N}}$	–	Subset of non-critical chemical reactions,	$\mathcal{C}^{\text{N}} \subset \mathcal{C}$
$\mathcal{C}^{\text{S}}$	–	Subset of chemical reactions where the slag variable appears,	$\mathcal{C}^{\text{S}} \subset \mathcal{C}$
$\mathcal{K}^{\text{C}}$	–	Subset of critical elements and oxides for end-products,	$\mathcal{K}^{\text{C}} \subset \mathcal{K}$
$\mathcal{K}^{\text{G}}$	–	Subset of gases,	$\mathcal{K}^{\text{G}} \subset \mathcal{K}$
$\mathcal{K}^{\text{N}}$	–	Subset of non-critical elements and oxides for end-products,	$\mathcal{K}^{\text{N}} \subset \mathcal{K}$
$\mathcal{K}^{\text{S}}$	–	Subset of elements and oxides in the slag,	$\mathcal{K}^{\text{S}} \subset \mathcal{K}$

Table 5.2: Indices.

Index		
p, g	–	Plant
f, h	–	Furnace
b	–	By-product
r, ρ	–	Raw material
e	–	End-product
k	–	Element
c	–	Chemical reaction number
v	–	Chemical reaction variable

Table 5.3: Parameters.

Parameter		
A_{fkcv}	–	Constant for element or oxide k in chemical reaction c for variable v in furnace f (constraints (a) in Appendix A).
A^{LS}_{fkcv}	–	Constant for element or oxide k in the left side ratio equation for chemical reaction c for variable v in furnace f (constraints (b) in Appendix A).
A^{RS}_{fkcv}	–	Constant for element or oxide k in the right side ratio equation for chemical reaction c for variable v in furnace f (constraints (c) in Appendix A).
B_{fkc}	–	1 if element or oxide k exists in chemical reaction c for furnace f, 0 otherwise.
C_r	–	Procurement cost per tonne raw material r.
C^{E}	–	Electricity cost per kWh.
C^{H}	–	End-product inventory holding cost per tonne.
C^{LSiL}	–	Reheating cost per tonne LC SiMn undersized lumps used.
C^{MFeL}	–	Reheating cost per tonne MC FeMn undersized lumps used.
C^{O}	–	Cost per tonne oxygen used. This includes procurement and electricity cost.
C^{S}	–	Discard cost per tonne slag.
C^{SiW}	–	Cost per tonne silicon waste used. This includes procurement and electricity cost.
C^{T}_{pg}	–	Transportation cost per tonne slag transported from plant p to plant g.
D^{F}_e	–	Fixed contract demand for end-product e.
D^{O}_e	–	Optional contract demand for end-product e.
I_{pr}	–	Initial inventory of raw material r at plant p in tonnes.
I^{E}_e	–	Total initial inventory of end-product e for all plants in tonnes.
I^{LSiL}_p	–	Initial inventory of LC SiMn undersized lumps at plant p in tonnes.
I^{MFeL}_p	–	Initial inventory of MC FeMn undersized lumps at plant p in tonnes.
I^{O}_p	–	Initial inventory of oxygen at plant p in tonnes.
I^{SiW}_p	–	Initial inventory of silicon waste at plant p in tonnes.
H^{F}_k	–	Formation enthalpy for element or oxide k, in kJ/tonne.
H^{S}_k	–	Sensible enthalpy for element or oxide k, in kJ/tonne.
L^{H}	–	Furnace heat loss factor.
M_k	–	Molar mass in moles/tonne for element or oxide k.
$\overline{P}_{pf}$	–	Net furnace power capacity for furnace f at plant p, in kW.
Q^{E}	–	Total end-product inventory capacity for all plants in tonnes.
Q^{F}_{pf}	–	Capacity of furnace f per day at plant p in tonnes.
Q^{MOR}_p	–	Total MOR capacity at plant p in tonnes.
Q^{REF}_p	–	Total LC SiMn refining station capacity at plant p in tonnes.
R^{B}_b	–	Revenue or discard cost per tonne by-product b.
R^{F}_e	–	Fixed contract revenue per tonne end-product e sold.
R^{O}_e	–	Optional contract revenue per tonne end-product e sold.
T_{kcv}	–	1 if element or oxide k exists in chemical reaction c for variable v, 0 otherwise.
ΔT	–	Time horizon for the production, given in days.

$\underline{\Gamma}_k^{\text{FeMn}}$	–	Lower limit weight percentage for non-critical element or oxide k in HC FeMn alloy.
$\overline{\Gamma}_k^{\text{FeMn}}$	–	Upper limit weight percentage for non-critical element or oxide k in HC FeMn alloy.
$\underline{\Gamma}_k^{\text{SiMn}}$	–	Lower limit weight percentage for non-critical element or oxide k in MC SiMn alloy.
$\overline{\Gamma}_k^{\text{SiMn}}$	–	Upper limit weight percentage for non-critical element or oxide k in MC SiMn alloy.
$\underline{\Lambda}$	–	Lower limit on the slag-to-metal ratio in the HC FeMn furnaces.
$\overline{\Lambda}$	–	Upper limit on slag-to-metal ratio in the HC FeMn furnaces.
Υ	–	Degree of pre-reduction in the HC FeMn furnaces.
$\underline{\Phi}_k$	–	Lower limit on the weight percentage for slag element or oxide k in slag.
$\overline{\Phi}_k$	–	Upper limit on the weight percentage for slag element or oxide k in slag.
Ψ_{fbk}^{B}	–	Weight percentage of element or oxide k in by-product b from furnace f.
Ψ_b^{CRUSH}	–	Weight percentage of by-product b from the crushing process.
Ψ_k^{FeMn}	–	Weight percentage of element or oxide k in HC FeMn alloy.
Ψ^{LSiL}	–	Weight percentage LC SiMn undersized lumps allowed to feed the LC SiMn refining station.
Ψ^{MFeL}	–	Weight percentage MC FeMn undersized lumps allowed to feed the MOR.
Ψ_b^{MOR}	–	Weight percentage of by-product b from the MOR.
Ψ_{rk}^{R}	–	Weight percentage of element or oxide k in raw material r.
Ψ_k^{SiMn}	–	Weight percentage of element or oxide k in MC SiMn alloy.
Ψ^{UL}	–	Weight percentage of undersized lumps allowed to feed a furnace.
Ω^{MOR}	–	Oxygen-HC FeMn weight relationship factor.
Ω^{REF}	–	Silicon-MC SiMn weight relationship factor.

Table 5.4: Variables.

Variable		
a_p	–	Tonnage of LC SiMn undersized lumps used in the LC SiMn refining station at plant p.
c_p	–	Tonnage of MC FeMn undersized lumps used in the MOR at plant p.
e_{pf}	–	Electric power consumed by furnace f at plant p, in kWh.
g_e^{F}	–	Tonnage end-product e sold on fixed contracts.
g_e^{O}	–	Tonnage end-product e sold on optional contracts.
h_p	–	Tonnage of LC SiMn produced at plant p sent to crushing.
i_e	–	Inventory of end-product e at the end of the production period.
m_{pf}	–	Tonnage of alloy produced in furnace f at plant p sent to the MOR or LC SiMn refining station.
n_{pfkcv}	–	Moles of element or oxide k in furnace f at plant p in reaction c for variable v.
o_p	–	Tonnage oxygen fed to the MOR at plant p.
q_{pf}	–	Tonnage slag produced in furnace f at plant p.
s_p	–	Tonnage silicon source fed to the LC SiMn refining station at plant p.
u_{pf}	–	Tonnage of alloy produced in furnace f at plant p sent to crushing.
v_p	–	Tonnage of MC FeMn produced at plant p sent to crushing.
x_{pe}^{E}	–	Tonnage of end-product e produced at plant p.
x_{pb}^{B}	–	Tonnage of by-product b produced at plant p.
y_{pfr}	–	Tonnage of raw material r fed to furnace f at plant p.
α_{pfkc}	–	Moles of element or oxide k in chemical reaction c extracted as slag from furnace f at plant p.
σ_{pfgh}	–	Tonnage slag sent from furnace f at plant p to furnace h at plant g.
ϕ_{pfk}	–	Weight percentage of element or oxide k in the slag produced by furnace f at plant p.

5.3 Pooling Problem Structure

Figure 5.1 illustrates the material flow within a plant and which processes the variables are describing, using a simplified superstructure. As an example, the variables y_{pfr} and n_{pfkcv} are related to the feeding of the furnaces from the raw material inventory, while a_p and s_p are related to the feeding of the LC SiMn refining station from refining resources. ϕ_{pfk}, e_{pf}, i_e, g_e^{F}, and g_e^{O} are not included in the figure since these are not process flow variables.

Figure 5.1 only illustrates the flow between two furnaces, the MAMP is, however, defined for multiple furnaces and several plants. Slag can be sent from an HC FeMn furnace at one plant to multiple MC SiMn furnaces, at the same plant or other plants. The flow between plants is illustrated in Figure 5.2.

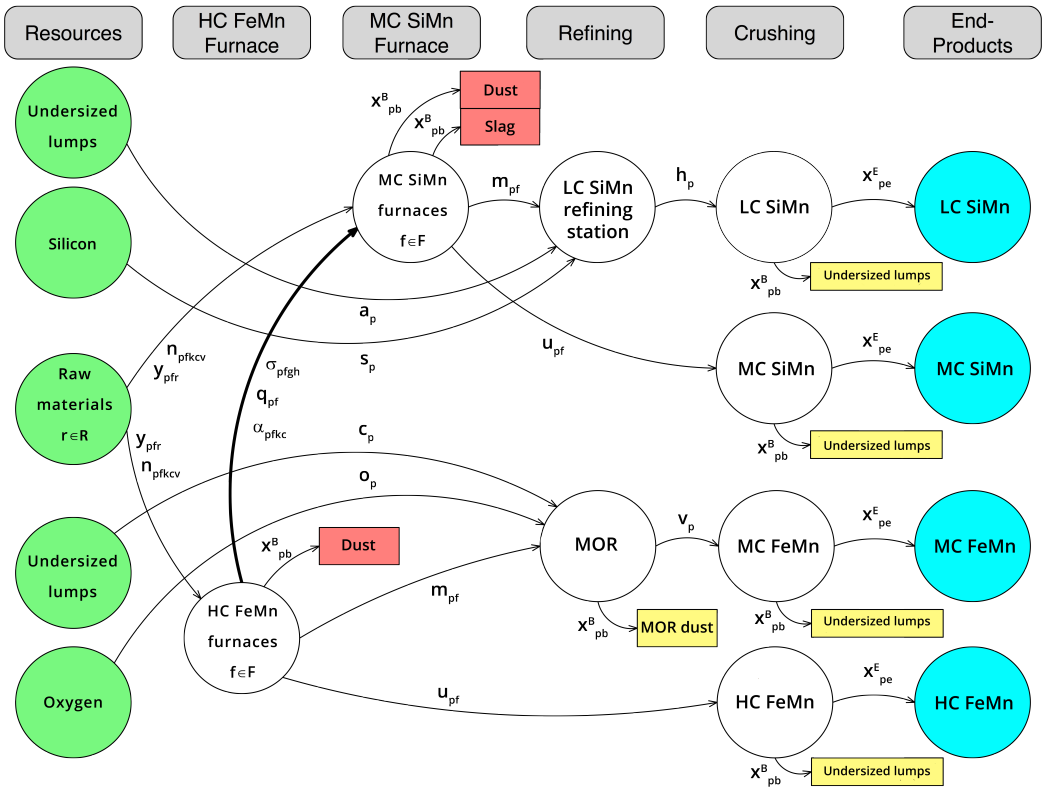

Figure 5.1: The MAMP superstructure for two furnaces, one HC FeMn and one MC SiMn furnace. The same colour coding as in Figure 2.6 is applied. Green: raw materials. Red: wastes. Yellow: reusable/saleable materials. Blue: final alloys.

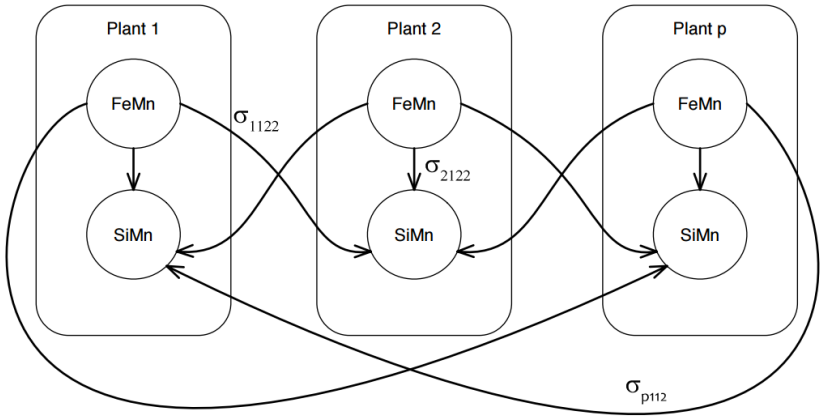

Figure 5.2: Potential flow from HC FeMn furnaces to MC SiMn furnaces within and between plants. The flows are denoted by σ_{pfgh}.

5.4 Mathematical Model

5.4.1 Objective Function

$$\max \quad z = \sum_{e \in \mathcal{E}} (R_e^{\mathrm{F}} g_e^{\mathrm{F}} + R_e^{\mathrm{O}} g_e^{\mathrm{O}}) \tag{5.1a}$$

$$+ \sum_{p \in \mathcal{P}} \sum_{b \in \mathcal{B}} R_b^{\mathrm{B}} x_{pb}^{\mathrm{B}} \tag{5.1b}$$

$$- \sum_{p \in \mathcal{P}} \sum_{f \in \mathcal{F}_p} \sum_{r \in \mathcal{R}} C_r y_{pfr} \tag{5.1c}$$

$$- \sum_{p \in \mathcal{P}} \sum_{f \in \mathcal{F}_p} C^{\mathrm{E}} e_{pf} \tag{5.1d}$$

$$- \sum_{p \in \mathcal{P}} (C^{\mathrm{O}} o_p + C^{\mathrm{MFeL}} c_p) \tag{5.1e}$$

$$- \sum_{p \in \mathcal{P}} (C^{\mathrm{SiW}} s_p + C^{\mathrm{LSiL}} a_p) \tag{5.1f}$$

$$- \sum_{p \in \mathcal{P}} \sum_{f \in \mathcal{F}_p^{\mathrm{FeMn}}} \sum_{g \in \mathcal{P}} \sum_{h \in \mathcal{F}_g^{\mathrm{SiMn}}} C_{pg}^{\mathrm{T}} \sigma_{pfgh} \tag{5.1g}$$

$$- \sum_{p \in \mathcal{P}} \sum_{f \in \mathcal{F}_p^{\mathrm{FeMn}}} C^{\mathrm{S}} (q_{pf} - \sum_{g \in \mathcal{P}} \sum_{h \in \mathcal{F}_g^{\mathrm{SiMn}}} \sigma_{pfgh}) \tag{5.1h}$$

$$- \sum_{e \in \mathcal{E}} C^{\mathrm{H}} i_e \tag{5.1i}$$

The objective function z maximises the total profit from selling end- and by-products from manganese alloy production. Part (5.1a) is the total revenue generated by selling end-products on fixed and optional contracts. Part (5.1b) is the total revenue generated by selling valuable by-products or the cost of discarding the non-profitable ones. Part (5.1c) is the total cost associated with the amounts of raw materials consumed in the production. Part (5.1d) is the total electricity cost from consuming energy in the furnaces. Part (5.1e) is the total cost associated with the amount of oxygen and MC FeMn undersized lumps added to the MOR process. Part (5.1f) is the total cost associated with the amounts of silicon waste and LC SiMn undersized lumps added to the LC SiMn refining station. Part (5.1g) is the total slag transportation cost between plants. Part (5.1h) accounts for the cost of discarding the slag that is not reused. Part (5.1i) accounts for the total holding cost of storing end-products.

5.4.2 Constraints

The constraints are presented in different sections to enhance readability and the understanding of which constraints restrict each process stage. Additionally, the constraint sections are presented in the order of process stage in Figure 5.1.

Resource Inventory Constraints

$$\sum_{f \in \mathcal{F}_p} y_{pfr} \leq I_{pr} \qquad p \in \mathcal{P},\ r \in \mathcal{R} \tag{5.2}$$

$$o_p \leq I_p^{\mathrm{O}} \qquad p \in \mathcal{P} \tag{5.3}$$

$$s_p \leq I_p^{\mathrm{SiW}} \qquad p \in \mathcal{P} \tag{5.4}$$

$$c_p \leq I_p^{\mathrm{MFeL}} \qquad p \in \mathcal{P} \tag{5.5}$$

$$a_p \leq I_p^{\mathrm{LSiL}} \qquad p \in \mathcal{P} \tag{5.6}$$

Constraints (5.2) ensure that the total flow of each raw material to the furnaces at each plant is less than or equal to the total supply of that raw material at the plant. Constraints (5.3) limit the feed of oxygen to the MOR to within the available inventory at the plant. Constraints (5.4) does the same for silicon waste fed to the LC SiMn refining station. Constraints (5.5) and (5.6) set the same restrictions for the use of undersized lumps of MC FeMn and LC SiMn, respectively.

Furnace Constraints

$$\sum_{r \in \mathcal{R}} y_{pfr} + \sum_{k \in \mathcal{K}^{\mathrm{S}}} \sum_{c \in \mathcal{C}^{\mathrm{S}}} M_k n_{pfkcv} \leq Q_{pf}^{\mathrm{F}} \Delta T \qquad p \in \mathcal{P},\ f \in \mathcal{F}_p,\ v \in \{\mathrm{SLAG}\} \tag{5.7}$$

Constraints (5.7) ensure that the total mass of raw materials and slag fed to a furnace does not exceed the mass capacity of the furnace. The capacity is given for one day and is scaled with the number of production days in the time period, ΔT. The term $\sum_{k \in \mathcal{K}^{\mathrm{S}}} \sum_{c \in \mathcal{C}^{\mathrm{S}}} M_k n_{pfkcv}$ is the amount of slag fed to a furnace and only contributes to the feed of MC SiMn furnaces. The term is zero for all HC FeMn furnaces as slag is not sent to HC FeMn furnaces.

$$y_{pfr} \leq \Psi^{\mathrm{UL}} \sum_{\rho \in \mathcal{R} \setminus r} y_{pf\rho} \qquad p \in \mathcal{P},\ f \in \mathcal{F}_p,\ r \in \{\text{HC FeMn}, \text{MC SiMn}\} \tag{5.8}$$

Constraints (5.8) handle the amount of undersized lumps it is possible to feed a furnace. The limit is set as a fraction of the total feed of raw materials excluding undersized lumps. This limit ensures that the feed of undersized lumps is proportional to the rest of the feed.

$$\begin{aligned}\sum_{r\in\mathcal{R}}\sum_{k\in\mathcal{K}}\Psi^{\mathrm{R}}_{rk}y_{pfr}+\sum_{k\in\mathcal{K}^{\mathrm{S}}}\sum_{c\in\mathcal{C}^{\mathrm{S}}}M_k n_{pfkc,\mathrm{SLAG}}+\sum_{c\in\mathcal{C}^{\mathrm{O}}}M_{\mathrm{O}}n_{pf,\mathrm{CO_2},c,\mathrm{TOT}}\\ +\sum_{c\in\mathcal{C}^{\mathrm{O}}}M_{\mathrm{CO}}n_{pf,\mathrm{CO},c,\mathrm{TOT}}-\sum_{b\in\mathcal{B}}\sum_{k\in\mathcal{K}}\sum_{r\in\mathcal{R}}\Psi^{\mathrm{B}}_{fbk}\Psi^{\mathrm{R}}_{rk}y_{pfr}\\ -\sum_{b\in\mathcal{B}}\sum_{k\in\mathcal{K}^{\mathrm{S}}}\sum_{c\in\mathcal{C}^{\mathrm{S}}}\Psi^{\mathrm{B}}_{fbk}M_k n_{pfkc,\mathrm{SLAG}}-\sum_{k\in\mathcal{K}^{\mathrm{G}}}\sum_{c\in\mathcal{C}^{\mathrm{O}}\setminus\{18\}}M_k n_{pfkc,\mathrm{RSRED}}\\ -m_{pf}-u_{pf}-q_{pf}\;=\;0\qquad p\in\mathcal{P},\;\;f\in\mathcal{F}_p\end{aligned}\tag{5.9}$$

Constraints (5.9) handle the mass balance in each furnace. Starting from the first term, the constraints include the following: the mass of the modelled elements and oxides fed to a furnace, the mass of the slag fed to a furnace, the mass of oxygen (O) subtracted twice due to the modelling of CO_2 entering the Boudouard reaction, the mass of CO taking part in the prereduction in the furnace, less the mass of the furnace by-products from the raw material and slag feed, the mass of CO and CO_2 off-gas emissions, the alloy output to either the MOR or the LC SiMn refining station, the alloy output to the crushing process, and the mass of the produced slag. The term $\sum_{k\in\mathcal{K}^{\mathrm{G}}}\sum_{c\in\mathcal{C}^{\mathrm{O}}\setminus\{18\}}M_k n_{pfkc,\mathrm{RSRED}}$ excludes chemical reaction 18, which is the Boudouard reaction, because it uses the variable name RSRED, but accounts for the off-gases leaving the furnace, and not the re-entering gas as in the Boudouard reaction.

For the HC FeMn furnaces, the slag terms $n_{pfkc,\mathrm{SLAG}}$ are zero as no slag is sent between HC FeMn furnaces. For MC SiMn furnaces, the produced slag terms q_{pf} are zero as the slag produced in these furnaces is assumed to be a discard slag. An extended explanation of the furnace mass balance in is given in Appendix C.

$$\begin{aligned}x^{\mathrm{B}}_{pb}\;=\;&\sum_{f\in\mathcal{F}_p}\sum_{r\in\mathcal{R}}\sum_{k\in\mathcal{K}}\Psi^{\mathrm{B}}_{fbk}\Psi^{\mathrm{R}}_{rk}y_{pfr}\\ &+\sum_{f\in\mathcal{F}_p}\sum_{k\in\mathcal{K}^{\mathrm{S}}}\sum_{c\in\mathcal{C}^{\mathrm{S}}}\Psi^{\mathrm{B}}_{fbk}M_k n_{pfkcv}\qquad p\in\mathcal{P},\;\;b\in\mathcal{B},\;\;v\in\{\mathrm{SLAG}\}\end{aligned}\tag{5.10}$$

Constraints (5.10) define the relationship between the total raw material and slag feed to the furnaces and the amount of a discardable by-product produced by the furnaces at a plant.

Furnace Power Consumption Constraints

The electric power consumption in a furnace is modelled by a thermodynamic relation based on enthalpy balances, as outlined in Section 2.5 in Chapter 2.

$$
\begin{aligned}
e_{pf} \;=\; L^{\mathrm{H}}\Bigg(& \sum_{k\in\mathcal{K}}\sum_{r\in\mathcal{R}} H^{\mathrm{F}}_{k}\Psi^{\mathrm{R}}_{rk}y_{pfr} \;+\; \sum_{g\in\mathcal{P}}\sum_{h\in\mathcal{F}^{\mathrm{FeMn}}_{g}}\sum_{k\in\mathcal{K}^{\mathrm{S}}} H^{\mathrm{F}}_{k}\phi_{ghk}\sigma_{ghpf} \\
- & \sum_{b\in\mathcal{B}}\sum_{k\in\mathcal{K}}\sum_{r\in\mathcal{R}} H^{\mathrm{F}}_{k}\Psi^{\mathrm{B}}_{fbk}\Psi^{\mathrm{R}}_{rk}y_{pfr} \;+\; \sum_{b\in\mathcal{B}}\sum_{k\in\mathcal{K}}\sum_{r\in\mathcal{R}} H^{\mathrm{S}}_{k}\Psi^{\mathrm{B}}_{fbk}\Psi^{\mathrm{R}}_{rk}y_{pfr} \\
- & \sum_{k\in\mathcal{K}^{\mathrm{S}}} H^{\mathrm{F}}_{k}\phi_{pfk}q_{pf} \;+\; \sum_{k\in\mathcal{K}^{\mathrm{S}}} H^{\mathrm{S}}_{k}\phi_{pfk}q_{pf} \\
+ & \sum_{g\in\mathcal{P}}\sum_{h\in\mathcal{F}^{\mathrm{FeMn}}_{g}}\sum_{b\in\mathcal{B}}\sum_{k\in\mathcal{K}^{\mathrm{S}}} H^{\mathrm{S}}_{k}\Psi^{\mathrm{B}}_{fbk}\phi_{ghk}\sigma_{ghpf} \\
- & \sum_{k\in\mathcal{K}^{\mathrm{G}}}\sum_{c\in C\setminus\{18\}} H^{\mathrm{F}}_{k}M_{k}n_{pfkc,\mathrm{RSRED}} \;+\; \sum_{k\in\mathcal{K}^{\mathrm{G}}}\sum_{c\in C} H^{\mathrm{S}}_{k}M_{k}n_{pfkc,\mathrm{RSRED}} \\
+ & \sum_{k\in\mathcal{K}^{\mathrm{G}}}\sum_{c\in C} H^{\mathrm{F}}_{k}M_{k}n_{pfkc,\mathrm{TOT}} \;-\; \sum_{k\in\mathcal{K}^{\mathrm{G}}}\sum_{c\in C} H^{\mathrm{S}}_{k}M_{k}n_{pfkc,\mathrm{TOT}} \\
+ & \sum_{k\in\mathcal{K}^{\mathrm{C}}}\sum_{c\in C^{\mathrm{C}}} H^{\mathrm{S}}_{k}M_{k}n_{pfkc,\mathrm{TOT}}\Bigg) \qquad\qquad p\in\mathcal{P},\;\; f\in\mathcal{F}_{p}
\end{aligned}
\tag{5.11}
$$

Constraints (5.11) ensure that the power used in each furnace equals the difference between the input and output enthalpy of the entering and exiting components. The terms involving H^{F}_{k} represent the formation enthalpies for each element and oxide. The terms involving H^{S}_{k} represent the sensible enthalpies. The sensible enthalpies are used to calculate the energy required to increase the temperature of each element and oxide from room temperature to the furnace temperature. Calculating the sensible enthalpies of the leaving compounds is sufficient, as shown in equation (2.4) in Chapter 2. The first line on the right side of the constraints describes the formation enthalpies of the raw materials and the slag fed to a furnace. The second line corresponds to the formation and sensible enthalpies of furnace by-products. The third line represents the formation and sensible enthalpies of the HC FeMn furnace slag, while the fourth line represents the sensible enthalpy required to reheat the HC FeMn slag in the MC SiMn furnace. The MC SiMn slag enthalpy from ores is accounted for in the terms on the second line of the constraints. The fifth line corresponds to the formation and sensible enthalpies of the gases produced by a furnace. The Boudouard reaction is excluded from the first term of line five for the same reasoning as in constraints (5.9). The sixth line accounts for the formation and sensible enthalpies from gases re-entering the furnace process through chemical reactions. The last term of the constraints represents the sensible enthalpy of the alloy output from a furnace. The whole right side of the constraints is multiplied by the heat loss factor L^{H} to account for the heat lost to the surroundings during production.

$$
e_{pf} \;\leq\; \overline{P}_{pf}\Delta T \qquad p\in\mathcal{P},\;\; f\in\mathcal{F}_{p} \tag{5.12}
$$

Constraints (5.12) ensure that a furnace cannot use more power than its maximum power capacity. Furnace effectiveness is included in the parameters $\overline{P}_{pf}$ such that the parameters represent the net available power capacity of the furnaces. ΔT should be converted from days to hours, to yield the conventional unit of energy, kWh. The power capacity is scaleable with time in the same way as in constraints (5.7).

Furnace - Slag Connection Constraints

$$\phi_{pfk} q_{pf} \;=\; M_k \sum_{c \in \mathcal{C}^{\mathrm{S}}} B_{fkc} \alpha_{pfkc} \qquad p \in \mathcal{P},\;\; f \in \mathcal{F}_p^{\mathrm{FeMn}},\;\; k \in \mathcal{K}^{\mathrm{S}} \tag{5.13}$$

Constraints (5.13) couple the mass of slag constituents $\phi_{pfk} q_{pf}$ to the mass of the constituents $M_k \alpha_{pfkc}$ subtracted from the chemical reactions occurring in an HC FeMn furnace. The left-hand side terms of the constraints are nonlinear and, therefore, complicates the MAMP. The constraints are specific to this problem because there are no pooling problems in the manganese alloy industry, to the authors' knowledge, that extracts a proportion of a specific constituent from a blending process. The closest similarities may be found in the separation processes in the crude oil industry.

$$\sum_{g \in \mathcal{P}} \sum_{h \in \mathcal{F}_g^{\mathrm{SiMn}}} \sigma_{pfgh} \;\leq\; q_{pf} \qquad p \in \mathcal{P},\;\; f \in \mathcal{F}_p^{\mathrm{FeMn}} \tag{5.14}$$

Constraints (5.14) state that sending slag to MC SiMn furnaces from an HC FeMn furnace is optional, by allowing less than the produced slag to be sent. If the slag is unfavourable to feed to MC SiMn furnaces, it is discarded.

$$\sum_{p \in \mathcal{P}} \sum_{f \in \mathcal{F}_p^{\mathrm{FeMn}}} \phi_{pfk} \sigma_{pfgh} = \;\; M_k \sum_{c \in \mathcal{C}^{\mathrm{S}}} n_{ghkcv} \qquad \begin{array}{l} g \in \mathcal{P},\;\; h \in \mathcal{F}_g^{\mathrm{SiMn}}, \\ k \in \mathcal{K}^{\mathrm{S}},\;\; v \in \{\mathrm{SLAG}\} \end{array} \tag{5.15}$$

The slag and raw material feed to the MC SiMn furnace are coupled by constraints (5.15). These constraints state that the total mass of the respective element or oxide k fed to an MC SiMn furnace through slag must equal the total mass of element or oxide present in the slag sent from the HC FeMn furnaces that feed the MC SiMn furnace. These are nonlinear terms common to the pooling problem.

$$\phi_{pfk} \;\geq\; \underline{\Phi}_k \qquad p \in \mathcal{P},\;\; f \in \mathcal{F}_p^{\mathrm{FeMn}},\;\; k \in \mathcal{K}^{\mathrm{S}} \tag{5.16}$$

$$\phi_{pfk} \;\leq\; \overline{\Phi}_k \qquad p \in \mathcal{P},\;\; f \in \mathcal{F}_p^{\mathrm{FeMn}},\;\; k \in \mathcal{K}^{\mathrm{S}} \tag{5.17}$$

$$\sum_{k \in \mathcal{K}^{\mathrm{S}}} \phi_{pfk} \;=\; 1 \qquad p \in \mathcal{P},\;\; f \in \mathcal{F}_p^{\mathrm{FeMn}} \tag{5.18}$$

Constraints (5.16) and (5.17) induce lower and upper bounds on the HC FeMn furnace slag composition, respectively. Constraints (5.18) enforce that the sum of the weight percentages of all the slag constituents must make up the total slag content.

$$q_{pf} \;\geq\; \underline{\Lambda}(m_{pf} + u_{pf}) \qquad p \in \mathcal{P},\;\; f \in \mathcal{F}_p^{\mathrm{FeMn}} \tag{5.19}$$

$$q_{pf} \leq \overline{\Lambda}(m_{pf} + u_{pf}) \qquad p \in \mathcal{P}, \ f \in \mathcal{F}_p^{\text{FeMn}} \tag{5.20}$$

In the manganese production industry, it is common to produce according to the slag-to-metal ratio. The $\overline{\Lambda}$ and $\underline{\Lambda}$ are the upper and lower bounds on this ratio. Constraints (5.19) make sure that it is always produced at least a minimum amount of slag in the HC FeMn furnaces relative to the alloy produced. Constraints (5.20) set the upper bound for the slag production relative to the alloy production.

MOR Constraints

$$\sum_{f \in \mathcal{F}_p^{\text{FeMn}}} m_{pf} + o_p + c_p \leq Q_p^{\text{MOR}} \qquad p \in \mathcal{P} \tag{5.21}$$

Each plant is modelled to have one MOR that processes HC FeMn from all the HC FeMn furnaces at the plant. The MOR has a capacity on the amount of feed it can process. Constraints (5.21) ensure that the feed of HC FeMn, oxygen, and undersized lumps added to the MOR do not surpass this capacity.

$$\sum_{f \in \mathcal{F}_p^{\text{FeMn}}} m_{pf} + o_p + c_p - v_p - x_{pb}^{\text{B}} = 0 \qquad p \in \mathcal{P}, \ b \in \{\text{MOR dust}\} \tag{5.22}$$

Constraints (5.22) handle the mass balance in the MOR. The HC FeMn, oxygen, and undersized lumps blended in the MOR equal the output of saleable dust and MC FeMn.

$$o_p = \Omega^{\text{MOR}} \sum_{f \in \mathcal{F}_p^{\text{FeMn}}} m_{pf} \qquad p \in \mathcal{P} \tag{5.23}$$

Constraints (5.23) state that the oxygen used in the MOR equals a fixed ratio of the added HC FeMn. According to the assumptions, all chemical reactions are complete. Thus, there has to be an HC FeMn-oxygen ratio that states the mass of oxygen that has to be added to the process to avoid leftovers of any reactants. By calculating this ratio, there is no need to include a chemical reaction when modelling this process. This ratio is calculated in Appendix B.

$$c_p \leq \Psi^{\text{MFeL}} \sum_{f \in \mathcal{F}_p^{\text{FeMn}}} m_{pf} \qquad p \in \mathcal{P} \tag{5.24}$$

Constraints (5.24) set the upper bound on how much MC FeMn undersized lumps it is possible to add to the MOR relative to the feed of HC FeMn alloy. The addition of undersized lumps decreases the temperature in the MOR, due to the higher energy required to re-melt the undersized lumps. This limitation on undersized lumps prevents too low temperatures from occurring in the MOR.

$$x^{\mathrm{B}}_{pb} \;=\; \Psi^{\mathrm{MOR}}_{b}\Big(\sum_{f\in\mathcal{F}^{\mathrm{FeMn}}_{p}} m_{pf} + o_p\Big) \qquad p\in\mathcal{P},\;\; b\in\{\text{MOR dust}\} \tag{5.25}$$

Constraints (5.25) state that a certain percentage of the mass fed to the MOR ends up as saleable MOR dust.

LC SiMn Refining Station Constraints

$$\sum_{f\in\mathcal{F}^{\mathrm{SiMn}}_{p}} m_{pf} + s_p + a_p \;\leq\; Q^{\mathrm{REF}}_{p} \qquad p\in\mathcal{P} \tag{5.26}$$

Constraints (5.26) handle the capacity of the LC SiMn refining station. The mass flow from all MC SiMn furnaces, the added mass of silicon waste, and LC SiMn undersized lumps must be less than or equal to the capacity of the LC SiMn refining station.

$$\sum_{f\in\mathcal{F}^{\mathrm{SiMn}}_{p}} m_{pf} + s_p + a_p - h_p \;=\; 0 \qquad p\in\mathcal{P} \tag{5.27}$$

The mass balance in the refining process is handled by constraints (5.27). The mass flow of LC SiMn from the refining process equals the total flow from the MC SiMn furnaces to the LC SiMn refining station at the plant, the added silicon waste, and LC SiMn undersized lumps.

$$s_p \;=\; \Omega^{\mathrm{REF}} \sum_{f\in\mathcal{F}^{\mathrm{SiMn}}_{p}} m_{pf} \qquad p\in\mathcal{P} \tag{5.28}$$

Constraints (5.28) relate the total amount of silicon waste needed to add to alter the product composition of MC SiMn to form LC SiMn. The constraints ensure that it is not possible to get LC SiMn out from the refining process without mixing the correct amount of silicon waste with the incoming feed of MC SiMn.

$$a_p \;\leq\; \Psi^{\mathrm{LSiL}}\Big(\sum_{f\in\mathcal{F}^{\mathrm{SiMn}}_{p}} m_{pf} + s_p\Big) \qquad p\in\mathcal{P} \tag{5.29}$$

There is an upper limit on how much LC SiMn undersized lumps it is possible to add to the refining process, given by constraints (5.29). Similar to the feeding of MC FeMn undersized lumps to the MOR, process temperature is the reason for this limit.

Crushing Constraints

$$\sum_{f \in \mathcal{F}_p^{\text{FeMn}}} u_{pf} = x_{pe}^{\text{E}} + x_{pb}^{\text{B}} \qquad p \in \mathcal{P},\ e \in \{\text{HC FeMn}\},\ b \in \{\text{HC FeMn}\} \tag{5.30}$$

$$\sum_{f \in \mathcal{F}_p^{\text{SiMn}}} u_{pf} = x_{pe}^{\text{E}} + x_{pb}^{\text{B}} \qquad p \in \mathcal{P},\ e \in \{\text{MC SiMn}\},\ b \in \{\text{MC SiMn}\} \tag{5.31}$$

$$v_p = x_{pe}^{\text{E}} + x_{pb}^{\text{B}} \qquad p \in \mathcal{P},\ e \in \{\text{MC FeMn}\},\ b \in \{\text{MC FeMn}\} \tag{5.32}$$

$$h_p = x_{pe}^{\text{E}} + x_{pb}^{\text{B}} \qquad p \in \mathcal{P},\ e \in \{\text{LC SiMn}\},\ b \in \{\text{LC SiMn}\} \tag{5.33}$$

The model must ensure that the mass balance of alloys from the furnaces and the MOR or LC SiMn refining station is equal to the amount of each end- and by-product that each plant produces. Constraints (5.30) and (5.31) ensure that the total amount of HC FeMn and MC SiMn from the respective set of furnaces equals the end- and by-products produced at the plant. The same balance applies to the crushing of MC FeMn and LC SiMn from the MOR and LC SiMn refining station. These are accounted for in constraints (5.32) and (5.33).

$$x_{pb}^{\text{B}} = \Psi_b^{\text{CRUSH}} \sum_{f \in \mathcal{F}_p^{\text{FeMn}}} u_{pf} \qquad p \in \mathcal{P},\ b \in \{\text{HC FeMn}\} \tag{5.34}$$

$$x_{pb}^{\text{B}} = \Psi_b^{\text{CRUSH}} \sum_{f \in \mathcal{F}_p^{\text{SiMn}}} u_{pf} \qquad p \in \mathcal{P},\ b \in \{\text{MC SiMn}\} \tag{5.35}$$

$$x_{pb}^{\text{B}} = \Psi_b^{\text{CRUSH}} v_p \qquad p \in \mathcal{P},\ b \in \{\text{MC FeMn}\} \tag{5.36}$$

$$x_{pb}^{\text{B}} = \Psi_b^{\text{CRUSH}} h_p \qquad p \in \mathcal{P},\ b \in \{\text{LC SiMn}\} \tag{5.37}$$

Constraints (5.34) - (5.37) ensure that a given percentage of the crushed end-products ends up as undersized lumps.

$$\sum_{f \in \mathcal{F}_p} y_{pfr} \leq x_{pb}^{\text{B}} \qquad p \in \mathcal{P},\ r \in \{\text{HC FeMn}, \text{MC SiMn}\},\ b \in \{\text{HC FeMn}, \text{MC SiMn}\} \tag{5.38}$$

$$c_p \leq x_{pb}^{\text{B}} \qquad p \in \mathcal{P},\ b \in \{\text{MC FeMn}\} \tag{5.39}$$

$$a_p \leq x_{pb}^{\text{B}} \qquad p \in \mathcal{P},\ b \in \{\text{LC SiMn}\} \tag{5.40}$$

To have a sustainable consumption of undersized lumps, the amount of undersized lumps used in the processes should be less than or equal to the amount of undersized lumps exiting the crushing process. Constraints (5.38) - (5.40) ensure that this condition is satisfied. Constraints (5.38) allow both types of lumps to be used in both the HC FeMn and MC SiMn furnaces.

Final Inventory and Demand Constraints

$$g_e^{\mathrm{F}} = D_e^{\mathrm{F}} \qquad e \in \mathcal{E} \tag{5.41}$$

$$g_e^{\mathrm{O}} \leq D_e^{\mathrm{O}} \qquad e \in \mathcal{E} \tag{5.42}$$

Constraints (5.41) handle the demand from fixed contracts, which must be satisfied. Constraints (5.42) handle the demand from optional contracts.

$$i_e = I_e^{\mathrm{E}} + \sum_{p \in \mathcal{P}} x_{pe}^{\mathrm{E}} - (g_e^{\mathrm{F}} + g_e^{\mathrm{O}}) \qquad e \in \mathcal{E} \tag{5.43}$$

$$\sum_{e \in \mathcal{E}} i_e \leq Q^{\mathrm{E}} \tag{5.44}$$

Constraints (5.43) and (5.44) control the total end-product inventory balance for each end-product and the total inventory capacity across all plants, respectively.

Chemical Balance Constraints

$$\sum_{c \in \mathcal{C}} T_{kcv} n_{pfkcv} = \frac{1 - \sum_{b \in \mathcal{B}} \Psi_{fbk}^{\mathrm{B}}}{M_k} \sum_{r \in \mathcal{R}} \Psi_{rk}^{\mathrm{R}} y_{pfr} \qquad p \in \mathcal{P},\ f \in \mathcal{F}_p,\ k \in \mathcal{K},\ v \in \{\mathrm{FED}\} \tag{5.45}$$

Constraints (5.45) connect the chemical processes in a furnace to the raw material feed. The left-hand side of the constraints states that the total amount of moles of an element or oxide k used in the chemical reactions in each furnace has to equal the feed of that element or oxide to the furnace. The parameters T_{kcv} ensure that n_{pfkcv} cannot take any other value than zero where element or oxide $k \in \mathcal{K}$ is not present in chemical reaction c for variable $v \in \{\mathrm{FED}\}$. The right-hand side of the constraints multiplies the weight percentage for each element or oxide k in raw material r with the total weight of the raw material to find the weight of the element or oxide in the raw material. The sum is taken over all raw materials so that the total feed of the respective element or oxide is found. It is then divided by molar mass in mole per tonne to determine the amount of mole fed to the furnace for element or oxide k. The term $(1 - \sum_{b \in \mathcal{B}} \Psi_{fbk}^{\mathrm{B}})$ removes the amount of moles that ends up as discardable by-products from the feed since the chemical reactions do not account for the production of these.

$$\begin{aligned} \sum_{v \in \mathcal{V} \setminus \{\mathrm{SLAG}\}} \sum_{k \in \mathcal{K}} A_{fkcv} n_{pfkcv} + \sum_{k \in \mathcal{K}^{\mathrm{S}}} (1 - \sum_{b \in \mathcal{B}} \Psi_{fbk}^{\mathrm{B}}) A_{fkc,\mathrm{SLAG}} n_{pfkc,\mathrm{SLAG}} \\ - \sum_{k \in \mathcal{K}} B_{fkc} \alpha_{pfkc} = 0 \qquad p \in \mathcal{P},\ f \in \mathcal{F}_p,\ c \in \mathcal{C}^{\mathrm{O}} \end{aligned} \tag{5.46}$$

$$\sum_{v\in\mathcal{V}\setminus\{\text{SLAG}\}}\sum_{k\in\mathcal{K}} A^{\text{LS}}_{fkcv} n_{pfkcv} + \sum_{k\in\mathcal{K}^{\text{S}}}(1-\sum_{b\in\mathcal{B}}\Psi^{\text{B}}_{fbk})A^{\text{LS}}_{fkc,\text{SLAG}} n_{pfkc,\text{SLAG}} - \sum_{k\in\mathcal{K}} B_{fkc}\alpha_{pfkc} = 0 \qquad p\in\mathcal{P},\ f\in\mathcal{F}_p,\ c\in\mathcal{C}^{\text{O}} \tag{5.47}$$

$$\sum_{v\in\mathcal{V}}\sum_{k\in\mathcal{K}} A^{\text{RS}}_{fkcv} n_{pfkcv} = 0 \qquad p\in\mathcal{P},\ f\in\mathcal{F}_p,\ c\in\mathcal{C}^{\text{O}} \tag{5.48}$$

The general form of the chemical reactions presented in reactions (2.5) - (2.17) in Chapter 2 are given by constraints (5.46) - (5.48). The constraints enforce that the mole balances equals zero. Each chemical reaction from Chapter 2 is represented by three constraints to ensure the correct relationships between reactants and resultants. Constraints (5.46) represent the complete chemical reaction, while constraints (5.47) ensure correct ratios between the reactants, and constraints (5.48) the resultants. The SLAG variable is removed from the set $\mathcal{V}$ in the first term of constraints (5.46) and (5.47) because slag is handled by a separate term.

$$\sum_{v\in\mathcal{V}}\sum_{k\in\mathcal{K}} A_{fkcv} n_{pfkcv} = 0 \qquad p\in\mathcal{P},\ f\in\mathcal{F}_p,\ c\in\mathcal{C}^{\text{C}} \tag{5.49}$$

$$n_{pfk,c+1,\text{RED}} = n_{pfkc,\text{RSRED}} \qquad p\in\mathcal{P},\ f\in\mathcal{F}_p, \quad k\in\{\text{Mn}_2\text{O}_3,\ \text{Mn}_3\text{O}_4,\ \text{MnO},\ \text{Fe}_2\text{O}_3,\ \text{Fe}_3\text{O}_4,\ \text{FeO}\},\ c\in\{1,2,3,6,7\} \tag{5.50}$$

The output of Mn, Fe, Si, and C from the redox reactions and the direct feed of the respective elements from ores and undersized lumps are added together in constraints (5.49) to find the total mass of each element in the furnace output alloy. Constraints (5.49) are general representations of constraints (A.5), (A.10), (A.11), and (A.12) in Appendix A. The reactants in some of the chemical reactions originate from a resultant in the previous reaction. Therefore, $n_{pfk,c+1,\text{RED}}$ in these chemical reactions equals $n_{pfkc,\text{RSRED}}$ in the previous reaction. This relation is given by constraints (5.50).

An example of the application of constraints (5.46) - (5.48) to model the chemical reaction (2.6) in Chapter 2, $3\,\text{Mn}_2\text{O}_3\text{(s)} + \text{CO(g)} \longrightarrow 2\,\text{Mn}_3\text{O}_4\text{(s)} + \text{CO}_2\text{(g)}$, is provided in equations (5.51a) - (5.51c). The full set of the constraints for the chemical reactions is given in Appendix A.

$$2n_{pf,\text{Mn}_2\text{O}_3,2,\text{FED}} + 2n_{pf,\text{Mn}_2\text{O}_3,2,\text{RED}} + 6n_{pf,\text{CO},2,\text{FED}} - 3n_{pf,\text{Mn}_3\text{O}_4,2,\text{RSRED}} - 6n_{pf,\text{CO}_2,2,\text{RSRED}} = 0 \qquad p\in\mathcal{P},\ f\in\mathcal{F}_p \tag{5.51a}$$

$$n_{pf,\text{Mn}_2\text{O}_3,2,\text{FED}} + n_{pf,\text{Mn}_2\text{O}_3,2,\text{RED}} - 3n_{pf,\text{CO},2,\text{FED}} = 0 \qquad p\in\mathcal{P},\ f\in\mathcal{F}_p \tag{5.51b}$$

$$n_{pf,\text{Mn}_3\text{O}_4,2,\text{RSRED}} - 2n_{pf,\text{CO}_2,2,\text{RSRED}} = 0 \qquad p\in\mathcal{P},\ f\in\mathcal{F}_p \tag{5.51c}$$

Boudouard Reaction Constraints

$$n_{pf,\mathrm{C},18,\mathrm{FED}} + n_{pf,\mathrm{CO_2},18,\mathrm{TOT}} - n_{pf,\mathrm{CO},18,\mathrm{RSRED}} = 0 \qquad p \in \mathcal{P},\ f \in \mathcal{F}_p \tag{5.52a}$$

$$n_{pf,\mathrm{C},18,\mathrm{FED}} - n_{pf,\mathrm{CO_2},18,\mathrm{TOT}} = 0 \qquad p \in \mathcal{P},\ f \in \mathcal{F}_p \tag{5.52b}$$

$$n_{pf,\mathrm{CO_2},18,\mathrm{TOT}} = (1-\Upsilon) \sum_{c \in \mathcal{C}\setminus\{1,2\}} n_{pf,\mathrm{CO_2},c,\mathrm{RSRED}} \qquad p \in \mathcal{P},\ f \in \mathcal{F}_p \tag{5.53a}$$

$$\sum_{c \in \mathcal{C}^{\mathrm{O}}} n_{pf,\mathrm{CO},c,\mathrm{TOT}} \leq n_{pf,\mathrm{CO},18,\mathrm{RSRED}} + \sum_{c \in \mathcal{C}^{\mathrm{S}}} n_{pf,\mathrm{CO},c,\mathrm{RSRED}} \qquad p \in \mathcal{P},\ f \in \mathcal{F}_p \tag{5.53b}$$

Constraints (5.52a) represent the Boudouard reaction given in reaction (2.14) in Chapter 2. Constraints (5.52b) ensure correct ratio between the left side reactants. No constraints are needed for the right side ratio as only one resultant exists. Constraints (5.53a) handle the degree of prereduction in a furnace, i.e. how much CO_2 that is consumed by the Boudouard reaction. Following the definition of pre-reduction given in Chapter 2, the term has to be formulated as $(1-\Upsilon)$ to model the amount of CO_2 re-entering the process correctly. The chemical reactions involving MnO_2 and Mn_2O_3 are not normally involved in prereduction and are therefore not included in the sum of the right side term. Constraints (5.53b) ensure that the total CO fed to reactions (2.5) - (2.7) and (2.10) - (2.11) is less than or equal to the CO resulting from the Boudouard reaction and reactions (2.8) and (2.12) - (2.13). The CO and CO_2 that do not re-enter the process are released as off-gases.

Chemical Content Constraints

$$M_k \sum_{c \in \mathcal{C}^{\mathrm{C}}} T_{kcv} n_{pfkcv} = \Psi_k^{\mathrm{FeMn}} (m_{pf} + u_{pf}) \qquad p \in \mathcal{P},\ f \in \mathcal{F}_p^{\mathrm{FeMn}},\ k \in \mathcal{K}^{\mathrm{C}},\ v \in \{\mathrm{TOT}\} \tag{5.54}$$

$$M_k \sum_{c \in \mathcal{C}^{\mathrm{C}}} T_{kcv} n_{pfkcv} = \Psi_k^{\mathrm{SiMn}} (m_{pf} + u_{pf}) \qquad p \in \mathcal{P},\ f \in \mathcal{F}_p^{\mathrm{SiMn}},\ k \in \mathcal{K}^{\mathrm{C}},\ v \in \{\mathrm{TOT}\} \tag{5.55}$$

Constraints (5.54) and (5.55) ensure that the required content of critical elements is satisfied in the HC FeMn and the MC SiMn furnaces, respectively.

$$M_k \sum_{c \in \mathcal{C}^{\mathrm{N}}} T_{kcv} n_{pfkcv} \leq \overline{\Gamma}_k^{\mathrm{FeMn}} (m_{pf} + u_{pf}) \qquad p \in \mathcal{P},\ f \in \mathcal{F}_p^{\mathrm{FeMn}},\ k \in \mathcal{K}^{\mathrm{N}},\ v \in \{\mathrm{TOT}\} \tag{5.56}$$

$$M_k \sum_{c \in \mathcal{C}^{\mathrm{N}}} T_{kcv} n_{pfkcv} \geq \underline{\Gamma}_k^{\mathrm{FeMn}} (m_{pf} + u_{pf}) \qquad p \in \mathcal{P},\ f \in \mathcal{F}_p^{\mathrm{FeMn}},\ k \in \mathcal{K}^{\mathrm{N}},\ v \in \{\mathrm{TOT}\} \tag{5.57}$$

$$M_k \sum_{c \in \mathcal{C}^{\mathrm{N}}} T_{kcv} n_{pfkcv} \leq \overline{\Gamma}_k^{\mathrm{SiMn}} (m_{pf} + u_{pf}) \qquad p \in \mathcal{P},\ f \in \mathcal{F}_p^{\mathrm{SiMn}},\ k \in \mathcal{K}^{\mathrm{N}},\ v \in \{\mathrm{TOT}\} \tag{5.58}$$

$$M_k \sum_{c \in \mathcal{C}^{\mathrm{N}}} T_{kcv} n_{pfkcv} \geq \underline{\Gamma}_k^{\mathrm{SiMn}} (m_{pf} + u_{pf}) \qquad p \in \mathcal{P},\ f \in \mathcal{F}_p^{\mathrm{SiMn}},\ k \in \mathcal{K}^{\mathrm{N}},\ v \in \{\mathrm{TOT}\} \tag{5.59}$$

To have some slack on the non-critical elements and oxides used in the production, upper and lower bounds are set for these elements. The bounds are given in constraints (5.56) - (5.59).

Non-negativity Constraints

$$a_p \geq 0 \qquad p \in \mathcal{P} \tag{5.60}$$

$$c_p \geq 0 \qquad p \in \mathcal{P} \tag{5.61}$$

$$e_{pf} \geq 0 \qquad p \in \mathcal{P},\ f \in \mathcal{F}_p \tag{5.62}$$

$$g_e^{\mathrm{F}} \geq 0 \qquad e \in \mathcal{E} \tag{5.63}$$

$$g_e^{\mathrm{O}} \geq 0 \qquad e \in \mathcal{E} \tag{5.64}$$

$$h_p \geq 0 \qquad p \in \mathcal{P} \tag{5.65}$$

$$i_e \geq 0 \qquad e \in \mathcal{E} \tag{5.66}$$

$$m_{pf} \geq 0 \qquad p \in \mathcal{P},\ f \in \mathcal{F}_p \tag{5.67}$$

$$n_{pfkcv} \geq 0 \qquad p \in \mathcal{P},\ f \in \mathcal{F}_p,\ k \in \mathcal{K},\ c \in \mathcal{C},\ v \in \mathcal{V} \tag{5.68}$$

$$o_p \geq 0 \qquad p \in \mathcal{P} \tag{5.69}$$

$$q_{pf} \geq 0 \qquad p \in \mathcal{P},\ f \in \mathcal{F}_p \tag{5.70}$$

$$s_p \geq 0 \qquad p \in \mathcal{P} \tag{5.71}$$

$$u_{pf} \geq 0 \qquad p \in \mathcal{P},\ f \in \mathcal{F}_p \tag{5.72}$$

$$v_p \geq 0 \qquad p \in \mathcal{P} \tag{5.73}$$

$$x_{pe}^{\mathrm{E}} \geq 0 \qquad p \in \mathcal{P},\ e \in \mathcal{E} \tag{5.74}$$

$$x_{pb}^{\mathrm{B}} \geq 0 \qquad p \in \mathcal{P},\ b \in \mathcal{B} \tag{5.75}$$

$$y_{pfr} \geq 0 \qquad p \in \mathcal{P},\ f \in \mathcal{F}_p,\ r \in \mathcal{R} \tag{5.76}$$

$$\alpha_{pfkc} \geq 0 \qquad p \in \mathcal{P},\ f \in \mathcal{F}_p,\ k \in \mathcal{K},\ c \in \mathcal{C} \tag{5.77}$$

$$\sigma_{pfgh} \geq 0 \qquad p \in \mathcal{P},\ f \in \mathcal{F}_p,\ g \in \mathcal{P},\ h \in \mathcal{F}_g \tag{5.78}$$

$$\phi_{pfk} \geq 0 \qquad p \in \mathcal{P},\ f \in \mathcal{F}_p,\ k \in \mathcal{K}^{\mathrm{S}} \tag{5.79}$$

5.5 Multi-period Model

To extend the MAMP to a multi-period model, the planning horizon is divided into time periods and the possibility to choose to hold an end-product inventory between time periods is included. This extension makes the MAMP better able to account for changing demands over time as the model accounts for when a contract must be fulfilled, and decide whether to produce and sell excess end-products or hold them in an inventory for later contracts.

The multi-period model is simplified by only allowing end-products to flow between time periods. The decision at the end of each time period is to sell or keep end-products in stock for future time periods. A series of assumptions are made to model this: the fixed and optional contracts' demands and revenues are defined for each time period. The specifications for the different end-products do not change between time periods. Demand, sales, and procurement prices are considered constant within a time period. The raw material inventory is assumed to be restocked to the initial inventory level for each time period. All of the produced slags are either reused or discarded within the same time period.

A set of time periods must be defined with a corresponding index. The demand, sales and procurement prices, and all of the variables must be indexed on time, and the end-product inventory balance is updated to handle sequential periods. New sets are defined in Table 5.5, new indices are defined in Table 5.6, the updated parameters are listed in Table 5.7, and updated variables used in the new restrictions are defined in Table 5.8. The updated constraints are provided by constraints (5.80) and (5.81). Besides this, every constraint in the single-period formulation must be valid for all time periods and the sum over time periods must be included in all the terms of the objective function. The full multi-period formulation of the MAMP is omitted for readability.

Table 5.5: Definition of sets for the multi-period MAMP.

Set			
$\mathcal{T}$	–	Set of time periods,	$\mathcal{T}$: {1, ..., $\lvert\mathcal{T}\rvert$}

Table 5.6: Definition of indices for the multi-period MAMP.

Index		
t	–	Time period

Table 5.7: Definition of parameters for the multi-period MAMP.

Parameter		
C_{rt}	–	Procurement cost per tonne raw material r in time period t.
D^{F}_{et}	–	Demand for end-product e from fixed contracts in time period t in tonnes.
D^{O}_{et}	–	Demand for end-product e from optional contracts in time period t in tonnes.
R^{F}_{et}	–	Fixed contract revenue per tonne end-product e sold in time period t.
R^{O}_{et}	–	Optional contract revenue per tonne end-product e sold in time period t.

Table 5.8: Definition of variables for the multi-period MAMP.

Variable		
i_{et}	–	Inventory of end-product e at the end of time period t.
x^{E}_{pet}	–	Tonnage of end-product e produced at plant p in time period t.

$$i_{et} \;=\; I^{\mathrm{E}}_{e} \;+\; \sum_{p\in\mathcal{P}} x^{\mathrm{E}}_{pet} \;-\; (g^{\mathrm{F}}_{et} + g^{\mathrm{O}}_{et}) \quad e \in \mathcal{E},\;\; t \in \{1\} \tag{5.80}$$

$$i_{et} \;=\; i_{e,t-1} \;+\; \sum_{p\in\mathcal{P}} x^{\mathrm{E}}_{pet} \;-\; (g^{\mathrm{F}}_{et} + g^{\mathrm{O}}_{et}) \quad e \in \mathcal{E},\;\; t \in \mathcal{T}\backslash\{1\} \tag{5.81}$$

Including the considerations mentioned above and constraints (5.80) - (5.81) completes the formulation of a multi-period model of the MAMP.

Chapter 6

Solution Method

The bilinear constraints in the model formulation in Chapter 5 cannot be solved using a linear solver in their present state. This inability motivates the use of the Multiparametric Disaggregation Technique (MDT), introduced in the literature review in Chapter 4, to linearise the bilinear terms. The global optimum can then be verified by implementing the formulation in a linear solver. This chapter describes the linearisation of the bilinear terms and how to apply this new formulation to verify the global optimum.

New sets, indices, parameters, and variables necessary for the MDT linearisation are introduced in Section 6.1. A general description of how the MDT locates the global optimum is given in Section 6.2. Section 6.3 and Section 6.4 cover the derivation of the linearisation of the lower and upper bound problem, respectively. Section 6.5 describes the algorithm used to verify global optimality. Lastly, Section 6.6 describe different approaches to reduce the computational time.

6.1 Definition of Sets, Indices, Parameters, and Variables

The MDT applied to linearise the bilinear terms in the Manganese Alloy Multi-plant Production problem (MAMP) is based on the descriptions found in *Teles et al. (2013)*, *Teles et al. (2012)*, *Kolodziej et al. (2013b)*, and *Kolodziej et al. (2013a)*. To be able to parameterise and discretise the bilinear constraints, new sets, indices, parameters, and variables have to be defined. These definitions are found in Tables 6.1, 6.2, 6.3, and 6.4, respectively.

Table 6.1: Definition of sets for the MDT.

Set		
$\mathcal{M}$	–	Set of integers, indexed by m
$\mathcal{L}$	–	Set of integers, indexed by l
$\mathbb{Z}$	–	Set of all integers

Table 6.2: Definition of indices for the MDT.

Index		
l	–	Integer in the set $\mathcal{L}$
m	–	Integer in the set $\mathcal{M}$

Table 6.3: Definition of parameters for the MDT.

Parameter		
$\underline{q}_{pf}$	–	Lower bound on the slag produced by furnace f at plant p in tonnes.
$\overline{q}_{pf}$	–	Upper bound on the slag produced by furnace f at plant p in tonnes.
ϵ	–	Optimality gap between the objective value of the lower bound problem and the best bound of the upper bound problem.
$\underline{\sigma}_{pfgh}$	–	Lower bound on the slag sent from furnace f at plant p to furnace h at plant g in tonnes.
$\overline{\sigma}_{pfgh}$	–	Upper bound on the slag sent from furnace f at plant p to furnace h at plant g in tonnes.

Table 6.4: Definition of variables for the MDT.

Variable		
b_{pfghk}	–	The product of $\phi_{pfk}\sigma_{pfgh}$. Represents tonnage of element or oxide k sent from furnace f at plant p to furnace h at plant g.
$\hat{q}_{pfkml}$	–	The disaggregated flow variable of the product $q_{pf}\mu_{pfkml}$.
w_{pfk}	–	The product of $\phi_{pfk}q_{pf}$. Represents tonnage of element or oxide k produced in furnace f at plant p.
Δw_{pfk}	–	Slack variable for the continuous representation of the product $\Delta\phi_{pfk}q_{pf}$.
μ_{pfkml}	–	1 if the decimal power l is active for integer m for element or oxide k in furnace f at plant p, 0 otherwise.
μ'_{pfkml}	–	1 if the decimal power l is active for integer m for element or oxide k in furnace f at plant p, 0 otherwise.
λ_{pfkl}	–	Discretisation variable for use in reformulating ϕ_{pfk}.
$\hat{\sigma}_{pfghkml}$	–	The disaggregated flow variable of the product $\sigma_{pfgh}\mu'_{pfkml}$.
$\Delta\phi_{pfk}$	–	Slack variable for the continuous representation of the discretised variable ϕ_{pfk}.

6.2 The Multiparametric Disaggregation Technique

By applying the MDT, a lower bound problem (LBP) and an upper bound problem (UBP) for the MAMP can be derived, such that the problems are in the form of MILPs. The LBP and UBP can then be solved with increasing accuracy until the global optimality gap ϵ is satisfactory.

As described in *Kolodziej et al. (2013a)*, the LBP solution yields a lower bound for the original problem, denoted $\underline{z} \leq z$, where $\underline{z}$ is the LBP objective value and z is the original problem objective value. When the precision is increased, the LBP and the UBP converge to the same value as $l \to -\infty$ *(Kolodziej et al., 2013a)*.

6.3 The Lower Bound Problem

6.3.1 HC FeMn Furnace - Slag Connection

This section describes the linearisation of constraints (5.13) in Chapter 5 for the LBP formulation. The constraints are reproduced as constraints (6.1) for readability.

$$\phi_{pfk} q_{pf} = M_k \sum_{c \in \mathcal{C}^{\mathrm{S}}} B_{fkc} \alpha_{pfkc} \qquad p \in \mathcal{P},\ f \in \mathcal{F}_p^{\mathrm{FeMn}},\ k \in \mathcal{K}^{\mathrm{S}} \tag{6.1}$$

Of the two variables appearing in the bilinear term, one variable must be parameterised and the other disaggregated *(Teles et al., 2012)*. A continuous variable can be disaggregated into a set of non-negative continuous variables, which can only assume positive values up to the upper bound of the original variable *(Teles et al., 2013)*. The ϕ_{pfk} variables are chosen to be parameterised since they are limited between zero and one, and a given decimal precision. This parametrisation reduces the feasible region of the problem compared to disaggregating ϕ_{pfk} and parameterising the q_{pf} variables instead, which have a range between zero and the maximum amount of slag possible to produce in a furnace.

$$w_{pfk} = \phi_{pfk} q_{pf} \qquad p \in \mathcal{P},\ f \in \mathcal{F}_p^{\mathrm{FeMn}},\ k \in \mathcal{K}^{\mathrm{S}} \tag{6.2}$$

$$\phi_{pfk} = \sum_{l \in \mathbb{Z}} \lambda_{pfkl} \qquad p \in \mathcal{P},\ f \in \mathcal{F}_p^{\mathrm{FeMn}},\ k \in \mathcal{K}^{\mathrm{S}} \tag{6.3}$$

$$\lambda_{pfkl} = \sum_{m=0}^{9} 10^l m \qquad p \in \mathcal{P},\ f \in \mathcal{F}_p^{\mathrm{FeMn}},\ k \in \mathcal{K}^{\mathrm{S}},\ l \in \mathbb{Z} \tag{6.4}$$

Constraints (6.1) contain a nonconvex bilinear term in the form of $\phi_{pfk} q_{pf}$. The bilinear term is precisely represented by (6.2), (6.3), and the disjunction in (6.4) *(Kolodziej et al., 2013a)*. Constraints (6.4) is a result of the fact, that in numerical theory, every real number has possibly an infinite decimal representation *(Teles et al., 2013)*. A number $m \in \{0, ..., 9\}$ is selected for each

power $l \in \mathbb{Z}$. Every $l \in \mathbb{Z}^+$ represents the integral part of the number, while $l \in \mathbb{Z}^-$ represents the decimal part. The disjunction is based on a basis of 10 to represent the decimal system. Also, the disjunction is defined over the domain of all integers; thus an infinite number of disjunctions is theoretically possible. For practical reasons, however, the disjunction is defined over a finite domain $l \in \mathcal{L} = \{j, j+1, ..., |\mathcal{L}|\}$, where j is the position of the last digit desired. If a precision of two decimal numbers is desired, then j = (-2). The variables ϕ_{pfk} are discretised through the disjunction given in (6.4). This discretisation leads to a continuous, but approximate representation of (6.2).

$$\lambda_{pfkl} = \sum_{m \in \mathcal{M}} 10^l m \cdot \mu_{pfkml} \qquad p \in \mathcal{P},\ f \in \mathcal{F}_p^{\text{FeMn}},\ k \in \mathcal{K}^{\text{S}},\ l \in \mathcal{L} \tag{6.5}$$

$$\sum_{m \in \mathcal{M}} \mu_{pfkml} = 1 \qquad p \in \mathcal{P},\ f \in \mathcal{F}_p^{\text{FeMn}},\ k \in \mathcal{K}^{\text{S}},\ l \in \mathcal{L} \tag{6.6}$$

$$\mu_{pfkml} \in \{0,1\} \qquad p \in \mathcal{P},\ f \in \mathcal{F}_p^{\text{FeMn}},\ k \in \mathcal{K}^{\text{S}},\ m \in M,\ l \in \mathcal{L} \tag{6.7}$$

After a convex hull reformulation of the disjunction given in (6.4), the disaggregated variables are introduced in (6.5) - (6.7) *(Kolodziej et al., 2013a)*.

$$\phi_{pfk} = \sum_{l \in \mathcal{L}} \sum_{m \in \mathcal{M}} 10^l m \cdot \mu_{pfkml} \qquad p \in \mathcal{P},\ f \in \mathcal{F}_p^{\text{FeMn}},\ k \in \mathcal{K}^{\text{S}} \tag{6.8}$$

Substituting (6.5) into (6.3), results in (6.8). In (6.8), the variables ϕ_{pfk} are fully parameterised, and the correct representation of the original variables is ensured.

$$w_{pfk} = \left[\sum_{l \in \mathcal{L}} \sum_{m \in \mathcal{M}} 10^l m \cdot \mu_{pfkml}\right] \cdot q_{pf} \qquad p \in \mathcal{P},\ f \in \mathcal{F}_p^{\text{FeMn}},\ k \in \mathcal{K}^{\text{S}} \tag{6.9}$$

Substituting the term for ϕ_{pfk} from (6.8) into (6.2) yields (6.9) and transforms the problem from an NLP to an MINLP.

$$\hat{q}_{pfkml} = q_{pf}\mu_{pfkml} \qquad p \in \mathcal{P},\ f \in \mathcal{F}_p^{\text{FeMn}},\ k \in \mathcal{K}^{\text{S}},\ m \in M,\ l \in \mathcal{L} \tag{6.10}$$

$$q_{pf} \sum_{m \in \mathcal{M}} \mu_{pfkml} = q_{pf} \qquad p \in \mathcal{P},\ f \in \mathcal{F}_p^{\text{FeMn}},\ k \in \mathcal{K}^{\text{S}},\ l \in \mathcal{L} \tag{6.11}$$

$$q_{pf} = \sum_{m \in \mathcal{M}} \hat{q}_{pfkml} \qquad p \in \mathcal{P},\ f \in \mathcal{F}_p^{\text{FeMn}},\ k \in \mathcal{K}^{\text{S}},\ l \in \mathcal{L} \tag{6.12}$$

The mixed integer nonlinear term $q_{pf}\mu_{pfkml}$ is substituted by the variables in (6.10) to transform the formulation into an MILP. Multiplying (6.6) by q_{pf} yields (6.11). Substituting (6.10) into (6.11) gives the relationship between q_{pf} and the disaggregated variables $\hat{q}_{pfkml}$, provided by (6.12).

$$\hat{q}_{pfkml} \geq \underline{q}_{pf}\mu_{pfkml} \qquad p \in \mathcal{P},\ f \in \mathcal{F}_p^{\text{FeMn}},\ k \in \mathcal{K}^{\text{S}},\ m \in M,\ l \in \mathcal{L} \tag{6.13}$$

$$\hat{q}_{pfkml} \leq \overline{q}_{pf}\mu_{pfkml} \qquad p \in \mathcal{P},\ f \in \mathcal{F}_p^{\text{FeMn}},\ k \in \mathcal{K}^{\text{S}},\ m \in M,\ l \in \mathcal{L} \tag{6.14}$$

μ_{pfkml} is a binary variable, meaning the term $\phi_{pfk}\mu_{pfkml}$ is zero if μ_{pfkml} is equal to zero, and ϕ_{pfk} if μ_{pfkml} is equal to one. None of the variables are negative. Thus, $\underline{q}_{pf}$ and $\overline{q}_{pf}$ are non-negative, resulting in the upper and lower bounds given by (6.13) and (6.14).

$$w_{pfk} = \sum_{l\in\mathcal{L}}\sum_{m\in\mathcal{M}} 10^l m \cdot \hat{q}_{pfkml} \qquad p \in \mathcal{P},\ f \in \mathcal{F}_p^{\text{FeMn}},\ k \in \mathcal{K}^{\text{S}} \tag{6.15}$$

Substituting $q_{pf}\mu_{pfkml}$ by $\hat{q}_{pfkml}$ in (6.9) results in (6.15).

This substitution completes the lower bound linearisation of the bilinear term in constraints (6.1), and it is an exact representation of the original term *(Kolodziej et al., 2013a)*. The bilinear term in (6.1) is substituted by w_{pfk} from (6.2). The linearisation is then given by constraints (6.6) - (6.8) and (6.12) - (6.15).

6.3.2 MC SiMn Furnace - Slag Connection

This section describes the linearisation of constraints (5.15) in Chapter 5 for the LBP formulation. The constraints are reproduced as constraints (6.16) for readability.

$$\sum_{p\in\mathcal{P}}\sum_{f\in\mathcal{F}_p^{\text{FeMn}}} \phi_{pfk}\sigma_{pfgh} = M_k \sum_{c\in\mathcal{C}^{\text{S}}} n_{ghkcv} \qquad \begin{array}{l} g \in \mathcal{P},\ h \in \mathcal{F}_g^{\text{SiMn}}, \\ k \in \mathcal{K}^{\text{S}},\ v \in \{\text{SLAG}\} \end{array} \tag{6.16}$$

Constraints (6.16) are linearised using the same procedure as applied to constraints (6.1) in the previous section, resulting in the following substitution and constraints:

$$b_{pfghk} = \phi_{pfk}\sigma_{pfgh} \qquad p \in \mathcal{P},\ f \in \mathcal{F}_p^{\text{FeMn}},\ g \in \mathcal{P},\ h \in \mathcal{F}_g^{\text{SiMn}},\ k \in \mathcal{K}^{\text{S}} \tag{6.17}$$

$$b_{pfghk} = \sum_{l\in\mathcal{L}}\sum_{m\in\mathcal{M}} 10^l m \cdot \hat{\sigma}_{pfghkml} \qquad \begin{array}{l} p \in \mathcal{P},\ f \in \mathcal{F}_p^{\text{FeMn}},\ g \in \mathcal{P}, \\ h \in \mathcal{F}_g^{\text{SiMn}},\ k \in \mathcal{K}^{\text{S}} \end{array} \tag{6.18}$$

$$\phi_{pfk} = \sum_{l\in\mathcal{L}}\sum_{m\in\mathcal{M}} 10^l m\cdot\mu'_{pfkml} \qquad p\in\mathcal{P},\ f\in\mathcal{F}_p^{\text{FeMn}},\ k\in\mathcal{K}^{\text{S}} \tag{6.19}$$

$$\sigma_{pfgh} = \sum_{m\in\mathcal{M}} \hat{\sigma}_{pfghkml} \qquad p\in\mathcal{P},\ f\in\mathcal{F}_p^{\text{FeMn}},\ g\in\mathcal{P},\ h\in\mathcal{F}_g^{\text{SiMn}},\ k\in\mathcal{K}^{\text{S}},\ l\in\mathcal{L} \tag{6.20}$$

$$\hat{\sigma}_{pfghkml} \geq \underline{\sigma}_{pfgh}\mu'_{pfkml} \qquad p\in\mathcal{P},\ f\in\mathcal{F}_p^{\text{FeMn}},\ g\in\mathcal{P},\ h\in\mathcal{F}_g^{\text{SiMn}},\ k\in\mathcal{K}^{\text{S}},\ m\in M,\ l\in\mathcal{L} \tag{6.21}$$

$$\hat{\sigma}_{pfghkml} \leq \overline{\sigma}_{pfgh}\mu'_{pfkml} \qquad p\in\mathcal{P},\ f\in\mathcal{F}_p^{\text{FeMn}},\ g\in\mathcal{P},\ h\in\mathcal{F}_g^{\text{SiMn}},\ k\in\mathcal{K}^{\text{S}},\ m\in M,\ l\in\mathcal{L} \tag{6.22}$$

$$\sum_{m\in\mathcal{M}} \mu'_{pfkml} = 1 \qquad p\in\mathcal{P},\ f\in\mathcal{F}_p^{\text{FeMn}},\ k\in\mathcal{K}^{\text{S}},\ l\in\mathcal{L} \tag{6.23}$$

$$\mu'_{pfkml}\in\{0,1\} \qquad p\in\mathcal{P},\ f\in\mathcal{F}_p^{\text{FeMn}},\ k\in\mathcal{K}^{\text{S}},\ m\in M,\ l\in\mathcal{L} \tag{6.24}$$

These constraints complete the lower bound linearisation of the bilinear term in constraints (6.16) and the linearisation is an exact representation of the original term. The linearisation is given by (6.18) - (6.24). Implementing the linearisations of constraints (6.1) and (6.16) in the MAMP formulation yields the LBP formulation.

6.4 The Upper Bound Problem

6.4.1 HC FeMn Furnace - Slag Connection

This section describes the linearisation of constraints (6.1) for the UBP formulation. The same derivation as for the LBP is used, but with the inclusion of slack variables, leading to a continuous representation of the discretised variables.

$$w_{pfk} = \phi_{pfk}q_{pf} \qquad p\in\mathcal{P},\ f\in\mathcal{F}_p^{\text{FeMn}},\ k\in\mathcal{K}^{\text{S}} \tag{6.25}$$

$$\phi_{pfk} = \sum_{l\in\mathcal{L}}\sum_{m\in\mathcal{M}} 10^l m\cdot\mu_{pfkml} + \Delta\phi_{pfk} \qquad p\in\mathcal{P},\ f\in\mathcal{F}_p^{\text{FeMn}},\ k\in\mathcal{K}^{\text{S}} \tag{6.26}$$

$$w_{pfk} = \left(\sum_{l \in \mathcal{L}} \sum_{m \in \mathcal{M}} 10^l m \cdot \mu_{pfkml} + \Delta\phi_{pfk} \right) \cdot q_{pf} \tag{6.27a}$$

$$w_{pfk} = \sum_{l \in \mathcal{L}} \sum_{m \in \mathcal{M}} 10^l m \cdot \hat{q}_{pfkml} + \Delta\phi_{pfk} \cdot q_{pf} \tag{6.27b}$$

$$w_{pfk} = \sum_{l \in \mathcal{L}} \sum_{m \in \mathcal{M}} 10^l m \cdot \hat{q}_{pfkml} + \Delta w_{pfk} \qquad p \in \mathcal{P},\ f \in \mathcal{F}_p^{\text{FeMn}},\ k \in \mathcal{K}^{\text{S}} \tag{6.28}$$

Substituting the parametrisation of ϕ_{pfk} in (6.26) into (6.25), gives (6.27a). Using the substitution from (6.10) and realising that $\Delta\phi_{pfk} \cdot q_{pf} = \Delta w_{pfk}$ in (6.27b), results in (6.28).

$$q_{pf} = \sum_{m \in \mathcal{M}} \hat{q}_{pfkml} \qquad p \in \mathcal{P},\ f \in \mathcal{F}_p^{\text{FeMn}},\ k \in \mathcal{K}^{\text{S}},\ l \in \mathcal{L} \tag{6.29}$$

$$\sum_{m \in \mathcal{M}} \mu_{pfkml} = 1 \qquad p \in \mathcal{P},\ f \in \mathcal{F}_p^{\text{FeMn}},\ k \in \mathcal{K}^{\text{S}},\ l \in \mathcal{L} \tag{6.30}$$

$$\mu_{pfkml} \in \{0,1\} \qquad p \in \mathcal{P},\ f \in \mathcal{F}_p^{\text{FeMn}},\ k \in \mathcal{K}^{\text{S}},\ m \in M,\ l \in \mathcal{L} \tag{6.31}$$

$$\hat{q}_{pfkml} \geq \underline{q}_{pf} \mu_{pfkml} \qquad p \in \mathcal{P},\ f \in \mathcal{F}_p^{\text{FeMn}},\ k \in \mathcal{K}^{\text{S}},\ m \in M,\ l \in \mathcal{L} \tag{6.32}$$

$$\hat{q}_{pfkml} \leq \overline{q}_{pf} \mu_{pfkml} \qquad p \in \mathcal{P},\ f \in \mathcal{F}_p^{\text{FeMn}},\ k \in \mathcal{K}^{\text{S}},\ m \in M,\ l \in \mathcal{L} \tag{6.33}$$

Constraints (6.25) - (6.26) and (6.28) - (6.33) are identical to the lower bound formulation, except that the slack variables $\Delta\phi_{pfk}$ and Δw_{pfk} are introduced in (6.26) and (6.28), respectively. The slack variables lead to a continuous representation of the discretised variables as the gap that exists between discretisation points for a finite l is eliminated *(Kolodziej et al., 2013a)*.

$$\Delta w_{pfk} \geq \underline{q}_{pf} \Delta\phi_{pfk} \qquad p \in \mathcal{P},\ f \in \mathcal{F}_p^{\text{FeMn}},\ k \in \mathcal{K}^{\text{S}} \tag{6.34}$$

$$\Delta w_{pfk} \leq \overline{q}_{pf} \Delta\phi_{pfk} \qquad p \in \mathcal{P},\ f \in \mathcal{F}_p^{\text{FeMn}},\ k \in \mathcal{K}^{\text{S}} \tag{6.35}$$

$$\Delta w_{pfk} \geq (q_{pf} - \overline{q}_{pf}) 10^j + \overline{q}_{pf} \Delta\phi_{pfk} \qquad p \in \mathcal{P},\ f \in \mathcal{F}_p^{\text{FeMn}},\ k \in \mathcal{K}^{\text{S}} \tag{6.36}$$

$$\Delta w_{pfk} \;\leq\; (q_{pf} \;-\; \underline{q}_{pf})10^{j} \;+\; \underline{q}_{pf}\Delta\phi_{pfk} \qquad p \in \mathcal{P},\;\; f \in \mathcal{F}_p^{\text{FeMn}},\;\; k \in \mathcal{K}^{\text{S}} \tag{6.37}$$

Constraints (6.34) - (6.37) are the McCormick envelopes relaxing the slack variables Δw_{pfk} that replaces the quadratic term $\Delta\phi_{pfk} \cdot q_{pf}$ in (6.27b), as done in *Kolodziej et al. (2013a)*. Note that j denotes the first element in $\mathcal{L}$.

$$\Delta\phi_{pfk} \;\geq\; 0 \qquad p \in \mathcal{P},\;\; f \in \mathcal{F}_p^{\text{FeMn}},\;\; k \in \mathcal{K}^{\text{S}} \tag{6.38}$$

$$\Delta\phi_{pfk} \;\leq\; 10^{j} \qquad p \in \mathcal{P},\;\; f \in \mathcal{F}_p^{\text{FeMn}},\;\; k \in \mathcal{K}^{\text{S}} \tag{6.39}$$

The slack variables are bounded by the gap between the discretisation points; thus constraints (6.38) and (6.39) must be included in the formulation *(Kolodziej et al., 2013a)*. The linearisation is then given by (6.26) and (6.28) - (6.39).

6.4.2 MC SiMn Furnace - Slag Connection

This section describes the linearisation of constraints (6.16) for the UBP formulation. The constraints are linearised using the same procedure as for the linearisation in Section 6.4.1, but with the introduction of slack variables to create a continuous representation of the discretised variables. This results in the following substitution and constraints:

$$b_{pfghk} \;=\; \phi_{pfk}\sigma_{pfgh} \qquad p \in \mathcal{P},\;\; f \in \mathcal{F}_p^{\text{FeMn}},\;\; g \in \mathcal{P},\;\; h \in \mathcal{F}_g^{\text{SiMn}},\;\; k \in \mathcal{K}^{\text{S}} \tag{6.40}$$

$$b_{pfghk} \;=\; \sum_{l\in\mathcal{L}}\sum_{m\in\mathcal{M}} 10^{l} m \cdot \hat{\sigma}_{pfghkml} \;+\; \Delta b_{pfghk} \qquad \begin{array}{l} p \in \mathcal{P},\;\; f \in \mathcal{F}_p^{\text{FeMn}}, \\ g \in \mathcal{P},\;\; h \in \mathcal{F}_g^{\text{SiMn}},\;\; k \in \mathcal{K}^{\text{S}} \end{array} \tag{6.41}$$

$$\phi_{pfk} \;=\; \sum_{l\in\mathcal{L}}\sum_{m\in\mathcal{M}} 10^{l} m \cdot \mu'_{pfkml} \;+\; \Delta\phi_{pfk} \qquad p \in \mathcal{P},\;\; f \in \mathcal{F}_p^{\text{FeMn}},\;\; k \in \mathcal{K}^{\text{S}} \tag{6.42}$$

$$\sigma_{pfgh} \;=\; \sum_{m\in\mathcal{M}} \hat{\sigma}_{pfghkml} \qquad \begin{array}{l} p \in \mathcal{P},\;\; f \in \mathcal{F}_p^{\text{FeMn}},\;\; g \in \mathcal{P}, \\ h \in \mathcal{F}_g^{\text{SiMn}},\;\; k \in \mathcal{K}^{\text{S}},\;\; l \in \mathcal{L} \end{array} \tag{6.43}$$

$$\sum_{m \in \mathcal{M}} \mu'_{pfkml} = 1 \qquad p \in \mathcal{P},\ f \in \mathcal{F}_p^{\text{FeMn}},\ k \in \mathcal{K}^{\text{S}},\ l \in \mathcal{L} \tag{6.44}$$

$$\mu'_{pfkml} \in \{0,1\} \qquad p \in \mathcal{P},\ f \in \mathcal{F}_p^{\text{FeMn}},\ k \in \mathcal{K}^{\text{S}},\ m \in M,\ l \in \mathcal{L} \tag{6.45}$$

$$\hat{\sigma}_{pfghkml} \geq \underline{\sigma}_{pfgh}\mu'_{pfkml} \qquad \begin{array}{r} p \in \mathcal{P},\ f \in \mathcal{F}_p^{\text{FeMn}},\ g \in \mathcal{P}, \\ h \in \mathcal{F}_g^{\text{SiMn}},\ k \in \mathcal{K}^{\text{S}},\ m \in \mathcal{M},\ l \in \mathcal{L} \end{array} \tag{6.46}$$

$$\hat{\sigma}_{pfghkml} \leq \overline{\sigma}_{pfgh}\mu'_{pfkml} \qquad \begin{array}{r} p \in \mathcal{P},\ f \in \mathcal{F}_p^{\text{FeMn}},\ g \in \mathcal{P}, \\ h \in \mathcal{F}_g^{\text{SiMn}},\ k \in \mathcal{K}^{\text{S}},\ m \in \mathcal{M},\ l \in \mathcal{L} \end{array} \tag{6.47}$$

$$\Delta b_{pfghk} \geq \underline{\sigma}_{pfgh}\Delta\phi_{pfk} \qquad p \in \mathcal{P},\ f \in \mathcal{F}_p^{\text{FeMn}},\ g \in \mathcal{P},\ h \in \mathcal{F}_g^{\text{SiMn}},\ k \in \mathcal{K}^{\text{S}} \tag{6.48}$$

$$\Delta b_{pfghk} \leq \overline{\sigma}_{pfgh}\Delta\phi_{pfk} \qquad p \in \mathcal{P},\ f \in \mathcal{F}_p^{\text{FeMn}},\ g \in \mathcal{P},\ h \in \mathcal{F}_g^{\text{SiMn}},\ k \in \mathcal{K}^{\text{S}} \tag{6.49}$$

$$\Delta b_{pfghk} \geq (\sigma_{pfgh} - \overline{\sigma}_{pfgh})10^j + \overline{\sigma}_{pfgh}\Delta\phi_{pfk} \qquad \begin{array}{r} p \in \mathcal{P},\ f \in \mathcal{F}_p^{\text{FeMn}}, \\ g \in \mathcal{P},\ h \in \mathcal{F}_g^{\text{SiMn}},\ k \in \mathcal{K}^{\text{S}} \end{array} \tag{6.50}$$

$$\Delta b_{pfghk} \leq (\sigma_{pfgh} - \underline{\sigma}_{pfgh})10^j + \underline{\sigma}_{pfgh}\Delta\phi_{pfk} \qquad \begin{array}{r} p \in \mathcal{P},\ f \in \mathcal{F}_p^{\text{FeMn}}, \\ g \in \mathcal{P},\ h \in \mathcal{F}_g^{\text{SiMn}},\ k \in \mathcal{K}^{\text{S}} \end{array} \tag{6.51}$$

$$\Delta\phi_{pfk} \geq 0 \qquad p \in \mathcal{P},\ f \in \mathcal{F}_p^{\text{FeMn}},\ k \in \mathcal{K}^{\text{S}} \tag{6.52}$$

$$\Delta\phi_{pfk} \leq 10^j \qquad p \in \mathcal{P},\ f \in \mathcal{F}_p^{\text{FeMn}},\ k \in \mathcal{K}^{\text{S}} \tag{6.53}$$

These constraints complete the upper bound linearisation of the bilinear term in constraints (6.16). The linearisation is given by (6.41) - (6.53). Implementing the linearisations of constraints (6.1) and (6.16) in the MAMP formulation yields the UBP formulation.

6.5 The Global Optimality Algorithm

An algorithm is applied to verify that the global optimum is found. The algorithm initiates with a coarse discretisation and solves both the LBP and UBP. If the difference between the LBP objective value and the UBP best bound is less than a given global optimality gap ϵ, the program ends, if not, the precision is increased, and the problems are resolved *(Kolodziej et al., 2013a)*. The algorithm is more formally presented in Algorithm 1. It is inspired by the algorithm presented in *Kolodziej et al. (2013a)*.

Algorithm 1 Algorithm for verifying global optimum.

1: **procedure** VERIFYGLOBALOPTIMUM
2: Select solution gap for the LBP and UBP
3: Select $j = \mathcal{L} = \lfloor \log_{10} \overline{\phi}_{pfk} \rfloor$
4: Solve the LBP to find the solution $\underline{z}$
5: Solve the UBP to find the best bound $\hat{z}$
6: **if** $\underline{z}$ is infeasible **then**
7: Let $\underline{z} = -\infty$
8: **if** $\left| \frac{\hat{z} - \underline{z}}{\underline{z}} \right| \leq \epsilon$ **then**
9: **stop**, solution $\underline{z}$ is global optimum
10: **else**
11: set $j = j - 1$, return to step 4

There may be infeasibilities in the discretised problem even if the original problem is feasible. To avoid this, j and $|\mathcal{L}|$ have to be chosen appropriately. There are some general guidelines to help ensure precision based feasibility. The highest power of 10 ($\mathcal{L}$) must be large enough to ensure that 10^j is of the same order of magnitude as the upper bound on ϕ_{pfk}, given as $\mathcal{L} = \lfloor \log_{10} \overline{\phi}_{pfk} \rfloor$. Also, j need to be sufficiently small to ensure that at least one discretisation point is located between the upper and lower bounds for ϕ_{pfk}, meaning $j \leq |\mathcal{L}|$ is the minimum requirement. Feasibility is more likely as j decreases since this results in increased precision. The guidelines do not guarantee feasibility of the LBP and UBP in all cases but represent the minimum precision level required to have reasonable bounds on ϕ_{pfk} *(Kolodziej et al., 2013a)*.

6.6 Decreasing the Computational Time

The water-using network design problem studied by *Kolodziej et al. (2013a)* shows that finding the global optimal solution can involve significant computational time. It is reasonable to believe that computational time is significant for the MAMP as well, therefore, different approaches to reduce the computational time is presented. The feasible region of the MAMP can be unnecessary large due to symmetry in the problem, for instance as a result of homogeneous furnaces. Elimination of potential symmetry in the problem can yield the same solution in a shorter time.

6.6.1 Merging Identical Furnaces

One approach to remove symmetry is to merge furnaces of the same type at the same plant into one larger furnace, thus, reducing the feasible region of the problem by reducing the number of furnaces and slag transportation possibilities. The changes are done in the parameter settings, so they do not have any impact on the mathematical formulation. When using this approach, it is critical to set the correct upper bound on the disaggregated variables q_{pf} and σ_{pfgh} from the MDT, as these parameters impact the computational time and the solution. Illustrations of the furnace setup at each plant before and after the furnace merging for a case of three HC FeMn and four MC SiMn furnaces distributed between three plants are given in Figures 6.1a and 6.1b.

When the furnaces produce only one end-product for each furnace type, it is possible that the optimal slag composition and combination of ores are the same for all furnaces of identical setup. It might, however, lead to the loss of better solutions as a result of fewer slag mixing possibilities. When there are multiple HC FeMn and MC SiMn products to produce, merging furnaces is not an option since each furnace can produce output products of different compositions. Thus, the furnaces must be kept separate in this case. As multiple HC FeMn and MC SiMn end-products are not currently modelled, it is of interest to compare furnace merging with the original setup to see how it affects the solution and the computational time.

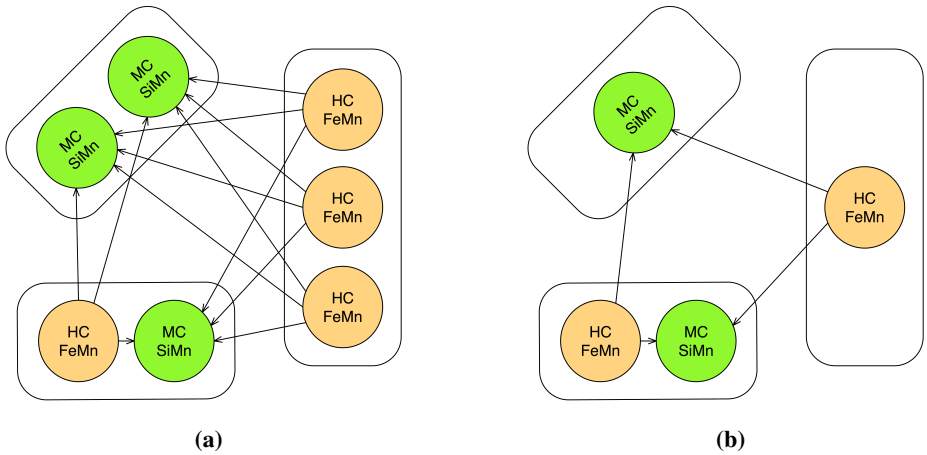

Figure 6.1: **(a)** Plant layouts with original furnace setups. **(b)** Plant layouts with merged furnace setups.

6.6.2 Symmetry Breaking Constraints

Another approach to remove symmetry in the problem is to formulate symmetry breaking constraints. These constraints could prioritise furnaces on the volume of alloy they send to refining or crushing processes, the weight fraction of one oxide in the slag from the furnaces, or the amount of slag chosen to be sent to homogeneous MC SiMn furnaces.

The complicating constraints are the ones involving the slag composition. Eliminating symmetry in this part of the problem can decrease the computational time. This elimination can be done by removing symmetry in one of the three variables present in the complicating constraints: ϕ_{pfk}, q_{pf}, and σ_{pfgh}. Proposed symmetry breaking constraints for these variables are found in (6.54) - (6.56).

$$\phi_{p,f+1,k} \geq \phi_{pfk} \qquad p \in \mathcal{P},\ f \in \mathcal{F}_p^{\text{FeMn}},\ k \in \mathcal{K}^{\text{S}} \tag{6.54}$$

$$q_{p,f+1} \geq q_{pf} \qquad p \in \mathcal{P},\ f \in \mathcal{F}_p^{\text{FeMn}} \tag{6.55}$$

$$\sigma_{pfg,h+1} \geq \sigma_{pfgh} \qquad p \in \mathcal{P},\ f \in \mathcal{F}_p^{\text{FeMn}},\ g \in \mathcal{P},\ h \in \mathcal{F}_p^{\text{SiMn}} \tag{6.56}$$

Adding symmetry breaking constraints may cut away global optimal solutions. The symmetry breaking constraints should optimally not have any effect on the optimal objective value, but a deviation in objective value may be acceptable if the computational time is significantly reduced.

It is also possible to explore if breaking symmetry in other parts of the production might contribute to lower computational times. The constraints considered are provided in (6.57) - (6.58).

$$m_{p,f+1} \geq m_{pf} \qquad p \in \mathcal{P},\ f \in \mathcal{F}_p^{\text{FeMn}} \tag{6.57}$$

$$u_{p,f+1} \geq u_{pf} \qquad p \in \mathcal{P},\ f \in \mathcal{F}_p^{\text{FeMn}} \tag{6.58}$$

Chapter 7

Computational Study

This chapter aims to evaluate the applicability and limitations of the Manganese Alloy Multi-plant Production problem (MAMP) formulation through a computational study. A comparison to actual production data would contribute to the validation of the model. However, it is not possible for us to evaluate the performance of the model against real production configurations and operational results since this is restricted data the authors have been unable to obtain from the industry partner. The computational study, therefore, consists of an extensive evaluation of model performance and economic aspects based on a semi-realistic instance.

A base instance is created to perform the computational study. The layout of the industry partner's plants in Norway has been used as an inspiration to create the base instance, in which different parameters can be varied. It is important to note that some of the parameters are taken from literature on manganese production, some are set by the authors, and that data provided by Eramet Norway is perturbed for confidentiality purposes. These imprecisions may lead to inaccurate costs, revenues, and consumption of raw materials compared to actual values. However, the intention of this computational study is not to accurately depict real production conditions, but rather to evaluate economic aspects of manganese alloy production in relation to variations in different parameters. Also, it is desirable to evaluate if the MAMP formulation can add value to manganese alloy multi-plant production planning when used as a decision support tool.

A description of the MAMP implementation is given in Section 7.1. Section 7.2 presents the base instance used in the computational study. The computational study is separated into a technical and an economic study. The technical study is conducted in Section 7.3 and the economic study in Section 7.4.

7.1 Implementation

The model is written in the algebraic modelling language Mosel and run in FICO® Xpress Optimisation Suite 7.9 using an HP EliteDesk 800 G2 SFF computer with Intel® Core™ i7-6700 3.40 GHz CPU and 32GB RAM. The operating system in use is Windows 10 Education 64-bit. The MAMP is formulated in a manner that requires some of the data provided by the industry partner to be pre-processed in Microsoft Excel before being imported into the optimisation software.

The Multiparametric Disaggregation Technique (MDT) is implemented to be able to solve the problem in the linear solver Xpress. The bilinear terms present in the model formulation must, therefore, be replaced by the variables in the MDT that substitute these terms. The implementation follows Algorithm 1 outlined in Chapter 6. Optimality gaps and maximal run times for the LBP and UBP can be varied, and a global optimality gap ϵ chosen for the main file. The algorithm describes that a precision in the range $\{0, -\infty\}$ is used to solve the pooling problem with the MDT. For practical purposes, values of $\{0, 1\}$ are too course to be able to model the chemical composition of the slag correctly. Producing alloy and slag with precisions of $\{-4, -\infty\}$ is not practically achievable. The algorithm is thus left with the precisions $\{-2, -3\}$.

7.2 Definition of the Base Instance

This section describes the setting of all input parameters. Data not provided by the industry partner have been sought out in literature on manganese alloy production or set to reasonable values by the authors in agreement with the problem owner to simulate realistic instances as closely as possible.

7.2.1 Plants, Furnaces, MORs, and LC SiMn Refining Stations

The base instance used to evaluate the MAMP formulation considers a single time period production. A single time period represents $\Delta T = 30$ days of production. The base instance considers three HC FeMn and four MC SiMn furnaces distributed over three plants, and is named *B1-3Fe4Si*. The plants, furnaces located at each plant, and furnace production setups are given in Table 7.1.

Table 7.1: Plant and furnace layout overview. Plant locations are numbered. Each furnace is numbered and located at a plant. The furnaces are divided into subsets based on the production setup of HC FeMn or MC SiMn for each plant.

Plant p	**Furnace set** F_p	**HC FeMn furnaces in the set** F_p^{FeMn}	**MC SiMn furnaces in the set** F_p^{SiMn}
1 Porsgrunn	{1, 2}	{1}	{2}
2 Kvinesdal	{3, 4, 5}		{3, 4, 5}
3 Sauda	{6, 7}	{6, 7}	

Each furnace is set to have a pre-reduction of 22%, as used in *Olsen et al. (2007)*, thus $\Upsilon = 0.22$. Each furnace loses 35% of the heat to the surroundings, thus $L^{\text{H}} = 1.35$. Alloy production companies often have lucrative electricity price agreements, therefore, the electricity price is set to $C^{\text{E}} = 0.00118$ USD/kWh. The mass and electrical power capacities of each furnace are listed in Table 7.2. The electrical power capacity is based on information about the furnaces at the industry partner's plants, and the mass capacity is set proportionally to this. In practice, it usually is the electrical power that limits furnace capacity. Each plant has, in addition to the furnaces, MOR and LC SiMn refining station capabilities. The input capacities for these are set sufficiently high not to be the limiting factors in the base instance.

Table 7.2: Furnace mass and electrical power capacity. Mass capacity given in tonnes. Power capacity given in kW.

Plant p	**Furnace** f	**Mass Capacity** Q_{pf}	**Power Capacity** P_{pf}
1 Porsgrunn	1	1 000	40 000
1 Porsgrunn	2	750	30 000
2 Kvinesdal	3	750	30 000
2 Kvinesdal	4	750	30 000
2 Kvinesdal	5	750	30 000
3 Sauda	6	1 000	40 000
3 Sauda	7	1 000	40 000

The feed limit for each type of undersized lumps is given as a weight fraction of the raw material feed to the furnaces, or the liquid alloy feed to the MOR and LC SiMn refining station. The weight fractions are presented in Table 7.3 and are based on values found in *Olsen et al. (2007)*.

Table 7.3: Undersized lump feed limit for different process stages. The feed is given as a weight fraction of the total raw materials feed to the furnaces, or liquid metal feed to the MOR or LC SiMn refining station.

Process stage	**Parameter**	**Undersized lump feed limit**
Furnace	Ψ^{UL}	0.10
MOR	Ψ^{MFeL}	0.10
LC SiMn refining station	Ψ^{LSiL}	0.10

7.2.2 End-products, By-products, and Slag

The plants produce one or more of the end-products listed in Table 7.4. The demands and revenues of fixed and optional contracts for the various end-products are also provided in this table. The fixed revenues have been obtained from the industry partner and are perturbed, while the revenues from optional contracts are set 5% higher than the fixed contract revenues. The authors have estimated the fixed demand based on that the demand for refined alloys is increasing *(Olsen et al., 2007)*. The demand is given as a total demand per end-product for the production period. The cumulative end-product demand is set greater than the total furnace capacity, as the authors assume that there are enough contracts available in the market to maximise production. This assumption is valid, as the furnaces always produce at maximum capacity in practice. The production is thus limited by the mass and electrical power capacity of the furnaces. The initial inventory of end-products is set to zero in the base instance. The choice of optional contracts to accept visualises which products are the most profitable since these are produced after the fixed demand is met.

Table 7.4: End-products with demands and revenues for fixed and optional contracts. Demand is given in tonnes, revenue in USD/tonne.

End-product e	**Demand** D_e^{F}	**Revenue** R_e^{F}	**Demand** D_e^{O}	**Revenue** R_e^{O}
HC FeMn	13500	771	6000	810
MC FeMn	15000	899	6000	944
MC SiMn	10500	783	6000	822
LC SiMn	12000	853	6000	896

Each end-product is produced to satisfy certain content specifications. Explicit specifications are only set for the contents of HC FeMn and MC SiMn, as these products are made in the furnaces where the chemical composition is modelled. Correct content specifications of MC FeMn and LC SiMn are given implicitly by predetermined parameters. The calculations to find these parameters are given in Appendix B. MC FeMn and LC SiMn have lower carbon contents than HC FeMn and MC SiMn, respectively. The weight percentage of every other constituent in MC FeMn and LC SiMn changes proportionally to the reduction of carbon as a result of the altered composition. The content specifications used in the base instance are listed in Table 7.5 and are obtained from *Olsen et al. (2007)*. Notice that each end-product composition sum up to 1.00.

Table 7.5: End-product compositions for metals exiting the furnace. Given as weight fractions of the total element or oxide content. Notice that the composition sums to 1.00 to ensure correct mass balances.

		Element or Oxide k			
End-product e	**Parameter**	**Mn**	**Fe**	**Si**	**C**
HC FeMn	Ψ_k^{FeMn}	0.790	0.136	0.004	0.070
MC SiMn	Ψ_k^{SiMn}	0.712	0.081	0.192	0.015

The mass output of slag is related to the total output of metal in an HC FeMn furnace. The maximum value is set to $\overline{\Lambda} = 1.0$ and the minimum value $\underline{\Lambda} = 0.5$. The slag exiting the HC FeMn furnaces has set quality specification intervals for oxides with metal-bearing capabilities. The upper and lower bound on the slag quality are defined by the parameters $\overline{\Phi}_k$ and $\underline{\Phi}_k$ and are given in Table 7.6 for the oxides $k \in K^S$. These values can be varied to test how different interval-ranges affect the solution and solution time. As stated in Section 2.4.2 of Chapter 2, the MnO content in the slag can vary in the range 30 - 50% for the duplex production method. The remaining intervals are set based on information provided by the industrial partner.

Table 7.6: Slag composition upper and lower bounds. Given in weight fractions of the total slag content.

		Element or Oxide k					
Product	**Parameter**	**MnO**	**FeO**	**SiO_2**	**Al_2O_3**	**MgO**	**CaO**
FeMn Slag Upper	$\overline{\Phi}_k$	0.50	0.02	0.35	0.20	0.20	0.30
FeMn Slag Lower	$\underline{\Phi}_k$	0.30	0.00	0.15	0.10	0.05	0.10

At every stage of the production, except at the LC SiMn refining station, by-products are produced as a fixed amount of the total feed to the process stage. The process stages, associated parameters, and parameter values used in the base instance are listed in Table 7.7 for the respective by-products. Values are based on those found in *Olsen et al. (2007)*. Al_2O_3, MgO, and CaO completely exit the MC SiMn furnace as slag dump.

Table 7.7: By-product yield from each process stage. Given as weight fractions of the total feed to the process.

Process stage	Parameter	By-product b	Weight Fraction for Element or Oxide k
HC FeMn furnace	Ψ^{B}_{fbk}	HC FeMn dust	0.02
MC SiMn furnace	Ψ^{B}_{fbk}	MC SiMn dust	0.02
MC SiMn furnace	Ψ^{B}_{fbk}	MC SiMn slag	1.00 for {Al_2O_3,MgO, CaO}, 0.10 for others
MOR	Ψ^{MOR}_{b}	MOR dust	0.08
Crushing	$\Psi^{\mathrm{CRUSH}}_{b}$	HC FeMn lumps	0.10
Crushing	$\Psi^{\mathrm{CRUSH}}_{b}$	MC FeMn lumps	0.10
Crushing	$\Psi^{\mathrm{CRUSH}}_{b}$	MC SiMn lumps	0.10
Crushing	$\Psi^{\mathrm{CRUSH}}_{b}$	LC SiMn lumps	0.10

7.2.3 Raw Materials and Refining Resources

A set of 19 raw materials is at disposal at each plant. These raw materials contain elements and oxides of various concentrations. Oxygen, silicon waste, and MC FeMn and LC SiMn undersized lumps, named refining resources for simplicity, are separated from the raw materials since these feed other processes than the furnace process. The inventories are assumed to be large enough to satisfy any demand, as the bottleneck of the production is the furnace mass and power capacity.

By industry practice, raw material content data is obtained through an ore content analysis which output is the total percentage of each pure element in the raw material. The data is modified in Microsoft Excel to obtain the correct weight fractions for all the elements and oxides in the raw materials to be compatible with the input data the MAMP requires. The content in each raw material is listed in Appendix D. Note that the data is perturbed.

7.2.4 Raw Material Costs, Discard Costs, and Slag Transportation Costs

Raw material procurement costs provided by the industrial partner are perturbed and can be found in Table 7.8. Refining resource costs are listed in Table 7.9 and are set low in agreement with the problem owner. There are also discard costs and revenues associated with the production of discardable and saleable by-products and transportation costs for transporting slag between furnaces. Discard costs and revenues for the respective by-products are listed in Table 7.10. The authors have been unsuccessful in obtaining accurate costs for discarding by-products, but have been informed by the problem owner that these can be assumed to be low compared to the raw material costs.

Table 7.8: Raw material procurement costs. Given in USD/tonne.

Raw material r	**Cost** C_r	**Raw material** r	**Cost** C_r	**Raw material** r	**Cost** C_r	**Raw material** r	**Cost** C_r
Ore 1	63.4	Ore 2	51.2	Ore 3	80.3	Ore 4	76.2
Ore 5	113.5	Ore 6	107.2	Ore 7	82.5	Ore 8	149.8
Ore 9	127.0	Ore 10	116.7	Coke 11	108.6	Coke 12	106.2
Coke 13	110.3	Flux 14	100.2	Flux 15	38.4	Flux 16	90.1
HC FeMn lumps	0.00	MC SiMn lumps	0.00	Quartz 19	61.6		

Table 7.9: Refining resource costs. Given in USD/tonne.

Refining resource	**Parameter**	**Cost**	**Refining resource**	**Parameter**	**Cost**
Oxygen	C^{O}	5	Silicon waste	C^{SiW}	5
MC FeMn lumps	C^{MFeL}	11	LC SiMn lumps	C^{LSiL}	15
Slag	C^{S}	150			

Table 7.10: By-product revenues and costs. Given in USD/tonne.

By-product b	**Revenue** R_b^{B}
MOR dust	50
HC FeMn dust	-10
MC SiMn slag	-10
MC SiMn dust	-10

Estimated slag transportation costs between plants are listed in Table 7.11. The transportation costs obtained from the industrial partner are from one of Eramet Norway's plants to another. The authors have been unable to obtain information about which plants the transportation cost applies. It has, therefore, been used as the cost for the shortest transportation route. For convenience, the transportation costs between other plants have been set proportional to the cost provided based on distance in kilometres.

Table 7.11: Slag transportation costs between plants. Distance given in kilometres, transportation costs in USD/tonne.

Plant p	**Plant** g	**Distance**	**Transportation cost** C_{pg}^{T}
1 Porsgrunn	2 Kvinesdal	300	8.4
1 Porsgrunn	3 Sauda	500	14.0
2 Kvinesdal	3 Sauda	150	4.2

7.2.5 MDT Parameters

The MDT defines two parameters it is crucial to determine correctly, namely $\overline{\sigma}_{pfgh}$ and $\overline{q}_{pf}$. These parameters greatly affect the run time and should be set as tight as possible. The parameters represent the upper bound on shipped and produced slag in an HC FeMn furnace. They are limited by the total amount of alloy a furnace can produce per day and the slag-to-metal ratio's lower and upper bound. The parameters are easily scaled by multiplying by ΔT. For the HC FeMn furnace mass and power capacities defined in *B1-3Fe4Si*, suitable values are found to be $\overline{\sigma}_{pfgh} = \overline{q}_{pf} = 500\Delta T$, to not be a limiting factor. The MDT parameters $\underline{\sigma}_{pfgh}$ and $\underline{q}_{pf}$ are set to zero as the HC FeMn furnace possibly can produce zero output.

7.2.6 Multiple Time Periods

The end-product inventories are assumed to be sufficiently large to hold any volume of end-products. Unit holding cost for all inventories is set to $C^{\mathrm{H}} = 2$ USD/tonne per time period. The multi-period instances are defined in Table 7.12. The first period in each instance has demands and revenues as defined in the base instance *B1-3Fe4Si* in Table 7.4. The decrease or increase in end-product demand and revenues are then based on these values for the subsequent time periods. All the other parameter settings remain as defined in the base instance.

Table 7.12: Increase in end-product demands and revenues for fixed and optional contracts for multiple time periods. The first time period is defined as in *B1-3Fe4Si* and changes in the values for subsequent time periods are given relative to the first.

Instance	Time Periods	Demand Increase D_e^{F} and D_e^{O}	Revenue Increase R_e^{F} and R_e^{O}
M2-LOW	2	{0, -2%}	{0, -2%}
M2-HIGH	2	{0, +2%}	{0, +2%}
M3-LOW	3	{0, -2%, -2%}	{0, -2%, -2%}
M3-HIGH	3	{0, +2%, +2%}	{0, +2%, +2%}

7.3 Technical Study

A technical study of the MAMP is conducted and the parameter settings for the base instance *B1-3Fe4Si* are used. Section 7.3.1 considers problem statistics, optimality gaps, and run times for different instance sizes. In Section 7.3.2, both furnace merging and symmetry breaking constraints are considered to decrease the computational time of the MAMP. In Section 7.3.3, changes to the global optimality gap are studied for increasing run time. The solution stability of the MAMP is studied in Section 7.3.4. The solution sensitivity for various slag compositions is presented in Section 7.3.5. The effect of changing the acceptable LBP and UBP optimality gaps is considered in Section 7.3.6. The effect of different MDT parameter settings is studied in Section 7.3.7. Lastly, the multi-period MAMP formulation run statistics are evaluated in Section 7.3.8.

The run time limits and optimality gaps for the LBP, UBP, and MAMP-main algorithm are set according to Table 7.13. The maximum run times permitted for the LBP and UBP are given in elapsed run time for each problem. Thus, should the LBP use 1 000 seconds to solve the {-2} precision, 6 200 seconds remains for the next iteration if the desired global optimality gap ϵ is not reached in the first iteration.

Table 7.13: Accepted optimality gaps and run times. The accepted run times are given in seconds.

Problem	Optimality Gap	Maximum Run Time
LBP	1%	7200
UBP	1%	7200
MAMP-main	ϵ =1%	*NA*

7.3.1 Solution Statistics

Instance testing of the MAMP starts with one plant and one HC FeMn furnace before expanding the instance to include several plants and furnaces. Definitions of the furnace setups used in the test instances are found in Table 7.14. The base instance furnace setup is included for readability. Original problem statistics and Xpress presolve statistics for each test instance are given in Table 7.15. The optimality gaps, run times, and solution precisions for the LBP and the UBP problems, as well as the total run time and global optimality gap ϵ for the test instances, are listed in Table 7.16.

Table 7.14: Definition of furnace setups for instances used in the technical study. The set of plants is given together with the furnace production setup at each plant. Each furnace has a unique number given in an increasing manner.

Instance	Set of Plants, $\mathcal{P}$	HC FeMn Furnaces at Plant p	MC SiMn Furnaces at Plant p
P1-1Fe	{1}	{1}	{}
P1-1Fe1Si	{1}	{1}	{2}
P1-2Fe2Si	{1}	{1,2}	{3,4}
P2-1Fe1Si	{1,2}	{1}, {}	{}, {2}
P2-2Fe2Si	{1,2}	{1,2}, {}	{}, {3,4}
B1-3Fe4Si	{1,2,3}	{1}, {}, {6,7}	{2}, {3,4,5}, {}
P5-5Fe5Si	{1,2,3,4,5}	{1,2}, {3,4}, {5}, {}, {}	{}, {}, {6}, {7,8}, {9,10}

Based on the results in Table 7.15, one can conclude that the number of furnaces is the dimension of the problem that makes it difficult to solve. This result is intuitive, as adding a furnace adds a new set of chemical balance and furnace constraints to the problem. Adding a plant and keeping the number of furnaces constant increases the rows and columns of the original problem minorly, but results in about the same number of rows and columns after the Xpress presolve.

It is worth noting the substantial reduction in the number of rows, columns, and elements from the original problem statistics to the Xpress presolve statistics. An explanation for this is that many of the chemical constraints in the MAMP formulation have linearly dependent rows. Also, there are many redundant variables of the n_{pfkcv} variables, as all of these are explicitly defined in the implementation, even though only a few are actively used in the chemical constraints.

Table 7.15: LBP computational statistics for the test instances.

	LBP Original Problem Statistics			LBP Xpress Presolve Statistics			Simplex
Instance	**Rows**	**Columns**	**Elements**	**Rows**	**Columns**	**Elements**	**Iterations**
P1-1Fe	18066	1347	23018	214	412	1302	77
P1-1Fe1Si	35350	2164	44196	378	592	2074	170
P1-2Fe2Si	70394	4184	87815	661	867	3459	393
P2-1Fe1Si	35882	2182	44975	376	591	2020	152
P2-2Fe2Si	70929	4202	88594	654	863	3337	355
B1-3Fe4Si	125477	7985	158517	1545	1810	7028	835
P5-5Fe5Si	183102	13280	235612	2976	3343	12864	1924

The basic operations in Xpress fixate variables explicitly defined by the problem formulation, eliminates redundant rows, and removes linearly dependent rows, among other things. The main reduction of the number of rows, columns, and elements can, thus, mainly be traced back to the explicit definition of the n_{pfkcv} variables.

Table 7.16: Optimality gaps and run times for the test instances. The run times are given in seconds. * denotes that the time limit was reached before the gap was closed. † denotes that the current precision was not finished within the time limit. * denotes that a valid upper bound, but no feasible solution was found for the current precision.

	LBP			UBP			MAMP Main	
Instance	**Gap**	**Time**	**Precision**	**Gap**	**Time**	**Precision**	**Time**	ϵ
P1-1Fe	1.00%	{<1,2}	{-2,-3}	1.00%	{1,13}	{-2,-3}	16	1.14%
P1-1Fe1Si	0.65%	{1,9}	{-2,-3}	1.00%	{2,17}	{-2,-3}	29	1.07%
P1-2Fe2Si	1.00%	{758,6440†}	{-2,-3†*}	1.00%	{763,6436†}	{-2,-3†*}	14406	1.47%
P2-1Fe1Si	0.17%	{<1,15}	{-2,-3}	1.00%	{2,43}	{-2,-3}	61	1.05%
P2-2Fe2Si	1.00%	{391,6808†}	{-2,-3†}	1.00%	{1019,6179†}	{-2,-3†}	14409	1.50%
B1-3Fe4Si	1.36%*	{7200†}	{-2†}	2.18%*	{7200†}	{-2†}	14409	2.55%
P5-5Fe5Si	3.33%*	{7200†}	{-2†}	7.08%*	{7200†}	{-2†}	14405	7.86%

From Table 7.16 it can be observed that both the LBP and the UBP are solved to the set optimality gaps for small instances with little computational effort. The resulting global optimality gap ϵ is close to the predefined optimality gap of 1.00%. For larger instances than *P2-2Fe2Si*, the set optimality gaps for the LBP and UBP are never reached within the time limits of two hours per problem. Consequently, the global optimality gap ϵ deteriorates for larger problems. The base instance *B1-3Fe4Si* is solved to a global optimality gap of 2.55% within the time limit. It is worth noting that the MAMP can find acceptable, feasible solutions even for large instances such as *P5-5Fe5Si* within a reasonable time.

Overall one can see that the solution time is most sensitive to the increase in the number of furnaces while increasing the number of plants barely has any effect. The applied precision also has a significant effect on the required computational time. For larger instances, the {-3} precision is never completed or even started within the time limit of the program. Generally, the solution to the LBP problem is better and located faster than for the UBP. This difference is due to that the UBP is a continuous representation of the solution space, while the LBP is discrete, therefore, the UBP requires a larger computational effort. Due to the relatively high computational time, different measures to reduce it should be considered.

7.3.2 Decreasing the Solution Time

The MAMP run duration is significant and different measures are considered to reduce the computational effort. First, the effect of merging identical furnaces is investigated. Second, symmetry breaking constraints are added to the formulation to see which one is the most effective, if any.

Merging Identical Furnaces

In the base instance, the MC SiMn furnaces at Plant 2 are identical and the HC FeMn furnaces at Plant 3 are identical. Merging these furnaces into one larger furnace at each plant may reduce the computational effort as it results in fewer pools to solve. Merging is acceptable for the base instance as there are only one furnace end-product per furnace type. If the set of furnace end-products had been larger, for instance by allowing multiple types of HC FeMn, furnace merging would not be feasible as the furnaces could potentially produce different HC FeMn end-products. Merging the furnaces may still remove too much of the solution space and, thus, cannot be applied to find optimal solutions. This section investigates whether furnace merging is an acceptable approach. Definitions of test instances with merged furnaces are given in Table 7.17. The base instance *B1-3Fe4Si* setup is provided for reference. It is important to note that when the capacity of the HC FeMn furnaces increases, the MDT parameters $\overline{\sigma}_{pfgh}$ and $\overline{q}_{pf}$ have to be scaled accordingly to account for the increased slag production capacity.

Table 7.17: Definition of test instances where identical furnaces from the base instance are merged. The furnace mass capacity in tonnes is the first number in the brackets, the furnace power capacity in MW is the second. The base instance *B1-3Fe4Si* setup is provided for reference.

	Plant 1		Plant 2			Plant 3	
Instance	**F1**	**F2**	**F3**	**F4**	**F5**	**F6**	**F7**
I1-2Fe4Si	{1000,40}	{750,30}	{750,30}	{750,30}	{750,30}	{2000,80}	*Merged*
I2-3Fe2Si	{1000,40}	{750,30}	{2250,90}	*Merged*	*Merged*	{1000,40}	{1000,40}
I3-2Fe2Si	{1000,40}	{750,30}	{2250,90}	*Merged*	*Merged*	{2000,80}	*Merged*
B1-3Fe4Si	{1000,40}	{750,30}	{750,30}	{750,30}	{750,30}	{1000,40}	{1000,40}

Table 7.18: Furnace merging results. The run times are given in seconds. * denotes that the time limit was reached before the gap was closed. † denotes that the current precision was not finished within the time limit. * denotes that a valid upper bound, but no feasible solution was found for the current precision.

	LBP			UBP			MAMP Main	
Instance	**Gap**	**Time**	**Precision**	**Gap**	**Time**	**Precision**	**Time**	ϵ
I1-2Fe4Si	1.00%	{293,4772}	{-2,-3}	1.00%	{622,6578†}	{-2,-3†}	12271	1.52%
I2-3Fe2Si	1.58%*	{7200†}	{-2†}	1.95%*	{7200†}	{-2†}	14410	2.53%
I3-2Fe2Si	1.00%	{307,6893†}	{-2,-3†}	1.34%*	{881,6319†}	{-2,-3†}	14625	1.41%

Based on the results from Table 7.18, merging HC FeMn furnaces improve the run time and optimality gaps compared to the base instance in Table 7.16. Merging MC SiMn furnaces does not seem to affect the solution time nor improve the optimality gap. The objective values and best bounds can be compared to the objective value and best bound of the base instance to get an indication of whether furnace merging reduces the solution space too much. This is done in Table 7.19.

Table 7.19: Furnace merging LBP objective value and UBP best bound for the base instance and instances with merged furnaces.

Instance	LBP Objective Value	UBP Best Bound
I1-2Fe4Si	35 414 595	35 952 989
I2-3Fe2Si	35 344 425	36 240 104
I3-2Fe2Si	35 397 570	35 897 540
B1-3Fe4Si	35 395 590	36 301 372

From Table 7.19 one can see that the objective values of the furnace merging instances are within the same range as for the base instance. The results indicate that merging MC SiMn furnaces lead to a poorer objective value. A tighter best bound is found in all the merged instances. The results imply that merging identical HC FeMn furnaces when implementing large instances can be an acceptable approach for removing problem symmetry and decreasing the computational effort. Merging furnaces is similar to stating that the furnaces must produce the same amount of alloy and slag with the same compositions. This approach is always feasible within the original problem, but it may remove some flexibility in the production by restricting multiple furnaces to the same slag volume and composition.

Merging furnaces reduces the problem size and, therefore, allows for a better solution to be found within the same time limit as for the base instance. The approach can be acceptable for locating good solutions in a short time. However, it does alter the original problem's parameter settings. The authors, therefore, choose to proceed with the original base instance *B1-3Fe4Si* without merged furnaces in the remainder of the computational study.

Symmetry Breaking Constraints

Definitions of test instances including the symmetry breaking constraints (6.54) - (6.58) presented in Chapter 6 are given in Table 7.20. The results of including the symmetry breaking constraints are provided in Table 7.21.

Table 7.20: Definition of test instances including symmetry breaking constraints.

Instance	Added Symmetry Breaking Constraints
S1-3Fe4Si	$\phi_{3,6,\text{MnO}} \leq \phi_{3,7,\text{MnO}}$
S2-3Fe4Si	$q_{3,6} \leq q_{3,7}$
S3-3Fe4Si	$\sigma_{3,6,2,3} \leq \sigma_{3,6,2,4} \leq \sigma_{3,6,2,5}$
S4-3Fe4Si	$m_{2,3} \leq m_{2,4} \leq m_{2,5}$ and $m_{3,6} \leq m_{3,7}$
S5-3Fe4Si	$u_{2,3} \leq u_{2,4} \leq u_{2,5}$ and $u_{3,6} \leq u_{3,7}$

Comparing the results in Table 7.21 to those of the base instance in Table 7.16 show that none of the implemented symmetry breaking constraints improve the computational time, nor the global optimality gap. Thus, nothing is gained from adding the symmetry breaking constraints and they are consequently not included further in the computational study.

Table 7.21: Results of including symmetry breaking constraints. The run times are given in seconds. * denotes that the time limit was reached before the gap was closed. † denotes that the current precision was not finished within the time limit.

	LBP			UBP			MAMP Main	
Instance	**Gap**	**Time**	**Precision**	**Gap**	**Time**	**Precision**	**Time**	ϵ
S1-3Fe4Si	1.37%*	{7200†}	{-2†}	2.21%*	{7215†}	{-2†}	14428	2.61%
S2-3Fe4Si	1.42%*	{7200†}	{-2†}	2.32%*	{7200†}	{-2†}	14412	2.85%
S3-3Fe4Si	1.49%*	{7200†}	{-2†}	2.42%*	{7200†}	{-2†}	14408	3.00%
S4-3Fe4Si	1.33%*	{7200†}	{-2†}	2.15%*	{7200†}	{-2†}	14410	2.56%
S5-3Fe4Si	1.46%*	{7200†}	{-2†}	2.24%*	{7200†}	{-2†}	14410	2.70%

7.3.3 Global Optimality Gap with Increasing Run Time

It can be interesting to observe how the global optimality gap ϵ changes with increasing run time. This relation is shown in Figure 7.1. The allowed run time for the LBP and UBP are set to twelve hours each. The base instance parameter settings are used.

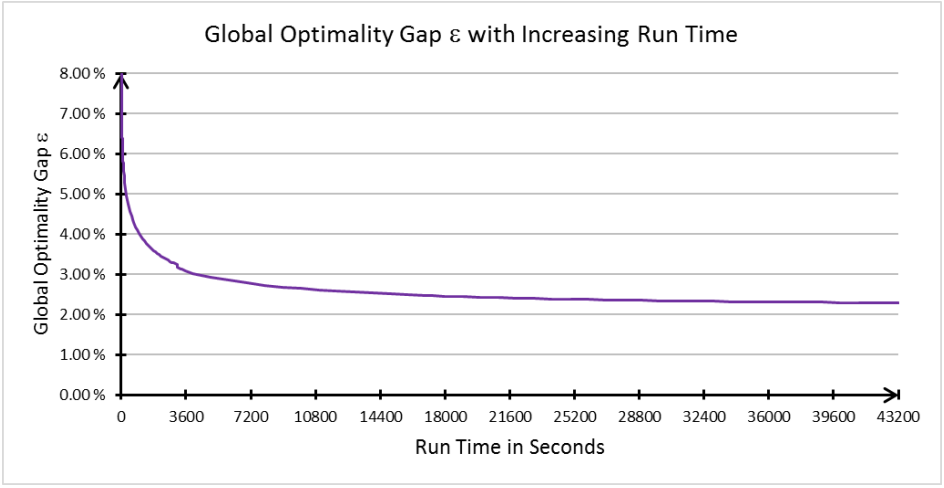

Figure 7.1: Global optimality gap ϵ with increasing run time. The run time is given as the individual LBP and UBP run times, thus, the run time of the MAMP main is twice the time of what is shown on the axis.

From Figure 7.1 one can see that the global optimality gap ϵ is approximately 3.10% after one hour of run time for both the LBP and the UBP. The decrease in the global optimality gap after one hour is small, improving to 2.52% in four hours. After four hours, the decrease is diminishing until it flattens out at approximately 2.30% after eight hours. At twelve hours, the MAMP main has run for a total of 24 hours, ending at a global optimality gap of 2.28%. It can be concluded that allowing run times of more than four hours for the LBP and UBP is of little value to the solution unless a very high solution accuracy is desired and sufficient time is available. Run times shorter than four hours allow for a good solution to be found within the time limit.

Note that small variations in the optimality gaps may come from variations between individual runs. In Table 7.16, the base instance is solved to an optimality gap of 2.55% in two hours, while as in this run, the global optimality gap after two hours is 2.76%. Such variations can be eliminated by running the model several times. Investigating the stability of the global optimality gap and objective value is, thus, desirable.

7.3.4 Solution Stability

Due to the nonconvexities in the original problem, the MAMP may provide different optimal solutions as the branch-and-bound tree can get stuck in a local optimum. The MDT should ensure that the global optimum is found, thus running the MAMP multiple times should yield the same optimal objective value, although the optimal solution may differ from run to run. To investigate this, the base instance *B1-3Fe4Si* is run ten times where the stability of the global optimality gap and the objective value of the runs are recorded and compared. The results of the runs are provided in Table 7.22. The solutions of the runs are also compared, but not presented here for readability; only the general findings are provided.

Table 7.22: Solution stability for ten different runs of *B1-3Fe4Si*. The solution times are given in seconds and the objective values in USD.

Run	Time	ϵ	Objective Value
1	14409	2.55%	35 395 590
2	14409	2.52%	35 406 342
3	14409	2.46%	35 534 028
4	14410	2.59%	35 377 497
5	14409	2.56%	35 368 170
6	14409	2.52%	35 400 270
7	14409	2.52%	35 400 270
8	14489	2.57%	35 368 170
9	14412	2.81%	35 380 737
10	14526	2.65%	35 395 590
Average		**2.58%**	**35 402 666**
Standard Deviation		**0.09%**	**45 689**

The average global optimality gap ϵ is found to be 2.58% for ten runs of the base instance, with a standard deviation of 0.09%. The average objective value is 35 402 666 USD, with a standard deviation of 45 689 USD. The standard deviation is small relative to the average objective value. Further, there are no extreme outliers in the results that significantly deviate from the average.

It seems that due to the MDT linearisation, the applied software does not necessarily find the same nodes to branch on in the branch-and-bound tree. The fact that the number of integer feasible solutions found by the program varies between four and 22 solutions within the allotted run time indicates that this is the case. The solutions from the runs are, although, quite similar, with only minor differences in the volumes of raw materials consumed in the furnaces, slag compositions, and the total end-products produced. One can conclude that the solution is sufficiently stable to accept that the solution of one run is a good representation of the optimal solution. For the remainder of the study, the solution from Run 1 of *B1-3Fe4Si* is used.

7.3.5 Solution Sensitivity For Different Slag Composition Intervals

As mentioned, different parameter settings can affect the problem size significantly. The upper and lower bounds on the slag composition are two such parameters. Allowing a wide interval may give a better solution to the MAMP, but can make the problem unsolvable within a reasonable time. Narrowing the interval can reduce the computational time significantly, but may limit how good and practical the solution is. If the upper and lower bounds are equal, or the sum of the upper bounds are 1.00, the bilinear terms vanish as only one slag composition is feasible. The slag composition is thus predetermined, and the MDT solution method is redundant in this case.

It is of interest to investigate how large slag composition intervals the MAMP can solve for within the allotted time. A trade-off between the interval size and the run time can then be established. In practice, there are process specific considerations that limit this interval to a certain degree; these values are as described in the base instance. Definitions of test instances with different slag intervals are given in Table 7.23. The upper and lower bounds on the slag composition are allowed to extend beyond the practical values to investigate the effects they have on the computational effort required to solve the MAMP. Values for the base instance *B1-3Fe4Si* are provided for readability.

Table 7.23: Test instances with various upper and lower bounds on the slag composition.

		Element or Oxide k						
Instance	**Parameter**	**MnO**	**FeO**	**SiO2**	**Al_2O_3**	**MgO**	**CaO**	**SUM**
C1-LOW	$\overline{\Phi}_k$	0.50	0.02	0.25	0.10	0.10	0.10	1.07
	$\underline{\Phi}_k$	0.45	0.00	0.20	0.05	0.05	0.05	0.80
C2-MED	$\overline{\Phi}_k$	0.50	0.05	0.25	0.20	0.15	0.15	1.30
	$\underline{\Phi}_k$	0.40	0.00	0.15	0.10	0.05	0.05	0.75
B1-3Fe4Si	$\overline{\Phi}_k$	0.50	0.02	0.35	0.20	0.20	0.30	1.57
	$\underline{\Phi}_k$	0.30	0.00	0.15	0.10	0.05	0.10	0.70
C3-HIGH	$\overline{\Phi}_k$	0.80	0.30	0.50	0.30	0.30	0.30	2.50
	$\underline{\Phi}_k$	0.10	0.00	0.10	0.05	0.05	0.00	0.30
C4-MAX	$\overline{\Phi}_k$	1.00	1.00	1.00	1.00	1.00	1.00	6.00
	$\underline{\Phi}_k$	0.00	0.00	0.00	0.00	0.00	0.00	0.00

The sum of the lower bounds on the slag compositions $\underline{\Phi}_k$ from Table 7.23 means that this amount of the slag composition is predetermined. In the base instance, 70% of the slag composition is already determined. 30% is then left for the MAMP to solve. The greater the sum of the upper bound on the slag compositions $\overline{\Phi}_k$, the greater the number of possible combinations of oxides with which to fill the remaining 30% of the slag composition. The test instance results for various slag intervals are given in Table 7.24.

Table 7.24 shows that the global optimality gap increases for increasing slag interval ranges. Solving *C1-LOW* results in that the {-2} precision is solved in a short time in contrast to not finishing for the other instances. Allowing maximum composition range, as in the instance *C4-MAX*, makes the problem harder to solve, thus the significantly worse global optimality gap ϵ. The conclusion is that the size of the interval greatly affects the computational effort required to solve a pooling problem like the MAMP, and that one should take great care in determining the slag interval parameters.

Table 7.24: Results for instances with various slag composition intervals. The run times are given in seconds. * denotes that the time limit was reached before the gap was closed. † denotes that the current precision was not finished within the time limit.

	LBP			UBP			MAMP Main	
Instance	**Gap**	**Time**	**Precision**	**Gap**	**Time**	**Precision**	**Time**	ϵ
C1-LOW	1.00%	{10, 3353}	{-2,-3}	1.16%*	{174,7026†}	{-2,-3†}	10566	1.19%
C2-MED	1.32%*	{7200†}	{-2†}	1.76%*	{7200†}	{-2†}	14415	2.28%
C3-HIGH	5.06%*	{7200†}	{-2†}	6.33%*	{7200†}	{-2†}	14405	6.90%
C4-MAX	8.66%*	{7200†}	{-2†}	8.93%*	{7200†}	{-2†}	14407	11.34%

7.3.6 The Effect of Changes to the LBP and UBP Optimality Gaps

Using different optimality gaps in the LBP and UBP can greatly affect the run time and the global optimality gap. One can investigate whether it is more effective to have a large optimality gap and thus allow multiple precisions to be solved within the time limit, or if it is better to solve one precision to a smaller optimality gap. The run time of the MAMP-main algorithm and the global optimality gap are plotted for various LBP and UBP optimality gaps in Figures 7.2 and 7.3, respectively.

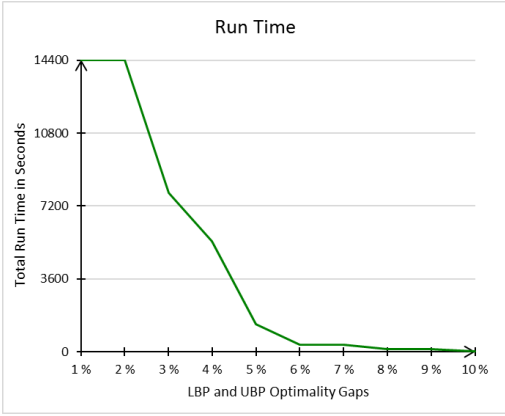

Figure 7.2: MAMP-main run time for increasing optimality gaps in the LBP and UBP.

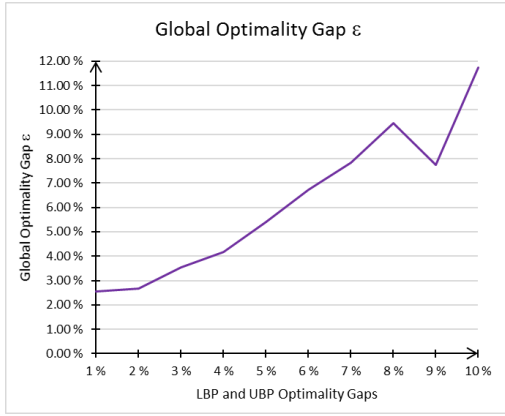

Figure 7.3: Global Optimality gap ϵ for increasing optimality gaps in the LBP and UBP.

Based on Figures 7.2 and 7.3 one can see that the run time decreases drastically for increasing LBP and UBP optimality gaps, but at the expense of a poorer global optimality gap. For optimality gaps in the range 4 - 10%, both precisions $\{-2, -3\}$ are solved within the time limit to the accepted optimality gaps. Here, the run time and global optimality gap ϵ fluctuate more based on whether the MAMP can quickly locate a solution in the next iteration with increased precision.

In the optimality gap range of 1 - 3%, the $\{-2\}$ precision is not completed within the time limit for the UBP, or for both the LBP and UBP. However, the achieved global optimality gap has the best values here at 2.70 - 3.50%. The conclusion is that it is best to set the optimality gaps of the LBP and UBP as small as possible and solve one precision to obtain the best solution from the MAMP. Thus, optimality gaps of 1% for the LBP and the UBP are continued to be used in the remainder of the computational study.

One should also take into consideration that there are uncertainties in the data provided by the industrial partner due to perturbation, and in the data estimated by the authors. This uncertainty may cumulatively be greater than the current global optimality gap found for the base instance, thus solving the problem to smaller optimality gaps may be academically interesting, but of no practical value.

7.3.7 MDT Parameter Setting Effects

Applying the MDT involves setting upper bounds on the parameterised variables. $\overline{q}_{pf}$ and $\overline{\sigma}_{pfgh}$ are big Ms in the linearisation and the selected upper bounds can have an impact on the computational results as it affects the q_{pf} and σ_{pfgh} variables' solution space. The results of the study are presented in Figure 7.4.

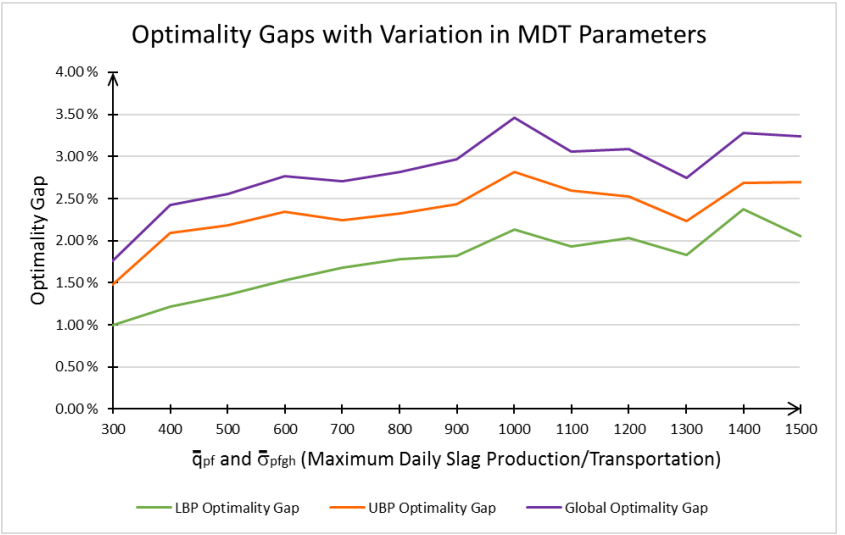

Figure 7.4: Global optimality gap for various $\overline{q}_{pf}$ and $\overline{\sigma}_{pfgh}$ settings.

Figure 7.4 shows that, in general, the tighter the upper bounds, the better optimality gaps in the LBP and the UBP, and global optimality gap ϵ are. Consequently, tighter bounds on $\overline{q}_{pf}$ and $\overline{\sigma}_{pfgh}$ use less computational time to reach any optimality gap. The small improvement in optimality gaps found in the interval $1000 \geq \overline{q}_{pf} = \overline{\sigma}_{pfgh} \leq 1400$ is likely due to the solver finding better solutions faster for these runs than for $\overline{q}_{pf} = \overline{\sigma}_{pfgh}$ equal to 900 and 1000.

Note that setting the upper bounds lower than 300 tonnes can only be done if one already knows that under the current production conditions, the slag-to-metal ratio is never optimal at 1.00. The slag production with a 1.00 slag-to-metal ratio in the base instance *B1-3Fe4Si* is around 260 - 300 tonnes slag per day, thus setting $\overline{q}_{pf}$ any lower results in a forced lower slag-to-metal ratio due to the removal of parts of the solution space. Overall, a bound close to 300 tonnes/day seems to be the optimal value for $\overline{q}_{pf}$ and $\overline{\sigma}_{pfgh}$, but for the continuity of the computational study, the original value of 500 tonnes/day is kept as an upper bound.

7.3.8 Multi-period MAMP Run Statistics

The time horizon is extended to include multiple time periods. It is of interest to identify how the global optimality gap behaves for an increasing number of time periods. The plant and furnace layouts of the base instance are also used here. The computational statistics are listed in Table 7.25.

Table 7.25: Optimality gaps and run times for the test instances. The run times are given in seconds. * denotes that the time limit was reached before the gap was closed. † denotes that the current precision was not finished within the time limit. ⋆ denotes that a valid upper bound, but no feasible solution was found for the current precision.

	LBP			UBP			MAMP Main	
Instance	**Gap**	**Time**	**Precision**	**Gap**	**Time**	**Precision**	**Time**	ϵ
M2-LOW	3.32%*	{7200†}	{-2†}	6.91%*	{7200†}	{-2†}	14404	7.55%
M2-HIGH	3.22%*	{7200†}	{-2†}	6.56%*	{7200†}	{-2†}	14404	7.28%
M3-LOW	4.46%*	{7200†}	{-2†}	*NA*⋆	{7200†}	{-2†⋆}	14405	8.90%
M3-HIGH	4.46%*	{7200†}	{-2†}	*NA*⋆	{7200†}	{-2†⋆}	14405	9.66%

The table shows that increasing the number of time periods to two leads to a significantly worse global optimality gap. The MAMP is still able to find feasible solutions, but they cannot be guaranteed to be good. Further increasing the number of time periods to three yields a global optimality gap close to 10%. No larger instances are tested. Observe that it is the UBP that is most difficult to solve and that for the case of three time periods a valid upper bound, but no integer feasible solution is found. Thus, the linear solver does not yield an optimality gap for the UBP with three time periods. *Lotero et al. (2016)* state that general purpose global optimisation solvers fail to find a solution for even small multi-period instances, while our results indicate that using the MDT enables linear solvers to find feasible solutions for such instances.

7.4 Economic Study

An economic study is conducted for two purposes; analysing and understanding how variations in input parameters affect the production and evaluating the applicability of the model. The base instance *B1-3Fe4Si* is used unless stated otherwise.

The value of increasing the run time of the LBP and UBP is studied in Section 7.4.1. In Section 7.4.2 a comparison of the MAMP to single furnace optimisation is conducted, followed by a study of the value of solving the pooling problem in Section 7.4.3. Changes to the slag production as a function of increasing demand is investigated in Section 7.4.4. The procurement cost's effect on the optimal raw material feed composition is studied in Section 7.4.5. A comparison of the MAMP to single furnace optimisation for a case with an optimal slag-to-metal ratio higher than the lower bound is conducted in Section 7.4.6. An evaluation of the optimal furnace setup for the base instance is performed in Section 7.4.7. A comparison of the multi-period MAMP to the single-period MAMP is presented in Section 7.4.8.

7.4.1 The Value of Increasing the Run Time

As seen previously, having the model run for a longer duration can give a lower global optimality gap. However, if the potential economic gain from increasing the run time is low, it may be better accept a shorter run time. This case occurs if no significantly better solutions are located with increasing run time. The LBP solution and the UBP best bound for a run time of twelve hours per problem is presented in Figure 7.5.

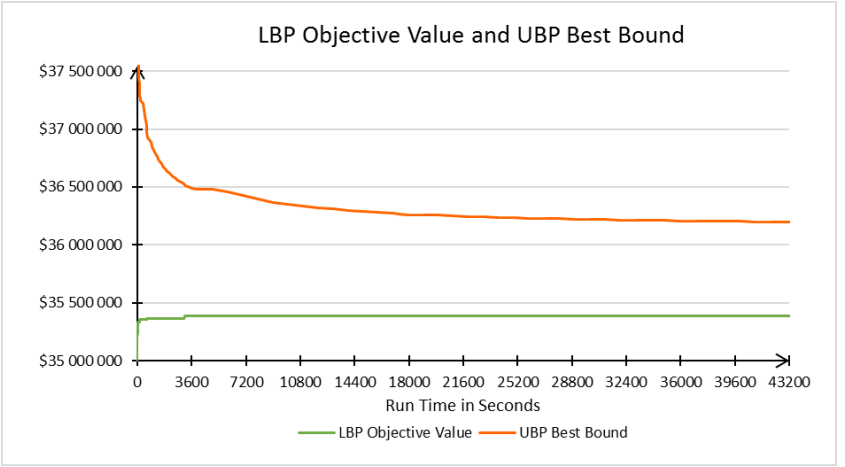

Figure 7.5: LBP objective value and UBP best bound for increasing the run times of the LBP and UBP. Values in USD.

As can be seen from Figure 7.5, a good LBP objective value is found within the first hour. After the first hour, no significantly better objective value is found. The best bound in the UBP decreases rapidly within the first hour and is diminishing for the remainder of the run. Increasing the run time ensures that the optimal objective value can be guaranteed with a better global optimality gap, but only a minimal improvement in the LBP objective value is found after the first three hours. The MAMP can thus provide a good feasible solution in a short time, but the model should be run for several hours to guarantee a small global optimality gap.

7.4.2 Comparison of the MAMP to Single Furnace Optimisation

The current industry practice is to optimise the production for individual furnaces based on software and expert judgement made by metallurgists. This practice is denoted single furnace optimisation and is the practice of optimising the profit of each single furnace and, consequently, the alloy it produces without regards to the overall production. This practice may be sub-optimal compared to planning the production when considering the entire production. The MAMP expands the production planning to cover all furnaces at all plants and is, therefore, a formulation that could potentially solve the complexity of multi-plant production. This section aims to evaluate how the MAMP performs against single furnace optimisation for the base instance *B1-3Fe4Si*. The results show if the MAMP can contribute to better production planning.

The following process is used to simulate single furnace optimisation. An instance only containing one HC FeMn furnace and an instance only containing one MC SiMn furnace are created. The authors assume that single furnace optimisation is done by satisfying the fixed contracts first, then the optional contracts with the highest profit. In the first iteration, the HC FeMn instance is solved with the total demand as input. The demand is then reduced with the production volumes obtained in the first iteration, and the instance is then solved again. This procedure is done for three iterations with the HC FeMn instance, followed by four iterations with the MC SiMn instance where the slag produced by the HC FeMn furnaces is made available to the MC SiMn furnaces. The results from the HC FeMn production iterations are shown in Table 7.26, together with the results from applying the MAMP formulation.

Table 7.26: Comparison of the MAMP formulation to single furnace optimisation for the FeMn production. Production values are given in tonnes. Objective values are given in thousand USD.

	Single Furnace Optimisation				**MAMP Optimisation**			
Plant p, Furnace f	**1, 1**	**3,6**	**3,7**	**Total**	**1, 1**	**3,6**	**3,7**	**Total**
Furnace Type	**FeMn**	**FeMn**	**FeMn**		**FeMn**	**FeMn**	**FeMn**	
u_{pf}**, to crushing**	0	8314	4175	12489	0	10688	3021	13709
m_{pf}**, to refining**	10439	2599	6519	19557	10998	0	8559	19557
q_{pf}**, produced slag**	5220	5456	5347	16023	5499	5344	5790	16633
x^{E}_{pe}**, HC FeMn**	0	7482	3758	11240	0	9620	2719	12339
x^{E}_{pe}**, MC FeMn**	9608	2392	6000	18000	10122	0	7878	18000
Obj. Val. FeMn	6668	5975	6741	19384	*NA*	*NA*	*NA*	*NA*

Table 7.26 shows that the MAMP produces 610 tonnes more slag than single furnace optimisation. The total demand of MC FeMn from fixed and optional contracts is satisfied for both production methods, while not all of the optional contract demand for HC FeMn is satisfied. This result indicates that MC FeMn is the most profitable FeMn end-product.

The slag-to-metal ratio is found to be optimal at the lower bound of 0.50 in both optimisation methods (can be verified by consulting $\frac{q_{pf}}{u_{pf}+m_{pf}}$). Single furnace optimisation minimises the amount of slag produced as the goal is to maximise the profit from FeMn alloys for the HC FeMn furnaces. Thus, the slag-to-metal ratio is at the lower bound. The MAMP chooses the slag production values based on the goal to optimise the entire production. In this case, it is more favourable to use the capacity of the furnace for HC FeMn production than to produce extra quantities of slag.

The authors assume that the slag transportation between furnaces in the single furnace optimisation is based on minimising transportation costs to make the two production planning methods as comparable as possible. This assumption implies that as much slag as possible is sent internally at a plant if a plant has both HC FeMn and MC SiMn furnaces, as is the case at Plant 1. When the internal capacity of slag is reached, slag is transported to the plant with MC SiMn furnaces incurring the lowest transportation costs. The results from the single furnace optimisation method and the MAMP for the SiMn production are given in Table 7.27.

One can observe from Table 7.27 that all of the produced slags are consumed in both production planning methods and that the total LC SiMn demand is satisfied. The difference lies in the produced volume of MC SiMn, where an additional 673 tonnes of MC SiMn is produced by using the MAMP due to different composition and allocation of the slag. One can argue that the slag could

have been distributed differently for the single furnace optimisation planning. Another approach for dividing the feed of slag between the remaining MC SiMn furnaces at Plant 2 could be to give them the average of the remaining feed, this would, however, still be sub-optimal compared to the allocation given by the MAMP. Having flexibility and decision support tools to help in the allocation of slag is an advantage. The authors are not aware if such tools exist or if the allocation of slag is based on calculations made by experts or rules of thumb.

Table 7.27: Comparison of the MAMP formulation to single furnace optimisation for the SiMn production and total profit. Production values are given in tonnes. Costs and objective values are given in thousand USD. *Transportation Costs* are not included in the *Cumulative Objective Value*. *Total profit* is the *Cumulative Objective Value* less the *Transportation Costs*.

	Single Furnace Optimisation					**MAMP Optimisation**				
Plant p, Furnace f	**1, 2**	**2,3**	**2,4**	**2,5**	**Total**	**1, 2**	**2,3**	**2,4**	**2,5**	**Total**
Furnace Type	**SiMn**	**SiMn**	**SiMn**	**SiMn**		**SiMn**	**SiMn**	**SiMn**	**SiMn**	
u_{pf}, **to crushing**	0	2786	5547	447	8780	2338	0	1381	5809	9528
m_{pf}, **to refining**	5021	2175	42	4755	11993	2856	5246	3892	0	11994
σ_{ghpf}, **used slag**	5220	5456	2674	2673	16023	5499	4095	3421	3618	16633
Leftover slag	0	0	0	0	0	0	0	0	0	0
x^{E}_{pe}, **MC SiMn**	0	2508	4992	402	7902	2104	0	1243	5228	8575
x^{E}_{pe}, **LC SiMn**	6280	2720	53	5947	15000	3571	6588	4841	0	15000
Obj. Val. SiMn	4418	3565	2929	4599	15511	*NA*	*NA*	*NA*	*NA*	*NA*
Cum. Obj. Val.					34895					35430
Transport. Costs	0	23	11	11	45	0	17	14	15	47
Discard Slag Cost					0					0
Total Profit					**34850**					**35383**

Table 7.27 summarises the cumulative objective values, transportation costs, and the total profits for the two production planning methods. One can observe that the slag transportation costs are quite similar in the two methods, although somewhat higher for the MAMP as it produces and sends additional tonnes of slag. The profit from using the MAMP is 1.53% greater than using single furnace optimisation in the case of the base instance *B1-3Fe4Si*. Two significant factors in making the MAMP formulation superior to single furnace optimisation are the volume and the composition of the slag produced. The average composition of the slag in the single furnace optimisation and the MAMP optimisation are presented in Figures 7.6 and 7.7, respectively.

Figures 7.6 and 7.7 show a considerable difference in the average slag composition for the HC FeMn furnaces between single furnace optimisation and the MAMP. The most notable differences are the MnO, CaO, MgO, and Al_2O_3 concentrations. In single furnace optimisation, it is favourable to keep the MnO concentration in the slag to a minimum, to maximise the HC FeMn output. Consequently, the oxides CaO, MgO, and Al_2O_3 that are not part of HC FeMn alloy are maximised in the slag output. In the MAMP, the slag compositions are changed to suit the overall production, and one can observe that the content of MnO is at the upper bound of 50%.

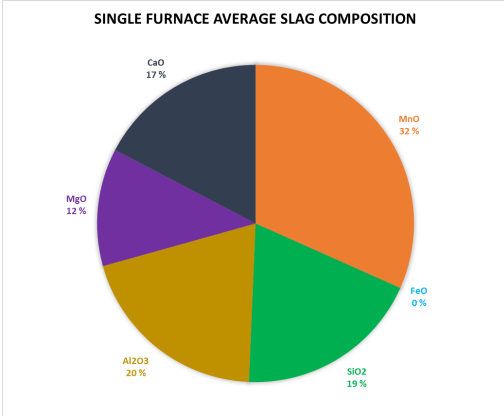

Figure 7.6: The average slag composition produced by the HC FeMn furnaces using single furnace optimisation.

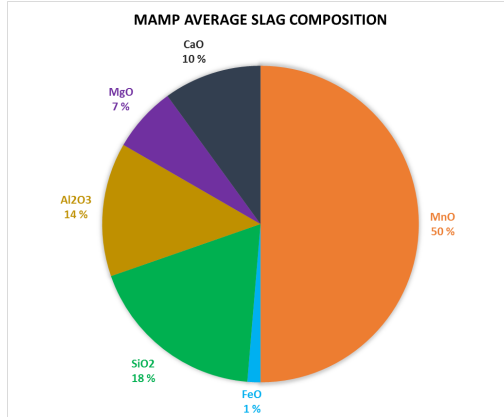

Figure 7.7: The average slag composition produced by the HC FeMn furnaces using the MAMP.

It is important to note that the slag composition from single furnace optimisation is a result of letting the optimisation software decide the optimal composition. This slag composition would probably have been different had it been predetermined by a metallurgist. It could, therefore, be of interest to solve the MAMP with predetermined slag compositions used in the industry today and compare it to solving the MAMP as a pooling problem to see if there is any value in having slack in the slag composition.

7.4.3 The Value of Solving the Pooling Problem

A large manganese alloy production company probably has a number of slag compositions they know to be effective. Comparing the objective values resulting from using these slag compositions to the MAMP objective value can give an indication of the value of solving the MAMP as a pooling problem. Definitions of test instances with pre-determined slag compositions are found in Table 7.28. The values are based on typical furnace production settings as described in *Olsen et al. (2007)* but have been modified slightly to ensure that the sum of the fractions are 1.00. The objective values for the predetermined slag composition instances are presented in Table 7.29.

Table 7.28: Definition of pre-determined slag composition instances. The values are slightly modified from compositions found in *Olsen et al. (2007)* to make the fractions sum up to 1.00.

		Element or Oxide k					
Instance	**Parameter**	**MnO**	**FeO**	**SiO_2**	**Al_2O_3**	**MgO**	**CaO**
D1-3Fe4Si	$\underline{\Phi}_k = \overline{\Phi}_k$	0.430	0.020	0.190	0.290	0.020	0.050
D2-3Fe4Si	$\underline{\Phi}_k = \overline{\Phi}_k$	0.380	0.020	0.240	0.130	0.040	0.190
D3-3Fe4Si	$\underline{\Phi}_k = \overline{\Phi}_k$	0.300	0.020	0.260	0.160	0.090	0.170
D4-3Fe4Si	$\underline{\Phi}_k = \overline{\Phi}_k$	0.403	0.014	0.228	0.125	0.063	0.167

Table 7.29: Objective values for the pre-determined slag composition instances. %-change is given relative to base instance *B1-3Fe4Si*.

Instance	LBP Objective Value	%-Change From B1-3Fe4Si
B1-3Fe4Si	35 395 590	0%
D1-3Fe4Si	26 660 700	-24.68%
D2-3Fe4Si	34 744 200	-1.84%
D3-3Fe4Si	34 751 800	-1.82%
D4-3Fe4Si	34 918 700	-1.35%

From Table 7.29 one can see that some of the pre-determined solutions are satisfactory, considering that they allow the MAMP to be solved in seconds. Although, from an economic perspective, even the best of the tested instances results in 1.35% less revenue compared to solving the MAMP with slack on the slag composition bounds. Also, note that fixating the slag composition yielded infeasible problems in many cases, thus, determining a good slag composition by using an educated guess is difficult. Overall, the results indicate that solving manganese alloy production as an optimisation problem can provide valuable decision support in deciding the optimal slag composition. One should keep in mind that the results are compared to the first run of the base instance, which is solved to a global optimality gap of 2.55%, and that the best predetermined solution is 1.35% worse than this. The potential gain from using the MAMP can, therefore, be even greater.

7.4.4 Slag Behaviour with Increasing Demand

In the comparison of the MAMP to single furnace optimisation, the slag-to-metal ratio is at the lower bound of 0.50 in all HC FeMn furnaces. This ratio can be up to 1.00, meaning one tonne slag is produced per tonne metal produced. It can, therefore, be of interest to investigate what conditions that can make this ratio prone to change from its lower bound. These conditions can, for instance, be variations in the demand volumes or sales prices of the end-products. The slag composition may also change when the slag-to-metal ratio changes. For instance, the optimal weight fraction of content in the slag, such as MnO and SiO_2, can fluctuate based on the production volumes of the most profitable end-products. It is, therefore, of interest to investigate how the slag-to-metal ratio and slag composition behaves under different demand volumes.

Three fixed demand cases are studied: one where the demand is assumed to be evenly distributed between all end-products, one where the demand is greater for FeMn alloys, and one where the demand is greater for SiMn alloys. The fixed demand for the end-products is set as optional to make the MAMP select the most profitable ones. Three solutions are computed for each demand to remove some of the effect instability may have on the solution. The end-product production volumes of the two first cases are also provided as these may help visualise the reason for the alteration in the slag-to-metal ratio and slag composition.

End-product Production Volumes

The slag-to-metal ratio is dependent on the relationship between the volumes of end-products to be produced. The produced volume of each end-product for increasing demand is shown in Figures 7.8 and 7.9 for evenly distributed demand and skewed demand towards FeMn alloys, respectively, to illustrate this relationship better.

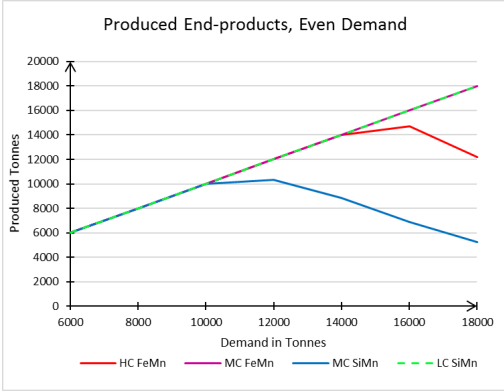

Figure 7.8: End-product production volumes for increasing demand when the demand is evenly distributed between FeMn and SiMn alloys.

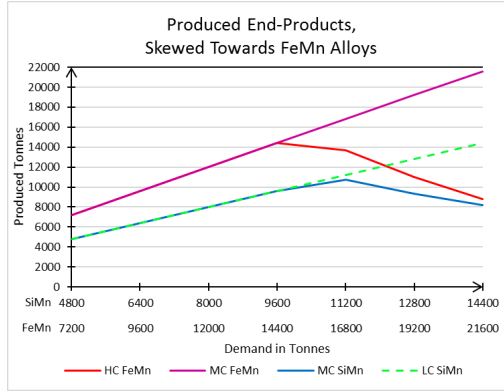

Figure 7.9: End-product production volumes for increasing demand when the demand is skewed towards FeMn alloys.

Observe from Figure 7.8 that MC SiMn and HC FeMn are the first end-products in each production to be reduced when reaching the total capacities of MC SiMn and HC FeMn furnaces of 12 000 tonnes and 16 000 tonnes, respectively. This graph behaviour occurs because an increasing part of the furnace metal output is further refined into LC SiMn and MC FeMn, which are more profitable. The same behaviour can be observed in Figure 7.9, but due to skewed demand towards FeMn alloys, the capacities in the HC FeMn furnaces are maxed out faster.

Evenly Distributed End-product Demand

In this case, the end-product demand is equally distributed between FeMn and SiMn alloys. A plot of the average slag-to-metal ratio in the HC FeMn furnaces as a function of demand is shown in Figure 7.10, and the average slag composition as a function of demand is shown in Figure 7.11.

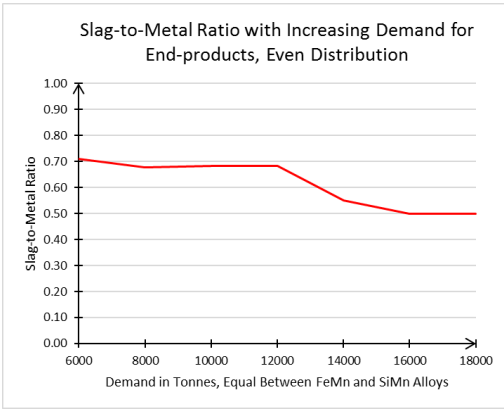

Figure 7.10: Average slag-to-metal ratio across all HC FeMn furnaces for increasing demand. The demand is evenly distributed between end-products.

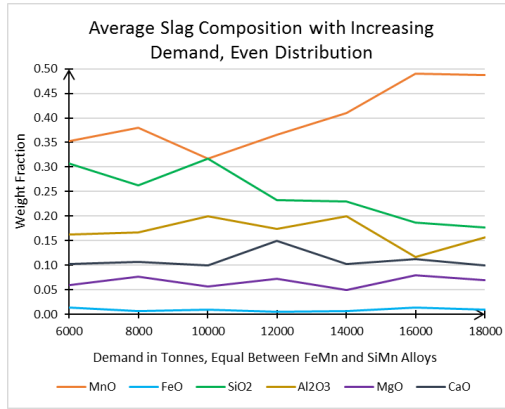

Figure 7.11: Average slag composition across the HC FeMn furnaces for increasing demand. The demand is evenly distributed between end-products.

The slag-to-metal ratio is in the range 0.68 - 0.71 for demands less than 12 000 tonnes. For greater demands, the slag-to-metal ratio decreases to the lower bound of 0.50. Here, production of the least profitable alloy MC SiMn cannot satisfy demand as the slag-to-metal ratio decreases to release capacity in the FeMn furnaces to satisfy the increasing demand for FeMn alloys. This behaviour can be seen from Figure 7.8. The trend continues for increasing demand until the lower bound of the slag-to-metal ratio is reached. The slight increase in production volumes of HC FeMn and MC SiMn before the constant decrease at the furnace capacities in Figure 7.8 are due to the alteration of the slag composition. As the slag-to-metal ratio decreases, it becomes more favourable to send slag with a greater MnO content and lowerSiO_2 content. Thus, as the volume of produced slag is reduced, the amount of MnO in the slag increases to carry more of the metal-bearing oxide to the MC SiMn furnace.

End-product Demand Skewed Towards FeMn Alloys

In this case, the end-product demand is skewed towards FeMn alloys. The cumulative demand for all end-products is the same as for the evenly distributed demand case. Of the total demand volume, 60% is demand for FeMn alloys and 40% is demand for SiMn alloys, divided equally between HC and MC, and MC and LC grades, respectively. A plot of the average slag-to-metal ratio for the HC FeMn furnaces as a function of demand is shown in Figure 7.12. A plot of the average slag composition for the HC FeMn furnaces as a function of demand is shown in Figure 7.13.

One can observe from Figure 7.12 that the slag-to-metal ratio is 0.70 when the demand for the end-products is low enough to maintain excess capacity in the furnaces. The excess capacity is then used to produce extra slag, as this is cheaper than using more raw materials in the MC SiMn furnaces. This observation seems to be valid for SiMn alloy demands less than 9 600 tonnes per product. The slag composition is stable at 0.70, but changes as the slag-to-metal ratio decreases, as can be seen in Figure 7.13.

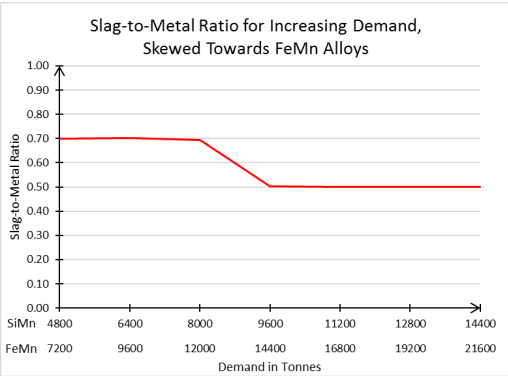

Figure 7.12: Average slag-to-metal ratio across all HC FeMn furnaces for increasing demand. The demand is skewed towards FeMn alloys.

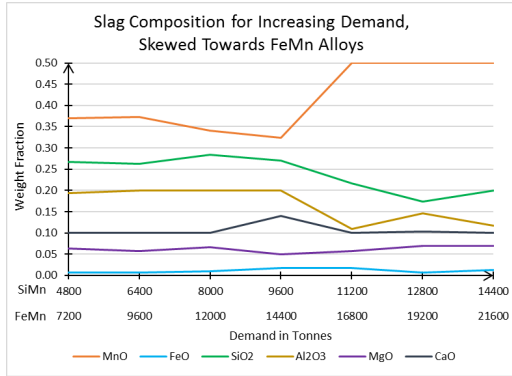

Figure 7.13: Average slag composition across all HC FeMn furnaces for increasing demand. The demand is skewed towards FeMn alloys.

When the end-product demand for SiMn alloys is 9 600 tonnes or greater, the slag-to-metal ratio is at the lower bound of 0.50. The drastic change is caused by the furnaces reaching their power capacity and then prioritise to produce more alloy instead of slag, as seen from Figure 7.9. At

the same time, the MnO content in the slag is increased to the upper bound of 50%, and the SiO_2 and Al_2O_3 decrease accordingly. At maximum furnace capacity, it is better to send slag that has a higher metal bearing capability for the most important elements in the end-product than to send larger volumes.

End-product Demand Skewed Towards SiMn Alloys

In this case, the end-product demand is skewed towards SiMn alloys. The cumulative demand for all end-products is the same as for the evenly distributed demand case. Of the total demand volume, 60% is demand for SiMn alloys and 40% is demand for FeMn alloys, divided equally between MC and LC, and HC and MC grades, respectively. A plot of the average slag-to-metal ratio for the HC FeMn furnaces as a function of demand is shown in Figure 7.14. A plot of the average slag composition for the HC FeMn furnaces as a function of demand is shown in Figure 7.15.

From Figure 7.14 one can observe that the slag-to-metal ratio is in the range 0.65 - 0.70 when the demand for the end-products is low enough to maintain excess capacity in the HC FeMn furnaces. From Figure 7.8 one can see that the HC FeMn furnace capacity is reached around 14 000 tonnes demand per FeMn alloy. The excess capacity in the HC FeMn furnaces is up to this point used to produce extra slag, as this is cheaper than using extra raw materials in the MC SiMn furnaces. As the demand for SiMn alloys is significantly higher in this case, it is advantageous to send larger volumes of slag and a higher MnO content in the slag as this lets the MC SiMn furnaces produce more MC SiMn alloy.

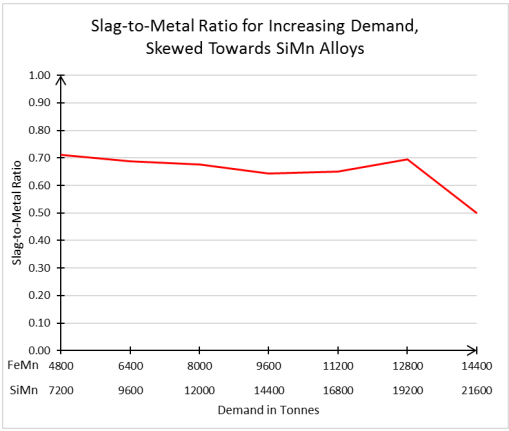

Figure 7.14: Average slag-to-metal ratio across all HC FeMn furnaces for increasing demand. The demand is skewed towards SiMn alloys.

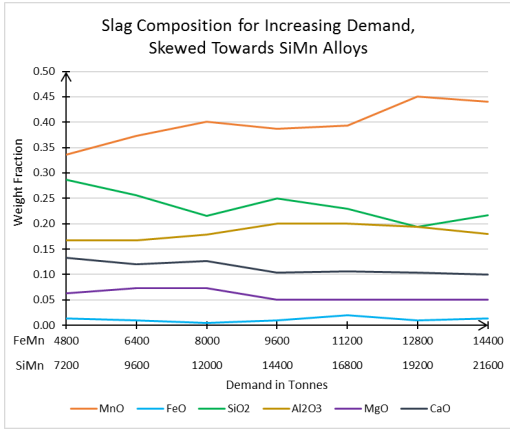

Figure 7.15: Average slag composition across all HC FeMn furnaces for increasing demand. The demand is skewed towards SiMn alloys.

Overall, one can notice that the slag-to-metal ratio is higher than the lower bound if the HC FeMn furnaces have excess capacity or if SiMn end-products are more profitable. Different demand scenarios consequently promote different optimal production strategies concerning the slag-to-metal ratio and slag composition. Locating the optimal operational strategy is not a trivial decision. Thus, it can be even more advantageous to use the MAMP when the parameter settings promote a slag-to-metal ratio greater than the lower bound.

7.4.5 Sensitivity to Changes in Raw Material Procurement Costs

The raw materials used in the production are essential cost factors as they incur different procurement and furnace electricity consumption costs due to their element and oxide content. Changes in the raw material procurement prices can, thus, alter the optimal raw material composition and volume used in the furnaces. Due to the many raw materials available to the production and no knowledge of how essential each raw material is, it is assumed that the cost changes affect all of the raw materials. Procurement cost increases in the range (-15)% - 15% have been studied, and the results on the raw material feed composition are presented in Figures 7.16 and 7.17 for HC FeMn furnaces and MC SiMn furnaces, respectively. Note that in the solution of the MAMP, the electric power consumption approximation is within the real power consumption ranges of about 2650 - 3100 kWh/tonne alloy for HC FeMn furnaces, and 3500 - 4500 kWh/tonne alloy for MC SiMn furnaces, as described in Chapter 2.

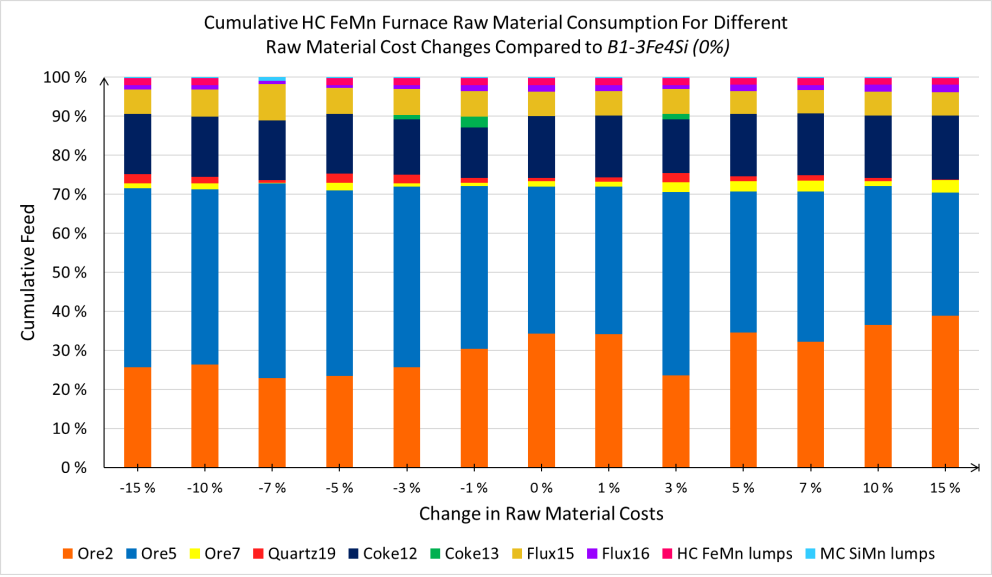

Figure 7.16: Cumulative HC FeMn furnace raw material consumption for changes in the raw material procurement costs, compared to *B1-3Fe4Si*.

It can be seen from Figure 7.16 that Ore 2 and Ore 5 are the primary resources used in the HC FeMn furnaces, accounting for about 70% of the feed, regardless of the change in raw material costs. The distribution between the two ores is, however, trending towards a higher usage of Ore 5 as the costs are reduced. The consumption of the other raw materials is stable with small fluctuations. Ore 7 and Quartz 19 seem to replace each other mostly, but with no apparent trend.

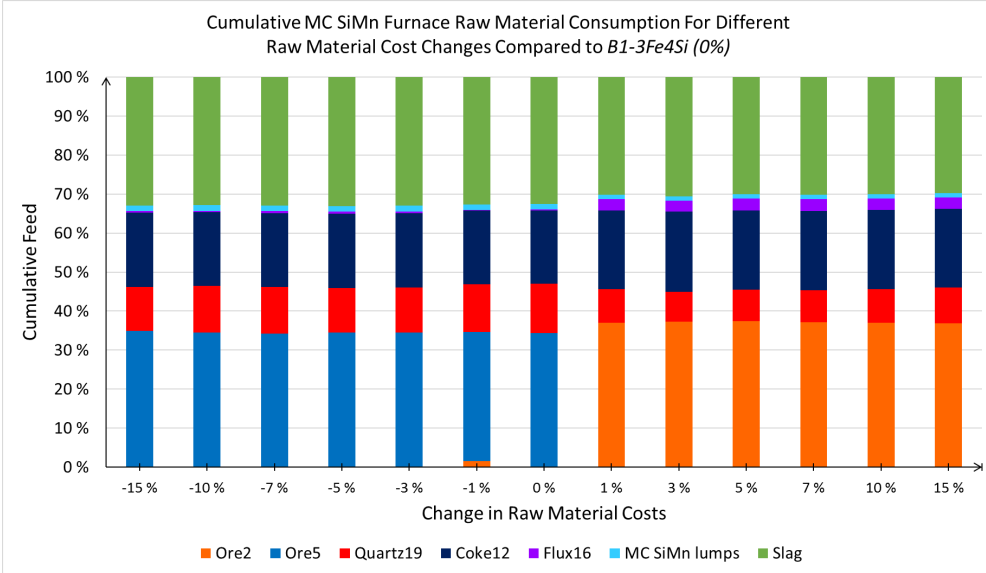

Figure 7.17: Cumulative MC SiMn furnace raw material consumption for changes in the raw material procurement costs, compared to *B1-3Fe4Si*.

Raw material costs have a much larger effect on the raw material feed composition in the MC SiMn furnaces. Increasing the costs makes Ore 2 favourable to use over Ore 5, thus, entirely replacing it in the feed. Consulting the raw material compositions in Table D.1 in Appendix D, it can be seen that Ore 2 consists mainly of MnO_2, while Ore 5 consists mainly of MnO. Ore 2 also contains a significantly higher content of SiO_2 than Ore 5, which explains the reduction in Quartz 19 usage for raw material cost increases of 1% or more. Note that Ore 2 is a much cheaper ore than Ore 5, thus the increase in procurement cost of ore 5 is greater. An increase in raw material costs thus offsets the economic gain from using a more expensive ore containing a greater MnO content, with a cheaper ore containing a greater MnO_2 content. Also, observe that the feed of Flux 16 significantly increases when increasing the raw material costs. This is to compensate for the reduction in iron oxides fed to a furnace as a result of replacing Ore 5 with Ore 2 in the feed.

The changes in slag production, slag transportation, and slag composition were also studied for changes in raw material costs. All the slag produced is transported and reused in the MC SiMn furnaces for all instances tested, and there are no changes in the optimal slag compositions. This result indicates that changes in the raw material costs do not affect the production of slag.

7.4.6 Comparison of the MAMP to Single Furnace Optimisation: High Slag-to-Metal Ratio

The results from Table 7.27 are for an instance where the slag-to-metal ratio is at its lower bound of 0.50. The authors suspect that the value of using the MAMP formulation is even greater in situations where the optimal slag-to-metal ratio is above the lower bound. The base instance is therefore updated with demands skewed towards SiMn alloys, as this results in an optimal slag-to-metal ratio of 0.70, illustrated in Figure 7.14. The demand is set to 19 200 tonnes for each SiMn alloy and 12 800 tonnes for each FeMn alloy, and a comparison of the MAMP formulation to the single furnace optimisation practice is conducted. The results are listed in Tables 7.30 and 7.31 for the FeMn and SiMn production, respectively.

Table 7.30: Comparison of the MAMP formulation to single furnace optimisation for the FeMn production. Low FeMn alloy demand, high SiMn alloy demand. Production values are given in tonnes. Objective values are given in thousand USD.

	Single Furnace Optimisation				**MAMP Optimisation**			
Plant p, Furnace f	**1, 1**	**3,6**	**3,7**	**Total**	**1, 1**	**3,6**	**3,7**	**Total**
Furnace Type	**FeMn**	**FeMn**	**FeMn**		**FeMn**	**FeMn**	**FeMn**	
u_{pf}, **to crushing**	0	7387	6839	14226	9685	4538	0	14223
m_{pf}, **to refining**	10439	3468	0	13907	0	4220	9687	13907
q_{pf}, **produced slag**	5220	5428	3420	14068	6737	6104	6705	19546
x^{E}_{pe}, **HC FeMn**	0	6645	6155	12800	8716	4084	0	12800
x^{E}_{pe}, **MC FeMn**	9608	3192	0	12800	0	3884	8916	12800
Obj. Val. FeMn	6668	6052	3588	16308	*NA*	*NA*	*NA*	*NA*

Table 7.31: Comparison of the MAMP formulation to single furnace optimisation for the SiMn production and total profit. Low FeMn alloy demand, high SiMn alloy demand. The demand is set for each end-product. Production values are given in tonnes. Costs and objective values are given in thousand USD. *Transportation Costs* are not included in the *Cumulative Objective Value*. Total profit is the *Cumulative Objective Value* less the *Transportation Costs*.

	Single Furnace Optimisation					**MAMP Optimisation**				
Plant p, Furnace f	**1, 2**	**2,3**	**2,4**	**2,5**	**Total**	**1, 2**	**2,3**	**2,4**	**2,5**	**Total**
Furnace Type	**SiMn**	**SiMn**	**SiMn**	**SiMn**		**SiMn**	**SiMn**	**SiMn**	**SiMn**	
u_{pf}, **to crushing**	0	0	0	5335	5335	5258	0	0	0	5258
m_{pf}, **to refining**	5021	4996	5189	146	15352	548	5074	4805	4926	15353
σ_{ghpf}, **used slag**	5220	5428	3420	0	14068	3651	0	9790	6105	19546
Leftover slag	0	0	0	0	0	0	0	0	0	0
x^{E}_{pe}, **MC SiMn**	0	0	0	4802	4802	4732	0	0	0	4732
x^{E}_{pe}, **LC SiMn**	6280	6248	6490	182	19200	686	6345	6009	6160	19200
Obj. Val. SiMn	4418	4400	4523	2960	16301	*NA*	*NA*	*NA*	*NA*	*NA*
Cum. Obj. Val.					32609					33298
Transport. Costs	0	23	14	0	37	0	0	53	26	79
Discard Slag Cost					0					0
Total Profit					**32572**					**33219**

Tables 7.30 and 7.31 show that single furnace optimisation minimises the slag-to-metal ratio, as it optimises the profit for single furnaces and, consequently, produces as much metal as possible. The MAMP, on the other hand, changes the slag-to-metal ratio according to what is optimal for the overall profit. A larger volume of slag is therefore produced and allocated efficiently to the MC SiMn furnaces. The decision to maximise metal output in single furnace optimisation could of course also be changed to maximise slag output, but this is not a trivial decision to make simply by consulting raw material costs and end-product revenues and demands.

More electricity is required to heat up the slag. Therefore, the furnace produces less MC SiMn in the MAMP, but the savings in raw material costs are greater than the extra revenue generated from selling more MC SiMn in the single furnace optimisation. The overall result is that the MAMP generates 1.99% more profit than single furnace optimisation under production conditions that favour

a higher slag-to-metal ratio. It should also be noted that the MAMP, for this instance, is solved to a global optimality gap of 1.60%, while single furnace optimisation is solved to optimality. This difference means that it could potentially exist an MAMP solution with an objective value that is even greater than the current objective value.

The results obtained so far are for a fixed furnace setup, however, the optimal furnace setup might be different from the one currently in use. Considering the production conditions, a plant manager, therefore, might want to identify the optimal furnace setup in advance of the production to achieve the highest profit. Evaluating different furnace setups under the current production conditions is, therefore, conducted next.

7.4.7 Switching Furnace Production Setups

As mentioned in Chapter 5, it is possible to switch the furnace setup between producing HC FeMn and MC SiMn. The analyses conducted in the previous sections suggest that deciding the optimal furnace setup is not a trivial decision to make based on the demand for the end-products. It may be preferable to have a greater total SiMn production capacity than total FeMn production capacity, at least to ensure the reuse of as much slag as possible from the HC FeMn furnaces. Reusing slag may still be sub-optimal for the profit of the operation, as adding more ores can be better than using slag in some of the procurement cost ranges studied. It may be preferable to have a greater total FeMn production capacity if the profit of making FeMn alloys outweighs the cost of discarding slag. Due to these options, it is of interest to investigate if switching the furnace setup can yield a greater profit under the production conditions considered in base instance *B1-3Fe4Si*.

To consider if this possibility can be of value, the furnace setup in base instance *B1-3Fe4Si* is updated, where the furnaces switch settings from either producing HC FeMn to MC SiMn or from MC SiMn to HC FeMn. It is assumed that the furnace mass and power capacity remain at the same level when changed, meaning a 40 MW HC FeMn furnace can become a 40 MW MC SiMn furnace. Table 7.32 defines the test instances with alternative furnace setups. The base instance *B1-3Fe4Si* setup is provided for readability. Every other parameter from the base instance remains the same to make the instances comparable. Production volumes of the different end-products and objective values from the respectable instances are given in Table 7.33.

Table 7.32: Test instances with alternative HC FeMn and MC SiMn furnace setups. The instances are sorted by increasing total HC FeMn furnace capacity.

Instance	HC FeMn furnaces at plant p	MC SiMn furnaces at plant p
A1-2Fe5Si	{1}, {}, {6}	{2}, {3, 4, 5}, {7}
A2-3Fe4Si	{1}, {3, 4}, {}	{2}, {5}, {6, 7}
A3-3Fe4Si	{1}, {3}, {6}	{2}, {4, 5}, {7}
B1-3Fe4Si	{1}, {}, {6, 7}	{2}, {3, 4, 5}, {}
A4-4Fe3Si	{1}, {3, 4, 5}, {}	{2}, {}, {6, 7}
A5-4Fe3Si	{1}, {3, 4}, {6}	{2}, {5}, {7}
A6-4Fe3Si	{1}, {3}, {6, 7}	{2}, {4, 5}, {}
A7-5Fe2Si	{1, 2}, {3, 4, 5},{}	{}, {}, {6, 7}

Table 7.33: End-product production volumes and objective values for alternative furnace production setups. The instances are sorted according to increasing total HC FeMn furnace capacity. The furnace mass capacity in tonnes is the first number in the brackets, while the furnace power capacity in MW is the second number. The production volumes are given in tonnes, objective values are given in thousand USD. The percentage change is given relative to the objective value of *B1-3Fe4Si*.

	Total Furnace Capacity		**End-Product Volume**					
Instance	**HC FeMn**	**MC SiMn**	**HC FeMn**	**MC FeMn**	**MC SiMn**	**LC SiMn**	**Obj. Val.**	**+/-%**
A1-2Fe5Si	{2000,80}	{4000,160}	*Infeasible solution. Unable to satisfy fixed HC and MC FeMn demand.*					
A2-3Fe4Si	{2500,100}	{3750,140}	10 500	15 509	11 625	15 000	34 203	-3.37%
A3-3Fe4Si	{2750,110}	{3250,130}	10 500	17 838	9 814	15 000	35 015	-1.07%
B1-3Fe4Si	{3000,120}	{3000,120}	12 565	18 000	8 594	15 000	35 395	0.00%
A4-4Fe3Si	{3250,130}	{2750,110}	14 915	18 000	7 500	14 121	**35 665**	**0.76%**
A5-4Fe3Si	{3500,140}	{2500,100}	16 500	18 000	7 500	12 220	**35 591**	**0.55%**
A6-4Fe3Si	{3750,150}	{2250,90}	16 500	18 000	7 500	9 975	34 636	-2.14%
A7-5Fe2Si	{4000,160}	{2000,80}	*Infeasible solution. Unable to satisfy fixed MC and LC SiMn demand.*					

The results from Table 7.33 indicate that the furnace setup used by Eramet Norway today may be sub-optimal under the base instance production conditions. The objective value increases with 196 000 - 270 000 USD for the instances *A5-4Fe3Si* and *A4-4Fe3Si*, respectively. This is an increase in profit of 0.55 - 0.76%, respectively, for a production period of thirty days. The possible gain of switching furnaces can be millions of dollars if one assume an equal production for the remaining eleven months of the year. One should also remember that there is a furnace switching cost that may be significant enough to undermine the possible profit of switching the furnace settings, considering that three or more furnaces must be switched in these instances. The authors are not aware of the actual costs of switching a furnace but assume that the costs are significant since switching setup results in furnace downtime.

In the other instances, switching the furnace setup only reduces the objective value under the current production conditions. Stray too far away from the base instance operational settings and the total furnace capacity is not able to produce satisfactory volumes for the fixed contracts, as in instance *A1-2Fe5Si* and *A7-5Fe2Si*. For these instances to be feasible, the fixed contracts must change.

Even if this study indicates that switching furnace setups can be more profitable, the results are valid only for the parameter settings used in base instance *B1-3Fe4Si*, and there may be aspects of the real production the MAMP is not able to capture. The optimal production is highly dependent on the availability of raw materials, raw material prices, and end-product contracts and revenues. Changes to these parameters may result in alternative setups being preferable. Having the flexibility to change a furnace's operational settings is, still, a great capability and a formulation like the MAMP can help utilise this capability.

7.4.8 Multi-period Production Planning

The production of manganese alloys is a continuous production with orders for multiple months into the future. Accounting for future deliveries and scheduling the production accordingly can provide a plant manager with valuable information and possibly increase the profit of manganese alloy production. A comparison is conducted to evaluate whether the multi-period model provides

the user with a better production plan than running the single-period model for each time period. The total run time for the multi-period instances is four hours. The time available for the single-period model to solve each time period is then the total run time divided by the number of time periods, to make the models comparable. The result of the comparison is summarised in Table 7.34.

Table 7.34: Comparison of the multi-period to the single-period MAMP formulation. The inventories indicate the tonnage of end-product stored at the end of each period for the multi-period model. The first number in the brackets is for the first period, then subsequent periods are given. The single-period model does not hold inventories at the end of each period, thus, inventories are always zero.

	Inventory				Objective Value	
Instance	**HC FeMn**	**MC FeMn**	**MC SiMn**	**LC SiMn**	**Multi-period**	**Single-period**
M2-LOW	{0,0}	{0,0}	{0,0}	{0,0}	69 601 823	**69 758 646**
M2-HIGH	{1758,0}	{0,0}	{1042,0}	{0,0}	71 658 877	**71 755 168**
M3-LOW	{0,0,0}	{0,0,0}	{0,0,0}	{0,0,0}	102 731 095	**103 153 630**
M3-HIGH	{0,0,0}	{1505,2515,0}	{1010,1640,0}	{0,0,0}	108 864 640	**109 131 318**

From Table 7.34 it can be observed that an inventory of end-products is only held in cases where it is excess capacity to produce to optional contracts and the contract revenues for later periods are greater. Reduction in sales prices in later periods, as in *M2-LOW* and *M3-LOW*, makes it undesirable to hold inventory. In all cases, the single-period model outperforms the multi-period model. This happens because the single-period model reaches significantly better global optimality gaps than the multi-period model within the allotted run time of four hours. The single-period cases were solved to within a global optimality gap of 2.80%, while the best global optimality gap found for a multi-period case is 7.28%, as seen in Table 7.25. Overall, Table 7.34 shows that the multi-period MAMP formulation does not provide any value in scheduling the production in its current state. Efforts should be made to reduce the optimality gaps of the LBP and the UBP to obtain a better global optimality gap to make the multi-period MAMP useful.

Chapter 8

Concluding Remarks

In this thesis, the manganese alloy multi-plant production problem is described and studied. The problem is to decide the optimal production of end-products and slag, in addition to the allocation of the produced slag, that results in the highest profit, given specified operational and market conditions. It is inspired by real production planning challenges faced by a manganese alloy manufacturer. The aim is to develop a decision support tool for multi-plant manganese alloy production planning that can improve the current operational practice, denoted single furnace optimisation. Single furnace optimisation is the practice of optimising the profit of each single furnace separately and, consequently, the output it produces without considering the overall production. Similar problems of blending raw materials into end-products are found in other processing industries, such as oil refining and wastewater treatment. These problems require extensive mixing of flows with different quality attributes and are in the optimisation literature defined as pooling problems.

A general nonlinear mathematical formulation of the problem is developed for the problem. The manganese alloy multi-plant production problem is unique in that the processes are different from other problems addressed; complex chemical reactions exist in the furnace process, it includes multiple layers of intermediate pools, and multi-plant production considerations. The formulation is a hybrid between the standard and the generalised pooling problem, using a flow and quality based formulation, called the P-formulation. Both a multi-period and a single-period formulation is developed, where the single-period formulation is a special case of the multi-period with only one time period. The model is formulated as generally as possible to ease implementation of future extensions and to be flexible in implementation for manufacturers with different production setups. It is important to note that the manganese alloy multi-plant production problem is formulated using simplifications and assumptions that may limit how realistic it is in its current state.

The mathematical formulation contains bilinear terms in constraints relating the chemical reactions in a furnace to the production of slag. These constraints are linearised using the multiparametric disaggregation technique. This solution method enables the model to be solved using a linear solver and to guarantee a global optimality gap. To our knowledge, this is the first optimisation model that applies this linearisation method on real, large-scale instances. The computational study shows that the multiparametric disaggregation technique scales well with problem sizes of up to ten pools.

The base instance of three high-carbon ferromanganese and four medium-carbon silicomanganese furnaces divided between three plants is solved to within a global optimality gap of 3% for a run time of four hours. Four hours of allowed run time is recommended for this problem size, as the improvement of the global optimality gap is marginally better for longer run times. The optimisation software's inability to always locate the same solutions within a given time can result in small deviations in the solution and the objective value between program runs. The multi-period version of the model yields poor global optimality gaps for instances of equal size as the base instance and is in its current state outperformed by the single-period model when scheduling production for multiple time periods.

The results from the computational study indicate that the number of furnaces is the dimension of the problem that makes it hard to solve. The upper bound problem in the multiparametric disaggregation technique algorithm proves to be the most difficult to solve due to its continuous representation of the solution space. Further, six parameters are identified as important to solve the model efficiently. These are: the accepted optimality gaps of the lower and upper bound problems, the upper bounds on the multiparametric disaggregation technique slag production and slag transportation volume parameters, and the upper and lower bounds on the slag composition.

To compare our model to the current practice of single furnace optimisation, single furnace optimisation is mimicked using a reduced version of our multi-plant formulation as the authors are unable to obtain real performance data. A comparison of the two production planning methods shows that our model is superior to single furnace optimisation. The two factors that make our model superior are the produced volume of slag and its composition. Where single furnace optimisation minimises slag production and selects the slag composition based on maximising alloy output from individual furnaces, our model produces slag that is optimal for the overall production.

Our model achieves close to 1.5% greater profit than single furnace optimisation for a case with evenly distributed demand between the end-products. For a case where the production conditions favour a slag-to-metal ratio greater than the set lower bound, as in the case where the demand is skewed towards silicomanganese alloys, our model achieves close to 2% greater profit. Alternative furnace setups are studied and indicate that our model can be used to evaluate the optimal setup of furnaces in advance of a production period. This flexibility allows for even better production planning and greater profit. It should be noted that furnace switching costs are not included in the formulation. Therefore, the increase in profit should be evaluated against the objective value obtained using the current furnace setup with switching costs accounted for to find the actual profit.

The conclusion is that there may be a considerable value of using the formulation proposed in this thesis to plan the production of manganese alloys, compared to continuing with the current practice of single furnace optimisation. The formulation may be the first step in the design of a decision support tool for multi-plant production planning of manganese alloys. However, assumptions have been made developing the model, and there are still many aspects of the formulation that can be extended to make the model more realistic.

Chapter 9

Future Research

This thesis formulates an extensive model for the Manganese Alloy Multi-plant Production problem (MAMP). The formulation includes simplifying assumptions, and the scope of the work has been limited to make the problem size manageable. As a result, there are aspects of the problem that can be improved upon to construct a more realistic and applicable formulation. This chapter presents thoughts on possible future improvements and reasons why these improvements can strengthen the formulation.

To better model the slag-to-metal ratio and account for the furnace temperature's influence on chemical reactions, it can be of value to the MAMP to include more complex thermodynamic relations in the furnaces, thus, improving the MAMP's realisticity. The MAMP models that each plant only has one MOR and one LC SiMn refining station for simplicity. Having one MOR and one LC SiMn refining station is sufficient for the production of only one refined product of FeMn and SiMn. However, in reality, the product range spans more end-products than the four to which the MAMP is currently limited. Extending the MAMP to account for more end-products would make the formulation more realistic and useful.

Switching production setup can currently be evaluated by the MAMP by running the same production scenario for different furnace setups. Including furnace setup switching as a decision variable gives the best production setup immediately instead of having to iterate through different setups manually. Including switching enables the MAMP to account for furnace switching costs and can be used as a decision tool for the production setup in advance of the production. This feature can be of interest to a company that is planning to build a new plant to evaluate the best starting furnace setup or if a company suspects that the current operational setup is sub-optimal and wants to change the setup configuration.

The MAMP is formulated as a deterministic problem where the production is assumed to be based on contracts. Thus, the demand is given ahead of the planning period. In reality, much of the production is, according to the problem owner, based on make-to-stock policies and the alloys are sold on the open market based on current market prices and demands. These prices and demands, as well as raw material, electricity, and transportation costs, are subject to uncertainty. Formulating the MAMP as a stochastic problem can widen its applicability by taking this uncertainty into account and, thus, provide a more robust production schedule.

In the MAMP formulation, it is assumed that the produced slag can be reused in the MC SiMn furnaces within the same time period. The production and the transportation of slag are likely to require a significant portion of the time period, such that the slag is not available to the MC SiMn furnaces before the next production period. The MAMP multi-period model should, therefore, be expanded to make the slag production consider the next production period. This extension allows for the correct volumes and compositions of slag to be located at the plants when the next production period starts.

Bibliography

Adhya, N., Tawarmalani, M., Sahinidis, N. V., 1999. A Lagrangian Approach to the Pooling Problem. Industrial & Engineering Chemistry Research 38 (5), 1956–1972.

Al-Khayyal, F. A., Falk, J. E., 1983. Jointly Constrained Biconvex Programming. Mathematics of Operations Research 8 (2), 273–286.

Alfaki, M., 2012. Models and Solution Methods for the Pooling Problem. Ph.D. thesis, The University of Bergen.

Alfaki, M., Haugland, D., 2013. Strong Formulations For the Pooling Problem. Journal of Global Optimization 56 (3), 897–916.

Almutairi, H., Elhedhli, S., 2009. A New Lagrangean Approach to the Pooling Problem. Journal of Global Optimization 45 (2), 237–257.

Amos, F., Rönnqvist, M., Gill, G., 1997. Modelling the Pooling Problem at the New Zealand Refining Company. Journal of the Operational Research Society 48 (8), 767–778.

Audet, C., Brimberg, J., Hansen, P., Digabel, S. L., Mladenović, N., 2004. Pooling Problem: Alternate Formulations and Solution Methods. Management Science 50 (6), 761–776.

Audet, C., Hansen, P., Jaumard, B., Savard, G., 2000. A Branch and Cut Algorithm for Nonconvex Quadratically Constrained Quadratic Programming. Mathematical Programming 87 (1), 131–152.

Ben-Tal, A., Eiger, G., Gershovitz, V., 1994. Global Minimization By Reducing the Duality Gap. Mathematical Programming 63 (1-3), 193–212.

Boland, N., Kalinowski, T., Rigterink, F., Savelsbergh, M., 2015. A Special Case of the Generalized Pooling Problem Arising in the Mining Industry. Optimization Online e-prints.

Cannon, W. F., 2014. Manganese – It Turns Iron Into Steel (and Does So Much More). URL https://pubs.usgs.gov/fs/2014/3087/pdf/fs2014-3087.pdf, Accessed 07.09.2016.

Digernes, M. N., Rudi, L., 2016. Manganese Alloy Multi-plant Production Planning. Norwegian University of Science and Technology.

Downing, J. H., 2013. Manganese Processing. URL https://global.britannica.com/technology/manganese-processing, Accessed 12.09.2016.

d'Harambure, A., 2015. Overview of the Global Manganese Industry. International Manganese Institute. URL http://www.manganese.org/images/uploads/board-documents/14._2015_AC_-_Aloys_dHarambure.pdf, Accessed 03.09.2016.

Eramet Group, 2016a. Site Locations. URL http://www.eramet.com/en/locations, Accessed 05.10.2016.

Eramet Group, 2016b. The Group. URL http://www.eramet.com/en, Accessed 05.10.2016.

Eramet Norway, 2013. Sustainability Report. URL http://eramet.no/wp-content/uploads/ErametNorway_2013ENG.pdf, Accessed 12.09.2016.

Eramet Norway, 2014. Sustainability Report. URL http://eramet.no/wp-content/uploads/Eramet_rapport2014_ENG.pdf, Accessed 12.09.2016.

Eramet Norway, 2016a. Eramet Norway. URL http://eramet.no/, Accessed 06.12.2016.

Eramet Norway, 2016b. Eramet Norway Kvinesdal. URL http://eramet.no/en/our-organization/kvinesdal/, Accessed 12.09.2016.

Floudas, C., Visweswaran, V., 1990. A Global Optimization Algorithm (GOP) for Certain Classes of nonconvex NLPs — I. Theory. Computers & Chemical Engineering 14 (12), 1397–1417.

Foulds, L., Haugland, D., Jörnsten, K., 1992. A Bilinear Approach to the Pooling Problem. Optimization 24 (1-2), 165–180.

Foundry Lexicon, 2016. Sintering. URL http://www.giessereilexikon.com/en/foundry-lexicon/Encyclopedia/show/sintering-4064/?cHash=b049d7a731c3b15a3b92c25fe27d3009, Accessed 19.09.2016.

Gasik, M., 2013. Handbook of Ferroalloys: Theory and Technology. Butterworth-Heinemann.

Ghosh, A., Ray, H. S., 1991. Principles of Extractive Metallurgy. New Age International.

Gounaris, C. E., Misener, R., Floudas, C. A., 2009. Computational Comparison of Piecewise- Linear Relaxations for Pooling Problems. Industrial & Engineering Chemistry Research 48 (12), 5742–5766.

Gulf Manganese Corp. Ltd., 2017. What Is Manganese. URL http://gulfmanganese.com/what-is-manganese/, Accessed 27.03.2017.

Haverly, C. A., 1978. Studies of the Behavior of Recursion for the Pooling Problem. ACM Sigmap Bulletin (25), 19–28.

Hellemo, L., Tomasgard, A., 2016. A Generalized Global Optimization Formulation of the Pooling Problem with Processing Facilities and Composite Quality Constraints. TOP, 1–36.

Inductotherm Corp., 2016. Ladle Refining Furnaces. URL http://inductotherm.com/blog/products/ladle-refining-furnaces-lrf/, Accessed 19.09.2016.

International Manganese Institute and Hatch, 2015. The Environmental Profile of Manganese Alloys. URL http://www.manganese.org/images/uploads/pdf/IMnI_LCA_Summary_Report_View_2015.pdf, Accessed 07.09.2016.

InvestmentMine, 2017. Historical Manganese Prices and Price Chart. Accessed 25.03.2017. URL http://www.infomine.com/investment/metal-prices/manganese/all/

Jezowski, J., 2010. Review of Water Network Design Methods With Literature Annotations. Industrial & Engineering Chemistry Research 49 (10), 4475–4516.

Jipnang, E., Monheim, P., Oterdoom, H., 2013. Process Optimisation Model For FeMn And SiMn Production. In: The Thirteenth International Ferroalloys Congress, Efficient Technologies in Ferroalloy Industry, Almaty, Kazakhstan. pp. 811–820.

Kalagadi Manganese, 2013. Manganese Industry Overview. URL http://www.kalahariresources.co.za/index.php/2013-12-09-10-15-39/manganese-industry-overview, Accessed 07.09.2016.

Kolodziej, S., Castro, P. M., Grossmann, I. E., 2013a. Global Optimization of Bilinear Programs with a Multiparametric Disaggregation Technique. Journal of Global Optimization 57 (4), 1039–1063.

Kolodziej, S. P., Grossmann, I. E., Furman, K. C., Sawaya, N. W., 2013b. A Discretization-Based Approach for the Optimization of the Multiperiod Blend Scheduling Problem. Computers & Chemical Engineering 53, 122–142.

Kubaschewski, O., Alcock, C. B., Spencer, P., 1993. Materials Thermochemistry. Pergamon Press.

Li, H.-L., Chang, C.-T., 1998. An Approximate Approach of Global Optimization for Polynomial Programming Problems. European Journal of Operational Research 107 (3), 625–632.

Liberti, L., Pantelides, C. C., 2006. An Exact Reformulation Algorithm for Large Nonconvex NLPs Involving

Bilinear Terms. Journal of Global Optimization 36 (2), 161–189.

Lotero, I., Trespalacios, F., Grossmann, I. E., Papageorgiou, D. J., Cheon, M.-S., 2016. An MILP-MINLP Decomposition Method for the Global Optimization of a Source Based Model of the Multiperiod Blending Problem. Computers & Chemical Engineering 87, 13–35.

Marmara Metal, 2016. Ferro Manganese. URL http://www.marmarametal.com/urun/detay/urunid/340#.V-IrwpN95bU, Accessed 21.09.2016.

McCormick, G. P., 1976. Computability of Global Solutions to Factorable Nonconvex Programs: Part I—Convex Underestimating Problems. Mathematical Programming 10 (1), 147–175.

Metalpedia, 2016. Manganese: Uses. URL http://metalpedia.asianmetal.com/metal/manganese/application.shtml, Accessed 13.12.2016.

Meyer, C. A., Floudas, C. A., 2006. Global Optimization of a Combinatorially Complex Generalized Pooling Problem. AIChE Journal 52 (3), 1027–1037.

Misener, R., Floudas, C. A., 2009. Advances for the Pooling Problem: Modeling, Global Optimization, and Computational Studies. Appl. Comput. Math 8 (1), 3–22.

Olsen, S. E., Tangstad, M., 2004. Silicomanganese Production - Process Uunderstanding. In: Tenth International Ferroalloys Congress. pp. 231–238.

Olsen, S. E., Tangstad, M., Lindstad, T., 2007. Production of Manganese Ferroalloys. Tapir Academic Press.

Quesada, I., Grossmann, I. E., 1995. Global Optimization of Bilinear Process Networks With Multicomponent Flows. Computers & Chemical Engineering 19 (12), 1219–1242.

Risk & Policy Analysts Limited, 2015. Manganese, The Global Picture - A Socio Economic Assessment, Report for the International Manganese Institute. URL http://www.manganese.org/images/uploads/publications/Manganese_SEA_-_Complete.pdf, Accessed 03.09.2016.

Royal Society of Chemistry, 2016. Manganese - Element Information, Properties and Uses. URL http://www.rsc.org/periodic-table/element/25/manganese, Accessed 13.12.2016.

Sahinidis, N. V., Tawarmalani, M., 2005. Accelerating Branch-and-Bound through a Modeling Language Construct for Relaxation-specific Constraints. Journal of Global Optimization 32 (2), 259–280.

Sherali, H. D., Adams, W. P., 2013. A Reformulation-linearization Technique for Solving Discrete and Continuous Nonconvex Problems. Vol. 31. Springer Science & Business Media.

Sherali, H. D., Adams, W. P., Driscoll, P. J., 1998. Exploiting Special Structures in Constructing a Hierarchy of Relaxations for 0-1 Mixed Integer Problems. Operations Research 46 (3), 396–405.

Sherali, H. D., Alameddine, A., 1992. A New Reformulation-Linearization Technique for Bilinear Programming Problems. Journal of Global Optimization 2 (4), 379–410.

Tawarmalani, M., Sahinidis, N. V., 2002. Convexification and Global Optimization in Continuous and Mixed-Integer Nonlinear Programming: Theory, Algorithms, Software, and Applications. Vol. 65. Springer Science & Business Media.

Teles, J. P., Castro, P. M., Matos, H. A., 2012. Global Optimization of Water Networks Design Using Multiparametric Disaggregation. Computers & Chemical Engineering 40, 132–147.

Teles, J. P., Castro, P. M., Matos, H. A., 2013. Multi-parametric Disaggregation Technique for Global Optimization of Polynomial Programming Problems. Journal of Global Optimization 55 (2), 227–251.

United Nations Environment Programme, 2016. Changing Consumption Patterns. URL http://www.unep.org/Documents.Multilingual/Default.asp?DocumentID=52&ArticleID=52, Accessed 06.12.2016.

Visweswaran, V., Floudas, C., 1990. A Global Optimization Algorithm (GOP) for Certain Classes of Nonconvex NLPs — II. Application of Theory and Test Problems. Computers & Chemical Engineering 14 (12), 1419–1434.

Westfall, L. A., Davourie, J., Ali, M., McGough, D., 2016. Cradle-to-gate Life Cycle Assessment of Global Manganese Alloy Production. The International Journal of Life Cycle Assessment.

Wicaksono, D. S., Karimi, I. A., 2008. Piecewise MILP Under-and Overestimators for Global Optimization of Bilinear Programs. AIChE Journal 54 (4), 991–1008.

Appendix A

Chemical Constraints

The chemical reaction variables are defined as $v \in \{\text{FED, RED, SLAG, RSRED, TOT}\}$ and α_{pfkc}, where the FED, RED, SLAG, and α_{pfkc} are left side reactant variables, and RSRED is the right side resultant variable, the TOT variable is dependent on the reaction. The main chemical constraints are numbered according to the order of appearance of the chemical reactions (2.5) - (2.17) in Chapter 2.

A.1 Main Chemical Constraints

The main chemical constraints are defined as equality constraints. These are the constraints handling the elements and oxides directly related to the output of alloy from the furnaces. The (*a*) constraints ensure the correct balance between the left and right side components. The (*b*) constraints ensure the correct relationships between the left side components. The (*c*) constraints ensure the correct relationships between the right side components.

Reaction (2.5), $2\,MnO_2(l) + CO(g) \longrightarrow Mn_2O_3(l) + CO_2(g)$, constraints:

$$\begin{aligned} n_{pf,\mathrm{MnO_2},1,\text{FED}} \;+\; 2n_{pf,\mathrm{CO},1,\text{TOT}} \\ -\; 2n_{pf,\mathrm{Mn_2O_3},1,\text{RSRED}} \;-\; 2n_{pf,\mathrm{CO_2},1,\text{RSRED}} = 0 \end{aligned} \qquad p \in \mathcal{P},\;\; f \in \mathcal{F}_p \tag{A.1a}$$

$$n_{pf,\mathrm{MnO_2},1,\text{FED}} \;-\; 2n_{pf,\mathrm{CO},1,\text{TOT}} = 0 \qquad p \in \mathcal{P},\;\; f \in \mathcal{F}_p \tag{A.1b}$$

$$n_{pf,\mathrm{Mn_2O_3},1,\text{RSRED}} \;-\; n_{pf,\mathrm{CO_2},1,\text{RSRED}} = 0 \qquad p \in \mathcal{P},\;\; f \in \mathcal{F}_p \tag{A.1c}$$

Reaction (2.6), $3\,Mn_2O_3(l) + CO(g) \longrightarrow 2\,Mn_3O_4(l) + CO_2(g)$, constraints:

$$\begin{aligned} 2n_{pf,\mathrm{Mn_2O_3},2,\text{FED}} \;+\; 2n_{pf,\mathrm{Mn_2O_3},2,\text{RED}} \;+\; 6n_{pf,\mathrm{CO},2,\text{TOT}} \\ -\; 3n_{pf,\mathrm{Mn_3O_4},2,\text{RSRED}} \;-\; 6n_{pf,\mathrm{CO_2},2,\text{RSRED}} = 0 \end{aligned} \qquad p \in \mathcal{P},\;\; f \in \mathcal{F}_p \tag{A.2a}$$

$$n_{pf,\mathrm{Mn_2O_3},2,\text{FED}} \;+\; n_{pf,\mathrm{Mn_2O_3},2,\text{RED}} \;-\; 3n_{pf,\mathrm{CO},2,\text{TOT}} = 0 \qquad p \in \mathcal{P},\;\; f \in \mathcal{F}_p \tag{A.2b}$$

$$n_{pf,\mathrm{Mn_3O_4},2,\text{RSRED}} \;-\; 2n_{pf,\mathrm{CO_2},2,\text{RSRED}} = 0 \qquad p \in \mathcal{P},\;\; f \in \mathcal{F}_p \tag{A.2c}$$

Reaction (2.7), Mn_3O_4(l) + CO(g) $\longrightarrow$ 3 (MnO) + CO_2(g), constraints:

$$\begin{aligned} 3n_{pf,\mathrm{Mn_3O_4},3,\text{FED}} \;+\; 3n_{pf,\mathrm{Mn_3O_4},3,\text{RED}} \;+\; 3n_{pf,\mathrm{CO},3,\text{TOT}} \\ -n_{pf,\mathrm{MnO},3,\text{RSRED}} \;-\; 3n_{pf,\mathrm{CO_2},3,\text{RSRED}} = 0 \qquad p \in \mathcal{P},\;\; f \in \mathcal{F}_p \end{aligned} \tag{A.3a}$$

$$n_{pf,\mathrm{Mn_3O_4},3,\text{FED}} \;+\; n_{pf,\mathrm{Mn_3O_4},3,\text{RED}} \;-\; n_{pf,\mathrm{CO},3,\text{TOT}} = 0 \qquad p \in \mathcal{P},\;\; f \in \mathcal{F}_p \tag{A.3b}$$

$$n_{pf,\mathrm{MnO},3,\text{RSRED}} \;-\; 3n_{pf,\mathrm{CO_2},3,\text{RSRED}} = 0 \qquad p \in \mathcal{P},\;\; f \in \mathcal{F}_p \tag{A.3c}$$

Reaction (2.8), (MnO) + C(s) $\longrightarrow$ $\underline{\text{Mn}}$ + CO(g), constraints:

$$\begin{aligned} n_{pf,\mathrm{MnO},4,\text{FED}} \;+\; n_{pf,\mathrm{MnO},4,\text{RED}} \\ +\; (1 - \sum\nolimits_{b\in\mathcal{B}} \Psi^{\mathrm{B}}_{fb,\mathrm{MnO}}) n_{pf,\mathrm{MnO},4,\text{SLAG}} \;-\; \alpha_{pf,\mathrm{MnO},4} \\ +\; n_{pf,\mathrm{C},4,\text{FED}} \;-\; n_{pf,\mathrm{Mn},4,\text{RSRED}} \;-\; n_{pf,\mathrm{CO},4,\text{RSRED}} = 0 \qquad p \in \mathcal{P},\;\; f \in \mathcal{F}_p \end{aligned} \tag{A.4a}$$

$$\begin{aligned} n_{pf,\mathrm{MnO},4,\text{FED}} \;+\; n_{pf,\mathrm{MnO},4,\text{RED}} \\ +\; (1 - \sum\nolimits_{b\in\mathcal{B}} \Psi^{\mathrm{B}}_{fb,\mathrm{MnO}}) n_{pf,\mathrm{MnO},4,\text{SLAG}} \\ -\; \alpha_{pf,\mathrm{MnO},4} \;-\; n_{pf,\mathrm{C},4,\text{FED}} = 0 \qquad p \in \mathcal{P},\;\; f \in \mathcal{F}_p \end{aligned} \tag{A.4b}$$

$$n_{pf,\mathrm{Mn},4,\text{RSRED}} \;-\; n_{pf,\mathrm{CO},4,\text{RSRED}} = 0 \qquad p \in \mathcal{P},\;\; f \in \mathcal{F}_p \tag{A.4c}$$

Reaction (2.9), C(s) $\longrightarrow$ $\underline{\text{C}}$, constraints:

$$n_{pf,\mathrm{C},5,\text{FED}} \;-\; n_{pf,\mathrm{C},5,\text{TOT}} = 0 \qquad p \in \mathcal{P},\;\; f \in \mathcal{F}_p \tag{A.5}$$

Reaction (2.10), 3 Fe_2O_3(l) + CO(g) $\longrightarrow$ 2 Fe_3O_4(l) + CO_2(g), constraints:

$$\begin{aligned} 2n_{pf,\mathrm{Fe_2O_3},6,\text{FED}} \;+\; 6n_{pf,\mathrm{CO},6,\text{TOT}} \\ -\; 3n_{pf,\mathrm{Fe_3O_4},6,\text{RSRED}} \;-\; 6n_{pf,\mathrm{CO_2},6,\text{RSRED}} = 0 \qquad p \in \mathcal{P},\;\; f \in \mathcal{F}_p \end{aligned} \tag{A.6a}$$

$$n_{pf,\mathrm{Fe_2O_3},6,\text{FED}} \;-\; 3n_{pf,\mathrm{CO},6,\text{TOT}} = 0 \qquad p \in \mathcal{P},\;\; f \in \mathcal{F}_p \tag{A.6b}$$

$$n_{pf,\mathrm{Fe_3O_4},6,\text{RSRED}} \;-\; 2n_{pf,\mathrm{CO_2},6,\text{RSRED}} = 0 \qquad p \in \mathcal{P},\;\; f \in \mathcal{F}_p \tag{A.6c}$$

Reaction (2.11), Fe_3O_4(l) + CO(g) $\longrightarrow$ 3 (FeO) + CO_2(g), constraints:

$$\begin{aligned} 3n_{pf,\mathrm{Fe_3O_4},7,\text{FED}} \;+\; 3n_{pf,\mathrm{Fe_3O_4},7,\text{RED}} \;+\; 3n_{pf,\mathrm{CO},7,\text{TOT}} \\ -\; n_{pf,\mathrm{FeO},7,\text{RSRED}} \;-\; 3n_{pf,\mathrm{CO_2},7,\text{RSRED}} = 0 \qquad p \in \mathcal{P},\;\; f \in \mathcal{F}_p \end{aligned} \tag{A.7a}$$

$$n_{pf,\mathrm{Fe_3O_4},7,\text{FED}} \;+\; n_{pf,\mathrm{Fe_3O_4},7,\text{RED}} \;-\; n_{pf,\mathrm{CO},7,\text{TOT}} = 0 \qquad p \in \mathcal{P},\;\; f \in \mathcal{F}_p \tag{A.7b}$$

$$n_{pf,\mathrm{FeO},7,\text{RSRED}} \;-\; 3n_{pf,\mathrm{CO_2},7,\text{RSRED}} = 0 \qquad p \in \mathcal{P},\;\; f \in \mathcal{F}_p \tag{A.7c}$$

Reaction (2.12), (FeO) + C(s) $\longrightarrow$ Fe + CO(g), constraints:

$$\begin{aligned} & n_{pf,\mathrm{FeO},8,\mathrm{FED}} + n_{pf,\mathrm{FeO},8,\mathrm{RED}} \\ + \ & (1 - \sum\nolimits_{b\in\mathcal{B}} \Psi^{\mathrm{B}}_{fb,\mathrm{FeO}}) n_{pf,\mathrm{FeO},8,\mathrm{SLAG}} - \alpha_{pf,\mathrm{FeO},8} \\ + \ & n_{pf,\mathrm{C},8,\mathrm{FED}} - n_{pf,\mathrm{Fe},8,\mathrm{RSRED}} - n_{pf,\mathrm{CO},8,\mathrm{RSRED}} = 0 \qquad p \in \mathcal{P}, \ \ f \in \mathcal{F}_p \end{aligned} \tag{A.8a}$$

$$\begin{aligned} & n_{pf,\mathrm{FeO},8,\mathrm{FED}} + n_{pf,\mathrm{FeO},8,\mathrm{RED}} \\ + \ & (1 - \sum\nolimits_{b\in\mathcal{B}} \Psi^{\mathrm{B}}_{fb,\mathrm{FeO}}) n_{pf,\mathrm{FeO},8,\mathrm{SLAG}} \\ - \ & \alpha_{pf,\mathrm{FeO},8} - n_{pf,\mathrm{C},8,\mathrm{FED}} = 0 \qquad p \in \mathcal{P}, \ \ f \in \mathcal{F}_p \end{aligned} \tag{A.8b}$$

$$n_{pf,\mathrm{Fe},8,\mathrm{RSRED}} - n_{pf,\mathrm{CO},8,\mathrm{RSRED}} = 0 \qquad p \in \mathcal{P}, \ \ f \in \mathcal{F}_p \tag{A.8c}$$

Reaction (2.13), (SiO_2) + 2 C(s) $\longrightarrow$ Si + 2 CO(g), constraints:

$$\begin{aligned} & 2n_{pf,\mathrm{SiO_2},9,\mathrm{FED}} \\ + \ & (1 - \sum\nolimits_{b\in\mathcal{B}} \Psi^{\mathrm{B}}_{fb,\mathrm{SiO_2}}) 2n_{pf,\mathrm{SiO_2},9,\mathrm{SLAG}} \\ - \ & 2\alpha_{pf,\mathrm{SiO_2},9} + n_{pf,\mathrm{C},9,\mathrm{FED}} \\ - \ & 2n_{pf,\mathrm{Si},9,\mathrm{RSRED}} - n_{pf,\mathrm{CO},9,\mathrm{RSRED}} = 0 \qquad p \in \mathcal{P}, \ \ f \in \mathcal{F}_p \end{aligned} \tag{A.9a}$$

$$\begin{aligned} & 2n_{pf,\mathrm{SiO_2},9,\mathrm{FED}} \\ + \ & (1 - \sum\nolimits_{b\in\mathcal{B}} \Psi^{\mathrm{B}}_{fb,\mathrm{SiO_2}}) 2n_{pf,\mathrm{SiO_2},9,\mathrm{SLAG}} \\ - \ & 2\alpha_{pf,\mathrm{SiO_2},9} - n_{pf,\mathrm{C},9,\mathrm{FED}} = 0 \qquad p \in \mathcal{P}, \ \ f \in \mathcal{F}_p \end{aligned} \tag{A.9b}$$

$$2n_{pf,\mathrm{Si},9,\mathrm{RSRED}} - n_{pf,\mathrm{CO},9,\mathrm{RSRED}} = 0 \qquad p \in \mathcal{P}, \ \ f \in \mathcal{F}_p \tag{A.9c}$$

A.2 Critical Chemical Constraints

The critical chemical constraints sum the moles of reduced metals from the main chemical constraints defined in the previous section and pure metal originating directly from the ores. Constraints (A.5) are also included in the critical chemical constraints, as carbon is an essential part of the output alloy.

$$n_{pf,\mathrm{Mn},10,\mathrm{TOT}} = n_{pf,\mathrm{Mn},4,\mathrm{RSRED}} + n_{pf,\mathrm{Mn},10,\mathrm{FED}} \qquad p \in \mathcal{P}, \ \ f \in \mathcal{F}_p \tag{A.10}$$

$$n_{pf,\mathrm{Fe},11,\mathrm{TOT}} = n_{pf,\mathrm{Fe},8,\mathrm{RSRED}} + n_{pf,\mathrm{Fe},11,\mathrm{FED}} \qquad p \in \mathcal{P}, \ \ f \in \mathcal{F}_p \tag{A.11}$$

$$n_{pf,\mathrm{Si},12,\mathrm{TOT}} = n_{pf,\mathrm{Si},9,\mathrm{RSRED}} + n_{pf,\mathrm{Si},12,\mathrm{FED}} \qquad p \in \mathcal{P}, \ \ f \in \mathcal{F}_p \tag{A.12}$$

A.3 Reduction Relating Chemical Constraints

The reduction relating chemical constraints relates the right side reduction variable RSRED and the left side reduction variable RED, which handles the feed of reduced oxides, for the respective oxides in different chemical constraints.

$$n_{pf,\mathrm{Mn_2O_3},2,\mathrm{RED}} = n_{pf,\mathrm{Mn_2O_3},1,\mathrm{RSRED}} \qquad p \in \mathcal{P},\ f \in \mathcal{F}_p \tag{A.13}$$

$$n_{pf,\mathrm{Mn_3O_4},3,\mathrm{RED}} = n_{pf,\mathrm{Mn_3O_4},2,\mathrm{RSRED}} \qquad p \in \mathcal{P},\ f \in \mathcal{F}_p \tag{A.14}$$

$$n_{pf,\mathrm{MnO},4,\mathrm{RED}} = n_{pf,\mathrm{MnO},3,\mathrm{RSRED}} \qquad p \in \mathcal{P},\ f \in \mathcal{F}_p \tag{A.15}$$

$$n_{pf,\mathrm{Fe_3O_4},7,\mathrm{RED}} = n_{pf,\mathrm{Fe_3O_4},6,\mathrm{RSRED}} \qquad p \in \mathcal{P},\ f \in \mathcal{F}_p \tag{A.16}$$

$$n_{pf,\mathrm{FeO},8,\mathrm{RED}} = n_{pf,\mathrm{FeO},7,\mathrm{RSRED}} \qquad p \in \mathcal{P},\ f \in \mathcal{F}_p \tag{A.17}$$

A.4 The Boudouard Reaction Chemical Constraints

The Boudouard reaction is special in the form that CO_2 resulting from the main chemical constraints (2.5) - (2.7) and (2.10) - (2.11) reacts with carbon feed and forms CO that supplies the same main chemical reactions. Constraints (A.18a) describes the chemical reaction and (A.18b) ensure correct relationships between the left side components of the reaction.

Reaction (2.14), $\mathrm{C(s) + CO_2(g) \longrightarrow 2\,CO(g)}$, constraints:

$$n_{pf,\mathrm{C},18,\mathrm{FED}} + n_{pf,\mathrm{CO_2},18,\mathrm{TOT}} - n_{pf,\mathrm{CO},18,\mathrm{RSRED}} = 0 \quad p \in \mathcal{P},\ f \in \mathcal{F}_p \tag{A.18a}$$

$$n_{pf,\mathrm{C},18,\mathrm{FED}} - n_{pf,\mathrm{CO_2},18,\mathrm{TOT}} = 0 \quad p \in \mathcal{P},\ f \in \mathcal{F}_p \tag{A.18b}$$

Constraints (A.19a) are defined as equality constraints, as the pre-reduction term $(1 - \Upsilon)$ defines how much CO_2 is being reused. The amount of CO fed to reactions (2.5) - (2.7) and (2.10) - (2.11) is given by constraints (A.19b). They are formulated as inequality constraints since not all of the CO resulting from the main chemical constraints and the Boudouard reaction is reused as reactants, but released as off-gases to the atmosphere.

$$n_{pf,\mathrm{CO_2},18,\mathrm{TOT}} = (1-\Upsilon) \sum_{c \in \mathcal{C}\setminus\{1,2\}} n_{pf,\mathrm{CO_2},c,\mathrm{RSRED}} \qquad p \in \mathcal{P},\ f \in \mathcal{F}_p \tag{A.19a}$$

$$\sum_{c \in \mathcal{C}^{\mathrm{O}}} n_{pf,\mathrm{CO},c,\mathrm{TOT}} \leq n_{pf,\mathrm{CO},18,\mathrm{RSRED}} + \sum_{c \in \mathcal{C}^{\mathrm{S}}} n_{pf,\mathrm{CO},c,\mathrm{RSRED}} \qquad p \in \mathcal{P},\ f \in \mathcal{F}_p \tag{A.19b}$$

A.5 Slag Specific Oxide Constraints

The slag specific oxide constraints describe the oxides that flow from the HC FeMn furnace to the MC SiMn furnace through the slag. These oxides completely exit the MC SiMn furnace as discardable slag.

Reaction (2.15), $Al_2O_3(l) \longrightarrow (Al_2O_3)$, constraints:

$$n_{pf,\mathrm{Al_2O_3},20,\mathrm{FED}} = \alpha_{pf,\mathrm{Al_2O_3},20} \qquad p \in \mathcal{P},\ \ f \in \mathcal{F}_p^{\mathrm{FeMn}} \tag{A.20}$$

Reaction (2.17), $CaO(l) \longrightarrow (CaO)$, constraints:

$$n_{pf,\mathrm{CaO},21,\mathrm{FED}} = \alpha_{pf,\mathrm{CaO},21} \qquad p \in \mathcal{P},\ \ f \in \mathcal{F}_p^{\mathrm{FeMn}} \tag{A.21}$$

Reaction (2.16), $MgO(l) \longrightarrow (MgO)$, constraints:

$$n_{pf,\mathrm{MgO},22,\mathrm{FED}} = \alpha_{pf,\mathrm{MgO},22} \qquad p \in \mathcal{P},\ \ f \in \mathcal{F}_p^{\mathrm{FeMn}} \tag{A.22}$$

Appendix B

Weight Relationship Parameters

This appendix presents the calculations done to determine the values for the parameters Ω^{MOR} and Ω^{REF} to omit the need to include the chemical reactions occurring in the MOR and the LC SiMn refining station in the model formulation.

Defining the values for the carbon content in HC and MC alloys: $C^{\text{HC}} = 0.07$ and $C^{\text{MC}} = 0.015$ based on values from *Olsen et al. (2007)*. Molar mass for the required elements to calculate the parameters: carbon: $M_{\text{C}} = 12.0107 \cdot 10^{-3}$ kg/mole, and oxygen: $M_{\text{O}_2} = 31.9988 \cdot 10^{-3}$ kg/mole.

The value of the Ω^{MOR} parameter can be found by consulting the relationship:

$$\frac{1}{2}\,\text{O}_2(\text{g}) + \text{C}(\text{s}) \longrightarrow \text{CO}(\text{g})$$

$\frac{1}{2}$ mole O_2 is consumed per mole C in the alloy. Ω^{MOR} is given as a weight fraction of the feed of HC FeMn alloy to the MOR. Ω^{MOR} times the mass of the HC FeMn alloy fed to the MOR gives the amount of oxygen that must be added to the process to reduce the carbon content to the desired specification. Define input mass of HC FeMn: $m_{\text{HC FeMn}} = 1$ kg, where the weight of carbon is $m_{\text{C}} = m_{\text{HC FeMn}} \cdot C^{\text{HC}} = 0.07$ kg. The Ω^{MOR} is given by:

$$\Omega^{\text{MOR}} = \frac{(C^{\text{HC}} - C^{\text{MC}}) \cdot \dfrac{m_{\text{C}} \cdot M_{\text{C}}}{\frac{1}{2} \cdot M_{\text{O}_2}}}{m_{\text{HC FeMn}}} = \frac{(0.07 - 0.015) \cdot \dfrac{0.07\ \text{kg} \cdot 12.0107 \cdot 10^{-3}\ \text{kg/mole}}{\frac{1}{2} \cdot 31.9988 \cdot 10^{-3}\ \text{kg/mole}}}{1\ \text{kg}}$$

$$\Omega^{\text{MOR}} = 0.00289$$

According to *Olsen et al. (2007)*, the silicon refining process consumes 250 kg FeSi per 950 kg MC SiMn alloy entered into the process to achieve a carbon content of C^{LC} = 0.005. Ω^{REF} is given as a weight fraction of the feed of MC SiMn to the LC SiMn refining station. Ω^{REF} times the mass of the MC SiMn alloy fed to the LC SiMn refining station gives the amount of silicon-waste that must be added to the process to reduce the carbon content to the desired specification.

$$\Omega^{\text{REF}} = \frac{250\ \text{kg}}{950\ \text{kg}} = 0.2632$$

Appendix C

Furnace Mass Balance

This appendix illustrates the flow of different components through the HC FeMn and MC SiMn furnaces. The modelling of looping elements due to re-entering gas and the Boudouard reaction is also illustrated. Figure C.1 shows the flow of the different components through an arbitrary furnace.

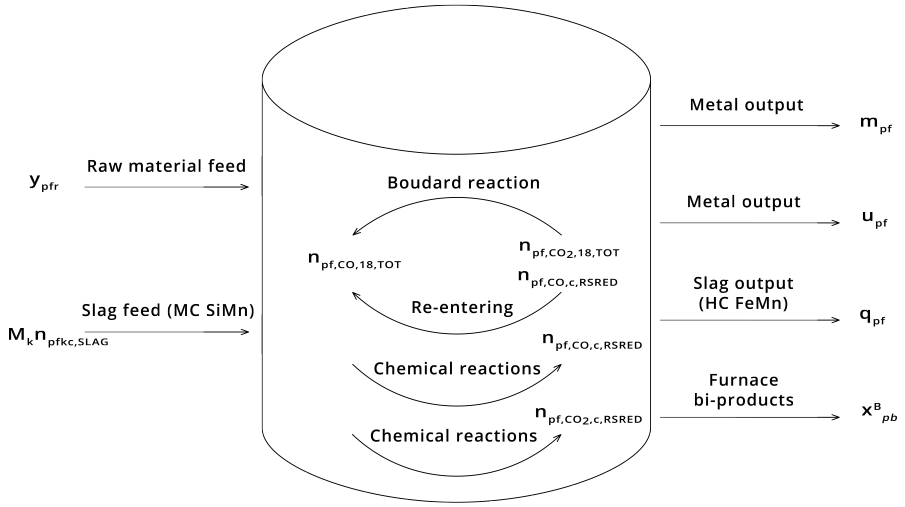

Figure C.1: Furnace mass balance overview.

As seen from Figure C.1, an amount of raw materials y_{pfr} is fed to the furnace, where the mass of the modelled elements and oxides enter the n_{pfkcv} variables. Slag originating from the HC FeMn furnace is an entering component in the MC SiMn furnace.

In the furnace, large amounts of CO and CO_2 gas is produced. A certain amount of these gases re-enters the chemical process, while the remainder is released into the atmosphere. CO_2 is consumed by the Boudouard reaction according to the specified degree of pre-reduction Υ. Thus, the CO_2 reacts with C and forms CO for use in the original chemical reactions. Consequently, when the amount of CO produced from the Boudouard reaction is consumed, the mass of the O-atoms in CO_2 is accounted for twice in the furnace mass balance. Therefore, to have a correct mass balance, the weight of the O-atoms accounted for twice must be subtracted. The mass is found by multiplying

the molar mass of O with the number of CO_2 molecules $n_{pf,\mathrm{CO}_2,18,\mathrm{TOT}}$ consumed in the Boudouard reaction, as the number of moles of O-atoms and re-entering CO_2 molecules are equal.

Leaving the furnace are the produced amount of metal m_{pf} and u_{pf}, as well as with discardable by-products x^{B}_{pb}. Produced slag q_{pf} is leaving the HC FeMn furnace. Gases are not modelled to leave the furnace, therefore, the remaining gas is left in the n_{pfkcv} variables for simplicity. This mass can be considered as the volume of gases that is released into the atmosphere.

Appendix D

Raw Material Compositions

Table D.1 gives the weight fractions of all relevant elements and oxides modelled by the chemical constraints in the MAMP for all raw materials. The sum of the weight fractions is also given for reference. When the sum is less than 1.00, it means there are other elements or contaminants in the raw materials that are not modelled. When a raw material is added to the furnace operation, it occupies 1 kg of the capacity regardless of the sum of the weight fractions, but only the sum of the weight fraction enters as moles into the chemical reactions. An example is provided for Ore 8: when 1 kg of the Ore 8 enters the furnace, only 0.7710722 kg is converted to moles and used in the respectable chemical constraints (0.4381950 kg as Mn_2O_3, 0.0108540 kg as Mn_3O_4, and so forth as described in Table D.1). This modelling choice ensures that the mass capacity of the furnace is respected and that consumption of low-, medium- and high-grade ores can be modelled correctly. Raw material contents are provided by the industry partner, and the data is perturbed.

Table D.1: Composition of elements and oxides in all raw materials. Given as weight fractions.

Type	MnO_2	Mn_2O_3	Mn_3O_4	MnO	Mn	Fe_2O_3	Fe_3O_4	FeO
Ore 1	0.6843442	0.0961908	0.0000000	0.0000000	0.0000000	0.0313739	0.0023511	0.0000000
Ore 2	0.6816263	0.0639357	0.0000000	0.0000000	0.0000000	0.0362813	0.0018557	0.0000000
Ore 3	0.0000000	0.0453822	0.4585738	0.0000000	0.0000000	0.0732689	0.0014021	0.0000000
Ore 4	0.6104011	0.1044539	0.0000000	0.0000000	0.0000000	0.0338087	0.0010603	0.0000000
Ore 5	0.0000000	0.0000000	0.0000000	0.7662274	0.0000000	0.0000000	0.0018332	0.1134918
Ore 6	0.0000000	0.0000000	0.4476948	0.2252482	0.0000000	0.0000000	0.0129852	0.0224588
Ore 7	0.0141170	0.6655660	0.0000000	0.0000000	0.0000000	0.1441404	0.0035526	0.0000000
Ore 8	0.0000000	0.4381950	0.0108540	0.0000000	0.0758821	0.0159827	0.0007583	0.0000000
Ore 9	0.0000000	0.0000000	0.4537059	0.3296261	0.0000000	0.0301467	0.0106333	0.0000000
Ore 10	0.0000000	0.0000000	0.4295173	0.3501277	0.0000000	0.0000000	0.0003689	0.0363201
Coke 11	0.0000000	0.0000000	0.0001676	0.0002264	0.0000000	0.0529452	0.0011628	0.0000000
Coke 12	0.0001262	0.0001698	0.0000000	0.0000000	0.0000000	0.0066660	0.0020250	0.0000000
Coke 13	0.0001253	0.0001697	0.0000000	0.0000000	0.0000000	0.0080001	0.0012499	0.0000000
Flux 14	0.0000000	0.0000000	0.0000000	0.4435092	0.0000000	0.0662746	0.0011034	0.0000000
Flux 15	0.0000000	0.0000000	0.0005538	0.0058262	0.0000000	0.0000000	0.0001745	0.0011015
Flux 16	0.0015364	0.0000316	0.0000000	0.0000000	0.0000003	0.8753059	0.0633831	0.0000000
HCFe 17	0.0000000	0.0000000	0.0000000	0.0000000	0.7900000	0.0000000	0.0000000	0.0000000
MCSi 18	0.0000000	0.0000000	0.0000000	0.0000000	0.7120000	0.0000000	0.0000000	0.0000000
Quart 19	0.0000000	0.0000000	0.0000000	0.0000000	0.0000000	0.0000000	0.0000000	0.0000000

Type	Fe	SiO_2	Si	C	Al_2O_3	MgO	CaO	Sum
Ore 1	0.0000000	0.0420830	0.0000000	0.0000000	0.0560790	0.0000970	0.0003890	0.9129080
Ore 2	0.0000000	0.0558950	0.0000000	0.0000000	0.0651140	0.0017470	0.0010670	0.9075220
Ore 3	0.0000000	0.0648590	0.0000000	0.0000000	0.0043170	0.0393470	0.1346240	0.8217740
Ore 4	0.0000000	0.0488950	0.0000000	0.0000000	0.0799110	0.0000000	0.0014820	0.8800120
Ore 5	0.0000000	0.0066970	0.0000000	0.0000000	0.0019700	0.0019700	0.0003940	0.8925834
Ore 6	0.0000348	0.0847320	0.0009820	0.0083460	0.0500730	0.0046150	0.0765820	0.9337518
Ore 7	0.0000000	0.0405910	0.0000000	0.0000000	0.0049880	0.0049880	0.0724770	0.9504200
Ore 8	0.0008391	0.0842950	0.0009850	0.0014770	0.0530780	0.0217630	0.0669630	0.7710722
Ore 9	0.0000000	0.0690430	0.0000000	0.0008800	0.0603390	0.0000980	0.0017600	0.9562320
Ore 10	0.0000000	0.0694750	0.0000000	0.0011710	0.0588390	0.0000980	0.0021470	0.9480640
Coke 11	0.0000000	0.0644560	0.0000000	0.8041230	0.0308480	0.0020700	0.0068000	0.9627990
Coke 12	0.0000000	0.0445430	0.0000000	0.8660720	0.0312100	0.0022720	0.0042470	0.9573310
Coke 13	0.0000000	0.0431020	0.0000000	0.8786730	0.0286360	0.0019680	0.0033460	0.9652700
Flux 14	0.0000000	0.1613140	0.0000000	0.0982640	0.0855750	0.0476070	0.0711160	0.9747632
Flux 15	0.0000000	0.0090300	0.0000000	0.0000000	0.0027480	0.2051370	0.3003440	0.5249150
Flux 16	0.0000000	0.0195970	0.0000000	0.0000000	0.0023520	0.0051930	0.0051930	0.9725923
HCFe 17	0.1360000	0.0000000	0.0040000	0.0700000	0.0000000	0.0000000	0.0000000	1.0000000
MCSi 18	0.0810000	0.0000000	0.1920000	0.0150000	0.0000000	0.0000000	0.0000000	1.0000000
Quart 19	0.0000000	0.9700000	0.0000000	0.0000000	0.0000000	0.0000000	0.0000000	0.9700000

Appendix E

Thermodynamic Properties

The enthalpy values used to calculate the electrical power consumption in the furnaces are presented in this appendix. It is assumed that all of the raw materials enter the furnace at 25°C and that slag, by-products, and tapped metal leave the furnace at 1500°C. The temperature of the gas leaving the furnace is assumed to be 200°C. These assumptions are in cohesion with the assumptions done for a furnace energy consumption calculation performed in *Olsen et al. (2007)*. Values for the formation and sensible enthalpies are given in Table E.1. The values are either supplied by the problem owner or calculated based on thermodynamic relations and tables found in *Kubaschewski et al. (1993)*. The values for H_2O are also provided, as a each ore contain some moisture not accounted for in the raw material composition. This moisture evaporates when exposed to the heat in the furnace, thus consuming energy.

Table E.1: Formation enthalpy H_k^{F} and sensible enthalpy H_k^{S} for each element or oxide. H_k^{F} given in (-10^{-3}) kJ/tonne, H_k^{S} in 10^{-3} kJ/tonne.

	Element or Oxide k								
Parameter	**MnO_2**	**Mn_2O_3**	**Mn_3O_4**	**MnO**	**Mn**	**Fe_2O_3**	**Fe_3O_4**	**FeO**	**Fe**
H_k^{F}	5991.7	6068.8	6063.5	5425.9	0	5156.3	4789.0	3660.7	0
H_k^{S}	1450.1	1560.5	1376.9	1236.9	1256.5	1349.9	1382.5	1278.2	1388.2
Parameter	**CO**	**CO_2**	**SiO_2**	**Si**	**C**	**Al_2O_3**	**MgO**	**CaO**	**H_2O**
H_k^{F}	3945.0	8941.3	15160.4	0	0	16434.7	14926.4	11321.9	44.0
H_k^{S}	200.5	111.8	2714.3	1452.7	2957.9	1933.2	1996.0	1506.3	505.0

Appendix F

Paper: Optimisation of Manganese Alloy Production

A paper has been written by the authors in collaboration with the supervisors. It is to be submitted to the journal Computers & Chemical Engineering for review during the summer of 2017. The unreviewed and unpublished version of the paper is appended here. As the paper is based on this thesis, there is overlapping content.

Optimisation of Manganese Alloy Production

Martin Naterstad Digernes[a,1], Lars Rudi[a,1],
Henrik Andersson[a], Magnus Stålhane[a], Stein O. Wasbø[b], Brage Rugstad Knudsen[b,c,d,*]

[a]*Department of Industrial Economics and Technology Management, NTNU, Alfred Getz veg 3, NO-7491 Trondheim, Norway*
[b]*Cybernetica AS, Leirfossveien 27, NO-7038 Trondheim, Norway*
[c]*Department of Engineering Cybernetics, NTNU, O. S. Bragstads plass 2D, Building D, NO-7491 Trondheim, Norway*
[d]*SINTEF Energy Research, Sem Sløndsvei 11, NO-7465 Trondheim, Norway*

Abstract

This paper studies the problem of multi-plant manganese alloy production. The problem is to find the optimal combination of ores, fluxes, coke, and slag to feed the furnaces that yields output products which meet customer specifications, and to optimally decide the volume, composition, and allocation of the slag. To solve the problem, a pooling problem formulation is presented and the bilinear terms are linearised using the Multiparametric Disaggregation Technique (MDT). This enables global optimisation by means of commercial software for mixed integer linear programs. We demonstrate the model and solution approach through case studies of the Norwegian manganese alloy producer Eramet Norway, using their plant layout consisting of three plants and seven furnaces. The computational study shows that the optimisation model presented can solve problem sizes of up to ten furnaces to a reasonable global optimality gap within the allotted run time, that the MDT is able to scale well with larger, real problem instances, and that our model outperforms the current operational practice. It should be noted that the current operational practice is mimicked by using instances of our model, and not actual practice results. Comparing the model to real production data remains an objective, but the results indicate that using our model could be of considerable value to manganese alloy production.

Keywords: Pooling Problem, Manganese Alloy Production, Multiparametric Disaggregation Technique, Optimisation, Multi-plant Production, Linear Programming

1. Introduction

Manganese is a hard, brittle, silvery metal that occurs in nature in the form of minerals, mainly as oxides. It is an essential element in steel and aluminium alloys, commonly used in railway tracks and safes, and beverage cans and kitchenware, respectively. The total production of manganese alloys has been approximately twenty million tonnes annually in the recent years *(d'Harambure, 2015)*. An average price of manganese alloys around 2 USD/kg *(InvestmentMine, 2017)* makes the manganese alloy production a multi-billion dollar industry.

There is an increasing focus on environmental impacts caused by production industries *(United Nations, 2016; Olsen et al., 2007)*. Consequences of unsustainable production of manganese alloys are environmental degradation, resource depletion, and CO_2-emissions. Manganese alloy production also produces a significant amount of slag and metallic dust that can have negative impacts on the environment if not handled properly. Producers of manganese are, therefore, looking for new ways to utilise available resources better and to make the production more sustainable.

Manganese alloy production can be divided into two categories: extraction and smelting. Extraction constitutes the processes of mining, hauling the ore to a processing plant, crushing, separation and beneficiation at the plant, transportation to sinter plants, and sintering *(Olsen et al., 2007)*. The smelting process constitutes the processes of smelting ores, fluxes, quartz, and coke in furnaces, tapping and casting, refining, crushing, and transportation of by-products back into processes or to disposal sites *(International Manganese Institute and Hatch, 2015)*.

*Corresponding author
Email address: brage.knudsen@ntnu.no (Brage Rugstad Knudsen)
[1]The first two authors contributed equally to this paper.

The focus of this paper is on the smelting process of the supply chain. Figure 1 provides an overview of the processes under consideration and the material flow between the processes. The raw material inventory supplies the necessary resources to the high-carbon ferromanganese (HC FeMn) and the medium-carbon silicomanganese (MC SiMn) furnaces. The output products from the HC FeMn furnace are HC FeMn alloy, reusable slag, and nonprofitable dust. The output products from the MC SiMn furnace are MC SiMn alloy, discard slag, and nonprofitable dust. The HC FeMn and MC SiMn alloys are either directly crushed into end-products or refined into medium-carbon ferromanganese (MC FeMn) and low-carbon silicomanganese (LC SiMn), respectively. MC FeMn is produced by adding oxygen to liquid HC FeMn in a Manganese Oxygen Refining (MOR) process, while LC SiMn can be produced by adding silicon sources to liquid MC SiMn in the LC SiMn refining station. In addition to the MC FeMn alloy, the MOR process also produces metal-oxide dust as a by-product that can be sold. After refining, the alloys are sent to crushing to produce end-products of the correct size. End-product lumps of adequate size are stored at sales inventories, while undersized lumps are kept at the respective undersized lumps inventories and reused in the associated processes.

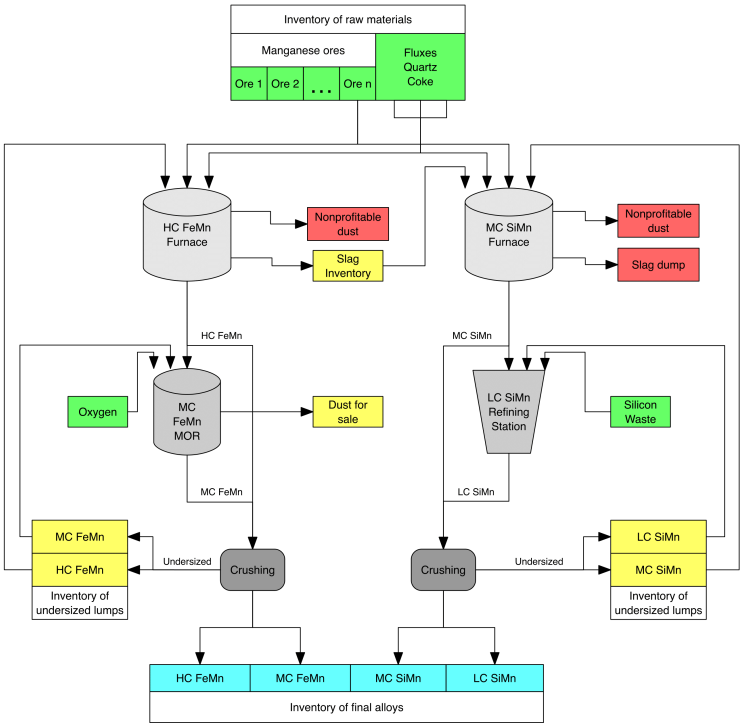

Figure 1: Overview of the material flow in manganese alloy production using the duplex method. The figure is inspired by *Olsen et al. (2007)*. Green colour: raw materials. Red: wastes. Yellow: inventory of reusable/saleable materials. Blue: end-products. Scales of grey: the furnace, refining, and crushing processes.

The slag produced by HC FeMn furnaces can either be discarded or reused to save raw material costs in the MC SiMn furnaces, the latter being the common industry practice. This practice is called the duplex method *(Olsen et al., 2007)* and couples the otherwise independent production paths. Both slag-to-metal ratio and slag composition can be manipulated, through ore combinations and furnace temperatures, to potentially achieve a more efficient production by blending different slags from different HC FeMn furnaces in the MC SiMn furnaces. As both furnace types are not necessarily located at the same plant, slag must be transported between plants. Thus, the decision-making process is complicated by the slag-to-metal-ratio, the slag composition, and the volume of slag to send to each MC SiMn furnace from each HC FeMn furnace. The blending of various qualities of varying volumes in pools is known as the pooling problem, originally introduced in *Haverly (1978)*.

Current operational practice in manganese alloy production is largely based on the process operator's experience and process knowledge, and to optimise production in furnaces separately without considering the overall production.

The slag produced in the HC FeMn furnaces is sent to the MC SiMn furnaces that incur the lowest transportation costs. An optimisation model that considers the integrated production of FeMn and SiMn alloys across multiple plants could improve on the current practice. The problem is to determine the optimal volumes of end-products and slag to produce while satisfying given quality specifications by mixing raw materials. Multiple plants and furnaces are involved in the production. In the remainder of the paper, the considered problem is denoted as the Manganese Alloy Multi-plant Production problem (MAMP).

The MAMP can be formulated as a pooling problem with side constraints. The pooling problem, a generalisation of the blending problem, is used to model systems that have intermediate mixing pools in the blending process *(Audet et al., 2004)*. Blending stream qualities result in nonlinear terms in the pooling problem formulation, yielding a nonlinear program (NLP) *(Audet et al., 2004; Alfaki, 2012)*. The objective of the pooling problem is according to *Gounaris et al. (2009)* to find the most efficient combination of flows through the network that produces final products with the correct quality properties. The pooling problem involves a network of source nodes, intermediate nodes, terminal nodes, and arcs connecting the nodes. The source nodes represent the inventory of feeds, the intermediate nodes represent the intermediate pools and other production processes, and the terminal nodes represent the end-products. The arcs are the possible flows between processes. Intermediate pools are process stages where mixing of feeds into products of specified quality occurs. Usually, the products mixed at an intermediate pool are sent to another intermediate pool for further mixing, but the flow can also go straight to a terminal node.

The flow structure of the MAMP can be treated as a pooling problem since intermediate pools are present in the form of furnaces, MORs, and LC SiMn refining stations. The raw material inventories are sources and end- and by-product inventories are terminals. The MAMP is complicated by the coupling of the intermediate pools. Slag flowing from the HC FeMn furnaces is of varying volume and quality and is sent to MC SiMn furnaces for further blending.

Multiple optimisation formulations of the pooling problem are found in the literature. Formulating the standard pooling problem in different ways have varying ramifications for the problem size and relaxation tightness, although the formulations are mathematically equivalent *(Misener and Floudas, 2009)*. The most common formulations for the standard and generalised pooling problem are the P-formulation *(Haverly, 1978)*, the Q-formulation *(Ben-Tal et al., 1994)*, and the PQ-formulation *(Quesada and Grossmann, 1995; Sherali et al., 1998; Tawarmalani and Sahinidis, 2002)*.

Solution methods for the pooling problem can generally be classified into local and global optimisation methods *(Alfaki and Haugland, 2013)*. Guaranteeing global optimality is of major importance, as the objective function typically is related to an economic metric *(Teles et al., 2012)*. A summary of some of the different solution methods is found in *Misener and Floudas (2009)*, including Successive Linear Programming (SLP), Global Optimisation Algorithm (GOP), Lagrangian approaches, convex envelopes, Reformulation Linearisation Technique (RLT), piecewise-affine underestimators, and different branch-and-bound schemes.

A more recent solution method is the Multiparametric Disaggregation Technique (MDT) found in *Teles et al. (2012, 2013); Kolodziej et al. (2013a,b)*. The method relies on a concept based on the characteristics of the decimal representation of real numbers. The NLP is transformed into a suitably reformulated problem containing new sets of continuous and discrete variables. By disaggregating and parameterising the variables in the nonlinear terms, it is shown how to approximate the original NLP formulation as a mixed integer linear program (MILP). The quality of the solution is dependent on the number of significant digits used to represent the number *(Teles et al., 2012)*.

Nonconvex NLPs yielding multiple local optima, such as the pooling problem, makes the application of local NLP solvers ineffective, due to a sub-optimal solution or failure to even locate a feasible one *(Teles et al., 2012; Wicaksono and Karimi, 2008)*. *Kolodziej et al. (2013a)* show that the MDT relaxation applied to large problems compares well with general global optimisation solvers. They also show that the solution from the upper and lower bounding formulations converge towards the original nonlinear formulation in the limit of an infinite number of discretisation intervals.

Compared to spatial branch-and-bound involving a continuous relaxation, the MDT involves a discrete partition of the feasible region. This partitioning means one can use standard MILP solvers to generate a near to optimal solution, given that one exists for the selected accuracy settings. Further, the MDT does not require the specification of an initial point *(Teles et al., 2012)*. For these reasons, the MDT is selected to be the method for linearising the bilinear constraints present in the MAMP.

The literature on manganese production optimisation is limited. To the authors' knowledge, only one article exists on the topic. *Jipnang et al. (2013)* present a single HC FeMn and MC SiMn furnace process optimisation model based

on mass and energy balances. The model only focuses on the production specific aspects of the problem. It optimises a target function such as total operating costs, energy consumption, Mn recovery, or the amount of slag. The model relies on software, hiding the modelling choices. It is only capable of calculating the production for single HC FeMn and MC SiMn furnaces and the paper states that connecting the two processes and adding possibilities for different production strategies are considered future research *(Jipnang et al., 2013)*.

The pooling problem has been applied in other industries, such as oil refining *(Ben-Tal et al., 1994; Amos et al., 1997)*, mining industry *(Boland et al., 2015)*, and wastewater network problems *(Meyer and Floudas, 2006; Jezowski, 2010)*, among others. These problems, classified as bilinear process networks, are generally difficult to solve to global optimality since bilinear constraints are required to model the mixing of different streams *(Kolodziej et al., 2013b)*.

Based on reviewed literature, little research has been done on formulating the production planning problem for manganese alloy production. Developing better production planning tools can increase the profit for a manganese alloy producer and contribute to a more sustainable industry by making production decisions based on the overall production. Efficient resource consumption and blending of raw materials meeting the end-product specifications are consequently important to address. An economically optimal production can result in a better utilisation of resources, less waste, and less energy consumption in the furnaces per tonne alloy produced, thus, resulting in savings for both the manganese alloy producer and the environment. The objective of this paper is thus to formulate a general model that can be used as a decision support tool for multi-plant production planning of manganese alloys. The optimisation model is tested on a case study based on the plant locations and furnace setup of Eramet Norway.

The contributions of this paper are:

- A clear description and definition of a multi-plant manganese alloy production problem previously not analysed.
- A general, nonlinear formulation of the problem in consideration, applicable to any alloy production with similar processes as manganese alloy production.
- Linearisation of the nonlinear formulation using the MDT so that the MAMP can be solved using a linear solver.
- Showing that the MDT can be applied to solve a large-scale industrial pooling problem.
- Results indicating that multi-plant production planning is superior to the current practice of single furnace optimisation.

The remainder of the paper is organised as follows. A brief introduction to the manganese alloy production problem is given. Then, the mathematical model is presented and the bilinear constraints present in the pooling problem are linearised using the MDT. Finally, a computational study is conducted based on a realistic case, followed by results, concluding remarks, and considerations for future research.

2. Problem Description

A manganese alloy manufacturer has a set of furnaces located at plants to produce manganese alloys. The alloys produced are given by customer specifications. The production is, therefore, based on contracts that must be satisfied. Customer specifications include order volume and alloy composition, resulting in a wide range of possible order sizes and end-products. To meet the end-product specifications set by the customers, a set of raw materials, including ores, fluxes, and coke sources, containing different concentrations of various elements and oxides is available to the production. The raw materials are blended in the furnaces and further processed to produce the desired end-products. Any excess end-product produced can be sold on optional contracts in the spot market or held as an inventory. Producing manganese alloys also yields various by-products, where some are valuable and may be sold.

The furnaces are used to smelt the raw materials. These can produce both HC FeMn and MC SiMn alloys, but only one alloy type at a time. Each furnace has a mass and electrical power capacity that limits the raw material feed to the furnace. The furnaces also have a limitation on the volume of undersized lumps from the crushing process it is possible to feed, since feeding too much undersized lumps is problematic for the furnace operation. An MOR and an LC SiMn refining station are required to produce MC FeMn and LC SiMn, respectively. These refining units have a mass and electrical power capacity limiting the feed to each process. The crushing process is where all the alloy types are crushed into lumps of adequate size.

Each plant has inventories for storing resources and end-products. The inventories at each plant are divided into raw material inventories, refining resource inventories, and end-product inventories. The raw material inventories store all resources used in the furnaces and the refining inventories store all resources used in the refining processes. All inventories have capacity limits.

The first step of the production is to blend raw materials together in a furnace to produce either HC FeMn or MC SiMn. Besides the alloys, by-products in the form of slag and nonprofitable dust are also outputs from the furnaces. The slag produced by the HC FeMn furnaces is in proportion to the metal produced, and this ratio can fluctuate between a lower and upper bound dependent on furnace alloy and slag characteristics. It is possible to produce slag of varying element and oxide content in each HC FeMn furnace. Further, the HC FeMn furnace slag can be reused in the MC SiMn furnaces. The reuse of slag in MC SiMn furnaces is the only coupling between the FeMn and SiMn productions, which otherwise would have been completely decoupled. Slag from the MC SiMn furnaces and the nonprofitable dust produced by both furnace types is discarded.

The next step is to send the produced HC FeMn and MC SiMn alloys either to further refining in the MOR and LC SiMn refining processes, or to the crushing process. In the MOR process, oxygen is added to the liquid HC FeMn to get MC FeMn. The MOR process also produces a by-product in the form of a metallic-oxide dust which can be sold. In the LC SiMn refining process, silicon waste is added to the liquid MC SiMn to get LC SiMn *(Olsen et al., 2007)*. In the crushing process, the alloys from the furnaces and the refining processes are crushed and then sent to the end-product inventories. A given percentage of the crushed end-product is undersized and cannot be sold to the customer and is, therefore, sent back to the respective process inventories for resmelting.

Revenues and costs are linked to various parts of the production. The resources used in the production, except the undersized lumps, are associated with a procurement cost. Smelting the raw materials in the furnaces requires energy in the form of electricity. Thus, the furnace process incurs electricity costs. Reusing slag produced by HC FeMn furnaces in MC SiMn furnaces at other plants incurs a transportation cost per tonne slag transported. Slag from the HC FeMn furnaces can also be discarded instead of reused, which incurs a discard cost. The other by-products that must be discarded also incur a discard cost. The metallic-oxide dust from the MOR process is associated with a revenue since it can be sold. Each end-product is associated with a revenue per tonne sold on fixed and optional contracts.

The purpose of the MAMP is to optimise the integrated production of FeMn and SiMn alloys across multiple plants to maximise profit. The profit is determined by deciding the optimal volumes of end-products to produce by mixing raw materials, while satisfying given quality specifications. Production costs are considerable, and the MAMP should, therefore, ensure optimal use of raw materials to the furnaces and refining processes. The solution to the MAMP should also describe the optimal slag volume and slag composition to be produced in the HC FeMn furnaces and the allocation of slag to the MC SiMn furnaces.

The MAMP must account for mass balancing in the furnaces. Therefore, mass balance reactions for Mn, Fe, Si, C, Al, Mg, Ca, and oxides of these elements must be included in the formulation. The main chemical reactions needed to represent the mass balance of the elements and oxides are given by reactions (1) - (13), where parentheses denote the slag phase and underlines the metal phase. We assume that all reactions happen at a steady state and that all of the following chemical reactions are complete. Note that the given reactions are simplified descriptions of a highly complex chemical process occurring over a wide range of temperatures.

$$2\,MnO_2(l) + CO(g) \longrightarrow Mn_2O_3(l) + CO_2(g) \tag{1}$$

$$3\,Mn_2O_3(l) + CO(g) \longrightarrow 2\,Mn_3O_4(l) + CO_2(g) \tag{2}$$

$$Mn_3O_4(l) + CO(g) \longrightarrow 3\,(MnO) + CO_2(g) \tag{3}$$

$$(MnO) + C(s) \longrightarrow \underline{Mn} + CO(g) \tag{4}$$

$$C(s) \longrightarrow \underline{C} \tag{5}$$

$$3\,Fe_2O_3(l) + CO(g) \longrightarrow 2\,Fe_3O_4(l) + CO_2(g) \tag{6}$$

$$Fe_3O_4(l) + CO(g) \longrightarrow 3\,(FeO) + CO_2(g) \tag{7}$$

$$(FeO) + C(s) \longrightarrow \underline{Fe} + CO(g) \tag{8}$$

$$(SiO_2) + 2\,C(s) \longrightarrow \underline{Si} + 2\,CO(g) \tag{9}$$

$$C(s) + CO_2(g) \longrightarrow 2\,CO(g) \tag{10}$$

$$Al_2O_3(l) \longrightarrow (Al_2O_3) \tag{11}$$

$$MgO(l) \longrightarrow (MgO) \tag{12}$$

$$CaO(l) \longrightarrow (CaO) \tag{13}$$

In contact with the CO-gas present in the furnace, the manganese oxides are reduced according to reactions (1) - (3). The reduced MnO, and supplied MnO from the ores, then reacts with solid C in the coke bed of the furnace, resulting in liquid manganese metal and CO-gas. This is shown in reaction (4).

The final alloy contains a certain amount of C. The C from the feed dissolute into the metal up to a saturation point *(Olsen et al., 2007)*. This is given by reaction (5). Similar to the reduction of manganese oxides, iron oxides and silicon oxides are also reduced in the furnace. The chemical reactions are shown in reactions (6) - (9).

In the furnace, fed C reacts with CO_2 resulting from the chemical reactions (1) - (3) and (6) - (7) and creates CO. This is known as the Boudouard reaction *(Olsen et al., 2007)* and is given in reaction (10). The Boudouard reaction is critical for the feeding of CO to the chemical reactions in reactions (1) - (3) and reactions (6) - (7), together with the feed of CO resulting from the chemical reactions in reactions (4), (8), and (9). The amount of CO_2 that enters the Boudouard reaction from reactions (3) and (6) - (7) is defined as the degree of pre-reduction. 100% pre-reduction is defined as when no CO_2 from the given reactions react with C in the Boudouard reaction, while 0% pre-reduction is defined as when all CO_2 from the given reactions react with C in the Boudouard reaction. CO_2 resulting from reactions (1) - (2) is not expected to react according to the Boudouard reaction under normal furnace operation. The specified degree of pre-reduction has a significant impact on consumed electrical power *(Olsen et al., 2007)*.

The feed to the furnace also contains oxides that do not enter the final alloy. These are important constituents of the slag, giving it different properties. The oxides enter the furnace as solids and dissolute into the slag. The reactions are given in reactions (11) - (13). By using mass-to-mole conversion, and applying reactions (1) - (13), it is possible to find the relation between the weight of each element in a raw material entered into a furnace and the weight and content of each output product from the furnace.

The furnace power consumption is an essential cost driver in manganese alloy production and different oxides require different amounts of energy for the chemical processes to occur. An approximation of the power consumption in a furnace should, therefore, be included, as the power consumption greatly affects the choice of raw materials to consume. The energy consumption in a furnace is determined by the net effect of exothermic and endothermic reactions and the enthalpy of the materials entering and leaving the furnace *(Olsen et al., 2007)*. The total enthalpy consists of formation enthalpy and sensible enthalpy. An approximation of the power consumption is then given by equation (14), where $H^{\mathrm{F}}_{\mathrm{out}}$ represents the formation enthalpy and $H^{\mathrm{S}}_{\mathrm{out}}$ the sensible enthalpy of the resultants at the exit temperature, $H^{\mathrm{F}}_{\mathrm{in}}$ the formation enthalpy and $H^{\mathrm{S}}_{\mathrm{in}}$ the sensible enthalpy of the reactants at the entry temperature, Q the heat added to the system, and W the work done on the system.

$$W = (H^{\mathrm{F}}_{\mathrm{out}} + H^{\mathrm{S}}_{\mathrm{out}}) - (H^{\mathrm{F}}_{\mathrm{in}} + H^{\mathrm{S}}_{\mathrm{in}}) - Q \tag{14}$$

Gas emissions, both from CO, CO_2, and vaporised H_2O constitutes a significant part of the furnace power consumption *(Olsen et al., 2007)*. Consequently, minimising CO and CO_2 emissions in the production planning is, therefore, beneficial both from an economic and an environmental perspective.

3. Mathematical Formulation

Multi-plant production, blending, advanced chemistry, and the coupling of the FeMn and SiMn productions that make up the MAMP add a high degree of complexity to the formulation of the problem. To reduce the scope of the problem, model assumptions are made.

The MAMP is formulated in such a way that the model is solved once and the production plan given by the solution can be used for the given planning period. The end-product demands are assumed to originate from fixed and optional

contracts, where optional contracts are available in the spot market. Fixed contracts are known ahead of production for the entire planning horizon, making a deterministic model appropriate. Optional contracts in the spot market are assumed to be of any size, so the model provides the user with the quantity that should be sold in this market for each end-product. The chemical compositions of the products are also specified in the fixed contracts, while it is assumed that it is possible to sell any end-product quality in the spot market. Fixed contracts must be fulfilled while optional contracts can be chosen as desired. This means that the capacity of the production is assumed to be greater than the cumulative fixed contract demand and that it is possible to sell excess end-products on optional contracts or not produce to optional contracts at all. The raw material procurement prices, electricity prices, and end- and by-product sales prices are constant.

The production timeframe is accounted for in the furnace capacity parameter by setting it equivalent to the furnace capacity available to the production for the period in consideration. This could, for instance, be the daily, weekly, monthly, or yearly capacity. A potential limitation of the model is that it only describes how much it is possible to produce within the given production period, but not when the production happens. All furnaces are assumed to run at 100% capacity at all times, resulting in an even production over the planning horizon. Switching furnace settings or switching furnaces on and off are not included in the model.

There is an initial inventory of raw materials at each plant. A sustainable balance for the re-use of undersized lumps should be found; the process should not consume more undersized lumps than it produces for the result to be sustainable over time. The feed of undersized lumps is therefore bounded by the produced volume of undersized lumps, in addition to an initial inventory.

A large set of chemical reactions is involved in the production of manganese alloys. The model aims to keep the number of chemical reactions to a minimum, but still at a sufficient level to include the main reactions occurring in the furnaces to ensure the correct weight fractions of elements in the final alloy. All chemical reactions are assumed to be complete. The reactions (1) - (13), therefore, translate into linear equality constraints. All reactions in the furnaces happen through mole balances as this often is the best way to model chemical relationships. Flows of raw materials to furnaces, refining processes, and crushing are given in tonnes (1000 kg).

In practice, many complicated and incomplete chemical reactions happen in the furnace. These may constitute a significant amount of the slag, in addition to the most important oxides. However, for simplicity, the slag is set to only consist of the most important oxides in the model. These oxides are MnO, FeO, SiO_2, Al_2O_3, MgO, and CaO. Process metallurgists typically want to determine a range of slag compositions, given by the lime basicity *(Olsen et al., 2007)*, to ensure a suitable viscosity of the slag. This is, however, not included in the model.

In the crushing process, the amount of crushed product that ends up as undersized lumps vary, but is for modelling purposes set as a fixed percentage of the total mass crushed of each end-product. In the furnaces, MOR, and LC SiMn refining station, we assume that a percentage of each element or oxide in the total feed to the processes ends up as by-products. The specific carbon content of a end-product is only considered within medium and high range for FeMn and low and medium range for SiMn. Detailed classifications of product types by percentage carbon content within these ranges are disregarded, yielding a reduced set of end-products.

The model is flow and quality based specifically developed for manganese alloy multi-plant production. To the authors' knowledge, it is the first detailed optimisation model for manganese alloy multi-plant production. *Jipnang et al. (2013)* mention that future extensions of their model are to introduce couplings between the HC FeMn and MC SiMn furnaces. The model presented in this paper includes this coupling. The P-formulation is used, as this is the most common formulation used in the chemical processing industry and it provides an intuitive understanding of the process flows and their qualities for this new problem.

Table 1: Sets and Indices.

Set	
$\mathcal{P}$	Set of plants, $\mathcal{P}$: {1,...,$\lvert\mathcal{P}\rvert$}, indexed by p, g
$\mathcal{F}_p$	Set of furnaces at plant p, $\mathcal{F}_p$: {1,...,$\lvert\mathcal{F}_p\rvert$}, indexed by f, t
$\mathcal{E}$	Set of end-products, $\mathcal{E}$: {1,...,$\lvert\mathcal{E}\rvert$}, indexed by e
$\mathcal{B}$	Set of by-products, $\mathcal{B}$: {1,...,$\lvert\mathcal{B}\rvert$}, indexed by b
$\mathcal{R}$	Set of raw materials, $\mathcal{R}$: {1,...,$\lvert\mathcal{R}\rvert$}, indexed by r, ρ
$\mathcal{K}$	Set of elements and oxides, $\mathcal{K}$: {1,...,$\lvert\mathcal{K}\rvert$}, indexed by k
$\mathcal{C}$	Set of chemical reactions, $\mathcal{C}$: {1,...,$\lvert\mathcal{C}\rvert$}, indexed by c
$\mathcal{V}$	Set of variables in the chemical reactions, $\mathcal{V}$: {1,...,$\lvert\mathcal{V}\rvert$}, indexed by v
$\mathcal{F}_p^{\text{FeMn}}$	Subset of all HC FeMn furnaces at plant p, $\mathcal{F}_p^{\text{FeMn}} \subseteq \mathcal{F}_p$
$\mathcal{F}_p^{\text{SiMn}}$	Subset of all MC SiMnfurnaces at plant p, $\mathcal{F}_p^{\text{SiMn}} \subseteq \mathcal{F}_p$
$\mathcal{C}^{\text{O}}$	Subset of original chemical reactions, $\mathcal{C}^{\text{O}} \subset \mathcal{C}$
$\mathcal{C}^{\text{C}}$	Subset of critical chemical reactions, $\mathcal{C}^{\text{C}} \subset \mathcal{C}$
$\mathcal{C}^{\text{S}}$	Subset of slag chemical reactions, $\mathcal{C}^{\text{S}} \subset \mathcal{C}$
$\mathcal{K}^{\text{C}}$	Subset of critical elements and oxides, $\mathcal{K}^{\text{C}} \subset \mathcal{K}$
$\mathcal{K}^{\text{G}}$	Subset of gases, $\mathcal{K}^{\text{G}} \subset \mathcal{K}$
$\mathcal{K}^{\text{S}}$	Subset of elements and oxides in the slag, $\mathcal{K}^{\text{S}} \subset \mathcal{K}$

Table 2: Parameters.

Parameter	
A_{fkcv}	Constant for an element or oxide k inchemical reaction c for variable v in furnace f.
A_{fkcv}^{LS}	Constant for an element or oxide k inthe left side ratio equation for chemical reaction c for variable v in furnace f.
A_{fkcv}^{RS}	Constant for an element or oxide k inthe right side ratio equation for chemical reaction c for variable v in furnace f.
B_{fkc}	1 if an element or oxide k exist in chemical equation c for furnace f, 0 otherwise.
C_r	Procurement cost per tonne raw material r.
C^{E}	Electricity cost per kWh.
C^{LSiL}	Cost per tonne LC SiMn undersized lumps used.
C^{MFeL}	Cost per tonne MC FeMn undersized lumps used.
C^{O}	Cost per tonne oxygen used. This includes procurement and electricity cost.
C^{S}	Discard cost per tonne slag.
C^{SiW}	Cost per tonne silicon waste used. This includes procurement and electricity cost.
C_{pg}^{T}	Transportation cost per tonne slag from plant p to plant g.
D_e^{F}	Fixed contract demand for end-product e.
D_e^{O}	Optional contract demand for end-product e.
I_{pr}	Initial inventory of raw material r at plant p in tonnes.
I_p^{LSiL}	Initial inventory of LC SiMn undersized lumps at plant p in tonnes.
I_p^{MFeL}	Initial inventory of MC FeMn undersized lumps at plant p in tonnes.
I_p^{O}	Initial inventory of oxygen at plant p in tonnes.
I_p^{SiW}	Initial inventory of silicon waste at plant p in tonnes.
H_k^{F}	Formation enthalpy for each element or oxide k, in kJ/tonne.
H_k^{S}	Sensible enthalpy for each element or oxide k, in kJ/tonne.
L^{H}	Furnace heat loss factor.
M_k	Molar mass in moles per tonne for element or oxide k.
$\overline{P}_{pf}$	Net furnace power capacity per day for furnace f at plant p, in kWh.
Q^{E}	Totalcapacity for end-product inventory across all plants.
Q_{pf}^{F}	Capacity of furnace f at plant p in tonnes.
Q_p^{MOR}	Total MOR capacity at plant p in tonnes.
Q_p^{REF}	Total LC SiMn refining station capacity at plant p in tonnes.
R_b^{B}	Revenue or discard cost per tonne of by-product b.
R_e^{F}	Fixed contract revenue per tonne end-product e sold.
R_e^{O}	Optional contract revenue per tonne end-product e sold on optional contracts.
T_{kcv}	1 if element or oxide k exist in chemical equation c for variable v, 0 otherwise.

ΔT	Time horizon for the production, given in days.
$\underline{\Lambda}$	Lower limit on the weight percentage for slag production in an HC FeMn furnace.
$\overline{\Lambda}$	Upper limit on the weight percentage for slag production in an HC FeMn furnace.
Υ	Degree of pre-reduction in the HC FeMn furnaces.
$\underline{\Phi}_k$	Lower limit on the weight percentage for element or oxide k in slag.
$\overline{\Phi}_k$	Upper limit on the weight percentage for element or oxide k in slag.
Ψ^{B}_{fbk}	Weight percentage of element or oxide k in by-product b from furnace f.
$\Psi^{\mathrm{CRUSH}}_{b}$	Weight percentage of by-product b from the crushing process.
Ψ^{FeMn}_{k}	Weight percentage of element or oxide k in HC FeMn.
Ψ^{LSiL}	Weight percentage LC SiMn undersized lumps allowed to feed LC SiMn refining station.
Ψ^{MFeL}	Weight percentage MC FeMn undersized lumps allowed to feed MOR.
Ψ^{MOR}_{b}	Weight percentage of by-product b from MOR.
Ψ^{R}_{rk}	Weight percentage of element or oxide k in raw material r.
Ψ^{SiMn}_{k}	Weight percentage of element or oxide k in MC SiMn.
Ψ^{UL}	Weight percentage of undersized lumps allowed to feed a furnace.
Ω^{MOR}	Oxygen-HC FeMn weight relationship factor.
Ω^{REF}	Silicon-MC SiMn weight relationship factor.

Table 3: Variables.

Variable	
a_p	Tonnage of LC SiMn undersized lumps used in the LC SiMn refining station at plant p.
c_p	Tonnage of MC FeMn undersized lumps used in MOR at plant p.
e_{pf}	Electric power consumed by furnace f at plant p, in kWh.
g^{F}_e	Sale of end-product e made on fixed contracts.
g^{O}_e	Sale of end-product e made on optional contracts.
h_p	Tonnage of LC SiMn produced at plant p sent to crushing.
m_{pf}	Tonnage of alloy produced in furnace f at plant p sent to refining processes.
n_{pfkcv}	Moles of element or oxide k in furnace f at plant p in equation c for variable v.
o_p	Tonnage oxygen fed to the MOR at plant p.
q_{pf}	Tonnage slag produced in furnace f at plant p.
s_p	Tonnage silicon fed to the LC SiMn refining at plant p.
u_{pf}	Tonnage of alloy produced in furnace f at plant p sent to crushing.
v_p	Tonnage of MC FeMn produced at plant p sent to crushing.
x^{E}_{pe}	Tonnage of end-product e produced at plant p.
x^{B}_{pb}	Tonnage of by-product b produced at plant p.
y_{pfr}	Tonnage of raw material r fed to furnace f at plant p.
α_{pfkc}	Moles of element or oxide k in chemical equation c extracted as slag from furnace f at plant p.
σ_{pfgt}	Tonnage slag sent from furnace f at plant p to furnace t at plant g.
ϕ_{pfk}	Weight percentage of element or oxide k in the slag produced by furnace f at plant p.

Figure 2 illustrates the material flow within a plant and which processes the variables are describing, using a simplified superstructure. As an example, the variables y_{pfr} and n_{pfkcv} are related to the feeding of the furnaces from the raw material inventory, while a_p and s_p are related to the feeding of the LC SiMn refining station from refining resources. ϕ_{pfk}, e_{pf}, g^{F}_e, and g^{O}_e are not included in the figure since these are quality variables and not flow variables.

Figure 2 illustrates only the flow within one plant, the MAMP is, however, defined for multiple plants. Slag can be sent from an HC FeMn furnace at one plant to multiple MC SiMn furnaces, at the same plant or other plants. The flow between plants is illustrated in Figure 3.

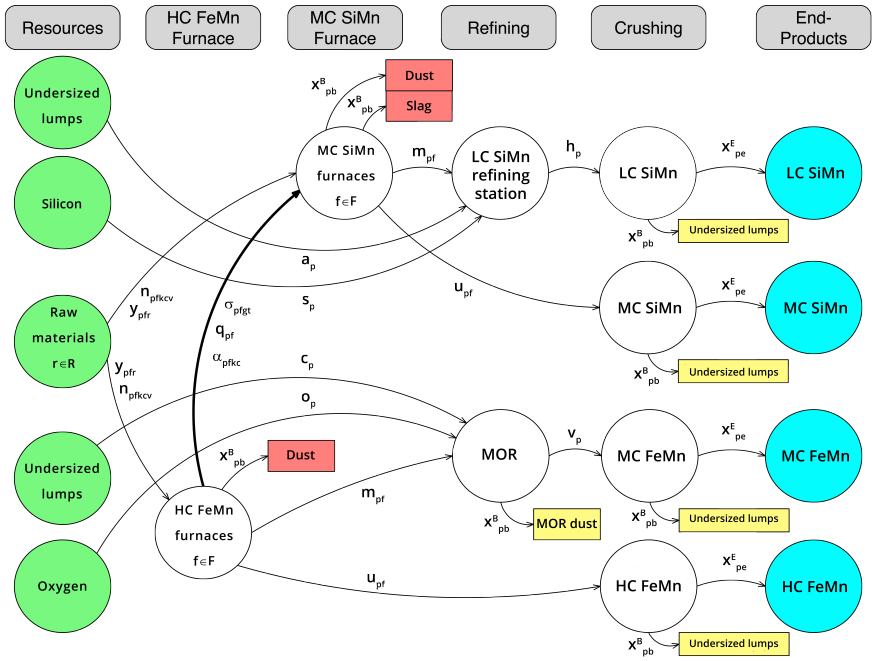

Figure 2: The MAMP superstructure for one plant. The same colour coding is applied as in Figure 1. Green: raw materials. Red: wastes. Yellow: inventory of reusable/saleable materials. Blue: final alloys.

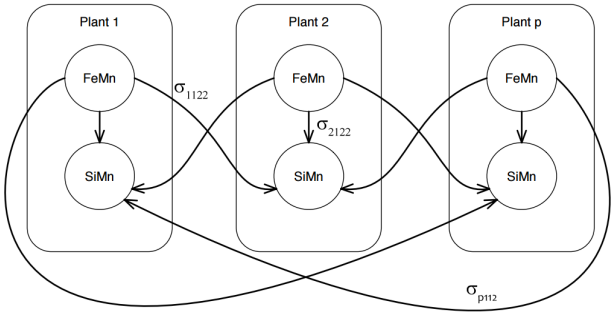

Figure 3: Potential flow between furnaces within and between plants. The flows are denoted by σ_{pfgt}.

3.1. Model

$$\max \; z = \sum_{e\in\mathcal{E}} (R^{\mathrm{F}}_e g^{\mathrm{F}}_e + R^{\mathrm{O}}_e g^{\mathrm{O}}_e) \tag{15a}$$

$$+ \sum_{p\in\mathcal{P}} \sum_{b\in\mathcal{B}} R^{\mathrm{B}}_b x^{\mathrm{B}}_{pb} \tag{15b}$$

$$- \sum_{p\in\mathcal{P}} \sum_{f\in\mathcal{F}_p} \sum_{r\in\mathcal{R}} C_r y_{pfr} \tag{15c}$$

$$- \sum_{p\in\mathcal{P}} \sum_{f\in\mathcal{F}_p} C^{\mathrm{E}} e_{pf} \tag{15d}$$

$$- \sum_{p \in \mathcal{P}} (C^{\mathrm{O}} o_p + C^{\mathrm{MFeL}} c_p) \tag{15e}$$

$$- \sum_{p \in \mathcal{P}} (C^{\mathrm{SiW}} s_p + C^{\mathrm{LSiL}} a_p) \tag{15f}$$

$$- \sum_{p \in \mathcal{P}} \sum_{f \in \mathcal{F}_p^{\mathrm{FeMn}}} \sum_{g \in \mathcal{P}} \sum_{t \in \mathcal{F}_g^{\mathrm{SiMn}}} C_{pg}^{\mathrm{T}} \sigma_{pfgt} \tag{15g}$$

$$- \sum_{p \in \mathcal{P}} \sum_{f \in \mathcal{F}_p^{\mathrm{FeMn}}} C^{\mathrm{S}} (q_{pf} - \sum_{g \in \mathcal{P}} \sum_{t \in \mathcal{F}_g^{\mathrm{SiMn}}} \sigma_{pfgt}) \tag{15h}$$

The objective function z maximises the total profit from selling end- and by-products from manganese alloy production. Part (15a) is the total revenue generated by selling end-products. Part (15b) is the net revenue generated by selling valuable by-products and discarding the non-profitable ones. Part (15c) is the total cost associated with the volume of raw materials used in the production. Part (15d) is the total electricity cost from the energy consumption in the furnaces. Part (15e) is the total cost associated with the amount of oxygen and MC FeMn undersized lumps added to the MOR process. Part (15f) is the total cost associated with the amount of silicon waste and LC SiMn undersized lumps added to the LC SiMn refining station process. Part (15g) is the total slag transportation cost between plants. Part (15h) accounts for the cost of discarding the slag that is not re-used.

To enhance readability and the understanding of which constraints restrict each process stage, the constraints are presented in different sections. The sections are presented in order of process stage according to Figure 2.

Resource inventory

$$\sum_{f \in \mathcal{F}_p} y_{pfr} \leq I_{pr} \qquad p \in \mathcal{P},\ r \in \mathcal{R} \tag{16}$$

$$o_p \leq I_p^{\mathrm{O}} \qquad p \in \mathcal{P} \tag{17}$$

$$s_p \leq I_p^{\mathrm{SiW}} \qquad p \in \mathcal{P} \tag{18}$$

$$c_p \leq I_p^{\mathrm{MFeL}} \qquad p \in \mathcal{P} \tag{19}$$

$$a_p \leq I_p^{\mathrm{LSiL}} \qquad p \in \mathcal{P} \tag{20}$$

Constraints (16) - (20) are resource inventory constraints limiting the feed of particular resources to within the initial inventories of the respective resources.

Furnace constraints

$$\sum_{r \in \mathcal{R}} y_{pfr} + \sum_{k \in \mathcal{K}^{\mathrm{S}}} \sum_{c \in \mathcal{C}^{\mathrm{S}}} M_k n_{pfkcv} \leq Q_{pf}^{\mathrm{F}} \Delta T \qquad p \in \mathcal{P},\ f \in \mathcal{F}_p,\ v \in \{\mathrm{SLAG}\} \tag{21}$$

$$y_{pfr} \leq \Psi^{\mathrm{UL}} \sum_{\rho \in \mathcal{R} \setminus r} y_{pf\rho} \qquad p \in \mathcal{P},\ f \in \mathcal{F}_p,\ r \in \{\text{HC FeMn}, \text{MC SiMn}\} \tag{22}$$

$$\begin{aligned} &\sum_{r \in \mathcal{R}} \sum_{k \in \mathcal{K}} \Psi_{rk}^{\mathrm{R}} y_{pfr} + \sum_{k \in \mathcal{K}^{\mathrm{S}}} \sum_{c \in \mathcal{C}^{\mathrm{S}}} M_k n_{pfkc,\mathrm{SLAG}} + \sum_{c \in \mathcal{C}^{\mathrm{O}}} M_{\mathrm{O}} n_{pf,\mathrm{CO_2},c,\mathrm{TOT}} \\ &+ \sum_{c \in \mathcal{C}^{\mathrm{O}}} M_{\mathrm{CO}} n_{pf,\mathrm{CO},c,\mathrm{TOT}} - \sum_{b \in \mathcal{B}} \sum_{k \in \mathcal{K}} \sum_{r \in \mathcal{R}} \Psi_{fbk}^{\mathrm{B}} \Psi_{rk}^{\mathrm{R}} y_{pfr} \qquad p \in \mathcal{P},\ f \in \mathcal{F}_p \\ &- \sum_{b \in \mathcal{B}} \sum_{k \in \mathcal{K}^{\mathrm{S}}} \sum_{c \in \mathcal{C}^{\mathrm{S}}} \Psi_{fbk}^{\mathrm{B}} M_k n_{pfkc,\mathrm{SLAG}} - \sum_{k \in \mathcal{K}^{\mathrm{G}}} \sum_{c \in \mathcal{C}^{\mathrm{O}} \setminus \{18\}} M_k n_{pfkc,\mathrm{RSRED}} - m_{pf} - u_{pf} - q_{pf} = 0 \end{aligned} \tag{23}$$

$$x^{\mathrm{B}}_{pb} = \sum_{f\in\mathcal{F}_p}\sum_{r\in\mathcal{R}}\sum_{k\in\mathcal{K}} \Psi^{\mathrm{B}}_{fbk}\Psi^{\mathrm{R}}_{rk}y_{pfr} + \sum_{f\in\mathcal{F}_p}\sum_{k\in\mathcal{K}^{\mathrm{S}}}\sum_{c\in C^{\mathrm{S}}} \Psi^{\mathrm{B}}_{fbk}M_k n_{pfkcv} \qquad p\in\mathcal{P},\ b\in\mathcal{B},\ v\in\{\mathrm{SLAG}\} \quad (24)$$

Constraints (21) restrict the feed of raw materials and slag to a furnace to within the capacity of the furnace for the time horizon. Constraints (22) handle the reuse of undersized lumps relative to the feed of other resources used in a furnace.

Constraints (23) handle the mass balance in a furnace. The constraints include the mass of the modelled elements and oxides fed to the furnace, the mass of the slag fed to the furnace, the mass of oxygen accounted for twice due to the modelling of CO_2 entering the Boudouard reaction, the mass of CO taking part in the prereduction in the furnace, less the mass of the furnace by-products from the raw material feed and slag feed, the mass of CO and CO_2 off-gas emissions, the metal output to either the MOR or LC SiMn refining and crushing processes and the mass of produced slag. For HC FeMn furnaces, the slag terms $n_{pfkc,\mathrm{SLAG}}$ are zero as no slag is sent to an HC FeMn furnace. For MC SiMn furnaces, the produced slag terms q_{pf} are zero as the slag is assumed to be a discard slag. The term $\sum_{k\in\mathcal{K}^{\mathrm{G}}}\sum_{c\in C^{\mathrm{O}}\setminus\{18\}} M_k n_{pfkc,\mathrm{RSRED}}$ excludes chemical reaction 18, which is the Boudouard reaction, because it uses the same variable name, but it accounts for the off-gases leaving the furnace, not the re-entering gas.

Constraints (24) state the relationship between the total feed of raw materials and slag sent to the furnaces and the amount of a discardable by-product produced by the furnaces at a plant. The constraints for electrical power consumption follows the given thermodynamic relations. They have the same structure as (23) using coefficients for formation and sensible enthalpies for the furnace temperature. The constraints are omitted for readability.

Furnace-Slag Connection Constraints

$$\phi_{pfk}q_{pf} = M_k\sum_{c\in C^{\mathrm{S}}} B_{fkc}\alpha_{pfkc} \qquad p\in\mathcal{P},\ f\in\mathcal{F}^{\mathrm{FeMn}}_p,\ k\in\mathcal{K}^{\mathrm{S}} \quad (25)$$

$$\sum_{g\in\mathcal{P}}\sum_{t\in\mathcal{F}^{\mathrm{SiMn}}_g}\sigma_{pfgt} \le q_{pf} \qquad p\in\mathcal{P},\ f\in\mathcal{F}^{\mathrm{FeMn}}_p \quad (26)$$

$$\sum_{p\in\mathcal{P}}\sum_{f\in\mathcal{F}^{\mathrm{FeMn}}_p}\phi_{pfk}\sigma_{pfgt} = M_k\sum_{c\in C^{\mathrm{S}}} n_{gtkcv} \qquad g\in\mathcal{P},\ t\in\mathcal{F}^{\mathrm{SiMn}}_g,\quad k\in\mathcal{K}^{\mathrm{S}},\ v\in\{\mathrm{SLAG}\} \quad (27)$$

$$\phi_{pfk} \ge \underline{\Phi}_k \qquad p\in\mathcal{P},\ f\in\mathcal{F}^{\mathrm{FeMn}}_p,\ k\in\mathcal{K}^{\mathrm{S}} \quad (28)$$

$$\phi_{pfk} \le \overline{\Phi}_k \qquad p\in\mathcal{P},\ f\in\mathcal{F}^{\mathrm{FeMn}}_p,\ k\in\mathcal{K}^{\mathrm{S}} \quad (29)$$

$$\sum_{k\in\mathcal{K}^{\mathrm{S}}}\phi_{pfk} = 1 \qquad p\in\mathcal{P},\ f\in\mathcal{F}^{\mathrm{FeMn}}_p \quad (30)$$

$$q_{pf} \ge \underline{\Lambda}(m_{pf}+u_{pf}) \qquad p\in\mathcal{P},\ f\in\mathcal{F}^{\mathrm{FeMn}}_p \quad (31)$$

$$q_{pf} \le \overline{\Lambda}(m_{pf}+u_{pf}) \qquad p\in\mathcal{P},\ f\in\mathcal{F}^{\mathrm{FeMn}}_p \quad (32)$$

Constraints (25) couple the produced amount of slag q_{pf} in an HC FeMn furnace and its constituent fractions ϕ_{pfk}, to the mass of the constituents $M_k\alpha_{pfkc}$ pulled from the chemical reactions occurring in the HC FeMn furnace. Thus, the mass of element or oxide k in the slag extracted from an HC FeMn furnace equals the amount of mass of element or oxide k removed from the redox reactions in the furnace. The left-hand side terms of the constraints are nonlinear and, therefore, complicates the problem. The constraints are unique to this problem because there are no pooling problems in the manganese alloy industry, to the authors' knowledge, that extracts a proportion of a specific constituent from a blending process. The closest similarities may be found in the separation processes in the crude oil industry.

Constraints (26) state that sending slag to MC SiMn furnaces from an HC FeMn furnace is optional, by allowing less than the produced slag to be sent. This allows the slag to be discarded if it is unfavourable to feed it to MC SiMn furnaces. The slag transportation and slag feed to an MC SiMn furnace are coupled by constraints (27). These are nonlinear terms common to the pooling problem. Constraints (28) induce lower and constraints (29) upper bounds on the slag compostition. Constraints (30) enforce that the sum of the weight percentages of all the slag constituents must make up the total slag content. Constraints (31) ensure that it is always produced at least a minimum amount of slag in a HC FeMn furnace relative to the metal produced. Constraints (32) set the upper bound on the slag production relative to the metal production.

MOR Constraints

$$\sum_{f \in \mathcal{F}_p^{\text{FeMn}}} m_{pf} + o_p + c_p \;\leq\; Q_p^{\text{MOR}} \qquad p \in \mathcal{P} \quad (33)$$

$$\sum_{f \in \mathcal{F}_p^{\text{FeMn}}} m_{pf} + o_p + c_p \; - v_p - x_{pb}^{\text{B}} = \; 0 \qquad p \in \mathcal{P},\;\; b \in \{\text{MOR dust}\} \quad (34)$$

$$o_p \;=\; \Omega^{\text{MOR}} \sum_{f \in \mathcal{F}_p^{\text{FeMn}}} m_{pf} \qquad p \in \mathcal{P} \quad (35)$$

$$c_p \;\leq\; \Psi^{\text{MFeL}} \sum_{f \in \mathcal{F}_p^{\text{FeMn}}} m_{pf} \qquad p \in \mathcal{P} \quad (36)$$

$$x_{pb}^{\text{B}} \;=\; \Psi_b^{\text{MOR}} \Big(\sum_{f \in \mathcal{F}_p^{\text{FeMn}}} m_{pf} + o_p \Big) \qquad p \in \mathcal{P},\;\; b \in \{\text{MOR dust}\} \quad (37)$$

Constraints (33) ensure that the feed of HC FeMn, oxygen, and undersized lumps added to the MOR do not surpass the MOR capacity. Constraints (34) handle the mass balance in the MOR. Constraints (35) state that the oxygen used in the MOR equals a fixed ratio of the added HC FeMn. By calculating this ratio, there is no need to include a chemical reaction in the model. Constraints (36) set the upper bound on how much MC FeMn undersized lumps it is possible to add to the MOR relative to the feed of metal. This is to prevent too low temperatures in the MOR. Constraints (37) state that a certain percentage of the mass fed to the MOR ends up as saleable MOR dust.

LC SiMn Refining Station Constraints

$$\sum_{f \in \mathcal{F}_p^{\text{SiMn}}} m_{pf} + s_p + a_p \;\leq\; Q_p^{\text{REF}} \qquad p \in \mathcal{P} \quad (38)$$

$$\sum_{f \in \mathcal{F}_p^{\text{SiMn}}} m_{pf} + s_p + a_p - h_p \;=\; 0 \qquad p \in \mathcal{P} \quad (39)$$

$$s_p \;=\; \Omega^{\text{REF}} \sum_{f \in \mathcal{F}_p^{\text{SiMn}}} m_{pf} \qquad p \in \mathcal{P} \quad (40)$$

$$a_p \;\leq\; \Psi^{\text{LSiL}} \Big(\sum_{f \in \mathcal{F}_p^{\text{SiMn}}} m_{pf} + s_p \Big) \qquad p \in \mathcal{P} \quad (41)$$

Constraints (38) handle the capacity of an LC SiMn refining station. The mass balance in the LC SiMn refining station is handled by constraints (39). Constraints (40) relate the total amount of silicon waste needed to add, relative to the amount of MC SiMn, to alter the product composition. The constraints ensure that it is not possible to get LC SiMn out from the refining process without mixing the correct amount of Si with the incoming feed of MC SiMn. The upper limit on how much LC SiMn undersized lumps it is possible to add to the LC SiMn refining station process is given by constraints (41).

Crushing Constraints

$$\sum_{f \in \mathcal{F}_p^{\text{FeMn}}} u_{pf} \;=\; x_{pe}^{\text{E}} + x_{pb}^{\text{B}} \qquad p \in \mathcal{P},\;\; e \in \{\text{HC FeMn}\},\;\; b \in \{\text{HC FeMn}\} \quad (42)$$

$$v_p \;=\; x_{pe}^{\text{E}} + x_{pb}^{\text{B}} \qquad p \in \mathcal{P},\;\; e \in \{\text{MC FeMn}\},\;\; b \in \{\text{MC FeMn}\} \quad (43)$$

$$x_{pb}^{\text{B}} = \; \Psi_b^{\text{CRUSH}} \sum_{f \in \mathcal{F}_p^{\text{FeMn}}} u_{pf} \qquad p \in \mathcal{P},\;\; b \in \{\text{HC FeMn}\} \quad (44)$$

$$x_{pb}^{\text{B}} = \; \Psi_b^{\text{CRUSH}} v_p \qquad p \in \mathcal{P},\;\; b \in \{\text{MC FeMn}\} \quad (45)$$

$$\sum_{f\in\mathcal{F}_p} y_{pfr} \;\leq\; x^{\mathrm{B}}_{pb} \qquad p\in\mathcal{P}, r\in\{\text{HC FeMn, MC SiMn}\}, b\in\{\text{HC FeMn, MC SiMn}\} \quad (46)$$

$$c_p \;\leq\; x^{\mathrm{B}}_{pb} \qquad p\in\mathcal{P},\;\; b\in\{\text{MC FeMn}\} \quad (47)$$

$$a_p \;\leq\; x^{\mathrm{B}}_{pb} \qquad p\in\mathcal{P},\;\; b\in\{\text{LC SiMn}\} \quad (48)$$

Constraints (42) ensure that the total amount of HC FeMn alloy from a plant's HC FeMn furnaces sent directly to crushing equals the HC FeMn end-product and by-products produced at the plant. The same balance applies to the crushing of MC FeMn alloy, restricted by constraints (43).

Constraints (44) - (45) ensure that a given percentage of the alloy that flows from the HC FeMn furnaces and the MOR ends up as undersized lumps. Similar constraints exist for the SiMn production for constraints (42) - (45). To have a sustainable consumption of undersized lumps, the volume of undersized lumps used in the process should be less than or equal to the volume of undersized lumps exiting the crushing process. Constraints (46) - (48) ensure that this condition is satisfied. Constraints (46) allow both HC FeMn and MC SiMn undersized lumps to be used in both furnace types.

Final Inventory and Demand Constraints

$$g^{\mathrm{F}}_e \;=\; D^{\mathrm{F}}_e \qquad e\in\mathcal{E} \quad (49)$$

$$g^{\mathrm{O}}_e \;\leq\; D^{\mathrm{O}}_e \qquad e\in\mathcal{E} \quad (50)$$

Constraints (49) handle the demand from fixed contracts while constraints (50) handle the demand from optional contracts.

Chemical Balance Constraints

$$\sum_{c\in C} T_{kcv} n_{pfkcv} \;=\; \frac{1-\sum_{b\in\mathcal{B}}\Psi^{\mathrm{B}}_{fbk}}{M_k}\sum_{r\in\mathcal{R}}\Psi^{\mathrm{R}}_{rk} y_{pfr} \qquad p\in\mathcal{P},\;\; f\in\mathcal{F}_p,\;\; k\in\mathcal{K},\;\; v\in\{\text{FED}\} \quad (51)$$

$$\sum_{v\in\mathcal{V}\setminus\{\text{SLAG}\}}\sum_{k\in\mathcal{K}} A_{fkcv} n_{pfkcv} + \sum_{k\in\mathcal{K}^{\mathrm{S}}}(1-\sum_{b\in\mathcal{B}}\Psi^{\mathrm{B}}_{fbk}) A_{fkc,\mathrm{SLAG}} n_{pfkc,\mathrm{SLAG}}$$
$$-\sum_{k\in\mathcal{K}} B_{fkc}\alpha_{pfkc} \;=\; 0 \qquad p\in\mathcal{P},\;\; f\in\mathcal{F}_p,\;\; c\in\mathcal{C}^{\mathrm{O}} \quad (52)$$

$$\sum_{v\in\mathcal{V}\setminus\{\text{SLAG}\}}\sum_{k\in\mathcal{K}} A^{\mathrm{LS}}_{fkcv} n_{pfkcv} + \sum_{k\in\mathcal{K}^{\mathrm{S}}}(1-\sum_{b\in\mathcal{B}}\Psi^{\mathrm{B}}_{fbk}) A^{\mathrm{LS}}_{fkc,\mathrm{SLAG}} n_{pfkc,\mathrm{SLAG}}$$
$$-\sum_{k\in\mathcal{K}} B_{fkc}\alpha_{pfkc} \;=\; 0 \qquad p\in\mathcal{P},\;\; f\in\mathcal{F}_p,\;\; c\in\mathcal{C}^{\mathrm{O}} \quad (53)$$

$$\sum_{v\in\mathcal{V}}\sum_{k\in\mathcal{K}} A^{\mathrm{RS}}_{fkcv} n_{pfkcv} \;=\; 0 \qquad p\in\mathcal{P},\;\; f\in\mathcal{F}_p,\;\; c\in\mathcal{C}^{\mathrm{O}} \quad (54)$$

$$\sum_{v\in\mathcal{V}}\sum_{k\in\mathcal{K}} A_{fkcv} n_{pfkcv} \;=\; 0 \qquad p\in\mathcal{P},\;\; f\in\mathcal{F}_p,\;\; c\in\mathcal{C}^{\mathrm{C}} \quad (55)$$

$$n_{pfk,c+1,\mathrm{RED}} \;=\; n_{pfkc,\mathrm{RSRED}} \qquad p\in\mathcal{P},\;\; f\in\mathcal{F}_p,\;\; k\in\{\mathrm{Mn_2O_3},\;\mathrm{Mn_3O_4},\;\mathrm{MnO},\;\mathrm{Fe_2O_3},\;\mathrm{Fe_3O_4},\;\mathrm{FeO}\},\;\; c\in\{1,2,3,6,7\} \quad (56)$$

Constraints (51) connect the chemical processes in a furnace to the raw material feed. The left-hand side of the constraints states that the total amount of moles of an element or oxide k used in the chemical reactions in each furnace has to equal the feed of that element or oxide to the furnace. The parameters T_{kcv} ensure that n_{pfkcv} cannot take any

other value than zero where element or oxide $k \in \mathcal{K}$ is not present in chemical reaction c for variable $v \in \{\text{FED}\}$. The right-hand side of the constraints multiplies the weight percentage for each element or oxide k in raw material r with the total weight of the raw material to find the weight of the element or oxide in the raw material. The sum is taken over all raw materials so that the total feed of the respective element or oxide is found. It is then divided by molar mass in mole per tonne to determine the amount of mole fed to the furnace for element or oxide k. The term $(1 - \sum_{b \in \mathcal{B}} \Psi^{\text{B}}_{fbk})$ removes the amount of moles that ends up as discardable by-products from the feed since the chemical reactions do not account for the production of these.

The general form of the chemical reactions is given by constraints (52) - (54). The constraints enforce that the mole balances equal zero. Each chemical reaction is represented by three constraints to ensure the correct relationships between reactants and resultants. Constraints (52) represent the complete chemical reaction, while constraints (53) ensure correct ratios between the reactants, and constraints (54) the resultants.

The output of Mn, Fe, Si, and C from the redox reactions and the direct feed of the respective elements from ores and undersized lumps are added together in constraints (55) to find the total mass of each element in the furnace output alloy. The reactants in some of the chemical reactions originate from a resultant in the previous reaction, therefore the $n_{pfk,c+1,\text{RED}}$ variables in these chemical reactions equals the $n_{pfkc,\text{RSRED}}$ in the previous reaction. This is handled by constraints (56).

An example of the application of constraints (52) - (54) to model chemical reaction (2), $3\,Mn_2O_3(s) + CO\,(g) \longrightarrow 2\,Mn_3O_4(s) + CO_2(g)$, is provided in equations (57a) - (57c).

$$2n_{pf,\text{Mn}_2\text{O}_3,2,\text{FED}} + 2n_{pf,\text{Mn}_2\text{O}_3,2,\text{RED}} + 6n_{pf,\text{CO},2,\text{FED}} - 3n_{pf,\text{Mn}_3\text{O}_4,2,\text{RSRED}} - 6n_{pf,\text{CO}_2,2,\text{RSRED}} = 0 \qquad p \in \mathcal{P},\ f \in \mathcal{F}_p \quad (57a)$$

$$n_{pf,\text{Mn}_2\text{O}_3,2,\text{FED}} + n_{pf,\text{Mn}_2\text{O}_3,2,\text{RED}} - 3n_{pf,\text{CO},2,\text{FED}} = 0 \qquad p \in \mathcal{P},\ f \in \mathcal{F}_p \quad (57b)$$

$$n_{pf,\text{Mn}_3\text{O}_4,2,\text{RSRED}} - 2n_{pf,\text{CO}_2,2,\text{RSRED}} = 0 \qquad p \in \mathcal{P},\ f \in \mathcal{F}_p \quad (57c)$$

Equation (57a) is the representation of reaction (2) with the correct mole ratios between the reactants and resultants. Equation (57b) and equation (57c) balance the reactants and the resultants, respectively.

Boudouard Reaction Constraints

$$n_{pf,\text{C},18,\text{FED}} + n_{pf,\text{CO}_2,18,\text{TOT}} - n_{pf,\text{CO},18,\text{RSRED}} = 0 \qquad p \in \mathcal{P},\ f \in \mathcal{F}_p \quad (58a)$$

$$n_{pf,\text{C},18,\text{FED}} - n_{pf,\text{CO}_2,18,\text{TOT}} = 0 \qquad p \in \mathcal{P},\ f \in \mathcal{F}_p \quad (58b)$$

$$n_{pf,\text{CO}_2,18,\text{TOT}} = (1 - \Upsilon) \sum_{c \in C \setminus \{1,2\}} n_{pf,\text{CO}_2,c,\text{RSRED}} \qquad p \in \mathcal{P},\ f \in \mathcal{F}_p \quad (58c)$$

$$\sum_{c \in C^{\text{O}}} n_{pf,\text{CO},c,\text{TOT}} \leq n_{pf,\text{CO},18,\text{RSRED}} + \sum_{c \in C^{\text{S}}} n_{pf,\text{CO},c,\text{RSRED}} \qquad p \in \mathcal{P},\ f \in \mathcal{F}_p \quad (58d)$$

Constraints (58a) are the Boudouard reaction given in reaction (10). Constraints (58b) ensure correct ratio between the left side reactants, no constraints are needed for the right side ratio as only one resultant exists. Constraints (58c) handle the degree of pre-reduction in the furnace, i.e. how much CO_2 that is consumed by the Boudouard reaction. Following the given definition of pre-reduction, the term has to be formulated as $(1 - \Upsilon)$ to model the amount of CO_2 re-entering the process correctly. The chemical reactions involving MnO_2 and Mn_2O_3 are not normally involved in prereduction and are therefore not included in the sum of the right side term. Constraints (58d) ensure that the total CO fed to reactions (1) - (3) and (6) - (7) is less than or equal to the CO resulting from the Boudouard reaction and the reactions (4), (8), and (9). The CO and CO_2 that do not re-enter the process are released as off-gases.

Chemical Content Constraints

$$M_k \sum_{c \in \mathcal{C}^{\mathrm{C}}} T_{kcv} n_{pfkcv} = \Psi_k^{\mathrm{FeMn}}(m_{pf} + u_{pf}) \qquad p \in \mathcal{P},\ f \in \mathcal{F}_p^{\mathrm{FeMn}},\ k \in \mathcal{K}^{\mathrm{C}},\ v \in \{\mathrm{TOT}\} \quad (59)$$

$$M_k \sum_{c \in \mathcal{C}^{\mathrm{C}}} T_{kcv} n_{pfkcv} = \Psi_k^{\mathrm{SiMn}}(m_{pf} + u_{pf}) \qquad p \in \mathcal{P},\ f \in \mathcal{F}_p^{\mathrm{SiMn}},\ k \in \mathcal{K}^{\mathrm{C}},\ v \in \{\mathrm{TOT}\} \quad (60)$$

Constraints (59) and (60) ensure that the required content of critical elements is satisfied in the HC FeMn and the MC SiMn furnace, respectively.

Non-negativity Constraints

$$a_p, c_p, h_p, o_p, s_p, v_p \geq 0 \qquad p \in \mathcal{P} \quad (61)$$

$$g_e^{\mathrm{F}}, g_e^{\mathrm{O}} \geq 0 \qquad e \in \mathcal{E} \quad (62)$$

$$x_{pb}^{\mathrm{B}} \geq 0 \qquad p \in \mathcal{P},\ b \in \mathcal{B} \quad (63)$$

$$x_{pe}^{\mathrm{E}} \geq 0 \qquad p \in \mathcal{P},\ e \in \mathcal{E} \quad (64)$$

$$e_{pf}, m_{pf}, q_{pf}, u_{pf} \geq 0 \qquad p \in \mathcal{P},\ f \in \mathcal{F}_p \quad (65)$$

$$\phi_{pfk} \geq 0 \qquad p \in \mathcal{P},\ f \in \mathcal{F}_p,\ k \in \mathcal{K}^{\mathrm{S}} \quad (66)$$

$$y_{pfr} \geq 0 \qquad p \in \mathcal{P},\ f \in \mathcal{F}_p,\ r \in \mathcal{R} \quad (67)$$

$$\sigma_{pfgt} \geq 0 \qquad p \in \mathcal{P},\ f \in \mathcal{F}_p,\ g \in \mathcal{P},\ t \in \mathcal{F}_g \quad (68)$$

$$\alpha_{pfkc} \geq 0 \qquad p \in \mathcal{P},\ f \in \mathcal{F}_p,\ k \in \mathcal{K},\ c \in \mathcal{C} \quad (69)$$

$$n_{pfkcv} \geq 0 \qquad p \in \mathcal{P},\ f \in \mathcal{F}_p,\ k \in \mathcal{K},\ c \in \mathcal{C},\ v \in \mathcal{V} \quad (70)$$

4. Solution by the Multiparametric Disaggregation Technique

The model has bilinear terms to correctly model mixing of the slag quality components and is, therefore, a nonconvex NLP. The Multiparametric Disaggregation Technique (MDT) applied to linearise the bilinear terms in the MAMP is based on the descriptions found in *Teles et al. (2012, 2013); Kolodziej et al. (2013a,b)*. The problem can then be solved by linear solvers. To be able to parameterise and discretise the bilinear constraints, new sets, indices, parameters, and variables have to be defined. These are found in Tables 4 - 6, respectively.

Table 4: Definition of sets for the MDT.

Set	
$\mathcal{M}$	Set of integers, indexed by m
$\mathcal{L}$	Set of integers, indexed by l
$\mathbb{Z}$	Set of all integers

Table 5: Definition of parameters for the MDT.

Parameter	
j	The last significant number's position.
$\underline{q}_{pf}$	Lower bound on the slag produced by furnace f at plant p.
$\overline{q}_{pf}$	Upper bound on the slag produced by furnace f at plant p.
ϵ	Optimality gap between the lower bound problem objective value and the best bound of the upper bound problem.

Table 6: Definition of variables for the MDT.

Variable	
$\hat{q}_{pfkml}$	The disaggregated flow variables of the product $q_{pf}\mu_{pfkml}$.
μ_{pfkml}	1 if the decimal power l is active for integer m for element or oxide k in furnace f at plant p, 0 otherwise.
λ_{pfkl}	Discretisation variable for use in reformulating ϕ_{pfk}.
$\Delta\phi_{pfk}$	Slack variable for the continuous representation of the discretised variable ϕ_{pfk}.

By applying the MDT, a lower bound problem (LBP) and an upper bound problem (UBP) for the MAMP can be derived, such that the problems are in the form of MILPs. The LBP and UBP can then be solved with increasing accuracy until the global optimality gap ϵ is satisfactory.

As described in *Kolodziej et al. (2013a)*, the LBP solution yields a lower bound for the original problem, denoted $\underline{z} \leq z$, where $\underline{z}$ is the solution to the LBP and z is the solution to the original problem. The UBP gives an upper bound on the problem. The LBP and UBP converge such that $\overline{z} = \underline{z} = z$.

4.1. Lower Bound Problem

This section describes the linearisation of constraints (25) for the LBP formulation. Of the two variables appearing in a bilinear term, one variable must be parameterised and the other disaggregated *(Teles et al., 2012)*. A continuous variable can be disaggregated into a set of non-negative continuous variables, which can only assume positive values up to the upper bound of the original variable *(Teles et al., 2013)*. The ϕ_{pfk} variables are chosen to be parameterised since they are limited between zero and one, and a given decimal precision. This reduces the feasible region of the problem compared to disaggregating ϕ_{pfk} and parameterising the variables q_{pf} instead, which have a range between zero and the maximum slag production possible in a furnace. Linearisation of constraints (25) is based on the MDT linearisation found in *Kolodziej et al. (2013a)* and yields the following constraints:

$$\phi_{pfk}q_{pf} = \sum_{l\in\mathcal{L}}\sum_{m\in\mathcal{M}} 10^l m \cdot \hat{q}_{pfkml} \qquad p\in\mathcal{P},\ f\in\mathcal{F}_p^{\text{FeMn}},\ k\in\mathcal{K}^{\text{S}} \quad (71)$$

$$\phi_{pfk} = \sum_{l\in\mathcal{L}}\sum_{m\in\mathcal{M}} 10^l m \cdot \mu_{pfkml} \qquad p\in\mathcal{P},\ f\in\mathcal{F}_p^{\text{FeMn}},\ k\in\mathcal{K}^{\text{S}} \quad (72)$$

$$q_{pfk} = \sum_{m\in\mathcal{M}} \hat{q}_{pfkml} \qquad p\in\mathcal{P},\ f\in\mathcal{F}_p^{\text{FeMn}},\ k\in\mathcal{K}^{\text{S}},\ l\in\mathcal{L} \quad (73)$$

$$\hat{q}_{pfkml} \geq \underline{q}_{pf}\mu_{pfkml} \qquad p\in\mathcal{P},\ f\in\mathcal{F}_p^{\text{FeMn}},\ k\in\mathcal{K}^{\text{S}},\ m\in M,\ l\in\mathcal{L} \quad (74)$$

$$\hat{q}_{pfkml} \leq \overline{q}_{pf}\mu_{pfkml} \qquad p\in\mathcal{P},\ f\in\mathcal{F}_p^{\text{FeMn}},\ k\in\mathcal{K}^{\text{S}},\ m\in M,\ l\in\mathcal{L} \quad (75)$$

$$\sum_{m\in\mathcal{M}} \mu_{pfkml} = 1 \qquad p\in\mathcal{P},\ f\in\mathcal{F}_p^{\text{FeMn}}, k\in\mathcal{K}^{\text{S}},\ l\in\mathcal{L} \quad (76)$$

$$\mu_{pfkml} \in \{0,1\} \qquad p\in\mathcal{P},\ f\in\mathcal{F}_p^{\text{FeMn}},\ k\in\mathcal{K}^{\text{S}},\ m\in M,\ l\in\mathcal{L} \quad (77)$$

Constraints (27) are linearised in the same manner. Implementing the linearisations of constraints (25) and (27) in the MAMP formulation yields the LBP formulation.

4.2. Upper Bound Problem

This section describes the linearisation of constraints (25) for the UBP formulation. The same derivation as found in *Kolodziej et al. (2013a)* is used, leading to a continuous representation of the discretised variables. The result is the following constraints, which replaces constraints (25):

$$\phi_{pfk}q_{pf} = \sum_{l\in\mathcal{L}}\sum_{m\in\mathcal{M}} 10^l m \cdot \hat{q}_{pfkml} + \Delta\phi_{pfk}q_{pf} \qquad p\in\mathcal{P},\ f\in\mathcal{F}_p^{\text{FeMn}},\ k\in\mathcal{K}^{\text{S}} \quad (78)$$

$$\phi_{pfk} = \sum_{l\in\mathcal{L}}\sum_{m\in\mathcal{M}} 10^l m\cdot\mu_{pfkml} + \Delta\phi_{pfk} \qquad p\in\mathcal{P},\ f\in\mathcal{F}_p^{\text{FeMn}},\ k\in\mathcal{K}^{\text{S}} \quad (79)$$

$$q_{pf} = \sum_{m\in\mathcal{M}} \hat{q}_{pfkml} \qquad p\in\mathcal{P},\ f\in\mathcal{F}_p^{\text{FeMn}},\ k\in\mathcal{K}^{\text{S}},\ l\in\mathcal{L} \quad (80)$$

$$\sum_{m\in\mathcal{M}} \mu_{pfkml} = 1 \qquad p\in\mathcal{P},\ f\in\mathcal{F}_p^{\text{FeMn}},\ k\in\mathcal{K}^{\text{S}},\ l\in\mathcal{L} \quad (81)$$

$$\mu_{pfkml}\in\{0,1\} \qquad p\in\mathcal{P},\ f\in\mathcal{F}_p^{\text{FeMn}},\ k\in\mathcal{K}^{\text{S}},\ m\in M,\ l\in\mathcal{L} \quad (82)$$

$$\hat{q}_{pfkml} \geq \underline{q}_{pf}\mu_{pfkml} \qquad p\in\mathcal{P},\ f\in\mathcal{F}_p^{\text{FeMn}},\ k\in\mathcal{K}^{\text{S}},\ m\in M,\ l\in\mathcal{L} \quad (83)$$

$$\hat{q}_{pfkml} \leq \overline{q}_{pf}\mu_{pfkml} \qquad p\in\mathcal{P},\ f\in\mathcal{F}_p^{\text{FeMn}},\ k\in\mathcal{K}^{\text{S}},\ m\in M,\ l\in\mathcal{L} \quad (84)$$

$$\Delta\phi_{pfk}q_{pf} \geq \underline{q}_{pf}\Delta\phi_{pfk} \qquad p\in\mathcal{P},\ f\in\mathcal{F}_p^{\text{FeMn}},\ k\in\mathcal{K}^{\text{S}} \quad (85)$$

$$\Delta\phi_{pfk}q_{pf} \leq \overline{q}_{pf}\Delta\phi_{pfk} \qquad p\in\mathcal{P},\ f\in\mathcal{F}_p^{\text{FeMn}},\ k\in\mathcal{K}^{\text{S}} \quad (86)$$

$$\Delta\phi_{pfk}q_{pf} \geq (q_{pf} - \overline{q}_{pf})10^j + \overline{q}_{pf}\Delta\phi_{pfk} \qquad p\in\mathcal{P},\ f\in\mathcal{F}_p^{\text{FeMn}},\ k\in\mathcal{K}^{\text{S}} \quad (87)$$

$$\Delta\phi_{pfk}q_{pf} \leq (q_{pf} - \underline{q}_{pf})10^j + \underline{q}_{pf}\Delta\phi_{pfk} \qquad p\in\mathcal{P},\ f\in\mathcal{F}_p^{\text{FeMn}},\ k\in\mathcal{K}^{\text{S}} \quad (88)$$

$$\Delta\phi_{pfk} \geq 0 \qquad p\in\mathcal{P},\ f\in\mathcal{F}_p^{\text{FeMn}},\ k\in\mathcal{K}^{\text{S}} \quad (89)$$

$$\Delta\phi_{pfk} \leq 10^j \qquad p\in\mathcal{P},\ f\in\mathcal{F}_p^{\text{FeMn}},\ k\in\mathcal{K}^{\text{S}} \quad (90)$$

Constraints (27) are linearised in the same manner for the UBP. Implementing the linearisations of constraints (25) and (27) in the MAMP formulation, yields the UBP formulation.

An algorithm is applied to verify that the global optimum is found and it is based on the description found in *Kolodziej et al. (2013a)*. The algorithm initiates with a coarse discretisation and solves both the LBP and UBP. If the difference between the objective value of the LBP and the best bound of the UBP is less than a given ϵ, the program ends, if not, the precision is increased and the problems are resolved.

There may be infeasibilities in the discretised problem even if the original problem is feasible. To avoid this, j and $|\mathcal{L}|$ have to be chosen appropriately. There are some general guidelines to help ensure precision based feasibility. The highest power of 10 ($\mathcal{L}$) must be large enough to ensure that 10^j is of the same order of magnitude as the upper bound on ϕ_{pfk}, given as $\mathcal{L} = \lfloor\log_{10}\overline{\phi}_{pfk}\rfloor$. Also, j has to be sufficiently small to ensure that at least one discretisation point is located between the upper and lower bounds for ϕ_{pfk}, meaning $j \leq |\mathcal{L}|$ is the minimum requirement. Feasibility is more likely as j decreases since this results in increased precision. The guidelines do not guarantee feasibility of the LBP and UBP in all cases, but represent the minimum precision level required to have reasonable bounds on ϕ_{pfk} *(Kolodziej et al., 2013a)*.

5. Computational Study

We have evaluated the applicability and limitations of the MAMP through a computational study. A comparison to actual production data would contribute to the validation of the model. However, it is not possible for us to evaluate the performance of the model against real production configurations and operational results since this is restricted data the authors have been unable to obtain from the industry partner. The computational study, therefore, consists of a model performance evaluation and a study of the economic aspects of manganese alloy production based on a semi-realistic instance.

The model is written in the algebraic modelling language Mosel and run in FICO® Xpress Optimisation Suite 7.9 using an HP EliteDesk 800 G2 SFF computer with Intel® Core™ i7-6700 3.40 GHz CPU and 32GB RAM. The operating system in use is Windows 10 Education 64-bit. The MAMP is formulated in a manner that requires some of the data provided by the industry partner to be pre-processed in Microsoft Excel before being imported to the optimisation software.

The MDT is implemented in the MAMP formulation to be able to solve the problem in the linear solver Xpress. Optimality gaps and maximal run times for the LBP and UBP can be varied, and a global optimality gap ϵ can be defined. The algorithm uses a precision in the range $\{0, -\infty\}$ to solve the pooling problem with the MDT. For all practical purposes, values of $\{0, 1\}$ are too course to accurately model the chemical compositions in the production problem. Producing metal and slag with precision values of $\{-4, -\infty\}$ is not practically achievable. The algorithm is thus left with a precision of $\{-2, -3\}$.

A base instance is created to perform the computational study. Data provided by Eramet Norway are perturbed for confidentiality purposes. This may lead to inaccurate costs, revenues, and consumption of raw materials compared to actual values. The intention of this computational study is not to accurately depict real production conditions as closely as possible, but rather to evaluate economic aspects of manganese alloy production in relation to variations in different parameters. Also, it is desirable to evaluate if the formulation of the MAMP can add value to manganese alloy multi-plant production planning when used as a decision support tool.

The production period is set to $\Delta T = 30$ days. The layout of Eramet Norway's plants has been used as the setup for the base instance. Seven furnaces are distributed over three plants, where three are HC FeMn furnaces and four are MC SiMn furnaces. The base instance is denoted *B1-3Fe4Si*. Plant 1 has one HC FeMn furnace and one MC SiMn furnace, Plant 2 has three MC SiMn furnaces, and Plant 3 has two HC FeMn furnaces. Estimated slag transportation costs between plants are set to 8.4 USD/tonne between Plant 1 and Plant 2, 14.0 USD/tonne between Plant 1 and Plant 3 and, 4.2 USD/tonne between Plant 2 and Plant 3.

All furnaces are set to have 22% pre-reduction, as used in *Olsen et al. (2007)*, thus $\Upsilon = 0.22$. Each furnace lose 35% of the heat generated to the surroundings, thus $L^{\mathrm{H}} = 1.35$. The electricity price is set lower than the current market price, as alloy companies often have lucrative price agreements. The electricity price is, therefore, set to $C^{\mathrm{E}} = 0.00118$ USD/kWh.

The input mass and electrical power capacity of each furnace are set to 1000 tonnes/40 MW and 750 tonnes/30 MW for HC FeMn and MC SiMn furnaces, respectively. In practice, it is usually the electrical power that limits furnace capacity. The refining processes' input capacities are set sufficiently high not to be limiting factors. The feed limit for each type of undersized lump is given as a weight fraction of the raw material feed to the furnaces, or the liquid metal feed to the MORs and LC SiMn refining stations. The feed limit fractions are set to 0.10.

The plants produce one or more of the end-products, with demands and revenues for fixed and optional contracts. These values can be found in Table 7. The revenues and demands for fixed and optional contracts are fictitious for confidentiality purposes. They do, however, reflect the increasing demand and prices seen for refined alloys *(Olsen et al., 2007)*. The demand is given for a 30 day period. The cumulative demand is set greater than the total furnace capacity, as the authors assume there are enough contracts available in the market to maximise production. The production is thus limited by the mass and electrical power capacity of the furnaces.

Table 7: End-products with demands and revenues for fixed and optional contracts. Demand is given in tonnes, revenue is given in USD/tonne.

End-product e	**Demand** D_e^{F}	**Revenue** R_e^{F}	**Demand** D_e^{O}	**Revenue** R_e^{O}
HC FeMn	13500	771	6000	810
MC FeMn	15000	899	6000	944
MC SiMn	10500	783	6000	822
LC SiMn	12000	853	6000	896

Each end-product is produced to satisfy certain content specifications. Explicit specifications are only set for the contents of HC FeMn and MC SiMn as these products are made in the furnaces where chemical composition is modelled. The content specifications for HC FeMn are: 0.790 Mn, 0.136 Fe, 0.004 Si, and 0.070 C. The MC SiMn specifications are 0.712, 0.081, 0.192, and 0.015 for the same elements, respectively. Notice that the composition of each end-product sum up to one. Correct content specifications of MC FeMn and LC SiMn are given implicitly by predetermined parameters for the refining stations. The weight percentage of every other constituent in MC FeMn and LC SiMn changes proportionally to the reduction of carbon as a result of the altered composition.

The mass output of slag is in relation to the total output of metal in an HC FeMn furnace. The maximum slag-to-metal ratio is set to $\overline{\Lambda} = 1.00$ and the minimum value $\underline{\Lambda} = 0.50$. The slag exiting the HC FeMn furnaces has set quality

specification intervals for oxides with metal-bearing capabilities. The upper and lower bound on the slag quality are defined by the parameters $\overline{\Phi}_k$ and $\underline{\Phi}_k$, respectively. $\overline{\Phi}_k$ is 0.50 for MnO, 0.02 for FeO, 0.35 for SiO_2, 0.20 for Al_2O_3 and MgO, and 0.30 for CaO. $\underline{\Phi}_k$ is 0.30, 0.00, 0.15, 0.10, 0.5, and 0.10 for the same oxides, respectively. The sum of the lower bounds on the slag composition $\underline{\Phi}_k$ means that this amount of the slag composition is predetermined. As in the base instance, 70% of the slag composition is already determined. 30% of the slag composition is then left for the MAMP to solve. The greater the sum of the upper bound on the slag composition $\overline{\Phi}_k$, the greater the number of possible combinations of oxides with which to fill the remaining 30% of the slag composition.

At every stage of the production, except at the LC SiMn refining station, by-products are produced as a fixed amount of the total feed to the process stage. These values are set to 0.02 for by-products produced in HC FeMn furnaces and 0.10 in the MC SiMn furnaces. The oxides Al_2O_3, ceMgO, and CaO completely exit the MC SiMn furnace as slag and thus the associated by-product parameters are 1.00 for these. In the MOR, the by-product fraction is 0.08. Values are based on *Olsen et al. (2007)*.

A set of 19 raw materials is at disposal at each plant. These raw materials contain various elements and oxides of different concentrations. Oxygen, silicon waste, MC FeMn undersized lumps, and LC SiMn undersized lumps, named refining resources, are separated from the raw materials since these feed other processes than the furnace process. The inventories are assumed to be large enough to satisfy any demand.

The MDT defines the parameters $\overline{q}_{pf}$. These parameters greatly affect the run time as they set the solution space for the volume of slag produced for each furnace. $\overline{q}_{pf}$ should therefore be set as tight as possible to avoid a too large feasible region. The parameters are naturally limited by the total amount of slag a furnace can produce per day. They are easily scaled by multiplying with ΔT. For the defined HC FeMn furnace capacities, a suitable mathematical upper bound is set to $\overline{q}_{pf} = 500\Delta T$, to not be a limiting factor. The parameters $\underline{q}_{pf}$ are set to zero as the HC FeMn furnace possibly can produce zero output. A similar parameter is defined for constraints (27) through the MDT linearisation.

The run time limits and optimality gaps for the LBP, UBP, and main algorithm are set to 7200 seconds and 1% for each problem. Extra instances are created to test the model. Instance testing starts with one plant, one HC FeMn, and one MC SiMn furnace, denoted as *P1-1Fe1Si*, where *P1* denotes one plant. Then, the instances are expanded to include several plants and furnaces in *P2-2Fe2Si* and *P5-5Fe5Si*. The optimality gaps, run times, and solution precisions for the LBP and the UBP problems, as well as the total run time and global optimality gap ϵ for the test instances, are listed in Table 8.

Table 8: Optimality gaps and run times for the test instances. The run times are given in seconds. * denotes that the time limit was reached before the gap was closed. † denotes that the current precision vector was not finished within the time limit.

	LBP			UBP			MAMP Main	
Instance	**Gap**	**Time**	**Precision**	**Gap**	**Time**	**Precision**	**Time**	ϵ
P1-1Fe1Si	0.65%	{1,9}	{-2,-3}	1.00%	{2,17}	{-2,-3}	29	1.07%
P2-2Fe2Si	1.00%	{391,6808†}	{-2,-3†}	1.00%	{1019,6179†}	{-2,-3†}	14409	1.50%
B1-3Fe4Si	1.36%*	{7200†}	{-2†}	2.18%*	{7200†}	{-2†}	14409	2.55%
P5-5Fe5Si	3.33%*	{7200†}	{-2†}	7.08%*	{7200†}	{-2†}	14405	7.86%

The number of furnaces limits the scalability of the problem. Adding a furnace adds a new set of chemical balance constraints and furnace restrictions to the problem. Both the LBP and the UBP are solved to the accepted optimality gaps for small instances with little computational effort. The resulting ϵ is close to the accepted global optimality gap of 1.00%. For larger instances, the accepted optimality gaps for the LBP and UBP are never reached within the time limit. Consequently, ϵ deteriorates for larger problems. The base instance *B1-3Fe4Si* is solved to an $\epsilon = 2.55\%$ within the time limit. It is worth noting that the MAMP can find acceptable, feasible solutions even for large instances such as *P5-5Fe5Si*.

The applied precision has a significant effect on the required computational time. For larger instances, the {-3} precision is never completed or even started within the run limit of the program. Generally, the solution to the LBP problem is better and located faster than for the UBP. This is due to that the UBP is a continuous representation of the solution space, while the LBP is discrete, thus requiring a larger computational effort.

Different parameter settings can affect the problem size significantly. The upper and lower bounds on the slag composition are two such parameters. Allowing a wide interval may give a better solution to the planning problem, but can make the problem unsolvable within a reasonable time. Narrowing the interval can reduce the computational time significantly, but may limit how useful the solution is. If the upper and lower bounds are equal, or the sum of the upper bounds are 1.00, the bilinear terms vanish as only one slag composition is feasible. The slag composition is thus predetermined and the MDT solution method is redundant in this case.

It is of interest to investigate how large intervals the MAMP can solve to a certain global optimality gap ϵ within the allotted time. In practice, there are process specific considerations that limit this interval to a certain degree; these values are as described in the base instance. The upper and lower bounds on the slag composition are allowed to extend beyond the practical values to investigate the effects on the computational effort for different interval ranges. The run results for the test instances are given in Table 9.

Table 9: Run results for various slag composition intervals. Run times given in seconds.

Instance	Sum $\underline{\Phi}_k$	Sum $\overline{\Phi}_k$	LBP Gap	UBP Gap	Total Time	MAMP ϵ
C1-LOW	0.80	1.07	1.00%	1.16%	10566	1.19%
C2-MED	0.75	1.30	1.32%	1.76%	14415	2.28%
C3-HIGH	0.30	2.50	5.06%	6.33%	14405	6.90%
C4-MAX	0.00	6.00	8.66%	8.93%	14407	11.34%

Table 9 shows that ϵ increases for increasing slag interval ranges. Solving *C1-LOW* results in that the {-2} precision is solved in a short time in contrast to not finishing for the other instances. Allowing maximum composition range, as in the instance *C4-MAX*, makes the problem harder to solve, thus the significantly worse ϵ. The conclusion is that the size of the interval greatly affects the computational effort required to solve a pooling problem like the MAMP and that one should take great care in determining these parameters.

Having the model run for a longer time can give a better optimality gap. However, if the potential economic gain from increasing the run time is low, it may be better to have a shorter run time. The LBP objective value and UBP best bound for an individual run time of twelve hours are shown in Figure 4.

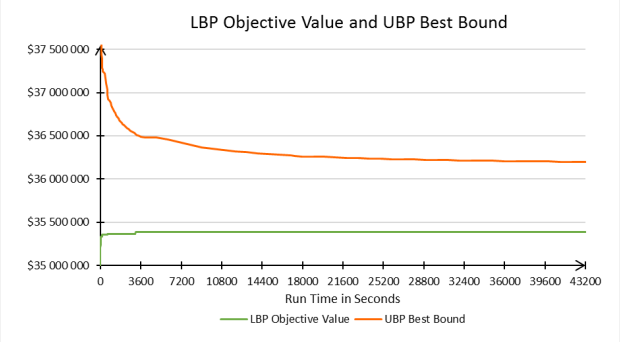

Figure 4: LBP objective value and UBP best bound for increasing run time of the LBP and the UBP. Values in USD.

A good LBP objective value is found within the first hour. After the first hour, no significantly better objective value is found. The best bound in the UBP decreases rapidly within the first hour and continues to decrease in a steady manner for the remainder of the run. Increasing the run time ensures that the solution can be guaranteed with a better ϵ. After four hours, the decrease in ϵ is diminishing until it flattens out at approximately 2.30% after eight hours. At twelve hours, the MAMP has run for a total of 24 hours, ending at an ϵ of 2.28%. It can be concluded that allowing run times of more than four hours for the LBP and UBP is of little value to the solution unless a very high solution accuracy is desired and sufficient time is available.

The current industry practice is to optimise the production for individual furnaces based on software and expert judgement made by metallurgists. This practice is denoted single furnace optimisation and is the practice of optimising

the profit of each single furnace, and consequently the metal it produces, without regards to the overall production. This may be sub-optimal compared with planning the production when taking the multi-plant production into consideration. The MAMP expands the production planning to cover all furnaces at all plants and is, therefore, a formulation that could potentially handle the complexity of multi-plant production. An evaluation on how the MAMP performs against single furnace optimisation can show if the MAMP can contribute to better production planning.

To simulate single furnace optimisation, the following process is used. An instance only containing one HC FeMn furnace and an instance only containing one MC SiMn furnace are created. The authors assume that the single furnace optimisation process is done by satisfying the fixed contracts first, then the optional contracts with the highest profit. In the first iteration, the HC FeMn instance is solved with the total demand as input. The demand is then reduced with the production in the first iteration and the instance is solved again. This is done for three iterations with the HC FeMn instance, followed by four iterations with the MC SiMn instance. The results from the HC FeMn production iterations are shown in Table 10, together with the results from applying the MAMP formulation.

Table 10: Comparison of the MAMP formulation to single furnace optimisation for the FeMn production. Production volumes are given in tonnes. Objective values are given in thousand USD.

	Single Furnace Optimisation				**MAMP Optimisation**			
Plant p, Furnace f	**1, 1**	**3,6**	**3,7**	**Total**	**1, 1**	**3,6**	**3,7**	**Total**
Furnace Type	**FeMn**	**FeMn**	**FeMn**		**FeMn**	**FeMn**	**FeMn**	
u_{pf}, **to crushing**	0	8314	4175	12489	0	10688	3021	13709
m_{pf}, **to refining**	10439	2599	6519	19557	10998	0	8559	19557
q_{pf}, **produced slag**	5220	5456	5347	16023	5499	5344	5790	16633
x^{E}_{pe}, **HC FeMn**	0	7482	3758	11240	0	9620	2719	12339
x^{E}_{pe}, **MC FeMn**	9608	2392	6000	18000	10122	0	7878	18000
Obj. Val. FeMn	6668	5975	6741	19384	*NA*	*NA*	*NA*	*NA*

The MAMP produces in total 610 tonnes more slag than single furnace optimisation. The total demand of MC FeMn from fixed and optional contracts are satisfied for both production methods, while not all of the optional contract demand for HC FeMn is satisfied. This indicates that MC FeMn is the most profitable FeMn end-product. Note that furnace 1 in single furnace optimisation is the result of the first iteration of the HC FeMn instance and furnace 6 and 7 are the second and third iteration, respectively.

The slag-to-metal ratio is optimal at the lower bound of 0.50 in both production methods (can be verified by consulting $\frac{q_{pf}}{u_{pf}+m_{pf}}$). As it is not advantageous to produce more slag than necessary, the MAMP yields the same ratio as the single furnace optimisation approach although the reasoning behind the slag production in the two planning methods are different. The single furnace optimisation practice always minimises the amount of slag produced as the goal is to maximise the profit from FeMn metal for the HC FeMn furnaces. Thus, ending at the lower bound slag-to-metal ratio. The MAMP chooses the slag production values based on the goal to optimise the entire production. The MAMP also uses a slag-to-metal ratio of 0.50 since producing slag in the HC FeMn furnaces is unfavourable compared to producing more HC FeMn for the given parameter settings. The produced slag is still used in MC SiMn furnaces as this is a better option than discarding it.

We assume that the slag transportation between furnaces in the single furnace optimisation is based on minimising transportation costs, to make the two production planning methods as comparable as possible. This implies that as much slag as possible is sent internally at a plant if a plant has both HC FeMn and MC SiMn furnaces, as is the case at Plant 1. When the internal capacity of slag is reached, slag is transported to the plant with MC SiMn furnaces incurring the lowest transportation costs. The results from the single furnace optimisation method and the MAMP for the SiMn production are given in Table 11.

All the produced slag is consumed in both production planning methods and all the LC SiMn demand is satisfied. The difference lies in the produced volume of MC SiMn, where an additional 673 tonnes of MC SiMn is produced by using the MAMP due to different composition and allocation of the slag. This is an 8.52% increase in production of MC SiMn alloy. One can argue that the slag could have been distributed in another manner for the single furnace optimisation planning. Another approach for dividing the feed of slag between the remaining MC SiMn furnaces at Plant 2 would be to give them the average of the remaining feed; this would however still be sub-optimal compared to

the allocation given by the MAMP. Having flexibility and decision support tools to help in the distribution of slag is clearly an advantage.

Table 11: Comparison of the MAMP to single furnace optimisation for the SiMn production and total profit. Production values are given in tonnes. Costs and objective values are given in thousand USD. *Cumulative Objective Value* is excluded the *Transportation Costs*. *Total profit* is the *Cumulative Objective Value* less the *Transportation Costs*.

	Single Furnace Optimisation					**MAMP Optimisation**				
Plant p, Furnace f	**1, 2**	**2,3**	**2,4**	**2,5**	**Total**	**1, 2**	**2,3**	**2,4**	**2,5**	**Total**
Furnace Type	**SiMn**	**SiMn**	**SiMn**	**SiMn**		**SiMn**	**SiMn**	**SiMn**	**SiMn**	
u_{pf}, **to crushing**	0	2786	5547	447	8780	2338	0	1381	5809	9528
m_{pf}, **to refining**	5021	2175	42	4755	11993	2856	5246	3892	0	11994
σ_{gtpf}, **used slag**	5220	5456	2674	2673	16023	5499	4095	3421	3618	16633
Leftover slag	0	0	0	0	0	0	0	0	0	0
x^{E}_{pe}, **MC SiMn**	0	2508	4992	402	7902	2104	0	1243	5228	8575
x^{E}_{pe}, **LC SiMn**	6280	2720	53	5947	15000	3571	6588	4841	0	15000
Obj. Val. SiMn	4418	3565	2929	4599	15511	*NA*	*NA*	*NA*	*NA*	*NA*
Cum. Obj. Val.					34895					35430
Transport. Costs	0	23	11	11	45	0	17	14	15	47
Discard Slag Cost					0					0
Total Profit					**34850**					**35383**

The MAMP transports more slag than the single furnace optimisation, thus, transportation costs are greater. Using the MAMP yields 1.53% higher profit compared to single furnace optimisation in the case of base instance *B1-3Fe4Si*. Two significant factors in making the MAMP formulation superior to single furnace optimisation are the volume of slag produced and the composition of the slag. The average composition of the slag in the single furnace optimisation and the MAMP optimisation are presented in Figures 5 and 6, respectively.

Figures 5 and 6 show a considerable difference between the average slag compositions of single furnace optimisation and MAMP optimisation. The most notable differences are the changes in the MnO, CaO, MgO, and Al_2O_3 concentrations. In optimising single furnaces, it is favourable to keep the MnO concentration in the slag to a minimum to maximise the HC FeMn output. Consequently, the oxides that are not substances of HC FeMn metal are maximised in the slag output. In MAMP optimisation, these concentrations are changed to suit the overall production.

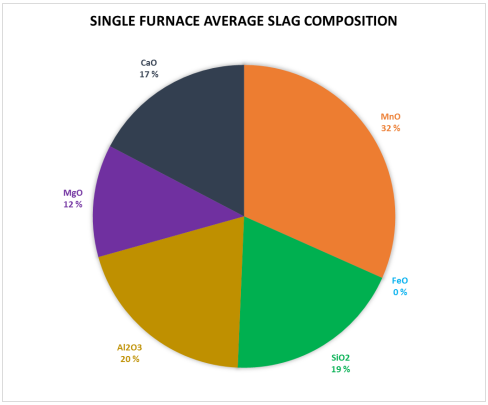

Figure 5: The average slag composition produced by the three HC FeMn furnaces using single furnace optimisation.

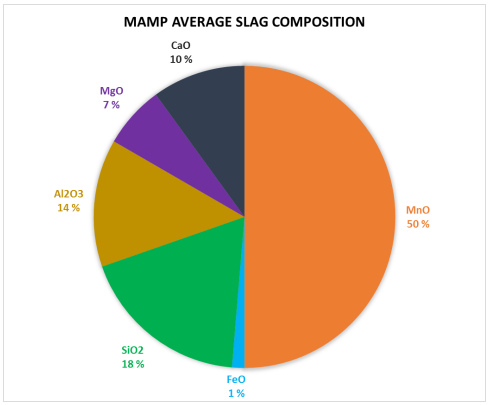

Figure 6: The average slag composition produced by the three HC FeMn furnaces using the MAMP formulation.

The measure slag-to-metal ratio is widely used in the manganese alloy production industry. In the previous section, it can be observed that the slag-to-metal ratio is at the lower bound of 0.50 in all furnaces. The ratio can be up to 1.00, meaning one tonne slag is produced per tonne metal produced. It can, therefore, be of interest to investigate which

conditions can make this ratio prone to change from its lower bound. These conditions can be variations in the demand volume of the end-products, which can affect the optimal slag-to-metal ratio. The composition of the slag may also change when the slag-to-metal ratio changes.

One case is studied where the demand is assumed to be equal for all end-products. The end-product demand is equally distributed between FeMn and SiMn alloys. The fixed demand for all end-products are set as optional to make the MAMP select the most profitable ones. The end-product production volumes are also provided as it may better visualise the changes occurring in the slag-to-metal ratio and slag composition. The volumes produced of each end-product for increasing demand are illustrated in Figure 7.

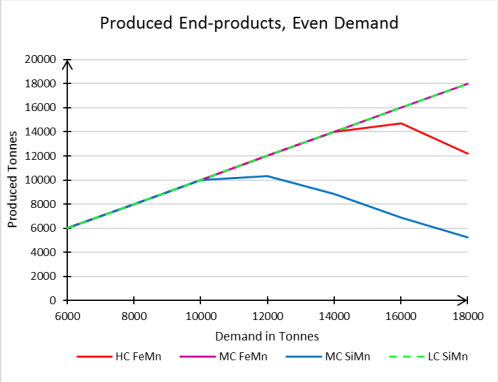

Figure 7: End-product production volumes for increasing demand when the demand is evenly distributed between FeMn and SiMn alloys.

Observe from Figure 7 that MC SiMn and HC FeMn are the first products in each production path to be reduced when reaching furnace capacities at 12 000 tonnes and 16 000 tonnes, respectively. The slight increase in productions before the steady decrease at the furnace capacities are due to the alteration of slag composition. A plot of the average slag-to-metal ratio as a function of demand is shown in Figure 8. A plot of the average slag composition as a function of demand is shown in Figure 9. Between 8 000 - 12 000 tonnes demand, a slight increase in slag-to-metal ratio can be observed. This is to accommodate the lacking MC SiMn furnace capacity better. At 12 000 tonnes, the HC FeMn furnace needs the capacity to produce more HC FeMn, and the slag-metal-ratio starts to decline. At 16 000 tonnes, it reaches the lower limit of the ratio and starts sending more of the metal output to MC FeMn refining, which is more profitable.

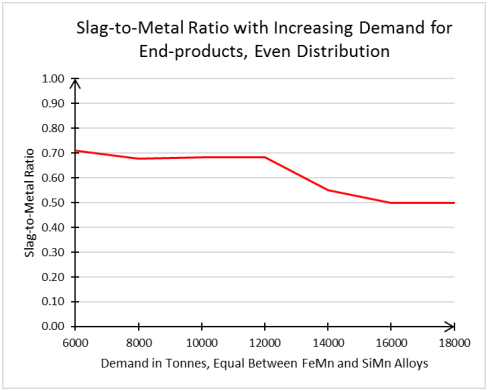

Figure 8: Average slag-to-metal ratio across all HC FeMn furnaces for increasing demand. Equal demand for each end-product.

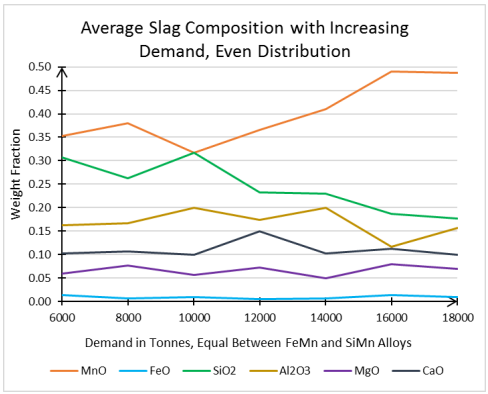

Figure 9: Average slag composition across all HC FeMn furnaces for increasing demand. Equal demand for each end-product.

The slag-to-metal ratio is 0.68 - 0.71 for demands less than 12 000 tonnes. For greater demands, the slag-to-metal ratio decreases to the lower bound of 0.50. Here, production of the least profitable alloy MC SiMn cannot satisfy

demand as the slag-to-metal ratio decreases to release capacity in the FeMn furnaces to satisfy the increasing demand of FeMn alloys which are more profitable. At a demand of 12 000 tonnes, the FeMn production needs the capacity to satisfy the FeMn alloy demand. Thus, less capacity is available to produce slag. This trend continues for increasing demand until the lower bound of the slag-to-metal ratio is reached. As the slag-to-metal ratio decreases, it becomes more favourable to send slag with a higher content of MnO and lower content of SiO_2. Thus, as the volume of slag goes down, the amount of MnO increases to make the slag carry more of the important oxides to form pure metals in the MC SiMn furnace, as can be seen from Figure 9.

The results from Table 11 are for an instance where the slag-to-metal ratio is at its lower bound of 0.50. The authors suspect that the value of using the MAMP formulation is even greater in situations where the optimal slag-to-metal ratio is above the lower bound. The single furnace optimisation practice always minimises the slag-to-metal ratio, as it optimises the profit for single furnaces, consequently produces as much metal as possible. The MAMP, on the other hand, changes the metal-to-slag ratio according to what is optimal for the overall profit. A larger volume of slag is therefore produced and allocated efficiently to the MC SiMn furnaces. The decision to maximise metal output in single furnace optimisation could of course also be changed to maximise slag output, but this is not a trivial decision to make simply by consulting raw material costs and end-product revenues.

The base instance is therefore updated with demands skewed towards SiMn alloys, as this results in an optimal slag-to-metal ratio of 0.70. The demands are set to be 19 200 tonnes for each SiMn alloy, and 12 800 tonnes for each FeMn alloy and an equal comparison of the MAMP formulation to the single furnace optimisation practice is performed. The overall result is that the MAMP generates 1.99% more profit than single furnace optimisation. It should be noted that the MAMP, for this instance, is solved to within 1.6% optimality gap while single furnace optimisation is solved to optimality.

6. Concluding Remarks

In this paper, the previously not analysed manganese alloy multi-plant production problem is defined and characterised. An optimisation model of the problem is presented and it is formulated as a pooling problem. The bilinear terms present in this formulation is linearised using the multiparametric disaggregation technique (MDT). To the authors' knowledge, it is the first model to implement the MDT to solve a large-scale pooling problem. A computational study shows that the optimisation model presented can solve problem sizes of up to seven furnaces spread across three plants to within a global optimality gap of 3% for a run time of four hours. The study also shows that the MDT is able to scale well with larger, real problem instances. The model outperforms the current operational practice of single furnace optimisation, which is based on process knowledge and expertise. The choice of optional contracts to accept visualise which products are the most profitable since these are the products produced after the fixed demand is met. Comparing the model to real production data can greatly improve the validation of the model presented in this paper. Overall, we are confident that our model can work as a decision support tool for the industry. Further work on this problem could include the following: allow an increased number of end-products to exit the furnaces and flow through the refining and crushing processes. Include furnace setup switching to allow for the best furnace setup to be determined by the model. Formulate the MAMP as a stochastic problem to account for uncertainty in market demand and raw material, electricity, and transportation costs, providing a more robust production schedule.

7. Acknowledgements

The authors gratefully acknowledge input and support to the model development and case studies from Benjamin Ravary and Helge Øsenstad, Eramet Norway. SOW and BRK gratefully acknowledge support from NFR grant 228460/030.

References

Alfaki, M., 2012. Models and solution methods for the pooling problem. Ph.D. thesis. The University of Bergen.

Alfaki, M., Haugland, D., 2013. Strong formulations for the pooling problem. Journal of Global Optimization 56, 897–916.

Amos, F., Rönnqvist, M., Gill, G., 1997. Modelling the pooling problem at the new zealand refining company. Journal of the Operational Research Society 48, 767–778.

Audet, C., Brimberg, J., Hansen, P., Digabel, S.L., Mladenović, N., 2004. Pooling problem: Alternate formulations and solution methods. Management science 50, 761–776.

Ben-Tal, A., Eiger, G., Gershovitz, V., 1994. Global minimization by reducing the duality gap. Mathematical programming 63, 193–212.

Boland, N., Kalinowski, T., Rigterink, F., Savelsbergh, M., 2015. A special case of the generalized pooling problem arising in the mining industry. Optimization Online e-prints .

d'Harambure, A., 2015. Overview of the global manganese industry. URL: http://www.manganese.org/images/uploads/board-documents/14._2015_AC_-_Aloys_dHarambure.pdf. Accessed 03.09.2016.

Gounaris, C.E., Misener, R., Floudas, C.A., 2009. Computational comparison of piecewise- linear relaxations for pooling problems. Industrial & Engineering Chemistry Research 48, 5742–5766.

Haverly, C.A., 1978. Studies of the behavior of recursion for the pooling problem. ACM Sigmap Bulletin , 19–28.

International Manganese Institute and Hatch, 2015. The environmental profile of manganese alloys. URL: http://www.manganese.org/images/uploads/pdf/IMnI_LCA_Summary_Report_View_2015.pdf. Accessed 07.09.2016.

InvestmentMine, 2017. Historical manganese prices and price chart. URL: http://www.infomine.com/investment/metal-prices/manganese/all/. Accessed 25.03.2017.

Jezowski, J., 2010. Review of water network design methods with literature annotations. Industrial & Engineering Chemistry Research 49, 4475–4516.

Jipnang, E., Monheim, P., Oterdoom, H., 2013. Process optimisation model for femn and simn production, in: The Thirteenth International Ferroalloys Congress, Efficient Technologies in Ferroalloy Industry, Almaty, Kazakhstan, pp. 811–820.

Kolodziej, S., Castro, P.M., Grossmann, I.E., 2013a. Global optimization of bilinear programs with a multiparametric disaggregation technique. Journal of Global Optimization 57, 1039–1063.

Kolodziej, S.P., Grossmann, I.E., Furman, K.C., Sawaya, N.W., 2013b. A discretization-based approach for the optimization of the multiperiod blend scheduling problem. Computers & Chemical Engineering 53, 122–142.

Meyer, C.A., Floudas, C.A., 2006. Global optimization of a combinatorially complex generalized pooling problem. AIChE journal 52, 1027–1037.

Misener, R., Floudas, C.A., 2009. Advances for the pooling problem: modeling, global optimization, and computational studies. Appl. Comput. Math 8, 3–22.

Olsen, S.E., Olsen, S., Tangstad, M., Lindstad, T., 2007. Production of manganese ferroalloys. Tapir Academic Press.

Quesada, I., Grossmann, I.E., 1995. Global optimization of bilinear process networks with multicomponent flows. Computers & Chemical Engineering 19, 1219–1242.

Sherali, H.D., Adams, W.P., Driscoll, P.J., 1998. Exploiting special structures in constructing a hierarchy of relaxations for 0-1 mixed integer problems. Operations research 46, 396–405.

Tawarmalani, M., Sahinidis, N.V., 2002. Convexification and global optimization in continuous and mixed-integer nonlinear programming: theory, algorithms, software, and applications. volume 65. Springer Science & Business Media.

Teles, J.P., Castro, P.M., Matos, H.A., 2012. Global optimization of water networks design using multiparametric disaggregation. Computers & Chemical Engineering 40, 132–147.

Teles, J.P., Castro, P.M., Matos, H.A., 2013. Multi-parametric disaggregation technique for global optimization of polynomial programming problems. Journal of Global Optimization 55, 227–251.

United Nations, 2016. Changing consumption patterns. URL: http://www.unep.org/Documents.Multilingual/Default.asp?DocumentID=52&ArticleID=52. Accessed 06.12.2016.

Wicaksono, D.S., Karimi, I.A., 2008. Piecewise milp under-and overestimators for global optimization of bilinear programs. AIChE Journal 54, 991–1008.